



PHD

Novel Applications of Cold Atmospheric Plasma for the Decontamination of Bacterial Biofilm-Associated Wound Infection

Patenall, Bethany

Award date:
2021

Awarding institution:
University of Bath

[Link to publication](#)

Alternative formats

If you require this document in an alternative format, please contact:
openaccess@bath.ac.uk

General rights

Copyright and moral rights for the publications made accessible in the public portal are retained by the authors and/or other copyright owners and it is a condition of accessing publications that users recognise and abide by the legal requirements associated with these rights.

- Users may download and print one copy of any publication from the public portal for the purpose of private study or research.
- You may not further distribute the material or use it for any profit-making activity or commercial gain
- You may freely distribute the URL identifying the publication in the public portal ?

Take down policy

If you believe that this document breaches copyright please contact us providing details, and we will remove access to the work immediately and investigate your claim.

**Novel Applications of Cold Atmospheric Plasma for the
Decontamination of Bacterial Biofilm-Associated Wound
Infection**

Bethany Patenall

A thesis submitted for the degree of a Doctor of Philosophy

University of Bath

Department of Chemistry

January 2021

“In the long history of humankind those who learned to collaborate and improve most effectively have prevailed”

-Sir Charles Darwin

Abstract

This research aims to investigate the biological interactions of cold atmospheric pressure plasma (CAP) with bacteria and to develop therapeutic hydrogel wound dressings which work in tandem with CAP treatment for the reduction of the bacterial bioburden of the wound while screening out any potentially harmful species generated by the CAP. The presence of a bacterial biofilm within a wound increases the risk of wound chronicity and bacterial biofilms are known to have increased antibiotic resistance. Wound infection can result in septicaemia.

Chapter 3 characterises a helium-driven CAP (He-CAP) device pertaining to its clinical use through the quantification of the biologically relevant reactive oxygen and nitrogen species (RONS) it produces, operating temperature, the effect upon pH under varying operating conditions and how the He-CAP device interacts with a model hydrogel wound dressing (polyvinyl alcohol (PVA)). The optimised He-CAP operating parameters were then applied to planktonic and biofilm bacteria.

Chapters 4 & 5 seek to understand the biological interactions between bacteria and He-CAP. *Chapter 4* concerns the interactions between He-CAP and bacterial biofilm formation and oxidative stress response, through the assessment of RONS delivery through the developing bacterial biofilm. *Chapter 5* assesses the mutagenic impact of sub-lethal He-CAP exposure, compares the mutagenic profile to known mutagens UV and ionising radiation and the impact upon antibiotic susceptibility.

The final chapters focus on the development and assessment of therapeutic hydrogel wound dressings. *Chapter 6* aims to develop a hydrogen peroxide responsive hydrogel which releases an antibiofilm agent to prevent biofilm formation. *Chapter 7* seeks to utilise and characterise a novel argon-driven CAP (Ar-CAP) jet and to use a known antimicrobial, povidone-iodine (PVP-I) in a PVA hydrogel for synergistic killing of a *Pseudomonas aeruginosa* bacterial biofilm.

For Freddie

Acknowledgements

Firstly, to my supervisors Professor Toby Jenkins and Dr Amber Young. Your support and guidance for the past 4 years have been incredible. Toby, thank you so much for your constant faith and support in all my outlandish endeavours, from letting me carry out a genetics-based project in a PhD that you assured me “won’t have any genetics in it”, your faith and encouragement to apply to medical school. Your worldly wisdom, ranging from the luxury booze cruise to Amsterdam to getting the train from Bath to Austria, will stay with me for a long time. Amber, thank you for your invaluable advice both academically and personally.

To the Jenkins research group, I cannot thank you all enough for your friendship, support and willingness to drink beer with me. Thank you to Thet, Adam, Jordan, Laura, George, Lauren, Rachel and Emily you have all made my PhD so fun. Hollie, thank you for your plasma-based guidance, hosting me in your house while I mutated bacteria and plying me with red wine after 12 hours of PCR. Your support and friendship have been invaluable. Scarlet, you were Frodo to my Sam, your constant berating of my grammar and spelling have made me a better writer. To you both, thank you for putting up with my endless string of nonsense. Finally, a huge thanks to Maisem for your endless supply of espressos, biology advice and comic relief.

To my friends and family, for your support and always listening to me exclusively talk about either my research or thesis for the past 3 years. I would not have been able to accomplish this without you all. To the Patenalls for your encouragement and Sunday dinners. To the McCanns, for keeping me grounded and cheering me on. The Gillsons for your support. To my dogs, Lupin, Sweep, Flash and Darwin giving you smooths always improves everything. Tom, thank you for your unwavering confidence and belief in me, always being there to remind me and educate me on what I can achieve. Your love (and endless cups of coffee) made this so much easier.

To my mother, you have taught me so much, how to pick myself up when things haven’t gone to plan (frequently utilised during my PhD), courage and resilience, you are a true inspiration.

Declarations

This thesis is the result of my own work and includes work done in collaboration which is specifically indicated here and in the text.

Chapter 4

Figure 4.4: Quantification of viable cells of MRSA and *P. aeruginosa* biofilms over time was performed by Dr Hollie Hathaway, University of Bath.

Figure 4.5: Recovery of H₂O₂ through MRSA and *P. aeruginosa* biofilms (normalised to TF) of varying maturity performed by Dr Hollie Hathaway, University of Bath.

Figure 4.6: H₂O₂ recovery beneath PVA/CMC hydrogel after varying post CAP treatment incubation times (A) and recovery beneath *P. aeruginosa* and MRSA biofilms after 4 hours rest (B). Error bars denote the standard deviation (n=3). (This graph was made in collaboration with Dr H. Hathaway and reproduced with her permission).

Chapter 6

Figure 6.8: UV-Vis absorption per gram of PBA-based hydrogel at 513 nm over time in PBS (pH 7.3) at 25 °C was performed by Dr George Williams, University of Bath.

Figure 6.9: UV-Vis absorption per gram of PBA-based hydrogel at 513 nm over time in PBS (pH 7.3) at 25 °C. Error bars indicate standard deviation (n = 3) was performed by Dr George Williams, University of Bath.

Figure 6.10: UV-Vis absorption per gram of PBA-based hydrogel in the presence of various concentrations of hydrogen peroxide (0.1 – 4 mM) in PBS (pH 7.3) after 3 hours. Absorbance was measured at 513 nm at 25 °C; error bars indicate standard deviation (n = 3). Increase in absorbance correlates with release of ARS from the hydrogel was performed by Dr George Williams, University of Bath.

Figure 6.18: Absorbance at 513 nm of release of ARS from PBA gel after incubation with PBS treated with CAP for varying amounts of time (0-30 minutes). Error bars represent standard deviation (n=3) was performed by Dr George Williams, University of Bath.

Dissemination of Research

- **Oral Presentation** – International Conference of Plasma Medicine, June 2020, South Korea (*Cancelled due to COVID-19*)
- **Poster Presentation** – European Wound Management Association (EWMA) May 2020, London, UK. (*Cancelled due to COVID-19*)
- **Delegate** – European Wound Management Association (EWMA) Conference, May 2019, Gottenberg, Sweden.
- **Oral Presentation** – British Burns Association Annual Meeting, May 2019, Leeds, UK.
- **Oral Presentation** – European Congress of Clinical Microbiology and Infectious Diseases (ECCMID), April 2019, Amsterdam, Netherlands.
- **Oral Presentation** – VBST Conference, February 2019, Hircheegg, Austria
- **Oral Presentation** – BioNano Summer School, August 2018 & 2019, Hirscheegg, Austria
- **Poster Presentation** – International Conference of Plasma Medicine, June 2018, Drexel University, Philadelphia, USA.
- **Delegate** – British Burns Association Annual Meeting, May 2018, Swansea, Wales.

Awards

- Santander Travel Grant 2020
- BBA Travel Grant 2020
- KCi/Acelity Scholarship 2019
- Images in Research 2018

Publications

- **Patenall BL**, Hathaway HJ, Sedgwick AC, Thet NT, Young AE, Allinson SL, Short RD & Jenkins ATA. Limiting *Pseudomonas aeruginosa* biofilm formation using cold atmospheric pressure plasma. (2018) Plasma Medicine 8(3)
- Hathaway HJ, **Patenall BL**, Thet NT, Sedgwick AC, Williams GT, Jenkins ATA, Allinson SL & Short RD. Delivery and quantification of hydrogen peroxide generated via cold atmospheric pressure plasma through biological material. (2019) Journal of Physics D Applied Physics 52(50)
- **Patenall BL**, Williams GT, Gwynne L, Stephens LJ, Lampard EV, Hathaway HJ, Thet NT, Young AE, Sutton MJ, Short RD, Bull SD, James TD, Sedgwick AC & Jenkins ATA. Reaction based indicator displacement assay (RIA) for the development of a triggered release system capable of biofilm inhibition. (2019) Chem Commun 12;55(100):15192-32
- Ghimire, B, Szili E, **Patenall BL**, Lamichane P, Gaur N, Robson A, Trivedi D, Thet N, Jenkins T, Choi E & Short R. Enhancement of hydrogen peroxide production for an atmospheric pressure argon plasma jet and implications to the antibacterial activity of plasma activated water. (2021) PSST 30 (3).
- **Patenall BL**, Hathaway HJ, Laabei M, Young AE, Thet NT, Jenkins A.T.A, Short R & Allinson SL. Assessment of mutations induced by cold atmospheric plasma jet treatment relative to known mutagens in *Escherichia coli*. (2021) Mutagenesis (*under review*)

Other

- Waterfield T, Lyttle MD, McKenna J, Maney J, Roland D, Corr M, Woolfall K, **Patenall B**, Shields M & Fairley D. Loop-mediated isothermal amplification for the early diagnosis of invasive meningococcal disease in children. (2020) Archives of Disease in Childhood.
- Waterfield T, Maney J, Lyttle MD, McKenna J, Roland D, Corr M, **Patenall B**, Shields M, Woolfall K & Fairley D. Diagnostic test accuracy of point-of-care procalcitonin to diagnose serious bacterial infections in children. (2020) BMC Paediatrics 20 (487)
- Waterfield T, Maney J, Lyttle MD, Fairley D, Lyttle MD, McKenna J, Roland D, Corr M, McFetridge L, Mitchell H, Woolfall K, Lynn F, **Patenall B** & Shields M. Validating clinical practice guidelines for the management of children with on-blanching rashes in the UK (PiC): a prospective, multicentre cohort study. (2020) The Lancet ID

- Califano D, **Patenall BL**, Kadowaki M, Mattia D, Scott J & Edler K. Enzyme-functionalized cellulose beads as a promising antimicrobial material. (2021) *Biomacromolecules* 22 (2).
- Milo S, Heylen R, Glancy J, Williams G, **Patenall BL**, Hathaway H, Thet N, Allinson S, Laabei M & Jenkins ATA. A small-molecular inhibitor against *Proteus mirabilis* urease to treat catheter-associated urinary tract infections. (2021) *Nature Scientific Reports* 11 (1).

Table of Contents

Abstract	IV
Acknowledgements	VIII
Declarations	X
List of Tables	XXI
List of Figures	XXII
Acronyms and Abbreviations	XXXIII
Chapter 1 : Introduction	1
1.1 The Clinical Problem – Biofilm-Associated Bacterial Wound Infection	1
1.2 Wounds	2
1.2.1 Wound Classification	2
1.2.2 Acute Wounds	2
1.2.3 Chronic Wounds.....	2
1.2.4 Burn Wounds.....	3
1.2.5 Wound Infection.....	4
1.2.6 Infection Diagnosis	5
1.2.7 Wound Dressings	7
1.2.8 Wound Healing	9
1.2.9 Bacterial Biofilms	10
1.2.10 <i>Staphylococcus aureus</i>	11
1.2.11 <i>Pseudomonas aeruginosa</i>	12
1.3 Bacterial Infection Treatments	13
1.3.1 Antibiotics	14
1.3.2 Antibiotic Resistance.....	18
1.3.3 Topical Antimicrobials.....	20
1.3.3.1 Hydrogen Peroxide.....	20
1.3.4 Drug Repurposing	21
1.4 Cold Atmospheric Plasma	22
1.4.1 Overview	22
1.4.2 Cold Plasma Devices.....	23
1.4.3 Applications	26
1.4.4 RONS	27
1.4.5 Antimicrobial Effects of Cold Plasma.....	30
1.4.5.1 Planktonic Bacteria.....	30
1.4.5.2 Biofilms	31
1.5 Hydrogels	32

1.6	Drug Delivery Systems	34
1.7	Hydrogels as Drug Delivery Systems	35
1.8	Aims and Objectives	37
1.9	References.....	38
Chapter 2	: Materials, Methods and Instrument Theory	53
2.1	Materials	53
2.1.1	Bacterial Strains	53
2.1.2	Chemicals.....	53
2.2	Bacterial Growth.....	54
2.2.1	Principles of Bacterial Growth.....	54
2.2.2	Growth Conditions	55
2.2.3	Quantification of Bacteria	55
2.3	Bacterial Biofilm Methods	56
2.3.1	96-well Plate Model	56
2.3.2	Crystal Violet Staining of 96-well Plate Model.....	56
2.3.3	Polycarbonate Membrane – <i>In vitro</i> Wound Biofilm Model	57
2.4	Drug Susceptibility Assays.....	57
2.4.1	Minimum Inhibitory Concentration (MIC).....	57
2.4.2	Minimum Biofilm Inhibitory Concentration (MBIC).....	58
2.4.3	Minimum Biofilm Eradication Concentration (MBEC)	58
2.5	Microscopy	58
2.5.1	Scanning Electron Microscopy	58
2.5.1.1	Theoretical Background	58
2.5.1.2	Sample Preparation.....	59
2.5.2	Confocal Laser Scanning Microscopy (CLSM).....	60
2.5.2.1	Theoretical Background	60
2.5.2.2	LIVE/DEAD Staining	61
2.6	Cold Atmospheric Pressure Plasma.....	61
2.6.1	Helium Jet Set Up	61
2.6.2	CAP Treatment of Biological Substances.....	62
2.6.3	PVA Hydrogels	62
2.6.4	Absorbance and Fluorescence.....	63
2.6.5	Quantification of CAP Produced RONS.....	63
2.6.5.1	H ₂ O ₂ Quantification - Potassium Iodide Method	63
2.6.5.2	H ₂ O ₂ Quantification - Titanium Oxysulphate Method.....	64
2.6.5.3	Nitrite Quantification – Griess Test	64

2.7	DNA Methods.....	64
2.7.1	Principles of PCR.....	64
2.7.2	Colony PCR.....	65
2.7.3	Agarose Gel Electrophoresis.....	65
2.8	Data Analysis.....	66
2.9	References.....	67
Chapter 3 : Characterisation of Helium Driven Cold Atmospheric Plasma Jet		71
3.1	Aims	71
3.2	Chapter Background.....	73
3.2.1	Characterisation of CAP.....	73
3.2.2	Biological Interactions of CAP	75
3.2.3	PVA Hydrogels	75
3.3	Methods	77
3.3.1	Thermal Imaging	77
3.3.2	pH and Temperature.....	77
3.3.3	Scanning Electron Microscopy of PVA Hydrogels	77
3.3.4	Rheology	77
3.4	Results and Discussion	78
3.4.1	Quantification of RONS from He-CAP Jet.....	78
3.4.1.1	Quantification of Hydrogen Peroxide	78
3.4.1.2	Quantification of Nitrites.....	81
3.4.2	Temperature and pH.....	82
3.4.3	Interaction of He-CAP Jet with PVA Hydrogel.....	85
3.4.4	He-CAP Killing of Planktonic Bacteria	89
3.4.5	He-CAP Eradication of Biofilms	91
3.4.6	He-CAP Inhibition of Biofilm Formation.....	93
3.4.6.1	Reduction in Viability	94
3.4.6.2	SEM Visualisation of Treated Biofilm.....	95
3.4.6.3	Confocal Scanning Laser Microscopy of Biofilms using LIVE/DEAD Staining.....	96
3.5	Conclusion	98
3.6	Future Work	100
3.7	References.....	101
3.8	Appendix.....	106
3.8.1	KI Standard Curve.....	106
3.8.2	Griess Test Standard Curve.....	106
3.8.3	Titanium Oxysulphate Standard Curve	107

3.8.4	MIC of H ₂ O ₂	107
Chapter 4 : Role of Biofilm Formation and Bacterially Produced Catalase in Mitigating CAP Damage..... 111		
4.1	Overview	111
4.2	Chapter Background	112
4.2.1	Delivery of CAP RONS into Tissue Model.....	112
4.2.2	Oxidative Stress.....	112
4.2.3	<i>E. coli</i> Oxidative Stress Response.....	113
4.2.4	Catalase	114
4.2.5	<i>E. coli</i> Catalase.....	114
4.2.6	Gene Knockout.....	115
4.2.7	<i>E. coli</i> Catalase Mutants.....	115
4.3	Methods.....	116
4.3.1	Materials.....	116
4.3.2	Recovery of RONS Through Bacterial Biofilm.....	116
4.3.3	PVA/CMC Hydrogel.....	116
4.3.4	Bacterial Lysis.....	117
4.3.5	Protein Quantification – Bradford Assay	117
4.3.6	Catalase Activity Assay	118
4.3.7	H ₂ O ₂ Susceptibility	118
4.4	Results and Discussion.....	119
4.4.1	Transmission of RONS through Bacterial Biofilm.....	119
4.4.2	Protective Role of Catalase Against CAP	122
4.4.3	Characterisation of Catalase Mutants.....	123
4.4.4	CAP Susceptibility	124
4.4.5	RONS Through Mutant Biofilm	127
4.4.6	Quantification of Catalase Activity.....	129
4.4.7	Role of Catalase Concentration.....	129
4.4.8	Susceptibility to H ₂ O ₂	130
4.5	Conclusion	131
4.6	Future Work.....	132
4.7	References.....	133
4.8	Appendix.....	135
4.8.1	Bradford Assay – Standard Curve.....	135
Chapter 5 : Cold Atmospheric Plasma Induced Mutagenesis..... 139		
5.1	Aims.....	139

5.2	Chapter background	140
5.2.1	Mutagenesis.....	140
5.2.2	Ionising Radiation	141
5.2.3	Ultraviolet.....	142
5.2.4	Ochre Stop Codon	143
5.2.5	Mutagenesis in Bacteria	144
5.3	Methods	146
5.3.1	Materials.....	146
5.3.2	Ames Test.....	146
5.3.2.1	Theory.....	146
5.3.2.2	<i>Salmonella</i> Ames Test	147
5.3.2.3	<i>E. coli</i> Ames Test	147
5.3.2.4	Theory.....	147
5.3.2.5	Bacterial strains	148
5.3.2.6	Minimal Agar	148
5.3.2.7	Bacterial Growth Conditions.....	149
5.3.3	Antibiotic Susceptibility Assay	150
5.3.4	Comet Assay	150
5.3.5	PCR	151
5.3.6	Sequencing	151
5.4	Results and Discussion	153
5.4.1	Comet Assay	153
5.4.2	Survival	154
5.4.3	Mutation Rate.....	156
5.4.4	He-CAP Induced Antibiotic Mutations.....	161
5.5	Conclusions.....	163
5.6	Future Work	164
5.7	References.....	165
Chapter 6	: Development of a Hydrogen Peroxide Responsive Hydrogel	171
6.1	Aim.....	171
6.2	Introduction	172
6.2.1	Boronic Acid and Ester Soft Materials.....	172
6.2.2	Dye Displacement Saccharide Detector Assay	172
6.2.3	Biofilm Inhibitors.....	174
6.2.4	Alizarin.....	174
6.3	Methods	176

6.3.1	General Information	176
6.3.2	Blank Gel Synthesis	176
6.3.3	PBA Gel Synthesis	176
6.3.4	PBA monomer synthesis	177
6.3.5	ARS loading	177
6.3.6	Removal of Excessive Dye	178
6.3.7	ARS Release Studies with H ₂ O ₂	178
6.3.8	Release Studies using Plasma Activated Buffer	178
6.3.9	Biofilm Inhibition Studies	178
6.4	Results and Discussion.....	179
6.4.1	Synthesis of Boronic Acid Containing Hydrogel.....	179
6.4.2	Determination of Loading of Hydrogel.....	179
6.4.2.1	Scheme for Triggered Release.....	180
6.4.2.2	Loading of ARS to PBA Gel.....	181
6.4.2.3	Triggered Release of ARS from PBA Hydrogel	183
6.5	Bacterial Studies	185
6.5.1	Minimum Inhibitory Concentrations.....	185
6.5.2	Minimum Biofilm Inhibitory Concentrations	185
6.5.3	Minimum Biofilm Eradication Concentrations (MBEC).....	189
6.5.4	Combination of ARS and H ₂ O ₂	192
6.5.5	ARS PBA Hydrogel Inhibition of Biofilm Formation	193
6.5.6	He-CAP Activation of PBA Gel	195
6.6	Conclusions.....	198
6.7	Future Work.....	199
6.8	References.....	200
6.9	Appendix.....	201
6.9.1	MIC H ₂ O ₂	201
6.9.2	MIC ARS.....	201
6.9.3	NMR Spectra.....	202
Chapter 7	: Povidone Based Hydrogel Wound Dressing	207
7.1	Aims.....	207
7.2	Chapter Background	208
7.2.1	Povidone-Iodine	208
7.2.2	Argon Plasma	210
7.3	Methods.....	212
7.3.1	Bacterial Strains	212

7.3.2	Argon Plasma Jet.....	212
7.3.3	PVP-I Hydrogel.....	213
7.3.4	Checkerboard Assay.....	213
7.3.5	Plasma Activation of Drug.....	213
7.3.5.1	Planktonic Treatment.....	213
7.3.5.2	Biofilm Treatment	214
7.3.6	FT-IR.....	214
7.3.7	MALDI-TOF.....	214
7.3.8	Pyocyanin Expression Assay	215
7.4	Results and Discussion	216
7.4.1	Bacterial Activity of PVP-I.....	216
7.4.1.1	Plasma Activation of PVP-I	218
7.4.1.2	Activity of CAP Activated PVP-I Against Model Wound Biofilms.....	221
7.4.1.3	Characterisation of Argon Plasma Jet	224
7.4.1.4	Characterisation of PVP-I Gel.....	227
7.4.1.5	Scanning Electron Microscopy.....	227
7.4.1.6	FT-IR	229
7.4.1.7	MALDI-TOF	230
7.4.1.8	Efficacy of PVP-I Hydrogel Against Established Model Wound Biofilms	230
7.5	Conclusions.....	234
7.6	Future Work	236
7.7	References.....	239
Chapter 8	: Conclusions & Future Perspectives.....	243

List of Tables

Table 1.1: Analysis of the different types of dressings available with description of function, examples and the wound type they are used to treat. ⁴¹	8
Table 1.2: Categorises of antibiotics, description of action, chemical structure and resistance mechanism.....	1
Table 3.1: All possible free-radical and non-radical RONS generated through cold atmospheric pressure plasma. ⁷	74
Table 4.1: Concentration of H ₂ O ₂ recovered beneath polycarbonate membrane impregnated with AWF after incubation for 8, 12 and 24 h at 37°C normalised to TF.....	121
Table 4.2: Characteristics of <i>E. coli</i> knock-out strains, description of gene knockout, catalase test results and H ₂ O ₂ MIC.....	123
Table 4.3: Quantification of <i>E. coli</i> catalase activity with and without He-CAP treatment.	129
Table 5.1: Nucleotide sequence for stop codons and their names.....	143
Table 5.2: Minimal agar recipe for modified Ames test.....	148
Table 5.3: Primer sequence for amplification of <i>trpE</i> gene.	151
Table 5.4: Thermocycler conditions for the amplification of <i>trpE</i> gene.....	151
Table 5.5: Within the ochre codon of the <i>trpE</i> gene of <i>E. coli</i> there are known to be 7 possible point mutations which result in a change in stop codon, these are outlined below.	159
Table 6.1: The amount of ARS release from PBA and Blank gels as abs g ⁻¹ at 513 nm..	173
Table 6.2: The MIC of MRSA (MRSA252), <i>S. aureus</i> (H560), <i>P. aeruginosa</i> (PAO1) and <i>E. coli</i> (NCTC10418) when treated with H ₂ O ₂ and ARS using standard microplate dilution method. For absorbance data see Appendix 6.9.1 & 6.9.2.....	185
Table 6.3: The MBIC of MRSA (MRSA252), <i>S. aureus</i> (H560), <i>P. aeruginosa</i> (PAO1) and <i>E. coli</i> (NCTC10418) when treated with H ₂ O ₂ and ARS using standard microplate dilution method. For absorbance data see Appendix.....	188
Table 6.4: The MBEC of MRSA (MRSA252), <i>S. aureus</i> (H560), <i>P. aeruginosa</i> (PAO1) and <i>E. coli</i> (NCTC10418) when treated with H ₂ O ₂ and ARS using standard microplate dilution method. For absorbance data see Appendix.....	191
Table 7.1: <i>P. aeruginosa</i> strains name and origin.....	212
Table 7.2: MIC and MBEC of H ₂ O ₂ and PVP-I for <i>P. aeruginosa</i> isolates.....	216
Table 7.3: FICI values for five <i>P. aeruginosa</i> strains used and FIC range (N=3).	217

List of Figures

Figure 1.1: Structure of healthy skin (A). Structure of burned skin showing the layers effected in the varying degree of burns (B). Photograph example of second-degree burn (C). (Image created in BioRender).	3
Figure 1.2: Schematic outlining the progression from bacterial contamination to systemic infection.....	5
Figure 1.3: MolecuLight device detects fluorescence emitted from bacteria colonising wound bed (A) handheld MolecuLight device with digital screen showing presence of bacteria (image found online molecuLight.com). (B) 12-days post lower limb split-thickness skin graft wound bed of a 58-year-old male. (C) MolecuLight fluorescent image showing cyan in wound bed. (Reproduced with permission from Journal of Woundcare) ³⁵	6
Figure 1.4: Fluorescent response of the prototype dressing in response to 24 h model burn infections of <i>P. aeruginosa</i> and <i>S. aureus</i> infections. (Reproduced with permission from ACS Applied Materials and Interfaces) ³⁸	7
Figure 1.5: Schematic representation of the stages of wound healing: inflammation (A) Proliferation & Re-epithelisation (B) and remodelling (C). (Reproduced with permission from Trends in Pharmacological Sciences) ⁴⁴	9
Figure 1.6: Schematic of the stages of bacterial biofilm formation on skins surface. (1) Planktonic bacteria attachment. (2) Irreversible bacterial attachment. (3) Cell proliferation. (4) Growth and maturation. (5) Dispersal. (Created using BioRender).	10
Figure 1.7: Structure of <i>P. aeruginosa</i> . (Created using BioRender).....	13
Figure 1.8: Schematic of DBD plasma (A) and CAPPJ (B). (Created using BioRender).	23
Figure 1.9: kINPen [®] MED apparatus (A) and ignited plasma jet plume (B) (Reproduced with permission from Springer Nature).....	25
Figure 1.10: Adtec SteriPlas apparatus (A) and ignited plasam plume (B). (Reproduced with permission from the Journal of Clinical Plasma Medicine).....	26
Figure 1.11: Synthesis of hydrogels through three-dimensional polymerisation (A). Synthesis of hydrogel by cross-linking of ready-made water-soluble polymers (B). (Created using BioRender).....	33
Figure 1.12: Classification of hydrogels based on subsequent route of delivery. (Reproduced with permission from Nature Reviews Materials). ¹⁶¹	35

Figure 2.1: Standard bacterial growth curve showing change in OD (dotted line) changing with viable bacterial cells (solid line) over time. (A) lag phase, (B) exponential phase, (C) stationary phase and (D) death phase. 54

Figure 2.2: Schematic demonstrating the Miles & Misra method. 55

Figure 2.3: Schematic of polycarbonate membrane wound biofilm model. 57

Figure 2.4: Schematic of CLSM optical pathway. (Reproduced with permission from Springer). 60

Figure 2.5: CAP jet set up. 62

Figure 3.1 Schematic representation of a hydrogel “screen” wound dressing applied to a bacterially infected wound. He-CAP treatment will then be applied atop the hydrogel dressing, allowing bactericidal RONS to diffuse through into the wound bed, where they will decontaminate the wound bed and potentially promote healing, whilst also screening out RONS which could be harmful to healthy mammalian cells such as keratinocytes. 71

Figure 3.2 He- CAP jet plume when ignited at 25 kHz, 10 kV using non-tapered glass tube (A-B) and tapered glass tube (C-D). (A) and (C) used 0.6 standard litres per minute (SLPM) and (B) and (D) used 2 SLPM. 78

Figure 3.3 H₂O₂ quantification for various He- CAP jet conditions 0.6 SLPM of helium through non-tapered jet (A), 2 SLPM of helium through non-tapered jet (B), 0.6 SLPM of helium through tapered jet (C) and 2 SLPM of helium through tapered jet (D). Measured after 30 mins post treatment incubation at 25°C using KI reporter system. Error bars denote standard deviation (n=3). 79

Figure 3.4 Chemical reaction for measuring NO₂⁻ using the Griess reagent system. 81

Figure 3.5 NO₂⁻ quantification for various He- CAP jet conditions: 0.6 SLPM of helium through non-tapered jet (A), 2 SLPM of helium through non-tapered jet (B), 0.6 SLPM of helium through tapered jet (C), and 2 SLPM of helium through tapered jet (D). Error bars denote standard deviation (n=3). 82

Figure 3.6 Temperature (shown in dark grey and recorded on the left axis) and pH change (shown in light grey and recorded on the right axis) in 2 mL of PBS (pH 7.4, 21°C) at varying times of exposure to He-CAP jet with different jet conformations: 0.6 SLPM He non-tapered jet (A), 2 SLPM He non-tapered jet (B), 0.6 SLPM tapered jet (C), & 2 SLPM tapered jet (D). Error bars denote standard deviation (n=3). 84

Figure 3.7 Thermal image of He-CAP jet demonstrating the variation in temperature between helium gas flow rates using Xenics GOBI-640-GigE thermal image camera 0.6

SLPM He flow rate (A) 2 SLPM He flow rate (B) when treating <i>P. aeruginosa</i> (PAO1) biofilm atop PBS buffer.	85
Figure 3.8 Photos of the visible, structural impact of He-CAP 0.6 SLPM of helium through tapered jet (A), 2 SLPM of helium through tapered jet (B), 0.6 SLPM of helium through non-tapered jet (C) and 2 SLPM of helium through non-tapered jet (D).	85
Figure 3.9 Microscopic analysis of the structural integrity of 5% (v/v) PVA gel treated with non-tapered He-CAP jet of varying conditions (x40 magnification) untreated control gel (A) 45 seconds with helium flow of 0.6 SLPM (B) 45 seconds with helium flow of 2 SLPM (C-D).....	86
Figure 3.10 SEM images of 5% (w/v) PVA hydrogel. Untreated control gel (A&B), 5% PVA hydrogel after 5 min treatment with He-CAP jet operated at 0.6 SLPM (C&D) & 5% PVA hydrogel after 5 min treatment with He-CAP jet operated at 2 SLPM (E&F). He-CAP induced damage is indicated (*).	87
Figure 3.11 Rheology data for 5% (w/v) PVA hydrogels after He-CAP treatment. Untreated 5% PVA gel (A), 0.6 SLPM He-CAP treated 5% PVA gel (B) and 2 SLPM He-CAP treated 5% PVA gel (C) (●) storage modulus (G') (■) loss modulus (G''). Error bars denote standard deviation (n=3).	88
Figure 3.12 recovery of H ₂ O ₂ and NO ₂ ⁻ below 5% (w/v) PVA hydrogel after 1 h incubation at 25°C after 5 min of He-CAP treatment using: 0.6 SLPM of helium through non-tapered jet (A), 2 SLPM of helium through non-tapered jet (B), 0.6 SLPM of helium through tapered jet (C) and 2 SLPM of helium through tapered jet (D). Error bars denote standard deviation (n=3).	89
Figure 3.13 Effects of varying He-CAP helium flow rate and exposure time, using non-tapered jet, on viability of stationary phase, planktonic <i>P. aeruginosa</i> (PAO1) (A), <i>S. aureus</i> (H560) (B) and MRSA (MRSA252) (C) cultures in PBS. Error bars denote standard deviation (n=3).	90
Figure 3.14 Reduction in viable cell count of <i>P. aeruginosa</i> (PAO1) (A), <i>S. aureus</i> (H560) (B) and MRSA (MRSA252) (C) 19 mm, 24 h biofilms after exposure to He-CAP for 5 mins at varying helium flow rate (0.6 & 2 SLPM). One-way ANOVA, (****) p<0.0001 and (***) p<0.001 compared to untreated. Error bars denote standard deviation (n=3).	92
Figure 3.15 Reduction in viable cell count of <i>S. aureus</i> (H560), <i>P. aeruginosa</i> (PAO1) and MRSA (MRSA252) 24 h biofilms after 5 mins treatment with He-CAP at helium flow rate 0.6 SLPM or 2 SLPM atop a 5% (w/v) PVA hydrogel. Students <i>t</i> -test were carried out for	

statistical analysis. * $p = 0.0265$, all other comparisons were not significant. Error bars denote standard deviation (n=3). 92

Figure 3.16 Comparison of viable bacterial cells at 24 h growth after varying He-CAP treatment intervention times during bacterial biofilm development. *P. aeruginosa* (PAO1) (A) MRSA (MRSA 252) (B). One-way ANOVA was performed (****) $p < 0.0001$ and (***) $p < 0.001$ (**) $p < 0.01$ (*) $p < 0.05$. Error bars denote standard deviation (n=3). 94

Figure 3.17 SEM images of *P. aeruginosa* (PAO1) biofilm after 24 h growth with varying treatment intervention times with 5 min exposure to He-CAP jet Untreated control (A) blue arrow indicating the biofilm extracellular matrix. Treatment was applied 8 h into biofilm development, red arrow indicating cellular debris (B). Treatment was applied 12 h into biofilm development. Green arrow indicating dead *P. aeruginosa* cell (C). 95

Figure 3.18 LIVE/DEAD results *P. aeruginosa* (PAO1) biofilm after 24 h growth with varying treatment intervention times with 5 min exposure to He-CAP jet (A) He-CAP intervention 8 h into growth (B) He-CAP intervention 12 h into growth. Images are inverted. 97

Figure 3.19 Standard curve using 1 M KI for the quantification of H_2O_2 . Error bars denote standard deviation (n=3). 106

Figure 3.20 Standard curve using Griess reagents against known concentrations of sodium nitrate (NO_2^-). Error bars denote standard deviation (n=3). 106

Figure 3.21 Standard curve of $TiOSO_4$ for the quantification of H_2O_2 . Error bars denote standard deviation (n=3). 107

Figure 3.22 MIC of H_2O_2 for *P. aeruginosa* (PAO1) (A), *S. aureus* (H560) (B) and MRSA (MRSA252) (C). Error bars 107

Figure 4.1: Schematic of reactive oxygen species induced damage in *E. coli* (Reproduce with permission from International Journal of Current Microbiology and Applied Sciences).¹⁰ 113

Figure 4.2: Structure of HP11 (A) and HP1 (B)..... 114

Figure 4.3: Experimental set up for the recovery of RONS beneath bacterial biofilm. ... 116

Figure 4.4: Quantification of viable cells of MRSA (MRSA252) and *P. aeruginosa* (PAO1) biofilms at 8, 12 and 24 hours of growth. Error bars denote the standard deviation (n=3). (This graph was made in collaboration with Dr H. Hathaway and reproduced with her permission). 120

Figure 4.5: Recovery of H_2O_2 through MRSA (MRSA252) and *P. aeruginosa* (PAO1) biofilms (normalised to TF) of varying maturity from 8 – 24 h. Error bars denote the standard

deviation (n=3). (This graph was made in collaboration with Dr H. Hathaway and reproduced with her permission).....	121
Figure 4.6: H ₂ O ₂ recovery beneath PVA/CMC hydrogel after varying post CAP treatment incubation times (A) and recovery beneath <i>P. aeruginosa</i> (PAO1) and MRSA (MRSA252) biofilms after 4 hours rest (B). Error bars denote the standard deviation (n=3). (This graph was made in collaboration with Dr H. Hathaway and reproduced with her permission).	122
Figure 4.7: Analysis of <i>E. coli</i> strain biofilm biomass using 96-well plate assay after 24 h growth at 37°C. Absorbance at 570 nm corresponds to bacterial biofilm biomass (n=4).	124
Figure 4.8: Log reduction of catalase mutant <i>E. coli</i> biofilms CFU/mL which were grown for 24 h and treated with CAP jet for 5 minutes using non-tapered jet at 5 mm distance. Error bars represent standard deviation, One-way ANOVA was carried out * p = 0.0122 (n=3).	125
Figure 4.9: Scanning electron microscopy images of <i>E. coli</i> 24 h biofilms untreated control (A,C,E & G) and after 5 mins CAP treatment (B,D,F & H) at x5000 magnification. <i>E. coli</i> BW25113 (A-B), PNW11-1 (C-D), PNW11-2 (E-F), and PNW11-4A (G-H).	126
Figure 4.10: Comparison on <i>E. coli</i> bacterial cell length in untreated biofilms (●) compared to cellular length in biofilms after 5 mins treatment with CAP (■).....	127
Figure 4.11: Recovery of H ₂ O ₂ through knockout <i>E. coli</i> biofilms relative to CFU/ mL after 8 h (A) 12 h (B) and 24 h (C) of growth. H ₂ O ₂ concentration is black and recorded on the left y-axis and CFU/mL is grey and recorded on the right y-axis. Error bars denote standard deviation (n=3).....	128
Figure 4.12: Inhibitor-response curve of H ₂ O ₂ recovered through 24 h <i>E. coli</i> PNW11-4A biofilm impregnated with varying doses of bovine catalase. Error bars denote standard deviation (n=3).	129
Figure 4.13: <i>E. coli</i> BW25113 was treated for 5 mins with CAP and then exposed to H ₂ O ₂ (20 mM) for 1 h at 37°C, survival was calculated. Error bars denote standard deviation (n=3) Students <i>t</i> -test was carried out, p<0.01.	130
Figure 4.14: Standard curve for Bradford assay using bovine serum albumin (BSA) of varying concentrations. LoD 2.5 µg/mL. Error bars represent the standard deviation (n=3).	135
Figure 5.1: Graphical abstract for He-CAP induced mutagenesis workflow.....	139
Figure 5.2: Formation of cyclobutane dimer in response to UV exposure.	142
Figure 5.3: Formation of 6,4 pyrimidine-pyrimidine in response to UV exposure.	143

Figure 5.4: <i>Salmonella</i> Ames Test workflow.....	147
Figure 5.5: PCR result of <i>trpE</i> positive and negative colonies against 100 bp ladder.....	151
Figure 5.6: Sequence of <i>trpE</i> gene showing forward and reverse primers in green, start codon in red and the mutation in blue	152
Figure 5.7: Diffusion-based DNA fragmentation assay was performed on <i>E. coli</i> WP2 cells to assess DNA damage. Untreated <i>E. coli</i> exhibit bright, dense nucleoids (A). After 5 min of He-CAP treatment evidence of DNA damage is observed, seen as speckling around the nucleoid (*) (B). <i>E. coli</i> treated with 1 mg/mL of Zeocin (C) DNA fragmentation (%) in Comet assay of <i>E. coli</i> WP2 after 5 minutes treatment with He-CAP jet compared to untreated control (D). The percentage of nucleoids with detectable fragmentation relative to intact nucleoids was calculated. A total of 138 nucleoids for He-CAP-treated and 157 nucleoids for untreated were analysed from 3 biological replicates. Error bars show standard deviation of the mean. Data was plotted using GraphPad 8.0, students t-test was performed (*) $p < 0.1$	154
Figure 5.8: Effects of varying dosages of He-CAP, treatment time (mins) (A), UV dosage(J/m^2) (B) and X-irradiation dosage (Gy) (C) on survival of <i>E. coli</i> WP2 strain. Plated to measure survival as per materials and methods and plotted as survival fraction relative to untreated control. Error bars represent the standard deviation of the mean (n=3).	156
Figure 5.9: <i>TrpE</i> revertant mutants for <i>E. coli</i> WP2 after exposure to varying dosage of He-CAP (A) X-ionising radiation (B) and UV (C). Data was plotted using GraphPad 8.0. Error bars represent the standard deviation of the mean (n=3), significance was analysed using a one-way ANOVA comparing significance to the untreated control (****) $p < 0.0001$, (***) $p < 0.001$, (**) $p < 0.01$ & (*) $p < 0.1$	157
Figure 5.10: Comparison of the mutation rate with increased He-CAP treatment time between <i>E. coli</i> WP2 strain than in the <i>E. coli</i> WP2 <i>uvrA</i> ⁻ strain. Error bars denote standard deviation of the mean (n=3). Data was plotted using GraphPad 8.0. Unpaired <i>t</i> -test performed to assess statistical significance. (**) $p < 0.01$	158
Figure 5.11: Amino acid sequence alignment data for comparison of mutations between a range of mutagen treatments.	160
Figure 5.12: After analysis of the <i>trpE</i> gene of <i>E. coli</i> WP2 a broad spectrum of point mutations was observed in the Ochre region (TAA)(details outlined in Table 5.5). The frequency was calculated as percentage relative to total number of samples sequenced per condition.	161

Figure 5.13: Normalised mutation rate of *E. coli* BW25113 in the presence of ciprofloxacin (0.03 µg/mL) after He-CAP treatment for varying amounts of time. Mutation rate is defined as number of ciprofloxacin-resistant *E. coli* cells per total surviving. Error bars represent standard deviation (n=3) Unpaired *t*-test performed to assess statistical significance. (*) p<0.1..... 162

Figure 6.1: Schematic outlining the concept of the ARS-PBA hydrogel triggered release system for the inhibition of biofilm formation. The release of ARS in response to H₂O₂ diffuses through the hydrogel into the wound inhibits *S. aureus* biofilm formation. 171

Figure 6.2: Displacement of ARS from PBA containing hydrogel matrices in the presence of saccharides owing to competitive binding. 173

Figure 6.3: Chemical structure of Alizarin (A) and Alizarin red S (B). 175

Figure 6.4 Structure of PBA..... 177

Figure 6.5: PBA hydrogel gel blank (A), loaded with ARS prewash step (B) and after washing in PBS (C). 180

Figure 6.6: Schematic for the binding and triggered release of ARS to PBA hydrogel in the presence of H₂O₂ with the oxidative release of the ARS indicated by the reverse colour change on addition of H₂O₂..... 181

Figure 6.7: UV-Vis absorption per gram of PBA-based hydrogel at 513 nm over time in PBS (pH 7.3) at 25°C. Error bars indicate the standard deviation (n=3). 182

Figure 6.8: UV-Vis absorption per gram of PBA-based hydrogel at 513 nm over time in PBS (pH 7.3) at 25 °C. Error bars indicate standard deviation (n = 3)..... 183

Figure 6.9: Absorbance at 513 nm of ARS released over time from PBA in the presence of varying concentrations of H₂O₂ (0-4 mM) in PBS..... 184

Figure 6.10: UV-Vis absorption per gram of PBA-based hydrogel in the presence of various concentrations of hydrogen peroxide (0.1 – 4 mM) in PBS (pH 7.3) after 3 hours. Absorbance was measured at 513 nm at 25 °C; error bars indicate standard deviation (n = 3). 184

Figure 6.11: Varying concentrations of ARS (2.5-100 µM) were added at lag phase to MRSA (MRSA252) (A), *S. aureus* (H560) (B), *P. aeruginosa* (PA01) (C) and *E. coli* NCTC 10418 (D). After 24 hours growth at 37 °C, absorbance was measured at 570 nm. Error bars indicate standard deviation (n = 4)..... 187

Figure 6.12: Varying concentrations of H₂O₂ (1-100 µM) were added at lag phase to MRSA (MRSA252) (A), *S. aureus* (H560) (B), *P. aeruginosa* (PA01) (C) and *E. coli* (NCTC 10418)

(D). After 24 hours growth at 37 °C, absorbance was measured at 570 nm. Error bars indicate standard deviation (n = 4). 188

Figure 6.13: XTT Viability of ARS against bacterial strains *P. aeruginosa* (PAO1) and *S. aureus* (H560). Error bars indicate the standard deviation (n=3). 189

Figure 6.14: Varying concentrations of ARS (2.5-100 µM) were added at stationary phase to MRSA (MRSA252) (A), *S. aureus* (H560) (B), *P. aeruginosa* (PAO1) (C) and *E. coli* (NCTC 10418) (D). After 24 hours growth at 37 °C, absorbance was measured at 570 nm. Error bars indicate standard deviation (n = 4). 190

Figure 6.15: Varying concentrations of H₂O₂ (1-100 mM) were added at stationary phase to MRSA (MRSA252) (A), *S. aureus* (H560) (B), *P. aeruginosa* (PAO1) (C) and *E. coli* (NCTC 10418) (D). After 24 hours growth at 37 °C, absorbance was measured at 570 nm. Error bars indicate standard deviation (n = 4). 191

Figure 6.16: H₂O₂ (2 mM) was added to ARS (50 and 100 µM) during lag phase to MRSA252 (A), *S. aureus* H560 (B), *P. aeruginosa* (PAO1) (C) and *E. coli* (NCTC 10418) (D). After 24 h growth at 37 °C whereby absorbance was measured at 570 nm. Error bars indicate standard deviation (n=4). 193

Figure 6.17: Biofilm biomass after 18 h growth at 37 °C in the presence of resultant solution after ARS loaded acrylamide gel was exposed to 2 mM H₂O₂, 2 mM H₂O₂ only, the resultant solution of PBA hydrogel in the presence of PBS compared to untreated bacterial control and broth only control for MRSA (MRSA252) (A), *S. aureus* (H560) (B), *P. aeruginosa* (PAO1) (C), and *E. coli* (NCTC10418) (D). Error bars represent standard deviation (n=3) One-way ANOVA was performed p<0.0001. 194

Figure 6.18: Absorbance at 513 nm of release of ARS from PBA gel after incubation with PBS treated with He-CAP for varying amounts of time (0-30 minutes). Error bars represent standard deviation (n=3). 195

Figure 6.19 He-CAP treated ARS-PBA hydrogel. Edges of the gel were taped down to prevent movement. 196

Figure 6.20: Bilayer ARS-PBA and PVA hydrogel before He-CAP treatment and after He-CAP treatment showing diffusion gradient of ARS post He-CAP treatment moving away from the wound. 196

Figure 6.21: Structure of Kanamycin, an aminoglycoside antibiotic 199

Figure 6.22: Minimum inhibitory concentration (MIC) of H₂O₂ against MRSA252, *S. aureus* (H560), *P. aeruginosa* (PAO1) and *E. coli* (NCTC10418). Absorbance at 600 nm corresponds to planktonic bacterial growth relative to untreated bacterial control (n=3). 201

Figure 6.23: Minimum inhibitory concentration (MIC) of ARS against MRSA (MRSA252), *S. aureus* (H560), *P. aeruginosa* (PAO1) and *E. coli* (NCTC10418). Absorbance at 600 nm corresponds to planktonic bacterial growth relative to untreated bacterial control (n=3). 201

Figure 7.1: Chemical structure of PVP-I..... 208

Figure 7.2: PVP-I antibacterial mechanism through the establishment of an equilibrium. (Reproduced with permission from Journal of Surgery)..... 209

Figure 7.3: Chart showing the selection of PVP-I formulation depending on requirements of the clinical wound.⁶..... 210

Figure 7.4: Schematic of Ar-CAP jet set up. 212

Figure 7.5: Structure of Pyocyanin (PCN)..... 215

Figure 7.6: Layout of synergy plate. Black circles show wells where combination of drug has successfully inhibited growth below the MIC of the drugs individually. Red square shows where the MIC of Drug A and Drug B falls..... 217

Figure 7.7: Optical density 600 nm of *P. aeruginosa* stains PAO1 (A), PAE45311 (B), PAE45321 (C), PAE45325 (D) & PAE45379 (E) after exposure to ½ MIC dose of PVP-I (0.33% (v/v), ½ MIC He-CAP (3 & 5 mins) treatment and combination treatment relative to untreated control. (n=3) Error bars represent standard deviation. One-way ANOVA was performed in GraphPad 8.0 **** $p < 0.0001$ *** $p = 0.0009$ respectively. 219

Figure 7.8 Visual analysis of PVP-I after He-CAP treatment of varying times (mins).. 219

Figure 7.9: (A) UV-Vis Spectra of 0.33% (v/v) PVP-I with increasing He-CAP treatment (B) Absorbance change at 288 nm (▲) and 350 nm (●) after varying treatment time of He-CAP jet. 220

Figure 7.10: Quantification of viable cells in 24 h *P. aeruginosa* biofilms stains PAO1 $p = 0.0021, 0.0026 & 0.0004$ (A), PAE45311 $p = 0.0006, 0.002 & < 0.0001$ (B), PAE45321 (C), PAE45325 $p = 0.0098, 0.0031 & 0.0031$ (D) & PAE45379 $p = 0.0295$ (E) after treatment with PVP-I, He-CAP and a combination of PVP-I and He-CAP. Error bars represent standard deviation (n=3), One-way ANOVA was performed (****) $p < 0.0001$, (***) $p < 0.001$, (**) $p < 0.01$ and (*) $p < 0.1$ 222

Figure 7.11: Pyocyanin for *P. aeruginosa* strains PAO1, PA45311, PA45325 & PA45321. Error bars represent standard deviation. One-way ANOVA performed (*) $p < 0.1$ 223

Figure 7.12: SEM at x5000 magnification, of 24h <i>P. aeruginosa</i> (PAO1) biofilm untreated control (A), He-CAP treatment for 5 mins (B), 10% (v/v) PVP-I (C) and and 5 min CAP treatment of 10% (v/v) PVP-I (D).	224
Figure 7.13 Quantification of H ₂ O ₂ produced by Ar-CAP jet treatment. Error bars represent standard deviation (n=3).	225
Figure 7.14: Minimum inhibitory Ar-CAP treatment time (MITT) for <i>P. aeruginosa</i> (PAO1) (A) and <i>S. aureus</i> (H560) (B) relative to untreated bacterial control. Error bars represent standard deviation (n=3).	225
Figure 7.15: Reduction in viable planktonic bacterial cells of <i>P. aeruginosa</i> (PAO1) (A) and <i>S. aureus</i> (H560) (B) after varying treatment times with Ar-CAP. Error bars represent standard deviation (n=3).	226
Figure 7.16: Analysis of 5% PVA hydrogel with varying Ar-CAP treatment. Recovery of H ₂ O ₂ beneath the 5% PVA hydrogel after varying Ar-CAP treatment times (A). Visual analysis of the 5% PVA hydrogels after varying treatment times (B). Error bars represent standard deviation (n=3).	226
Figure 7.17: Reduction in viable cells of 24 h biofilm after treatment Ar-CAP for 5 min atop a 5% PVA hydrogel screen <i>P. aeruginosa</i> (PAO1) (A) & <i>S. aureus</i> (H560) (B). Error bars represent standard deviation (n=3). One-way ANOVA (**) p<0.001.	227
Figure 7.18: SEM images of PVP-I/PVA Hydrogel. Untreated PVP-I/PVA hydrogel gel control (A-C), PVP-I/PVA hydrogel after 3 mins Ar-CAP treatment (D-F) & PVP-I/PVA hydrogel after 5 min Ar-CAP treatment (G-I).	228
Figure 7.19: Rheology data for PVP-I hydrogel. Untreated control (A) and after 5 minutes of Ar-CAP treatment (B). Error bars represent standard deviation (n=3).	229
Figure 7.20 FT-IR analysis of PVP-I Gel (-) and 5 % PVA Hydrogel (-).	229
Figure 7.21: MALDI-TOF analysis of PVP-I gel 1h after 3 mins treatment with Ar CAP jet (-) compared with untreated control (-).	230
Figure 7.22: Reduction in viable bacterial after treatment for 1 h with PVP-I hydrogel and PVP-I hydrogel with 3 mins of Ar CAP jet treatment applied atop relative to untreated control and Ar plasma treatment without hydrogel. <i>P. aeruginosa</i> PAO1 (A), PAE45311 (B), PAE45321 (C), PAE45325 (D) and PAE45379 (E). <i>t</i> -test was carried out with Welch's correction p = 0.0019, p = 0.0203 and p = 0.0033 respectively. Error bars represent standard deviation (n=3). (**) p<0.01 & (*) p<0.1.	232
Figure 7.23: Qualitative analysis of untreated and Ar-CAP treated PVP-I hydrogels before and after 1 h incubation at 37 °C.	233

Figure 7.24: Prototype multi-jet..... 236

Figure 7.25: MIC of PAA for *S. aureus* (H560) **(A)** and *P. aeruginosa* (PAO1) **(B)**. 237

Figure 7.26: Reduction in optical density of *S. aureus* (H56) after 18 h growth at 37°C in the presence of TAED-PLGA particles, Ar-CAP activated water, Ar-CAP activated TAED-PLGA particles compared to untreated bacterial control **(A)**, prototype TAED-PLGA wound dressing system **(B)**. 237

Acronyms and Abbreviations

Abbreviation	Full Name
Alizarin Red S	ARS
Antimicrobial Resistance	AMR
Argon driven Cold Atmospheric Pressure Plasma	Ar-CAP
Bovine Serum Albumin	BSA
Brain Heart Infused Agar	BHIA
Carboxymethylcellulose	CMC
Cold Atmospheric Pressure Plasma	CAP
Colony Forming Units	CFU
Confocal Laser Scanning Microscopy	CLSM
Critical Colonisation Threshold	CCT
Crystal Violet	CV
Cyclobutane Pyrimidine Dimers	CPD
Dielectric Barrier Discharge	DBD
Double-strand breaks	DSB
<i>Escherichia coli</i>	<i>E. coli</i>
Ethylenediaminetetraacetic acid	EDTA
Extracellular Matrix	ECM
Extracellular Polymeric Substance	EPS
Fractional Inhibitory Concentration	FIC
Fractional Inhibitory Concentration Index	FICI
Helium driven Cold Atmospheric Pressure Plasma	He-CAP
Horizontal Gene Transfer	HGT
Hydroperoxidase I	HPI
Hydroperoxidase II	HPII
Hypiodous acid	HOI
Intensive Care Unit	ICU
Limit of Detection	LoD
Luria-Bertani agar	LBA
Luria Broth	LB

Matrix-Assisted Laser Desorption/Ionisation Time of Flight Mass Spectroscopy	MALDI-TOF MS
Methicillin-resistant <i>S. aureus</i>	MRSA
Minimal Agar	MA
Minimum Biofilm Eradication Concentration	MBEC
Minimum Biofilm Inhibitory Concentration	MBIC
Minimum Inhibitory Concentration	MIC
Minimum Inhibitory Treatment Time	MITT
Multidrug Resistant	MDR
National Health Service	NHS
Nitric oxide	NO
Titanium oxysulphate	TiOSO ₄
Nucleotide Excision Repair	NER
Optical Density	OD
Overnight	ON
Oxidative Stress Response	OSR
Phenyl boronic acid	PBA
Phenylmethlysufonyl fluoride	PMSF
Phosphate Buffer Saline	PBS
Polyvinyl Alcohol	PVA
Polyvinylpyrrolidone	PVP
Potassium Iodide	KI
Povidone Iodine	PVP-I
Pressure Ulcers	PU
Propidium Iodide	PI
<i>Pseudomonas aeruginosa</i>	<i>P. aeruginosa</i>
Quorum Sensing	QS
Reactive Oxygen and Nitrogen Species	RONs
Scanning Electron microscopy	SEM
Skin and Soft Tissue Infections	SSTI
Standard Litres per Minute	SLPM
<i>Staphylococcus aureus</i>	<i>S. aureus</i>

Superoxide Dismutase	SOD
Total Body Surface Area	TBSA
Toxic Shock Syndrome Toxin	TSST
Transmission Factor	TF
Tryptic Soy agar	TSA
Tryptic Soy Broth	TSB
Vascular Ulcers	VU
World Health Organisation	WHO

Chapter 1

Chapter 1 : Introduction

1.1 The Clinical Problem – Biofilm-Associated Bacterial Wound Infection

By definition a wound is “an injury to living tissue through a cut, blow or trauma resulting in breakage of the skin”. Any break in the skins integrity puts the patient at risk of colonisation by pathogenic bacteria and can result in an infection. Overall, wound treatment accounts for 4% of the total cost of the healthcare budget within the UK.¹ Wound infections result in increased patient trauma, extending hospitalisation which can increase the associated costs, and in extreme cases, can lead to sepsis and death. The “ESKAPE” pathogens: *Enterococcus faecium*, *Staphylococcus aureus* (*S. aureus*), *Klebsiella pneumoniae*, *Acinetobacter baumannii*, *Pseudomonas aeruginosa* (*P. aeruginosa*) and *Enterobacter* are a group of nosocomial pathogens that are multidrug resistant (MDR) and virulence and thus are considered a great threat to human health.²

Populations of bacteria can bind to the surface of the wound forming complex communities known as biofilms, which are associated with increased virulence, need significantly higher doses of antibiotics for clearance, slow healing and can result in wound chronicity.³ Moreover, biofilm-associated infections have been shown to contribute to antimicrobial resistance (AMR). AMR is within the top global health threats, able to affect people of any age or nationality. The World Health Organisation (WHO) report that by 2050 more than 10 million people will die annually from antibiotic resistant bacterial infections.⁴ With between 60-100% of wounds cited as having biofilm-associated infections, the need for novel treatments of biofilm infections has never been higher.⁵

1.2 Wounds

1.2.1 Wound Classification

Wounds are classified according to a number of factors, the most important of which are: the form of injury which caused the wound, the depth of wound, site, contamination and the duration of existence.⁶ Wounds are subcategorised into two types, acute and chronic. An acute wound is defined as a wound which progresses through the 4 stages of healing: haemostasis, inflammation, proliferation and remodelling within a timely fashion.⁷ The exact appropriate time frame of healing is disputed. However, broadly speaking it is between 4-8 weeks.^{8,9} When a wound fails to progress through these stages of healing it is then defined as a chronic wound.¹⁰ There are three most common forms of chronic wounds: diabetic foot ulcers, venous/arterial ulcers and pressure ulcers.¹¹

1.2.2 Acute Wounds

An acute wound is any break in the skin that occurs suddenly and will heal at an expected rate. Acute wounds include traumatic wounds, which can be subcategorised into blunt and penetrating traumatic wounds, bite wounds of either human or animal origin and surgical site wounds and some burn wounds.¹² The decision to medically close an acute wound through use of stitches or glue, is based upon the age of the wound, the degree of contamination and whether the wound is infected. Human bite wounds, blast injuries and severely contaminated wounds are left open. Wounds are irrigated with saline or an antibiotic solution and dressed with a moist, absorbent gauze dressings.¹³

1.2.3 Chronic Wounds

Chronic wounds are classified into two groups: vascular ulcers (VU) which include diabetic ulcers, and venous/arterial ulcers or pressure ulcers (PU). They share common features including excessive inflammation and persistent infection, often caused by drug-resistant bacterial biofilms. Chronic wounds are often comorbidities, with patients who are bed bound, diabetic, smokers and the elderly, being at greater risk of their formation.¹⁴ Chronic wounds have a high rate of morbidity and mortality associated with them.¹⁵ Per annum,

wounds and their associated morbidity and mortality cost the National Health Service (NHS) an estimated £5.3 million.¹⁶ The care of chronic wounds is specialised and requires regular visitation to a wound clinic for treatment from a trained nurse. Wounds are routinely cleaned, debrided and dressed. Debridement is the removal of dead or inflamed tissue, often through the use of sharp items such as tweezers or a curette. Although enzymatic gels, high-pressure water jets and maggot therapy are also used.¹⁷

1.2.4 Burn Wounds

Burn wounds are classified based upon their causative agent: physical, thermal, electrical, chemical, radiation and laser burn each type differing in their presentation and clinical management. The skin has three main layers, epidermis, dermis and subcutaneous fat, the structure of healthy skin is shown in **Figure 1.1A**. The healing of a burn wound is heavily dependent on the depth of the burn. Burns are categorised into first-degree burns, where skin is erythematous without vesication, second-degree involves the epidermis and variable thickness of the dermis (**Figure 1.1C**), third-degree eschar formation and fourth degree burns, which extend into fat, muscle and bone (**Figure 1.1B**).¹⁸

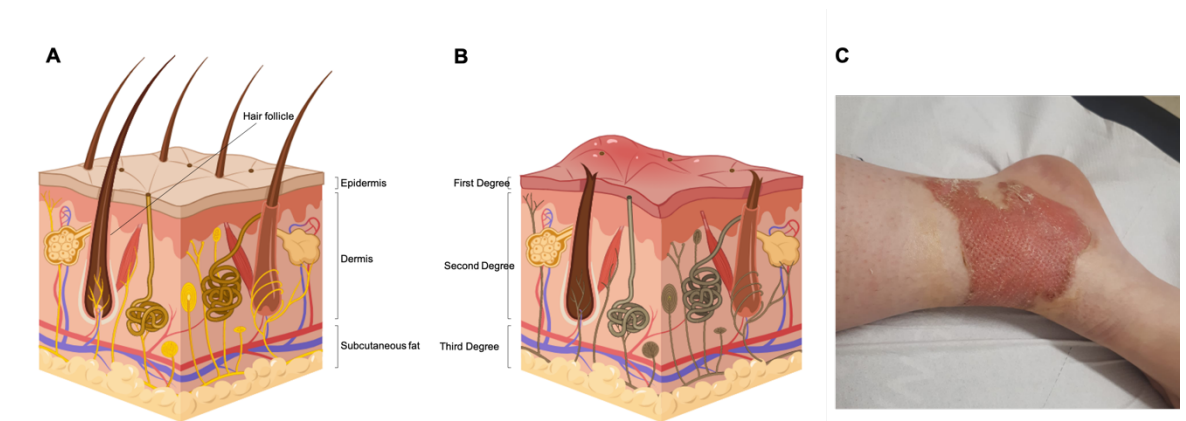


Figure 1.1: Structure of healthy skin (A). Structure of burned skin showing the layers effected in the varying degree of burns (B). Photograph example of second-degree burn (C). (Image created in BioRender).

The clinical management of burn injury is based upon the severity, minor burns are <15% total body surface area (TBSA) for adults and <10% in children and major burns are up to 35% TBSA in adults and 30% in children. Coverage greater than this is deemed life-threatening.¹⁹ While initially burn wounds are sterile, they quickly become contaminated. The only organisms present within a wound are those within the epithelial appendages of hair follicles and sebaceous glands. The formation of eschar acts as a cultural media for these

bacteria to proliferation and invade deeper tissue. This is thought to be a cause of burn wound sepsis. An effective antimicrobial for a burn wound must penetrate the eschar and kill these organisms. *S. aureus* and *P. aeruginosa* are the bacteria most frequently isolated from burn wounds.²⁰ Owing to the great surface area available for bacterial colonisation and infection burn wounds are dressed to prevent infection, antimicrobials are often applied topically to prevent infection.^{20,21}

1.2.5 Wound Infection

Nearly all open wounds will become colonised with microorganisms; while usually this has no clinical consequences, occasionally the patient will exhibit symptoms which suggest that they have become clinically infected. A wound is only said to be infected when pathogenic organisms have triggered an immune response.²² The risk of infection is increased with the size of the microbial inoculum, the virulence of the colonising microorganism, and the immunocompetency of the patient. Clinical manifestations of wound infection include redness, warmth, swelling, pain and purulent secretions.²³

The progression of infection occurs as follows: contamination, colonisation, critical colonisation threshold (CCT), localised infection, spreading infection and then systemic infection (**Figure 1.2**). Bacterial contamination is the first phase of infection, in which the bacteria are not multiplying or causing clinical problems. This progresses into colonisation where the bacteria are multiplying but wound tissues are not being damaged. The bacteria then reach the CCT, whereby the bacteria have multiplied to an extent that healing is impaired and the wound tissues are damaged and bacterial biofilms begin to form.^{24,25}

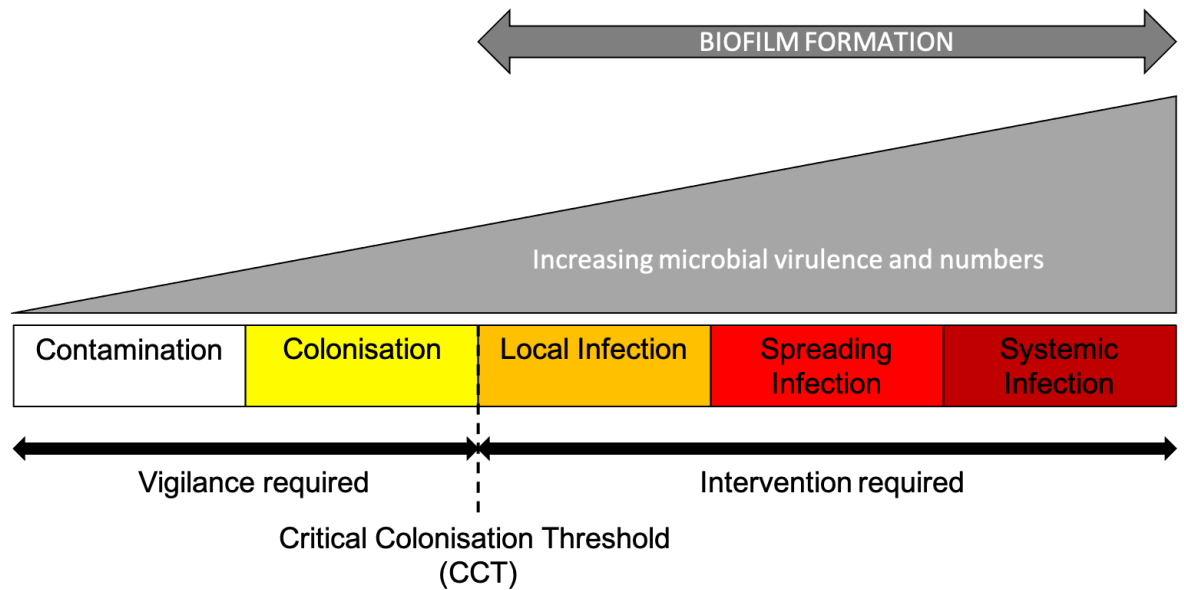


Figure 1.2: Schematic outlining the progression from bacterial contamination to systemic infection.

The human skin covers $\sim 1.6 \text{ m}^2$ with a range of specialist niches for the support of a range of bacterial species.²⁶ Often the source of contaminating bacteria is from the patient's skin, for example *S. aureus* are known to colonise the nasopharyngeal passage and contribute to the skin microbiota and are considered opportunistic pathogens.²⁷ Normal human skin is colonised with between $10^4 - 10^6$ colony forming units (CFU) per cm^2 .²⁸ Wound infection is characterised clinically through presentation with fever, erythema, oedema, pain and/or wound discharge of a purulent nature.²⁹ The nature of infection can vary from localised infection, requiring minimal intervention, or can spread to systemic infection. Serious complications of wound infection are cellulitis, sepsis and necrotising fasciitis.³⁰ To date there is no set classification for skin and soft tissue infection (SSTI) likely owing to the vast range of clinical presentation.³¹

1.2.6 Infection Diagnosis

The diagnostic challenge within wound infection diagnosis is the identification of wounds which are infected to a level that will impact healing and repair. Some wounds which are heavily colonised will heal in a spontaneous and timely fashion, whereas others which have significantly lower levels of bacterial colonisation will result in serious infection. While clinical presentation and the trained eye of a physician drive suspicion of infection, diagnosis is confirmed using clinical microbiology, however as yet, no gold standard for wound infection diagnosis exists.³² Wounds are swabbed and sent to pathology labs for

investigation, which is split into semi-quantitative and quantitative.³³ Semi-quantitative analysis involves the culture of any viable bacteria from patient sample and grading growth accordingly: light, moderate and heavy. This culture method is flawed owing to its propensity for growth of motile and quick growing organisms, leaving fastidious organisms, namely anaerobes, underrepresented.³⁴ Quantitative analyse of tissue samples and pus, while labour intensive, is a better method for the prediction of infection. A bacterial load of greater than 10^5 CFU/mm² of tissue is regarded as being significantly at risk of causing infection.³¹

There are a number of issues with microbiological testing for wound infection. Firstly, the turnaround time varies from 24-48 h, after which antibiotic treatment has likely already been administered or infection has increased in severity rendering the diagnosis irrelevant. Moreover, clinical microbiology can only confirm the presence of bacteria and indicate any antibiotic resistance the detectable species may have. There is no way to confirm that the detected bacteria are pathogenic or whether they will cause serious infection or sepsis. Point-of-care testing can offer a quicker time to diagnosis increasing the evidence for the requirement of antibiotic treatment thus potentially reducing unnecessary use of antibiotics. Such tests currently available are Woundchek and MolecuLight. MolecuLight uses UV light to detect the presence of fluorescent bacteria, *S. aureus* emits a red colour owing to the presence of endogenous porphyrins and *P. aeruginosa* cyan signal, shown in **Figure 1.3C** as a result of endogenous pyoverdine in otherwise clean looking wound bed **Figure 1.3B**.³⁵

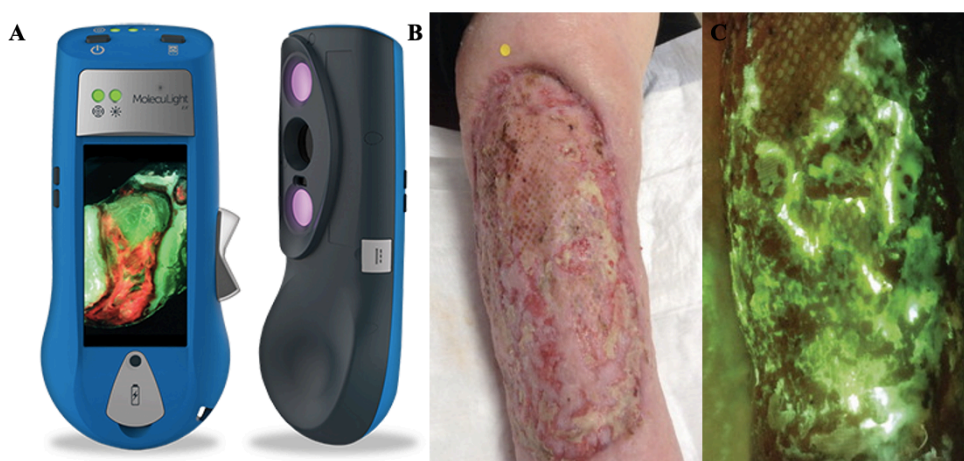


Figure 1.3: MolecuLight device detects fluorescence emitted from bacteria colonising wound bed (A) handheld MolecuLight device with digital screen showing presence of bacteria (image found online molecuLight.com). (B) 12-days post lower limb split-thickness skin graft wound bed of a 58-year-old male. (C) MolecuLight fluorescent image showing cyan in wound bed. (Reproduced with permission from Journal of Woundcare)³⁵

Woundchek is quick, taking 15 minutes and costing £30 per swab, it detects the presence of proteases within the wound. Proteases are produced by both Gram-positive and negative bacterial species which are associated with increased pathogenicity owing to their ability to degrade healthy host tissues and impair host immune response. However, WoundChek is only marketed for the diagnosis of infection within chronic wounds but currently has no application in detecting developing infection within acute patients.^{36,37}

Thet *et al.* describe an *in-situ* infection detecting hydrogel dressing, where bacterial toxins produced on the development of a biofilm rupture synthetic lipid vesicles, containing a fluorescent dye. On their release there an increase in their fluorescence, indicating the presence of infection. The dressing indicates bacterial presence after 4 h. Thus it can be concluded this device has the potential to detect developing pathogenic infection indicating to clinicians that a bacterial infection could be forming (**Figure 1.4**).³⁸

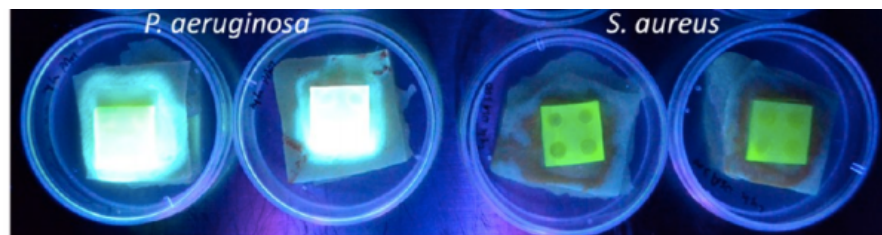


Figure 1.4: Fluorescent response of the prototype dressing in response to 24 h model burn infections of *P. aeruginosa* and *S. aureus* infections. (Reproduced with permission from ACS Applied Materials and Interfaces)³⁸

1.2.7 Wound Dressings

Owing to the dynamic nature of wounds in terms of size, purulence, depth, location and infection there is a wide range of available dressings available to meet the range of demands stretching from the common household plaster, to semi permeable, antimicrobial releasing hydrogels (**Table 1.1**). Regular dressing changes put the wound at greater risk of contamination and can hinder wound healing owing to the high risk of removing the developing layer of keratinocytes from the wound surface. In addition to this, frequent dressing changes are painful, especially within burn wounds, and can require many visits to the wound clinic.^{39,40}

Chapter 1

Table 1.1: Analysis of the different types of dressings available with description of function, examples and the wound type they are used to treat.⁴¹

Dressing Type	Description	Examples	Wound Type
Gauze	Made from woven or non-woven fibres of cotton or polyester, to form a protective barrier.	Xeroform ^T M	Non-exudating – slightly exudating.
Semi-permeable film dressings	Transparent and adhesive polyurethane allows for transmission of CO ₂ , O ₂ and water vapour from wound	Opsite TM Tegaderm ^T M	For epithelialising wounds, shallow wounds with low exudate & superficial wounds
Semi-permeable foam dressings	Consist of hydrophilic and hydrophobic foam. Allowing for protection from liquids but enabling gas exchange, silicone-based rubber foam enables the dressing to mould to the wound. Foam thickness dictates wound drainage capabilities.	Lyof foam TM	Highly exudative wounds. Not suitable for dry wounds.
Polymer hydrogels	Insoluble, hydrophilic materials made from synthetic polymers such as poly-vinyl-alcohol (PVA). They have a high water content helping granulation tissues and epithelium. Their elasticity enables easy application and the temperature of the wound is decreased upon application providing a cooling effect.	Aquaform ^T M Nu-gel TM	Low exudation
Hydrocolloid	Consist of two layers, inner colloidal layer and outer water-impermeable layer. Allowing water permeation while protecting from bacteria. They also have debriding properties and absorb exudate.	Comfeel TM Granuflex ^T M	Neuropathic ulcers or highly exudating wounds
Alginate hydrogels	Made up of mannuronic and guluronic acid units. Derived from seaweed, some studies have shown alginates accelerate healing through macrophage activation and TNF- α	Sorbsan TM	Moderate-heavy exudating wounds
Skin Substitutes	2 types available: one mimics keratinocytes and fibroblasts on collagen matrix, the other contains dermal elements.	Biobrane TM	Burns and ulcers
Medicated Dressings	Dressing impregnated with antimicrobials such as silver or iodine. Dressing can also contain proteolytic enzymes such as papain and collagenases.	Aquacell Ag+ Debridace ^T M	Ulcers, burns and necrotic wounds

1.2.8 Wound Healing

Wound healing begins with the inflammation phase. This early stage in wound healing is when the wound is at most risk of colonisation of pathogenic bacteria. Inflammation is split into two phases: vascular and cellular. Acute inflammatory response (**Figure 1.5A**) consists of localised vasodilation, extravasation and blocking in lymphatic drainage causing swelling, redness and heat, the main signs of infection. Tissue damage typically causes blood vessel damage which results in bleeding. The cellular response involves platelets, a key component of blood, adherence, aggregation and release a multitude of factors for coagulation. Further to this coagulation platelets also initiate healing through the release of chemoattractants and growth factors, attracting neutrophils, macrophages and leukocytes.⁴² Proliferation (**Figure 1.5B**) provides the necessary components for a new functional barrier, through re-epithelisation, establishment of a new blood supply through the generation of blood vessels (known as angiogenesis) and reinforcements of damaged dermal tissues. Re-epithelisation restores the remaining epidermal tissues through attraction of keratinocytes into the wound, then subsequent proliferation and differentiation of neoepithelium into stratified epidermis. Remodelling occurs throughout the wound repair process. Fibrin clots formed early in the inflammation phase, are replaced with granulation tissue rich in type III collagen and blood vessels during proliferation. This is then replaced with type I collagen and less mature blood vessels. Change in the extracellular wound matrix is a key characteristic of wound remodelling (**Figure 1.5C**).⁴³

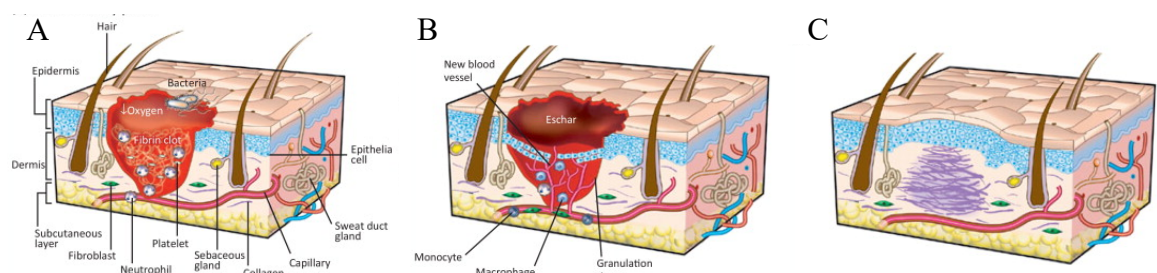


Figure 1.5: Schematic representation of the stages of wound healing: inflammation (**A**) Proliferation & Re-epithelisation (**B**) and remodelling (**C**). (Reproduced with permission from Trends in Pharmacological Sciences)⁴⁴

1.2.9 Bacterial Biofilms

Initially discovered in the 17th century by Antoine Von Leeuwenhoek, a biofilm is broadly defined as aggregated microorganisms irreversibly bound to a surface living within a complex matrix consisting of extracellular polymeric substances (EPS) that cannot be removed without force, **Figure 1.6**.⁴⁵

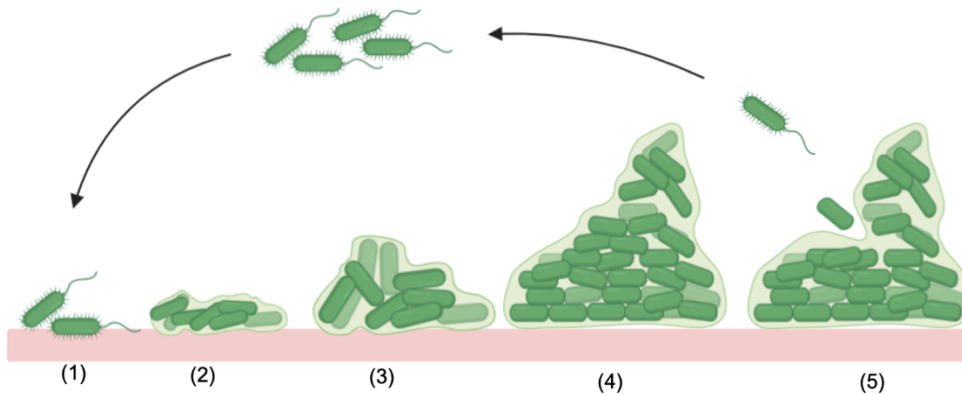


Figure 1.6: Schematic of the stages of bacterial biofilm formation on skins surface. (1) Planktonic bacteria attachment. (2) Irreversible bacterial attachment. (3) Cell proliferation. (4) Growth and maturation. (5) Dispersal. (Created using BioRender).

Planktonic bacteria are single “free living” microorganisms, they can reversibly attach to surfaces, which within a clinical environment include catheters, teeth, orthopaedic implants and importantly, wounds.⁴⁶ After attachment the community of bacteria forms a microcolony, stabilising their adhesion to the associated surfaces, and the cohesion between neighbouring bacteria increases making the microcolony stronger. At this stage the bacteria are now irreversibly bound to the surface owing to the formation of the EPS. The EPS “slime” is composed of nucleic acids, proteins and polysaccharides and makes up about 80% of the biofilm. The EPS surrounds the bacteria functioning as a protective barrier against the hosts immune response.⁴⁷ The bacteria begin to proliferate. Upon reaching a critical density, the activation of quorum sensing (QS) occurs, which enables communication between bacterial cells and results in alteration of bacterial phenotypes. Once QS molecules are present the upregulation of biofilm formation occurs through phenotype alteration. Bacteria excrete QS molecules which causes neighbouring bacteria to join the biofilm.⁴⁸ Within the bacterial biofilm there is a broad range of phenotypic and genotypic traits resulting in a community that is less susceptible to antimicrobials and the hosts immune response. Antimicrobials fail to eradicate biofilms owing to poor penetration into the biofilm, the metabolic inhibition, and the dormant bacteria, known as persister cells. Persister cells are

able to repopulate the community if a significant proportion of the biofilm is removed. Finally some cells will detach from the mature biofilm ready to colonise a new surface.⁴⁹

1.2.10 *Staphylococcus aureus*

Bacteria are categorised into Gram-positive and Gram-negative, using Gram's staining. Gram-positive bacteria, which have a single, thick peptidoglycan layer, retain crystal violet dye, whereas Gram-negative bacteria, which have a double peptidoglycan layer, will not retain crystal violet dye identifying themselves as Gram-negative. *S. aureus* is Gram-positive, and its cell wall is 50% peptidoglycan by weight.⁵⁰

S. aureus translates as golden, grape-cluster berry owing to its colour and shape. It is a catalase positive and a facultative anaerobe. *S. aureus* are commensal bacteria, persistently colonising the nasal-pharynx of between 20-25% of the population with 60% transient carriage. While it has a high level of asymptomatic carriage it is associated with a number of illnesses, from skin conditions like impetigo and folliculitis to life threatening conditions like meningitis and sepsis.⁵¹ *Staphylococci* produce a range of toxins, which are categorised based upon their action. Cytotoxins such as alpha toxin, can cause pore formation and inflammation in mammalian hosts resulting in sepsis. Toxic shock syndrome toxin (TSST) is found in 20% of *S. aureus* isolates and causes toxic shock syndrome. Epidermolytic toxins A & B causes skin erythema and separation which is seen in staphylococcal scalded skin syndrome.⁵²

A major component of *S. aureus* biofilms is polysaccharide intercellular adhesin (PIA) which is produced by enzymes encoded in the *icaADBC* locus, composed of β -1,6-linked *N*-acetylglucosamine. PIA plays an important role in the structural integrity of the biofilm.⁵³ Further to this *S. aureus* has surface -associated proteins which are important components in the attachment and development of the biofilm matrix such as protein A, fibrinogen-binding proteins, biofilm-associated protein (Bap) and clumping factor B (ClfB) the importance of which will vary between strains.⁵⁴ *S. aureus* biofilm regulation is controlled by staphylococcal accessory regulator (*sarA*) and accessory gene regulator (*agr*) which compose a two regulatory gene locus encoded by *arlRS*, a member of the OmpR-PhoB family. When upregulated *arlS* prevents biofilm formation, *sarA* transcripts are upregulated

in biofilms. The *agr* quorum sensing system has been shown to downregulate genes of cell-wall associated adherence factors and its expression is induced through auto-inducing peptides (AIP) resulting in the dispersal of mature biofilms. Additional levels of biofilm control are achieved through the *sigB* operon product σ^B . σ^B upregulates the expression of clumping factor, coagulase and fibronectin binding protein A (FnbpA) which are needed in the early stages of biofilm development.⁵⁵

S. aureus biofilm-associated infections are the key cause of a number of diseases. They are the most prevalent cause of osteomyelitis, an infection of the bone, where bacteria are often introduced through trauma or surgery.⁵⁶ *S. aureus* biofilms are also commonly isolated from medical devices such as prosthetic implants, intravenous catheters and stitch materials.⁵⁷ *S. aureus* is also recovered from 50% of chronic rhinosinusitis cases and within over 50% of endocarditis patients.⁵⁸

1.2.11 *Pseudomonas aeruginosa*

P. aeruginosa translates as “false unit” (Greek and Latin, referring to the rod-like shape) of “copper rust” colour (Latin), referring to the colour of the bacteria. *P. aeruginosa* is Gram-negative, owing to its double cell membrane. *P. aeruginosa* is considered an opportunistic infection, thriving in moist environments. It generally affects immunocompromised patient groups such as those with burns, cystic fibrosis or who are immunosuppressed.⁵⁹ But can also affect the immunocompetent via hot tub folliculitis, owing to its ability to thrive in moist environments. *P. aeruginosa* is frequently isolated from medical devices such as catheters and ventilators which can result in ventilator-associated pneumonia which is associated with high mortality rate within cystic fibrosis patients.⁶⁰

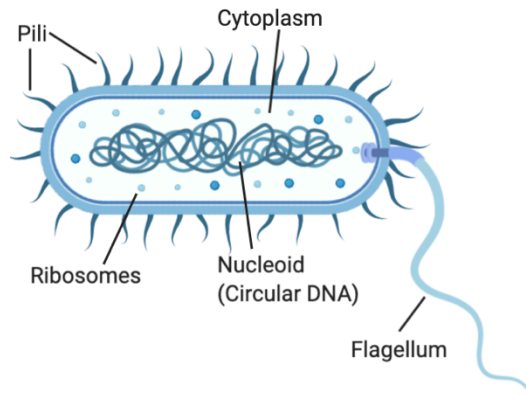


Figure 1.7: Structure of *P. aeruginosa*. (Created using BioRender)

Bacteria surface factors including lipopolysaccharides, pili and flagella as well as toxin production and biofilm formation contribute to *P. aeruginosa* virulence shown in **Figure 1.7**. Pyocyanin, a phenazine dye produced by *P. aeruginosa* which gives it its colour, is also a virulence factor. Pyocyanin is toxic to mammalian cells as well as bacterial cells enabling *P. aeruginosa* to outcompete other species.⁶¹ *P. aeruginosa* also produces a range of other virulence factors including elastases⁶² and exotoxins.⁶³

P. aeruginosa has two interconnected quorum sensing systems which rely upon acylhomoserine lactone (AHL) signalling molecules. The Las system uses N-(3-oxododecanoyl)-L-homoserine lactone and the Rhl system which uses N-butanoyl homoserine lactone. The Rhl system regulates swarming motility, which is implicated in the early stages of *P. aeruginosa* biofilm formation and also controls the production of rhamnolipids which play multiple roles within biofilm formation.⁶⁴

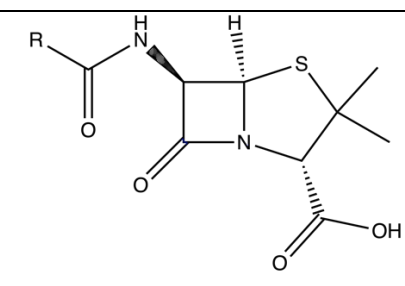
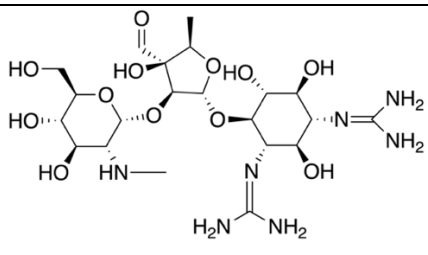
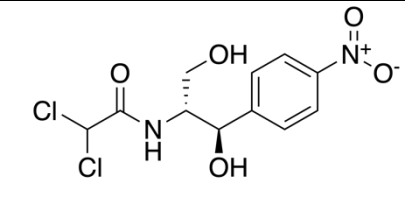
1.3 Bacterial Infection Treatments

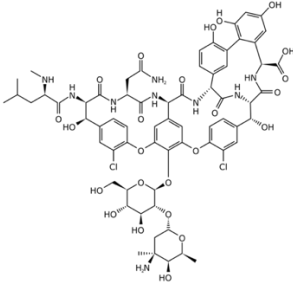
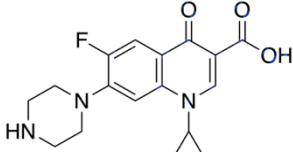
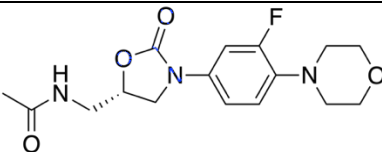
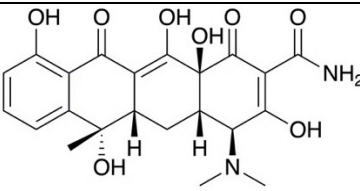
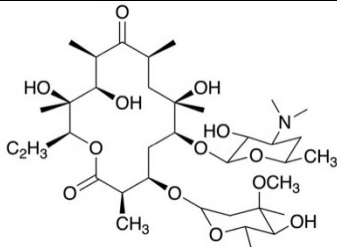
As all wounds will be colonised to some extent with microorganisms there is a requirement of effective and targeted treatments to reduce and prevent the impact and extent of potential infection in both acute and chronic wounds. There are three key groups of antimicrobials; antibiotics which destroy microorganisms within the body, antiseptics which are applied to living tissues with the aim of reducing infection (particularly during surgery) and disinfectants which are nonselective agents which kill a range of microbes on non-living surfaces, preventing the spread of disease.

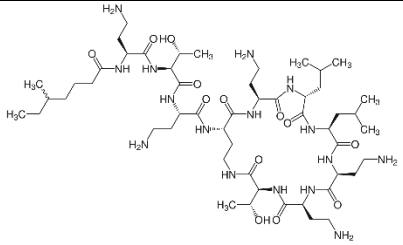
1.3.1 Antibiotics

The word antibiotic, translated from Greek, means “opposing life” and is defined as “a substance that is able to kill or inhibit a microorganism”. Penicillin, the first antibiotic, was famously discovered accidentally by Alexander Fleming in 1928. Derived from *Penicillium* moulds, penicillin was found to exert lytic action against *Staphylococci*.⁶⁵ Howard Florey, devised a method for the mass production of penicillin. This discovery won Florey and Fleming the Nobel prize, and in 1942 the first patient, a male with *Streptococcal* sepsis was treated with penicillin.⁶⁶ This discovery kicked off the “golden era” of antibiotic discovery. Since the discovery of penicillin the number of deaths caused by infectious diseases has been reduced by over 70%.⁶⁷ Antibiotics are classed based upon their structure. Common targets include bacterial cell wall synthesis, nucleic acid synthesis and protein synthesis, the chemical structure and mechanism of action of some examples is outlined in **Table 1.2**.

Table 1.2: Categorises of antibiotics, description of action, chemical structure and resistance mechanism.

Category of Antibiotic	Examples	Description	Structure	Resistance Mechanism	Ref
Beta-lactams	Penicillins e.g. penicillin (pictured), amoxicillin & flucloxacillin and cephalosporins	Beta-lactam ring (shown in blue) work through inhibiting bacterial cell wall synthesis. They achieve this by inhibiting the last step in the production of peptidoglycan, which is a vital component of the bacterial cell wall. This occurs when beta-lactams binds to the penicillin-binding proteins (PBP).		Bacteria synthesis beta-lactamase, an enzyme which cleaves the beta-lactam ring.	68
Aminoglycosides	Streptomycin, neomycin & kanamycin	Made up of amino-modified glycoside (sugar), aminoglycosides inhibit protein synthesis. They bind to the cytosolic membrane-associated ribosome, preventing the elongation and resulting in inaccurate mRNA translation.		While still broadly effective, some bacteria, have a reduced drug uptake by aminoglycoside-modifying enzymes.	69
Chloramphenicol	Chloramphenicol	Organochlorine compound that is dichloro-substituted acetamide containing a nitrobenzene ring. It diffuses through the cell wall and reversibly binds to the 50S ribosomal unit altering peptidyl transferase activity.		Bacterial enzymatic inactivation by acetylation mainly via acetyltransferases.	70

Glycopeptides	Vancomycin	Inhibit bacterial cell wall synthesis through binding to the terminal D-Ala-D-Ala in pentapeptide portion of N-acetylglucosamine-N-acetylmuramic acid peptidoglycan cell wall precursor.		Resistance is mediated by vancomycin resistance operon, transported chromosomal and extrachromosomal plasmid.	71
Quinolones	Ciprofloxacin, levofloxacin	Interferes with bacterial DNA replication and transcription through targeting DNA gyrase and DNA topoisomerase IV.		Mutations in the target enzymes, and through efflux pumps.	72
Oxazolidinones	Linezolid, posizolid	Inhibits synthesis of proteins preventing growth through binding to the 50S subunit.		Can occur through target modification.	73, 74
Tetracyclines	Tetracycline, doxycycline	Inhibits protein synthesis by preventing attachment of aminoacyl-tRNA to the ribosomal acceptor (A) site thus preventing growth.		Usually through acquiring mobile genetic elements carrying tetracycline-specific resistance genes.	75
Macrolides	Erythromycin, clarithromycin	Inhibits of bacterial protein synthesis through prevention of peptidyl transferase from adding the growing peptide attached to the tRNA to the next amino acid and through inhibition of ribosomal translation.		Post translational methylation of the 23S bacterial ribosomal RNA. This resistance can be acquired either through plasmid or through mutation.	76, 77

Polymyxin	Polymyxin B, Polymyxin E Colistin	Binds to LPS in Gram negative bacteria and disrupts lipid membranes of bacteria		Modification of LPS to decrease binding	66
-----------	---	---	---	--	----

1.3.2 Antibiotic Resistance

Antibiotic resistance occurs when bacteria develop the ability to combat the drug's effect, enabling them to either continue to grow in the presence of the drug, or are unable to be affected by the drug. Infections caused by antibiotic resistant bacteria are difficult and sometimes impossible to treat, often requiring extended hospital stays, more costly alternative treatments and frequent medical follow up appointments.

It is commonly misconceived that antibiotic resistance is as a result of the body becoming resistant to antibiotics, however, this is not the case. The inappropriate use and overuse of antibiotics has resulted in a surge of antibiotic resistant bacteria within a multitude of sectors including healthcare, veterinary and agricultural industries. Antibiotics not only save lives; they have also enabled a major advancement on modern medicine and surgery before antibiotics simple procedures such as caesarean sections and tooth removals had a high level of associated mortality.

Epidemiological studies have shown the direct relationship between antibiotic use and the emergence of resistant bacterial strains.⁷⁸ Resistance can occur spontaneously, or genes can be inherited from relatives or shared by non-relatives in close proximity through the transferral of mobile genetic elements such as plasmids. Horizontal gene transfer (HGT) enables the transferral of antibiotic resistance between different species of bacteria.⁷⁹ Yet despite warnings against overuse, antibiotics remain widely overprescribed across the world and in some countries are uncontrolled (sold over the counter). Furthermore, the incorrect prescribing of antibiotics has also contributed to the rise in antibiotic resistance, within intensive care units (ICUs) 30%-60% of antibiotic prescriptions have been found to be inappropriate, unnecessary or suboptimal.⁸⁰ Subinhibitory concentrations of antibiotics can promote resistance by supporting genetic alterations, including virulence, HGT and mutagenesis.⁸¹

Antibiotic administration to livestock is known to promote growth and limit infection resulting in larger yields and higher quality produce. However, antibiotic resistant bacteria pass from livestock to humans through the food chain. Further to this, antibiotics are excreted into the environment by livestock through stool and urine which is subsequently widely

distributed into rivers through groundwater, surface runoff and fertiliser. This environmental dissemination of antibiotics contributes to the exposure of microorganisms in the environment and increases the proportion of resistance.⁸²

There are a multitude of multidrug resistant (MDR) bacterial species which pose a serious threat to human health. These have been further categorised based on risk. Within Gram-positive bacteria *S. aureus* and *Enterococcus* pose the greatest threat owing to *S. aureus* strains with resistance to methicillin, known as methicillin-resistant *S. aureus* (MRSA) and *Enterococci* are broadly vancomycin resistant. Gram-negative bacteria are more threatening owing to their resistance to nearly all available antibiotic treatments. MDR nosocomial pathogens frequently cause infection and associated with a higher risk of mortality.² MDR infections often occur within a healthcare setting, yet other MDR infections are becoming prevalent within the community including *E. coli*⁸³ and *Neisseria gonorrhoea*.⁸⁴

Antibiotic resistance can either be acquired, as already outlined, or intrinsic owing to the inherent structural or functional characteristics. The simplest version of intrinsic resistance is the absence of the antibiotic target, for example, triclosan is broadly efficient against Gram-negative and Gram-positive bacteria, however, is ineffective against bacteria of the genus *Pseudomonas*. This is owing to *Pseudomonas* carrying an insensitive *fabI* gene which encodes the enzyme enoyl-ACP reductase, the target of triclosan.⁸⁵ Gram-negative bacteria are intrinsically less permeable to antibiotics owing to their outer membrane. Bacterial efflux pumps are also known to be a major component of intrinsic resistance. Efflux pumps actively transport antibiotics out of the cell.⁸⁶

Chloramphenicol florfenicol resistance (*cfr*) is achieved by methyltransferase specifically methylates A2503 in the 23S rRNA conferring resistance to a range of drugs that have targets near this site, including: streptogramins, phenicols and oxazolidinones (including linezolid). The *pnr* genes encode pentapeptide repeat proteins (PRPs). PRPs bind to topoisomerase IV and DNA gyrase and protect from the lethal action of quinolones i.e. ciprofloxacin.⁸⁷

1.3.3 Topical Antimicrobials

Clinically infected wounds typically require treatment with systemic antibiotics. However, some superficial wound infections such as impetigo, a skin infection caused by *S. aureus*, are routinely treated with topical antimicrobial therapies.⁸⁸ Topical antimicrobials aim to either kill colonising bacteria or prevent their replications without causing clinically significant damage to the patients cells. They can be used alone or in combination with antibiotics. Typically, topical antimicrobials are broad spectrum in their activity, with multiple microbial targets. Chlorohexidine and povidone iodine are commonly used within wound care, however, currently silver ions are being promoted as the main antimicrobial within wound disinfection.⁸⁹

The ease of application of topical antimicrobials makes them very appealing from a patient's point of view, they can be applied by either the patient or their caregiver thus reducing the need to attend the clinic. Pharmacologically speaking their high and sustained concentration at the infection site is advantageous, further, there is a reduced risk of systemic absorption and toxicity. Owing to reduced risk of toxicity, novel therapies that have yet to be approved for systemic use can be used.⁹⁰ However, topical antimicrobials are not without disadvantage, from a patients' perspective frequent reapplication can be tiresome, application can be difficult depending upon wound location and there is risk of contamination in multidose containers. There is also the potential for localised hypersensitivity or contact dermatitis associated with topical antimicrobials and a risk of systemic absorption in large wounds which may lead to toxicity.⁸⁹

1.3.3.1 Hydrogen Peroxide

Hydrogen peroxide (H_2O_2) is a commonly used topical antimicrobial for wound irrigation and in some cases for the removal of necrotic tissue from wounds. H_2O_2 for this use has a concentration of between 1-3 % (v/v) (324-972 mM).⁹¹ H_2O_2 is an oxidising agent which induces cellular toxicity through the generation of hydroxyl radicals which subsequently induce lipid peroxidation leading to DNA damage and cellular death. However, H_2O_2 is readily formed by immune cells, such as leukocytes, within the mammalian healing process.⁹²

The effects of H₂O₂ within wound healing are debated. Multiple studies have shown that low concentrations of H₂O₂ can promote re-epithelisation of the wound (250-500 μM)⁹³ and enhance healing (10-50 mM).⁹⁴ Yet these concentrations are significantly lower than the high concentrations used within wound care. High concentrations of H₂O₂ have been found to damage cells within the wound bed and healthy cells surrounding the wound. The toxic effect that H₂O₂ induced oxidative stress has on fibroblasts⁹⁵ and keratinocytes⁹⁶ have been widely reported. While the dermal penetration of H₂O₂ has not been reported owing to its instability and rapid decomposition by enzymes catalase and glutathione peroxidase, it is accepted that H₂O₂ rarely has systemic toxicity.⁹⁷ Importantly, however, there are no reports of H₂O₂ resistant bacteria.

1.3.4 Drug Repurposing

With the ever-growing threat of antimicrobial resistance, the need for novel antibacterial treatments increases concurrently. Yet, the development of *de novo* antibiotics is risky, with only 1 in 70 progressing from early screening. This process is expensive and lengthy, taking between 10-17 years and costing over \$1 billion. However, drug repurposing provides a potential solution, identifying new commercial opportunities for already approved drugs. There are two distinct principles for the identification of candidate drugs: (1) a drug may have unknown biological activities, evident through identification of many side-effects and (2) different diseases frequently share a common molecular pathway or genetic factors, this principle is commonly leveraged within cancer therapy. A famous example of drug repurposing is Sildenafil, originally used to treat hypertension, was repurposed for treatment of erectile dysfunction. To date approximately 46 approved drugs have been repurposed for novel therapeutic uses.^{98,99}

There is also a third approach of screening combinations of drugs to assess modulation of antimicrobial effects, and the identification of antibiotic drugs that potentiate antimicrobials. Extending the life span of said antimicrobial and overcoming antibacterial resistance is an attractive concept. A key example is the co-administration of β-lactamase inhibitors with β-lactam antibiotics or Fluoxetine (Prozac), which is an efflux pump inhibitor, being used in combination to modulate antibiotics activity.¹⁰⁰

1.4 Cold Atmospheric Plasma

1.4.1 Overview

First described by Irving Langmuir in the 1920's, plasma is affectionately referred to as “the fourth state of matter”. Plasma exists in a variety of forms, examples include lightning, the Northern Lights, solar flares, televisions and neon signs.¹⁰¹ Plasma is generated through the application of heat or electromagnetic field on an inert gas, causing ionisation of the gas which causes an increase in electrical conductivity. On application of an electric field electrons are subject to external energy, increasing their kinetic energy making them faster than the heavier ions of the gas, thus increasing their temperature to several thousand degrees before their environment heats up. In nonthermal plasma, cooling of the ions and uncharged molecules is more effective than the energy transfer from the heated electrons, resulting in the bulk gas temperature remaining cold. Owing to this, nonthermal plasmas are also referred to as non-equilibrium plasmas. Whereas, within a thermal plasma, the energy flux from electrons to heavy particles within the gas will cause the heavy gas particles to have a temperature equal to that of the electrons, which will in turn equilibrate with heavy particles in the external environment.¹⁰²

The application of plasma within medicine is a relatively new field known as “plasma medicine”. Early plasma medicine utilised the heating aspect of thermal plasmas for sterilisation of contaminated surfaces, cauterisation and tissue removal. Electrocautery, the application of heat to a tissue surface through application of high current, while effective, often results in the adhesion of charred tissue to the metal surface. Argon plasma coagulation resolved this issue owing to the absence of direct tissue contact. Thermal plasma has also been used for the cosmetic alteration of tissues.^{103,104}

Cold atmospheric pressure plasmas (CAP) have a greater range of applications within plasma medicine due to their temperature being within a physiologically tolerated range, typically <40°C, and their ability to operate under stable, easily reproducible atmospheric conditions. On interaction with the atmosphere the plasma produces a “cocktail” of reactive oxygen and nitrogen species, collectively known as reactive oxygen and nitrogen species (RONS), which have a range of biologically relevant applications. In addition to RONS,

CAP also generates UV, visible ultraviolet (VUV), infrared radiation/heat and electromagnetic fields.^{105,106}

1.4.2 Cold Plasma Devices

The characteristics of CAP can be incredibly variable and can be manipulated to favour the application of the device. The two types of CAP used within wound care are dielectric barrier discharge (DBD) and cold atmospheric pressure plasma jet (CAPPJ) illustrated in **Figure 1.8B**. In 1853 Theodose du Moncel discovered that discharge can be induced between two conducting plates separated by two glass plates. Moncel applied a Ruhmkorff coil to drive the discharge, which allowed for the generation of high alternating current (AC voltage from a low voltage DC source). Later, in 1857 Werner von Siemens reported the design of a DBD apparatus to generate ozone.¹⁰⁷

DBD generates large volume, non-equilibrium atmospheric pressure plasma using a dielectric material such as alumina or glass to cover at least one electrode. The electrodes are driven at high AC voltages within the kV range and at frequencies within the kHz range. DBD devices maintain a non-equilibrium state of plasma owing to the surface charge accumulation on the dielectric surface as soon as the discharge is ignited.^{108 107}

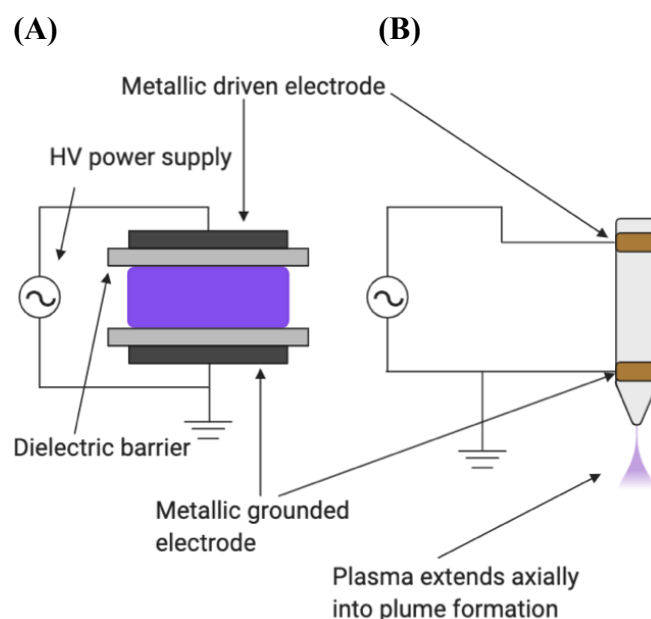


Figure 1.8: Schematic of DBD plasma (A) and CAPPJ (B). (Created using BioRender).

CAPPJs emit low temperature plumes into the surroundings and maintain temperatures below 40°C, enabling them to touch biological tissues without causing thermal damage. As such CAPPJs have proved useful within biomedical applications. As shown in **Figure 1.8A** the plasma plume is formed away from the high voltage electrode and into the atmosphere, which is free from high voltage, so the plasma does not cause electrical damage to the target tissue. However, there is a high electrical field at the tip of the CAPPJ which aids the propagation of the plasma plume and can affect the target tissue.¹⁰⁹

These CAP sources generate a cocktail of RONS, which play crucial biological roles. While RONS are thought to be the dominate biologically relevant species, there are other CAP components which will also interact with biological species: UV and VUV radiation and electric fields. There are now multiple plasma devices that are CE-certified medical devices and available for clinical use.

1.4.2.1.1 The kINPen®MED

The kINPen is a class IIa medical device, which been available since 2013 and was the first approved CAPPJ aimed at treating hard to heal wounds and pathogen induced skin diseases. Daeschlein *et al.* showed that the kINPen was effective in the inactivation of 105 wound infections on caused by 11 different bacterial species.¹¹⁰ Further to this Kramer *et al.* found that there was an increased proliferation rate on human cells that were treated with plasma. They also observed chronic wound remission after 3-24 weeks in four dogs and two cats.¹¹¹ Stratmann *et al.* reported significant improvement in the healing of 43 out of 62 diabetic foot ulcers after kINPen treatment.¹¹²

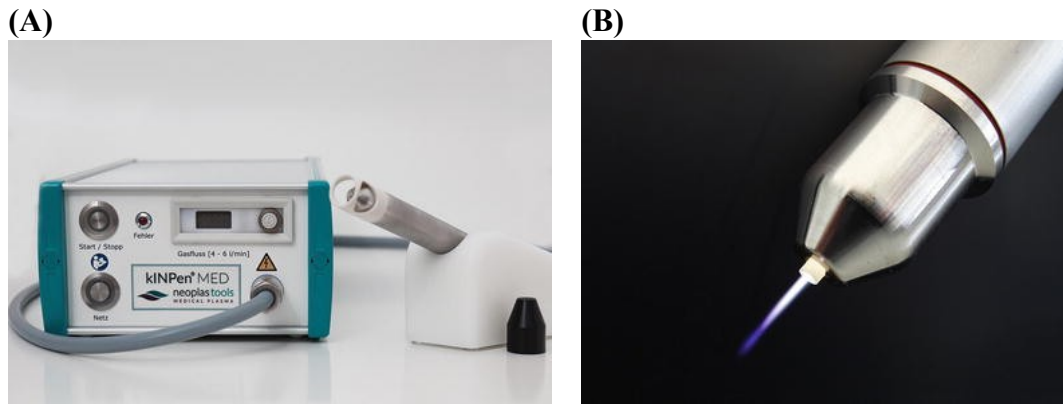


Figure 1.9: kINPen[®]MED apparatus (A) and ignited plasma jet plume (B) (Reproduced with permission from Springer Nature).

The plasma jet is handheld, moved vertically and precisely with over the affected area with a mean treatment time of 30-60 s/cm² (**Figure 1.9A**). The jet consists of a central pin electrode and the plasma is ignited at 2-6 kV at a frequency of 1 MHz using argon at a flow of between 3 to 5 standard litres per minute (SLPM). The plume has a length of between 8-13 mm and a diameter of 1 mm (**Figure 1.9B**).¹¹³ If the jet is not moved for 60 seconds the UV exposure locally is 8.8 J/m².¹¹³ Plasma treatment would be applied to the wound post debridement and prior to the application of any topical medications to avoid undesired interactions. Currently the kINPen[®]MED is licensed for the treatment of chronic wounds, acne vulgaris, herpes genitalis, eczema and athlete's foot.¹¹⁴

1.4.2.1.2 Adtec SteriPlas

The SteriPlas consists of a 6-electrode plasma torch and produces plasma by microwave-induced discharges using argon as the carrier gas (**Figure 1.10A**). The aperture of the plasma torch has a diameter of 3.5 cm resulting in a treatment area of 4-5 cm² (**Figure 1.10B**), both the apparatus and the treatment are significantly larger than the kINPen device. The distance between the plasma torch and the treatment tissue is 2 cm and treatment times were between 2-5 mins at an operating temperature of 33-37°C. The ignition conditions are 2.45 GHz and 80-110 W.¹¹⁵ A treatment time of two minutes was found to be effective in killing bacteria in infected wounds, further to this, 30 seconds of treatment was found to significantly influence the migration of fibroblasts however, it had no effect on the proliferation of keratinocytes of fibroblasts.¹¹⁶ SteriPlas was shown by Isbary *et al.* to relieve pain and

accelerate healing of herpes zoster infections and was found to reduce bacterial load in chronic wound patients.^{117,118}

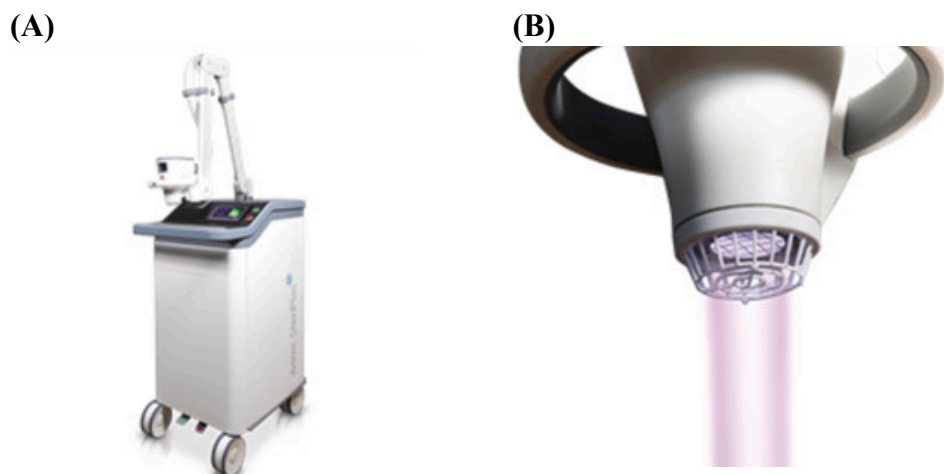


Figure 1.10: Adtec SteriPlas apparatus (A) and ignited plasam plume (B). (Reproduced with permission from the Journal of Clinical Plasma Medicine).

1.4.3 Applications

CAP devices have unique physical and chemical properties which can be tailored for the specific needs of the application, lending their utility to a variety of biomedical applications including dental treatment, cancer therapy, sterilisation, material preparation, tissue extrusion, and wound healing and decontamination.

Every year \$60 billion is spent on dental disease in the USA alone. Periodontal disease and caries are the most common diseases seen within dentistry. Dental caries are the localised destruction of tooth tissue owing to acids produced by bacteria, *Streptococcus mutans* (*S. mutans*) is one of the leading causes of caries.¹⁰⁶ Periodontal disease is caused by plaque which is a complex oral biofilm. CAP treatment has been shown to successfully treat oral biofilms caused by a variety of bacterial species including *S. mutans*^{119,120} and *Porphyromonas gingivalis*¹²¹ a common cause of periodontal disease. In addition to this, helium driven CAP has been found to be effective within cosmetic dentistry for tooth whitening in conjunction with H₂O₂, improving the bleaching efficacy.¹²²

Within the development of cancer therapies the goal is to hit the therapeutic “sweet spot”, where the treatment kills the cancerous cells without damaging normal cells of the diseased

tissue. CAP treatment is able to induce both necrosis and apoptosis within cancerous cells, depending on treatment time, a decrease in cell migration and induction of senescence in cancer cells, which is believed to be as a result of CAP produced ROS which are known to induce apoptosis.¹⁰⁶ Fridman *et al.* observed apoptosis and necrosis after DBD CAP treatment of melanoma cancer cells, after treatment with a low dose the cells became apoptotic several hours post treatment and at higher doses the melanoma cells became necrotic.¹²³ Further to this CAP has been shown to be effective against pancreatic cancer cells¹²⁴, neuroblastoma cells¹²⁵ and colorectal cancer.¹²⁶

The first application of CAP was the inactivation of bacteria on abiotic and biotic surfaces and in media. CAP was also found to be effective at treating biofilms and contaminated wound surfaces which will be discussed further in Section 1.4.5.2. In addition to its efficacy against bacteria CAP has also been found to inactivate viruses including HIV¹²⁷ and most recently COVID-19.¹²⁸ Aside from medical applications CAP has also been used within dermatology and aesthetic medicine. CAP has been effective in treating Ichthyosis and atopic dermatitis.¹²⁹ Within normal skin an acidic protective hydrolipid film, produced by the perspiratory glands and sebaceous glands covers the outer layer of skin and protects the skin from drying, this layer typically has a pH of between 5.4 and 5.9.¹³⁰ However, the pH value of patients with Ichthyosis or atopic dermatitis are significantly higher. CAP treatment lowers the pH of the hydrolipid film in diseased skin inhibiting colonisation by pathogenic bacteria.^{131,132} In addition to this, CAP has been shown to reduce scarring within patients with acne scars owing to its ability to promote tissue regeneration and work is an effective treatment for acne through its ability to reduce sebum production.¹³³

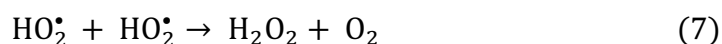
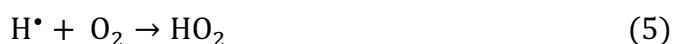
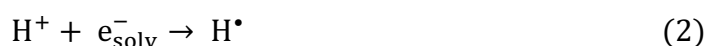
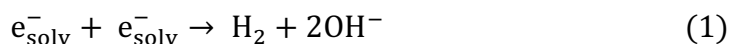
1.4.4 RONS

All living, aerobic, multicellular organisms require molecular oxygen to live. Due to its electronic structure O₂ is susceptible to radical formation owing to the presence of unpaired valence shell electrons. ROS are a natural by-product of metabolism and play a significant role in homeostasis and cell signalling, however, in the presence of environmental stresses, such as UV radiation or ionising radiation, their levels can drastically increase. At high concentrations ROS react readily with carbohydrates, proteins, lipids and DNA. This causes damage to cell structure and results in oxidative stress. Oxidative stress occurs when the

Chapter 1

balance between oxidants and antioxidants shifts resulting in an accumulation of oxidants which has an overall detrimental effect on the organism.¹³⁴

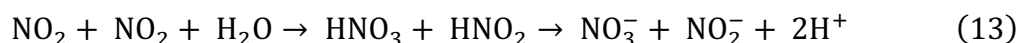
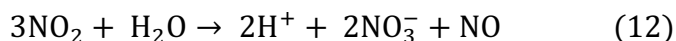
RONS are the key therapeutic component within CAP treatment, generated through CAP interactions with the atmosphere and upon contact with biological fluids, living tissues and other media. The cocktail of RONS generated through CAP treatment can be finely tuned and optimised for the desired purpose.¹³⁵ RONS can be generated within liquids through the dissociation of water molecules, resulting in the formation of short-lived species: such as OH• and H• radicles and hydrated (solvated) electrons (e_{solv}^-). Very quick reactions between these species results in the formation of transitory and more stable species (Shown in Equations 1-7), usually with a lifetime of more than one second, such as O₃, H₂, O₂ and H₂O₂.

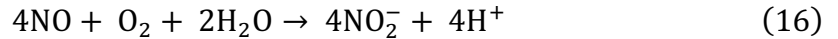
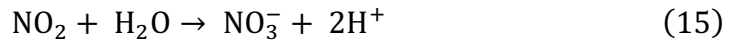
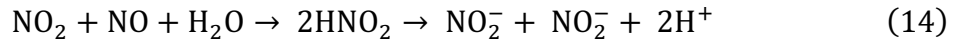


In the presence of air, RNS are also formed in liquids. Nitrogen oxides can be formed through the dissociation of nitrogen and oxygen (shown in Equations 8-11)



These nitrogen oxides subsequently react with water forming acids (shown in Equations 12-16), which alters the pH and conductivity of the CAP treated solution.

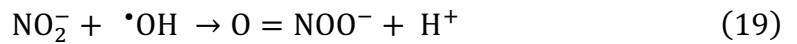
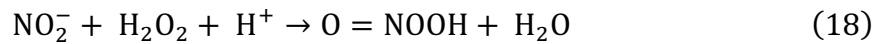




NO can be oxidised to NO₂ when oxygen is used as the working gas, mixed within the plasma plume, as in the case of atmospheric plasmas. This increases the concentration of NO₂. NO₂ can further react with hydroxyl radicals to form nitric acid (as per Equation 17).



Further reactions between different species can lead to the formation of peroxyxynitrous acid (for example in acidified conditions) (as per Equation 18) or peroxyxynitrite ions (in neutral conditions or basic conditions, i.e. PBS) (as per Equation 19).¹³⁶



1.4.4.1.1 Hydrogen peroxide

H₂O₂ is a biologically relevant CAP produced RONS, created as per equations 4 & 7 in CAP treated solutions, that is already present within host cells. H₂O₂ is thought to be the most prevalent of the CAP generated RONS and as such its production from CAP has been extensively characterised.¹³⁷ Throughout the literature a wide variation of CAP jet configurations and operating parameters are used, making it difficult to directly compare the generation of H₂O₂. However, these findings clearly demonstrate that through the tailoring of the CAP configuration the concentration of different RONS generated can be finely tuned.¹³⁶

1.4.4.1.2 Nitrite ions

NO₂⁻ are formed through the dissolution of NO, which are formed within the gaseous phase of the plasma jet. NO₂⁻ formation leads to the decrease of pH. The amount of NO₂⁻ decreases with an increase in flow rate. This is thought to be as a result of the decrease in mixing

between the CAP gas and the atmosphere, resulting in the production of fewer RONS.¹³⁸ The amount of NO_2^- formed has been found to decrease with increased flow rate owing to less air mixing with the plasma jet channel, resulting in less RONS.¹³⁸

1.4.5 Antimicrobial Effects of Cold Plasma

1.4.5.1 Planktonic Bacteria

CAP produces a spectrum of antibacterial RONS, which do not target one specific bacterial species. This is one of the major advantages of CAP treatment over traditional antibiotic therapy; owing to the range of components, bacteria struggle to mount resistance to CAP therapy, whereas antibiotics operate via one mechanism and as such are easy to mitigate against. Thus, it is unsurprising the CAP therapy has proven effective in the decontamination of foodstuffs, sporulating bacteria, protozoa and bacterial infections.

The use of low voltages limits damage to the fragile surfaces of fresh produce, and has enabled CAP to decontaminate eggshells with *Salmonella typhimurium* on the surface, as well as decontaminating lettuce, spinach and strawberries. *E. coli* O157:H7 is an enterohemorrhagic strain of *E. coli* that causes a number of deaths per annum when ingested from contaminated foods. Studies have shown CAP effectively reduces colonisation of *E. coli* in milk and on the leaves of spinach. It has also effectively decontaminated cheese of *Listeria monocytogenes* (*L. monocytogenes*). *Bacillus* and *Clostridium* species produce bacterial endospores exhibit high levels of tolerance to environmental stresses such as disinfectants and thermal inactivation owing to their impermeable outer layer and low water content. They can survive in a dormant state for prolonged periods of time, which is of particular concern on surfaces within clinical settings and within the food industry. CAP has demonstrated efficacy against *Clostridium difficile* (*C. difficile*) spores.¹³⁹ Often hospital-acquired and broadly resistant to antibiotics, *C. difficile* causes enteric disease and has a high morbidity and mortality within the elderly population.¹⁴⁰

CAP treatment has been found to result in a moderate reduction of protozoal viability. *Cryptosporidium parvum*, a common cause of water-borne disease in humans, produces oocysts which have exhibited resistance to chemical disinfectants such as chlorine and hypochlorous acid. However, CAP treatment resulted in a 4-log reduction of *C. parvum*

oocytes within 30 mins of CAP exposure. Further to this CAP has been found to inactivate cysts and trophozoites of *Acanthamoeba polyphagia* and *Acanthamoeba castellanii* which are ocular pathogens which can cause *Acanthamoeba* keratitis.^{141,142}

CAP has also been found to be effective in the decontamination of the ESKAPE pathogens.¹⁴³ Interestingly, it has been found that Gram-negative bacterial species are more susceptible to CAP treatment than Gram-positive species, despite their double outer membrane. This is thought to be due to their thinner cell wall (<10 nm, whereas Gram-positives are between 20-80 nm thick).¹⁴⁴

1.4.5.2 Biofilms

As previously discussed, bacteria often exist as biofilms which are significantly more resilient to environmental stresses and antimicrobial treatments. Biofilm formation poses a risk to human health when they form on the surfaces of contaminated foods, surfaces within a clinical setting, and within wounds. As such, these are potential areas where CAP therapy could be utilised.

Due to the great range of variables and potentially bactericidal products of CAP it is unsurprising that there are a multitude of mechanisms by which CAP treatment impacts bacterial biofilms. A number of studies have evaluated the depth of CAP generated RONS penetration into a bacterial biofilm matrix. Xiong *et al.* demonstrated that helium CAP was able to completely inactivate *Porphyromonas gingivalis* to a depth of 15 μm ¹⁴⁵ and Alkawareek *et al.* demonstrated that helium CAP was able to penetrate 40 and 80 μm into *P. aeruginosa* biofilms.¹⁴⁶ Importantly, findings by Duan *et al.* suggest that some RONS can penetrate through 500 μm of biological tissue, suggesting that the previous studies may have underestimated the penetration of RONS.¹⁴⁷ Further to this, CAP produced NO can signal the dispersal of the biofilm. NO is known to induce dispersal in multiple species including *P. aeruginosa* and *Vibrio cholera*.¹⁴⁸ CAP has also been shown to hinder QS within *P. aeruginosa* through the inactivation and chemical modification of N-acyl-homoserine lactone and inactivation of elastase and pyocyanin.¹⁴⁹

Whilst many studies that show the treatment and eradication of bacterial biofilms using CAP treatment, however, comparison is limited owing to the variability in both methodology of biofilm formation, bacterial species and plasma source. Despite this, the results are promising. Alkawareek *et al.* observed a 4-log reduction in *P. aeruginosa* biofilms after 4 minute treatment with He/O₂ plasma.¹⁴⁶ Denes *et al.* found that CAP is also effective in the treatment of mixed-species biofilms, decreasing the attachment of *S. epidermidis*, *P. fluorescens* and *S. typhimurium* by 56.5% and reducing biofilm formation by 72.2%.¹⁵⁰

1.5 Hydrogels

Hydrogels are three-dimensional, cross-linked, polymeric networks which are hydrophilic, and swollen with water. They can be produced through the simple reaction of one or more different monomers. Alternatively, they are polymeric materials which are able to swell and retain water without dissolving in it. Owing to their large water content hydrogels exhibit a degree of flexibility. Hydrogels can be made from naturally occurring or synthetically created polymers. Their high-water content and flexibility have resulted in great interest for application within biomedicine. Hydrogels can be synthesised in a number of ways, including polymerisation and parallel cross-linking of multifunctional monomers and multiple step procedures involving synthesis of polymer molecules and subsequent cross-linking of their reactive groups. This synthesis can be tailored for biodegradation, mechanical strength, chemical and biological response.

There are numerous ways of classifying a polymer. This can be based on their source in which they are classed as either natural or synthetic, according to polymeric composition. Homopolymer hydrogels are referred to as polymer network from a single species of monomer, copolymers are made up of two or more monomers. These often consist of one hydrophilic component and multipolymer interpenetrating polymeric hydrogel, made up of two independent cross-linked synthetic/natural polymer components in a network. Hydrogels can also be classified based on physical structure, into amorphous, semicrystalline and crystalline and physical appearance. They also vary in their electrical charge non-ionic, ionic, amphoteric and zwitterionic.¹⁵¹

Polymerisation is commonly initiated by compounds which generate free-radicals such as 2,2-azoisobutyronitrile (AIBN), benzoyl peroxide and ammonium peroxydisulphate or alternatively through the use of gamma, UV or electron radiation. As observed in **Figure 1.11A**, after polymerisation further purification is required to remove residual monomers. Yet this can be avoided through the use of ready-made water-soluble polymers as shown in **Figure 1.11B**. Frequently used polymers include poly(ethylene glycol), poly(acrylic acid), poly(vinylpyrrolidone) poly(vinyl alcohol), polyacrylamide and some polysaccharides.¹⁵²

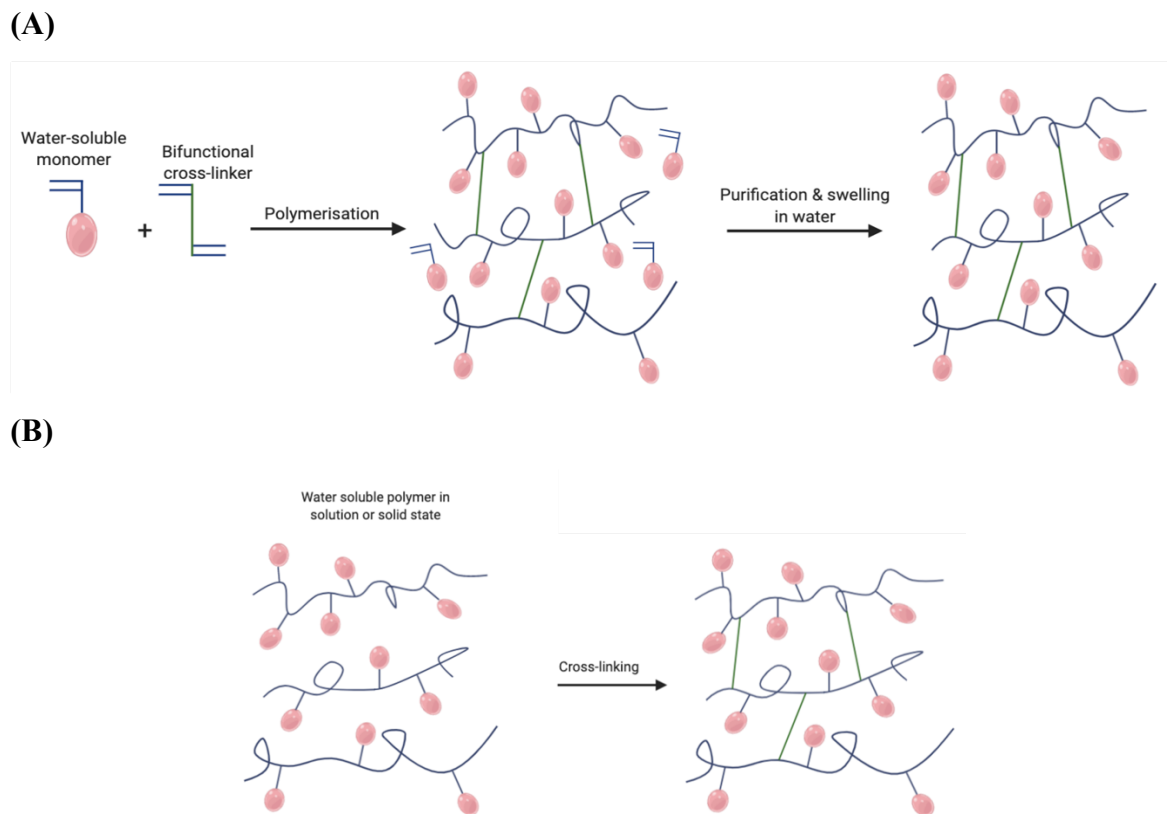


Figure 1.11: Synthesis of hydrogels through three-dimensional polymerisation (A). Synthesis of hydrogel by cross-linking of ready-made water-soluble polymers (B). (Created using BioRender).

Hydrogels are capable of holding large quantities of water, as water is the greatest component of the human body, thus providing great potential for biomedical applications such as tissue engineering, biosensors, wound dressings and drug delivery.¹⁵² One highly advantageous property of hydrogels within biomedicine is that they can be made to be responsive to various stimuli within the body such as temperature and pH or alternatively to an external stimulus such as light. Schoener *et al.* developed a pH-responsive hydrogel

which releases a therapeutic agent from a hydrogel in response to the change in pH from the stomach to the small intestines for the application of treatment of gastrointestinal (GI) and colon cancers.¹⁵³

1.6 Drug Delivery Systems

Drug delivery systems are designed to improve the therapeutic and pharmacological properties of a drug through either controlled release or targeted delivery of the drug. This is often done through the use of polymer or lipid-based nanoparticles. Traditional systemic delivery of drugs is associated with an increased risk of side effects and toxicity. This can be bypassed using drug delivery systems to administer the drug locally. Targeted drug delivery can be divided into two forms either passive, in which the system utilises tissue permeability altered either through disease pathology or owing to the properties of the delivery system, or active which is achieved through conjugation of the delivery system to a polymer or protein, enabling accumulation of the drug at a specific location.¹⁵⁴

The advantage of drug delivery systems is clearly highlighted within cancer therapies. Enabling the targeted delivery of often highly toxic chemotherapy drugs to the tumour site would significantly reduce side effects and increase the therapeutic dose being delivered to site. Nanoparticles are between 100-500 nm in size and can be modified for optimal bioavailability and increase stability which reduced clearance making them good drug delivery carriers.¹⁵⁵ Montero *et al.* describe a protein-based nanoparticle using human serum albumin-bound paclitaxel nanoparticles to deliver abraxane for improved solubility and tumour delivery to the tumour for the treatment of metastatic breast cancer.¹⁵⁶

Liposomes are spherical vesicles consisting of one or more phospholipid bilayers, whose biochemical and physiochemical properties can easily be manipulated, making attractive drug delivery systems.¹⁵⁷ Liposomes can encase hydrophilic and lipophilic compounds enabling them to carry a range of drugs, further, as they are composed of natural lipids that are pharmacologically inactive resulting in minimal toxicity.¹⁵⁸ Sriraman *et al.* report that doxorubicin can be administered via liposomes for the treatment of cancer.¹⁵⁹

1.7 Hydrogels as Drug Delivery Systems

As previously described the biocompatibility of hydrogels enables a broad range of biomedical applications of which drug delivery is one. Their cross-linking impedes the penetration of proteins reducing degradation risk particularly within the application of biological therapeutics.¹⁶⁰ The physical properties of hydrogels can be tuned to enable a range of pharmacological uses. There are three main categories: macroscopic gels, microgels and nanogels, as shown in **Figure 1.12**.

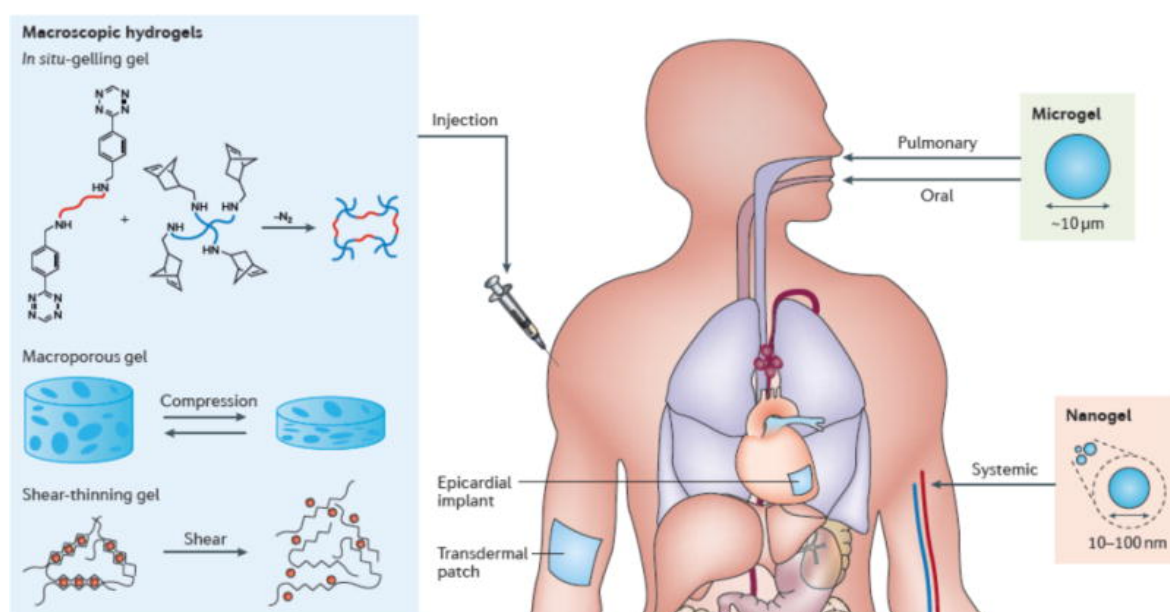


Figure 1.12: Classification of hydrogels based on subsequent route of delivery. (Reproduced with permission from Nature Reviews Materials).¹⁶¹

Microgels and nanogels are significantly smaller than macroscopic hydrogels, their size dictating the method of delivery. Microgels smaller than $5\ \mu\text{m}$ are delivered orally or through the pulmonary system but not intravascularly owing to their rapid clearance.¹⁶² Nanogels between 10-100 nm are suitable for intravascular delivery and are particularly favoured for the delivery of plasmid DNA within gene therapy, as they improve cellular uptake and increase circulation time.¹⁶³

Macroscopic hydrogels can be surgically implanted or placed on the body for transepithelial delivery. *In situ* gelling hydrogels, such as tetrazine-norbornene chemistry, microporous gels which can undergo reversible volume changes, which are frequently used within wound care

and shear thinning gels such as alginate hydrogels which are crosslinked with multivalent ions, shown in **Figure 1.12**.¹⁶¹

Within hydrogel drug delivery systems adhesion, toughness, mesh size and crosslinking network all play important roles in regulating drug delivery. The ability of a hydrogel to adhere to a surface will dictate its utility. For example, the mucosa and epithelial lining of the stomach is wet and slippery, as such, hydrogels will be unable to stick and thus will have limited utility.¹⁶⁴ Yet within wound care hydrogels adhere and are retained for a long time at the treatment site, maximising the delivery of the drug, the hydrogel needs to be tough to limit risk of tearing. Mesh size (typically 5-100 nm) is dictated by the crosslinking network and allows for liquids and small molecules to diffuse out of the hydrogel, the dynamics and rate of diffusion varying depending on mesh size.¹⁶¹ If the drug is smaller than the mesh size it will rapidly diffuse out. Where the mesh is equal to the drug size the drug release will be slow and if the drug is bigger than the mesh then the drug is physically trapped in the hydrogel. The entrapped drug can be released, or the rate of release can be increased through the degradation of the hydrogel network or increase swelling, owing to the increase the mesh size. This degradation can be achieved either through chemical reactions such as degradation of a polymer backbone, through enzymatic hydrolysis or enzymatic activity or mechanical means such as the application of ultrasound or a magnetic field.^{165,166}

1.8 Aims and Objectives

- The optimisation of a helium-driven cold atmospheric pressure plasma jet for the decontamination of bacterially infected wounds.
 - Quantify the biologically relevant RONS H_2O_2 and nitrates/nitrites
 - Maximise production of biologically relevant RONS while maintaining favourable mechanical interactions with a prototype PVA hydrogel wound dressing
- Investigate the interactions between bacteria and cold plasma.
 - Role of developing biofilm and bacterially produced enzyme catalase on mitigating plasma induced damage
 - Elucidate the mutagenic dose of helium-driven cold plasma
- Development of a CAP responsive hydrogel for the inhibition and eradication of bacterial biofilm-associated wound infection

1.9 References

1. Posnett, J., Gottrup, F., Lundgren, H. & Saal, G. The resource impact of wounds on health-care providers in Europe. *Journal of wound care* vol. 18 154–161 (2009).
2. Mulani, M. S., Kamble, E. E., Kumkar, S. N., Tawre, M. S. & Pardesi, K. R. Emerging strategies to combat ESKAPE pathogens in the era of antimicrobial resistance: A review. *Front. Microbiol.* **10**, 539 (2019).
3. Zhao, G. *et al.* Biofilms and Inflammation in Chronic Wounds. *Adv. Wound Care* **2**, 389–399 (2013).
4. de Kraker, M. E. A., Stewardson, A. J. & Harbarth, S. Will 10 Million People Die a Year due to Antimicrobial Resistance by 2050? *PLoS Med.* **13**, (2016).
5. Attinger, C. & Wolcott, R. Clinically Addressing Biofilm in Chronic Wounds. *Adv. Wound Care* **1**, 127–132 (2012).
6. Percival, N. J. Classification of Wounds and their Management. *Surg.* **20**, 114–117 (2002).
7. Monaco, J. A. L. & Lawrence, W. T. Acute wound healing: An overview. *Clinics in Plastic Surgery* vol. 30 1–12 (2003).
8. Fonder, M. A. *et al.* Treating the chronic wound: A practical approach to the care of nonhealing wounds and wound care dressings. *Journal of the American Academy of Dermatology* vol. 58 185–206 (2008).
9. Demidova-Rice, T. N., Hamblin, M. R. & Herman, I. M. Acute and impaired wound healing: Pathophysiology and current methods for drug delivery, part 1: Normal and chronic wounds: Biology, causes, and approaches to care. *Advances in Skin and Wound Care* vol. 25 304–314 (2012).
10. Eaglstein, W. H. & Falanga, V. Chronic wounds. *Surg. Clin. North Am.* **77**, 689–700 (1997).
11. Frykberg, R. G. & Banks, J. Challenges in the Treatment of Chronic Wounds. *Adv. Wound Care* **4**, 560–582 (2015).
12. Lee, C. K. & Hansen, S. L. Management of Acute Wounds. *Surgical Clinics of North America* vol. 89 659–676 (2009).
13. Ramasastry, S. S. Acute wounds. *Clinics in Plastic Surgery* vol. 32 195–208 (2005).
14. Anderson, K. & Hamm, R. L. Factors that impair wound healing. *Journal of the American College of Clinical Wound Specialists* vol. 4 84–91 (2012).
15. Wicke, C. *et al.* Aging influences wound healing in patients with chronic lower

- extremity wounds treated in a specialized wound care center. *Wound Repair Regen.* **17**, 25–33 (2009).
16. Guest, J. F. *et al.* Health economic burden that wounds impose on the National Health Service in the UK. *BMJ Open* **5**, (2015).
 17. Bonham, P. A. Identifying and treating wound infection: Topical and systemic antibiotic therapy. *J. Gerontol. Nurs.* **35**, 12–16 (2009).
 18. Morgan, E. D., Bledsoe, S. C. & Barker, J. Ambulatory Management of Burns. *Am. Fam. Physician* **62**, 2015–2026 (2000).
 19. Giretzlehner, M. *et al.* The determination of total burn surface area: How much difference? *Burns* **39**, 1107–1113 (2013).
 20. Tiwari, V. K. Burn wound: How it differs from other wounds. *Indian Journal of Plastic Surgery* vol. 45 364–373 (2012).
 21. Church, D., Elsayed, S., Reid, O., Winston, B. & Lindsay, R. Burn wound infections. *Clinical Microbiology Reviews* vol. 19 403–434 (2006).
 22. Salcido, R. ‘Sal’. What is Bioburden? *Adv. Skin Wound Care* **20**, 368–369 (2007).
 23. Moore, Z. & Cowman, S. Effective wound management: identifying criteria for infection - PubMed. *Nurs. Stand.* **21**, (2007).
 24. Leaper, D. J. *et al.* Extending the TIME concept: What have we learned in the past 10 years? *Int. Wound J.* **9**, 1–19 (2012).
 25. IWII. *WOUND INFECTION IN CLINICAL PRACTICE 2016 Principles of best practice.*
 26. Grice, E. A. & Segre, J. A. The skin microbiome. *Nature Reviews Microbiology* vol. 9 244–253 (2011).
 27. Sakr, A., Brégeon, F., Mège, J. L., Rolain, J. M. & Blin, O. Staphylococcus aureus nasal colonization: An update on mechanisms, epidemiology, risk factors, and subsequent infections. *Frontiers in Microbiology* vol. 9 (2018).
 28. Cundell, A. M. Microbial Ecology of the Human Skin. doi:10.1007/s00248-016-0789-6.
 29. White, R. J. The wound infection continuum. *Br. J. Community Nurs.* **7**, 7–9 (2002).
 30. ROBERTS, S. & CHAMBERS, S. Diagnosis and management of Staphylococcus aureus infections of the skin and soft tissue. *Intern. Med. J.* **35**, S97–S105 (2005).
 31. Healy, B. & Freedman, A. Infections. *BMJ* **332**, 838–841 (2006).
 32. Halstead, F. D. *et al.* A systematic review of quantitative burn wound microbiology in the management of burns patients. *Burns* **44**, 39–56 (2018).

Chapter 1

33. Bowler, P. G., Duerden, B. I. & Armstrong, D. G. Wound microbiology and associated approaches to wound management. *Clinical Microbiology Reviews* vol. 14 244–269 (2001).
34. Kallstrom, G. Are quantitative bacterial wound cultures useful? *Journal of Clinical Microbiology* vol. 52 2753–2756 (2014).
35. Hurley, C. M., McClusky, P., Sugrue, R. M., Clover, J. A. & Kelly, J. E. Efficacy of a bacterial fluorescence imaging device in an outpatient wound care clinic: a pilot study. *J. Wound Care* **28**, 438–443 (2019).
36. Horizon Scanning Centre, N. *WOUNDCHEK™ Protease Status point of care test for chronic wounds SUMMARY*. www.hsc.nihr.ac.uk.
37. (No Title). <http://www.io.nihr.ac.uk/wp-content/uploads/migrated/2274.5cdcae65.SystagenixWOUNDCHEKSep2012.pdf>.
38. Thet, N. T. *et al.* Prototype Development of the Intelligent Hydrogel Wound Dressing and Its Efficacy in the Detection of Model Pathogenic Wound Biofilms. (2015) doi:10.1021/acsami.5b07372.
39. Lindholm, C. & Searle, R. Wound management for the 21st century: combining effectiveness and efficiency. *Int. Wound J.* **13**, 5–15 (2016).
40. Sood, A., Granick, M. S. & Tomaselli, N. L. Wound Dressings and Comparative Effectiveness Data. *Adv. Wound Care* **3**, 511–529 (2014).
41. Dhivya, S., Padma, V. V. & Santhini, E. Wound dressings - A review. *BioMedicine (Netherlands)* vol. 5 24–28 (2015).
42. Guo, S. & DiPietro, L. A. Critical review in oral biology & medicine: Factors affecting wound healing. *J. Dent. Res.* **89**, 219–229 (2010).
43. Woodley, D. T., O’Keefe, E. J. & Prunieras, M. Cutaneous wound healing: A model for cell-matrix interactions. *J. Am. Acad. Dermatol.* **12**, 420–433 (1985).
44. Stein, C. & Kuchler, S. Targeting inflammation and wound healing by opioids. *Trends in Pharmacological Sciences* vol. 34 303–312 (2013).
45. Donlan, R. M. Biofilms: Microbial life on surfaces. *Emerging Infectious Diseases* vol. 8 881–890 (2002).
46. Khatoon, Z., McTiernan, C. D., Suuronen, E. J., Mah, T. F. & Alarcon, E. I. Bacterial biofilm formation on implantable devices and approaches to its treatment and prevention. *Heliyon* vol. 4 1067 (2018).
47. Flemming, H. C., Neu, T. R. & Wozniak, D. J. The EPS matrix: The ‘House of Biofilm Cells’. *Journal of Bacteriology* vol. 189 7945–7947 (2007).

48. Miller, M. B. & Bassler, B. L. Quorum sensing in bacteria. *Annual Review of Microbiology* vol. 55 165–199 (2001).
49. Jamal, M. *et al.* Bacterial biofilm and associated infections. *Journal of the Chinese Medical Association* vol. 81 7–11 (2018).
50. Wiegel, J. Distinction between the gram reaction and the gram type of bacteria. *Int. J. Syst. Bacteriol.* **31**, 88 (1981).
51. Taylor, T. A. & Unakal, C. G. *Staphylococcus Aureus*. (StatPearls Publishing, Treasure Island (FL), 2019).
52. Lowy, F. D. Staphylococcus aureus Infections. *N. Engl. J. Med.* **339**, 520–532 (1998).
53. Arciola, C. R., Campoccia, D., Ravaioli, S. & Montanaro, L. Polysaccharide intercellular adhesin in biofilm: Structural and regulatory aspects. *Frontiers in Cellular and Infection Microbiology* vol. 5 (2015).
54. Lister, J. L. & Horswill, A. R. Staphylococcus aureus biofilms: Recent developments in biofilm dispersal. *Front. Cell. Infect. Microbiol.* **4**, (2014).
55. Archer, N. K. *et al.* Staphylococcus aureus biofilms: Properties, regulation and roles in human disease. *Virulence* vol. 2 445–459 (2011).
56. Lew, P. D. P. & Waldvogel, P. F. A. Osteomyelitis. in *Lancet* vol. 364 369–379 (Lancet, 2004).
57. Costerton, J. W., Montanaro, L. & Arciola, C. R. Biofilm in implant infections: Its production and regulation. *Int. J. Artif. Organs* **28**, 1062–1068 (2005).
58. Røder, B. L. *et al.* Clinical features of Staphylococcus aureus endocarditis: A 10-year experience in Denmark. *Arch. Intern. Med.* **159**, 462–469 (1999).
59. Cross, A. *et al.* Nosocomial infections due to Pseudomonas aeruginosa: review of recent trends. *Reviews of infectious diseases* vol. 5 Suppl 5 (1983).
60. Bhagirath, A. Y. *et al.* Cystic fibrosis lung environment and Pseudomonas aeruginosa infection. *BMC Pulm. Med.* **16**, (2016).
61. Azam, M. W. & Khan, A. U. Updates on the pathogenicity status of Pseudomonas aeruginosa. *Drug Discovery Today* vol. 24 350–359 (2019).
62. Rasamiravaka, T., Labtani, Q., Duez, P. & El Jaziri, M. The formation of biofilms by pseudomonas aeruginosa: A review of the natural and synthetic compounds interfering with control mechanisms. *BioMed Research International* vol. 2015 (2015).
63. Vasil, M. L. Pseudomonas aeruginosa: Biology, mechanisms of virulence, epidemiology. *J. Pediatr.* **108**, 800–805 (1986).

Chapter 1

64. Maurice, N. M., Bedi, B. & Sadikot, R. T. *Pseudomonas aeruginosa* biofilms: Host response and clinical implications in lung infections. *American Journal of Respiratory Cell and Molecular Biology* vol. 58 428–439 (2018).
65. Bennett, J. W. & Chung, K. T. Alexander Fleming and the discovery of penicillin. *Advances in Applied Microbiology* vol. 49 163–184 (2001).
66. Gaynes, R. The discovery of penicillin—new insights after more than 75 years of clinical use. *Emerg. Infect. Dis.* **23**, 849–853 (2017).
67. Davies, J. Where have all the antibiotics gone? in *Canadian Journal of Infectious Diseases and Medical Microbiology* vol. 17 287–290 (Hindawi Limited, 2006).
68. Oates, J. A., Wood, A. J. j., Donowitz, G. R. & Mandell, G. L. Beta-Lactam Antibiotics. *New England Journal of Medicine* vol. 318 490–500 (1988).
69. Mingeot-Leclercq, M. P., Glupczynski, Y. & Tulkens, P. M. Aminoglycosides: Activity and resistance. *Antimicrobial Agents and Chemotherapy* vol. 43 727–737 (1999).
70. Fernández, M. *et al.* Mechanisms of resistance to chloramphenicol in *Pseudomonas putida* KT2440. *Antimicrob. Agents Chemother.* **56**, 1001–1009 (2012).
71. Faron, M. L., Ledebøer, N. A. & Buchan, B. W. Resistance mechanisms, epidemiology, and approaches to screening for vancomycin-resistant *Enterococcus* in the health care setting. *Journal of Clinical Microbiology* vol. 54 2436–2447 (2016).
72. Hooper, D. C. & Jacoby, G. A. Topoisomerase inhibitors: Fluoroquinolone mechanisms of action and resistance. *Cold Spring Harb. Perspect. Med.* **6**, a025320 (2016).
73. Bozdoğan, B. & Appelbaum, P. C. Oxazolidinones: Activity, mode of action, and mechanism of resistance. *International Journal of Antimicrobial Agents* vol. 23 113–119 (2004).
74. Chopra, I. & Roberts, M. Tetracycline Antibiotics: Mode of Action, Applications, Molecular Biology, and Epidemiology of Bacterial Resistance. *Microbiol. Mol. Biol. Rev.* **65**, 232–260 (2001).
75. Grossman, T. H. Tetracycline antibiotics and resistance. *Cold Spring Harb. Perspect. Med.* **6**, (2016).
76. Mazzei, T., Mini, E., Novelli, A. & Periti, P. Chemistry and mode of action of macrolides. *J. Antimicrob. Chemother.* **31**, 1–9 (1993).
77. Pechère, J. C. Macrolide resistance mechanisms in Gram-positive cocci. *Int. J. Antimicrob. Agents* **18**, 25–28 (2001).

78. Willemsen, I., Bogaers-Hofman, D., Winters, M. & Kluytmans, J. Correlation between antibiotic use and resistance in a hospital: Temporary and ward-specific observations. *Infection* **37**, 432–437 (2009).
79. Sun, D., Jeannot, K., Xiao, Y. & Knapp, C. W. Editorial: Horizontal Gene Transfer Mediated Bacterial Antibiotic Resistance. *Front. Microbiol.* **10**, 1933 (2019).
80. Llor, C. & Bjerrum, L. Antimicrobial resistance: Risk associated with antibiotic overuse and initiatives to reduce the problem. *Therapeutic Advances in Drug Safety* vol. 5 229–241 (2014).
81. Zhanel, G. G., Hoban, D. J. & Harding, G. K. Subinhibitory Antimicrobial Concentrations: A Review of In Vitro and In Vivo Data. *Can. J. Infect. Dis.* **3**, 193–201 (1992).
82. Landers, T. F., Cohen, B., Wittum, T. E. & Larson, E. L. A review of antibiotic use in food animals: Perspective, policy, and potential. *Public Health Reports* vol. 127 4–22 (2012).
83. Pormohammad, A., Nasiri, M. J. & Azimi, T. Prevalence of antibiotic resistance in escherichia coli strains simultaneously isolated from humans, animals, food, and the environment: A systematic review and meta-analysis. *Infection and Drug Resistance* vol. 12 1181–1197 (2019).
84. Unemo, M. & Shafer, W. M. Antibiotic resistance in *Neisseria gonorrhoeae*: origin, evolution, and lessons learned for the future. *Annals of the New York Academy of Sciences* vol. 1230 E19 (2011).
85. Zhu, L., Lin, J., Ma, J., Cronan, J. E. & Wang, H. Triclosan resistance of *Pseudomonas aeruginosa* PAO1 is due to FabV, a triclosan-resistant enoyl-acyl carrier protein reductase. *Antimicrob. Agents Chemother.* **54**, 689–698 (2010).
86. Webber, M. A. The importance of efflux pumps in bacterial antibiotic resistance. *J. Antimicrob. Chemother.* **51**, 9–11 (2003).
87. Long, K. S., Poehlsgaard, J., Kehrenberg, C., Schwarz, S. & Vester, B. The Cfr rRNA methyltransferase confers resistance to phenicols, lincosamides, oxazolidinones, pleuromutilins, and streptogramin A antibiotics. *Antimicrob. Agents Chemother.* **50**, 2500–2505 (2006).
88. Darmstadt, G. L. & Lane, A. T. Impetigo: An Overview. *Pediatr. Dermatol.* **11**, 293–303 (1994).
89. Lipsky, B. A., Hoey, C., Cruciani, M. & Mengoli, C. Topical antimicrobial agents for preventing and treating foot infections in people with diabetes. *Cochrane Database*

- Syst. Rev.* **2014**, (2014).
90. Gelmetti, C. Local antibiotics in dermatology. *Dermatol. Ther.* **21**, 187–195 (2008).
 91. Loo, A. E. K. *et al.* Effects of Hydrogen Peroxide on Wound Healing in Mice in Relation to Oxidative Damage. *PLoS One* **7**, e49215 (2012).
 92. Wittmann, C. *et al.* Hydrogen peroxide in inflammation: Messenger, guide, and assassin. *Advances in Hematology* vol. 2012 (2012).
 93. Loo, A. E. K. *et al.* Effects of Hydrogen Peroxide on Wound Healing in Mice in Relation to Oxidative Damage. *PLoS One* **7**, e49215 (2012).
 94. Bryan, N. *et al.* Reactive oxygen species (ROS) - A family of fate deciding molecules pivotal in constructive inflammation and wound healing. *Eur. Cells Mater.* **24**, 249–265 (2012).
 95. Hoffmann, M. E. & Meneghini, R. ACTION OF HYDROGEN PEROXIDE ON HUMAN FIBROBLAST IN CULTURE. *Photochem. Photobiol.* **30**, 151–155 (1979).
 96. Vessey, D. A., Lee, K. H. & Blacker, K. L. Characterization of the oxidative stress initiated in cultured human keratinocytes by treatment with peroxides. *J. Invest. Dermatol.* **99**, 859–863 (1992).
 97. Watt, B. E., Proudfoot, A. T. & Vale, J. A. Hydrogen peroxide poisoning. *Toxicological Reviews* vol. 23 51–57 (2004).
 98. Farha, M. A. & Brown, E. D. Drug repurposing for antimicrobial discovery. *Nat. Microbiol.* **2019 44 4**, 565–577 (2019).
 99. It's time to fix the antibiotic market. <https://wellcome.ac.uk/what-we-do/our-work/drug-resistant-infections/its-time-fix-broken-antibiotics-market>.
 100. Karine de Sousa, A. *et al.* New roles of fluoxetine in pharmacology: Antibacterial effect and modulation of antibiotic activity. *Microb. Pathog.* **123**, 368–371 (2018).
 101. Heinlin, J. *et al.* Plasma medicine: possible applications in dermatology. *JDDG J. der Dtsch. Dermatologischen Gesellschaft* **8**, 968–976 (2010).
 102. Fridman, G. *et al.* Applied Plasma Medicine. *Plasma Process. Polym.* **5**, 503–533 (2008).
 103. Ginsberg, G. G. *et al.* The argon plasma coagulator: February 2002. *Gastrointest. Endosc.* **55**, 807–810 (2002).
 104. Lord, M. J., Maltry, J. A. & Shall, L. M. Thermal injury resulting from arthroscopic lateral retinacular release by electrocautery: Report of three cases and a review of the literature. *Arthrosc. J. Arthrosc. Relat. Surg.* **7**, 33–37 (1991).

105. Weltmann, K. D. & Von Woedtke, T. Plasma medicine - Current state of research and medical application. *Plasma Phys. Control. Fusion* **59**, (2017).
106. Hoffmann, C., Berganza, C. & Zhang, J. Cold Atmospheric Plasma: Methods of production and application in dentistry and oncology. *Medical Gas Research* vol. 3 (2013).
107. Laroussi, M., Lu, X. & Keidar, M. Perspective: The physics, diagnostics, and applications of atmospheric pressure low temperature plasma sources used in plasma medicine. *J. Appl. Phys.* **122**, 20901 (2017).
108. Laroussi, M. Cold Plasma in Medicine and Healthcare: The New Frontier in Low Temperature Plasma Applications. *Front. Phys.* **8**, 74 (2020).
109. Slikboer, E., Acharya, K., Sobota, A., Garcia-Caurel, E. & Guaitella, O. Revealing Plasma-Surface Interaction at Atmospheric Pressure: Imaging of Electric Field and Temperature inside the Targeted Material. *Sci. Rep.* **10**, 1–10 (2020).
110. Daeschlein, G. *et al.* Skin decontamination by low-temperature atmospheric pressure plasma jet and dielectric barrier discharge plasma. *J. Hosp. Infect.* **81**, 177–183 (2012).
111. Kramer, A. *et al.* Suitability of tissue tolerable plasmas (TTP) for the management of chronic wounds. *Clinical Plasma Medicine* vol. 1 11–18 (2013).
112. Stratmann, B. *et al.* Effect of Cold Atmospheric Plasma Therapy vs Standard Therapy Placebo on Wound Healing in Patients With Diabetic Foot Ulcers: A Randomized Clinical Trial. *JAMA Netw. open* **3**, e2010411 (2020).
113. Bekeschus, S., Schmidt, A., Weltmann, K. D. & von Woedtke, T. The plasma jet kINPen – A powerful tool for wound healing. *Clin. Plasma Med.* **4**, 19–28 (2016).
114. Schönebeck, R. kINPen MED®. in *Comprehensive Clinical Plasma Medicine: Cold Physical Plasma for Medical Application* 485–494 (Springer International Publishing, 2018). doi:10.1007/978-3-319-67627-2_32.
115. Shimizu, T. *et al.* Characterization of microwave plasma torch for decontamination. *Plasma Process. Polym.* **5**, 577–582 (2008).
116. Arndt, S., Schmidt, A., Karrer, S. & von Woedtke, T. Comparing two different plasma devices kINPen and Adtec SteriPlas regarding their molecular and cellular effects on wound healing. *Clinical Plasma Medicine* vol. 9 24–33 (2018).
117. Isbary, G. *et al.* Randomized placebo-controlled clinical trial showed cold atmospheric argon plasma relieved acute pain and accelerated healing in herpes zoster. *Clin. Plasma Med.* **2**, 50–55 (2014).

118. Isbary, G. *et al.* A first prospective randomized controlled trial to decrease bacterial load using cold atmospheric argon plasma on chronic wounds in patients. *Br. J. Dermatol.* **163**, 78–82 (2010).
119. Goree, J., Liu, B., Drake, D. & Stoffels, E. Killing of *S. mutans* bacteria using a plasma needle at atmospheric pressure. *IEEE Trans. Plasma Sci.* **34**, 1317–1324 (2006).
120. Kang, S. K. *et al.* Reactive hydroxyl radical-driven oral bacterial inactivation by radio frequency atmospheric plasma. *Appl. Phys. Lett.* **98**, 143702 (2011).
121. Mahasneh, A. *et al.* Inactivation of *Porphyromonas gingivalis* by low-temperature atmospheric pressure plasma. *Plasma Med.* **1**, 191–204 (2011).
122. Lee, H. W. *et al.* Tooth Bleaching with Nonthermal Atmospheric Pressure Plasma. *J. Endod.* **35**, 587–591 (2009).
123. Fridman, G. *et al.* Floating electrode dielectric barrier discharge plasma in air promoting apoptotic behavior in Melanoma skin cancer cell lines. *Plasma Chem. Plasma Process.* **27**, 163–176 (2007).
124. Partecke, L. I. *et al.* Tissue Tolerable Plasma (TTP) induces apoptosis in pancreatic cancer cells in vitro and in vivo. *BMC Cancer* **12**, 473 (2012).
125. Walk, R. M. *et al.* Cold atmospheric plasma for the ablative treatment of neuroblastoma. *J. Pediatr. Surg.* **48**, 67–73 (2013).
126. Kim, C. H. *et al.* Effects of atmospheric nonthermal plasma on invasion of colorectal cancer cells. *Appl. Phys. Lett.* **96**, 243701 (2010).
127. Volotskova, O., Dubrovsky, L., Keidar, M. & Bukrinsky, M. Cold atmospheric plasma inhibits HIV-1 replication in macrophages by targeting both the virus and the cells. *PLoS One* **11**, (2016).
128. Chen, Z., Garcia, G., Arumugaswami, V. & Wirz, R. E. Cold atmospheric plasma for SARS-CoV-2 inactivation. *Phys. Fluids* **32**, 111702 (2020).
129. Bernhardt, T. *et al.* Plasma Medicine: Applications of Cold Atmospheric Pressure Plasma in Dermatology. (2019) doi:10.1155/2019/3873928.
130. Schmid-Wendtner, M.-H. & Korting, H. C. The pH of the Skin Surface and Its Impact on the Barrier Function. *Skin Pharmacol. Physiol.* **19**, 296–302 (2006).
131. Öhman, H. & Vahlquist, A. The pH gradient over the stratum corneum differs in X-linked recessive and autosomal dominant ichthyosis: A clue to the molecular origin of the ‘acid skin mantle’? *J. Invest. Dermatol.* **111**, 674–677 (1998).
132. Seidenari, S. & Giusti, G. Objective assessment of the skin of children affected by

- atopic dermatitis: A study of pH, capacitance and TEWL in eczematous and clinically uninvolved skin. *Acta Derm. Venereol.* **75**, 429–433 (1995).
133. Chutsirimongkol, C., Boonyawan, D., Polnikorn, N., Techawatthanawisan, W. & Kundilokchai, T. Non-thermal plasma for acne treatment and aesthetic skin improvement. *Plasma Med.* **4**, 79–88 (2014).
 134. Kim, S. J. & Chung, T. H. Cold atmospheric plasma jet-generated RONS and their selective effects on normal and carcinoma cells. *Sci. Rep.* **6**, (2016).
 135. Chaple, S. *et al.* Effect of atmospheric cold plasma on the functional properties of whole wheat (*Triticum aestivum* L.) grain and wheat flour. *Innov. Food Sci. Emerg. Technol.* **66**, 102529 (2020).
 136. Khlyustova, A., Labay, C., Machala, Z., Ginebra, M.-P. & Canal, C. Important parameters in plasma jets for the production of RONS in liquids for plasma medicine: A brief review. *Front. Chem. Sci. Eng.* **13**, 238–252 (2019).
 137. Oehmigen, K. *et al.* The role of acidification for antimicrobial activity of atmospheric pressure plasma in liquids. *Plasma Process. Polym.* **7**, 250–257 (2010).
 138. Girard, P. M. *et al.* Synergistic Effect of H₂O₂ and NO₂ in Cell Death Induced by Cold Atmospheric He Plasma. *Sci. Rep.* **6**, (2016).
 139. Connor, M. *et al.* Evolutionary clade affects resistance of *Clostridium difficile* spores to Cold Atmospheric Plasma. *Sci. Rep.* **7**, (2017).
 140. Claro, T., Cahill, O. J., O'Connor, N., Daniels, S. & Humphreys, H. Cold-Air Atmospheric Pressure Plasma Against *Clostridium difficile* Spores: A Potential Alternative for the Decontamination of Hospital Inanimate Surfaces. *Infect. Control Hosp. Epidemiol.* **36**, 742–744 (2015).
 141. Hayes, J., Kirf, D., Garvey, M. & Rowan, N. Disinfection and toxicological assessments of pulsed UV and pulsed-plasma gas-discharge treated-water containing the waterborne protozoan enteroparasite *Cryptosporidium parvum*. *J. Microbiol. Methods* **94**, 325–337 (2013).
 142. Heaselgrave, W., Shama, G., Andrew, P. W. & Kong, M. G. Inactivation of *Acanthamoeba* spp. and other ocular pathogens by application of cold atmospheric gas plasma. *Appl. Environ. Microbiol.* **82**, 3143–3148 (2016).
 143. Theinkom, F. *et al.* Antibacterial efficacy of cold atmospheric plasma against *Enterococcus faecalis* planktonic cultures and biofilms in vitro. *PLoS One* **14**, e0223925 (2019).
 144. Mai-Prochnow, A., Clauson, M., Hong, J. & Murphy, A. B. Gram positive and Gram

- negative bacteria differ in their sensitivity to cold plasma. *Sci. Rep.* **6**, (2016).
145. Xiong, Z., Du, T., Lu, X., Cao, Y. & Pan, Y. How deep can plasma penetrate into a biofilm? *Appl. Phys. Lett.* **98**, 221503 (2011).
 146. Alkawareek, M. Y. *et al.* Eradication of *Pseudomonas aeruginosa* Biofilms by Atmospheric Pressure Non-Thermal Plasma. *PLoS One* **7**, (2012).
 147. Duan, J., Lu, X. & He, G. On the penetration depth of reactive oxygen and nitrogen species generated by a plasma jet through real biological tissue. *Phys. Plasmas* **24**, 073506 (2017).
 148. Barraud, N. *et al.* Involvement of nitric oxide in biofilm dispersal of *Pseudomonas aeruginosa*. *J. Bacteriol.* **188**, 7344–7353 (2006).
 149. Ziuzina, D., Boehm, D., Patil, S., Cullen, P. J. & Bourke, P. Cold plasma inactivation of bacterial biofilms and reduction of quorum sensing regulated virulence factors. *PLoS One* **10**, (2015).
 150. Denes, A. R., Somers, E. B., Wong, A. C. L. & Denes, F. 12-crown-4-ether and tri(ethylene glycol) dimethyl-ether plasma-coated stainless steel surfaces and their ability to reduce bacterial biofilm deposition. *J. Appl. Polym. Sci.* **81**, 3425–3438 (2001).
 151. Ahmed, E. M. Hydrogel: Preparation, characterization, and applications: A review. *Journal of Advanced Research* vol. 6 105–121 (2015).
 152. Caló, E. & Khutoryanskiy, V. V. Biomedical applications of hydrogels: A review of patents and commercial products. *European Polymer Journal* vol. 65 252–267 (2015).
 153. Schoener, C. A., Hutson, H. N. & Peppas, N. A. PH-responsive hydrogels with dispersed hydrophobic nanoparticles for the oral delivery of chemotherapeutics. *J. Biomed. Mater. Res. - Part A* **101 A**, 2229–2236 (2013).
 154. Tiwari, G. *et al.* Drug delivery systems: An updated review. *Int. J. Pharm. Investig.* **2**, 2 (2012).
 155. Rizvi, S. A. A. & Saleh, A. M. Applications of nanoparticle systems in drug delivery technology. *Saudi Pharmaceutical Journal* vol. 26 64–70 (2018).
 156. Montero, A. J., Adams, B., Diaz-Montero, C. M. & Glück, S. Nab-paclitaxel in the treatment of metastatic breast cancer: A comprehensive review. *Expert Review of Clinical Pharmacology* vol. 4 329–334 (2011).
 157. Dimov, N., Kastner, E., Hussain, M., Perrie, Y. & Szita, N. Formation and purification of tailored liposomes for drug delivery using a module-based micro

- continuous-flow system. *Sci. Rep.* **7**, 1–13 (2017).
158. Sercombe, L. *et al.* Advances and challenges of liposome assisted drug delivery. *Frontiers in Pharmacology* vol. 6 286 (2015).
159. Sriraman, S. K., Salzano, G., Sarisozen, C. & Torchilin, V. Anti-cancer activity of doxorubicin-loaded liposomes co-modified with transferrin and folic acid. *Eur. J. Pharm. Biopharm.* **105**, 40–49 (2016).
160. Wang, K. *et al.* Functional Hydrogels and Their Application in Drug Delivery, Biosensors, and Tissue Engineering. *Int. J. Polym. Sci.* **2019**, 3160732 (2019).
161. Li, J. & Mooney, D. J. Designing hydrogels for controlled drug delivery. *Nature Reviews Materials* vol. 1 (2016).
162. Wang, K. *et al.* Functional Hydrogels and Their Application in Drug Delivery, Biosensors, and Tissue Engineering. *International Journal of Polymer Science* vol. 2019 (2019).
163. Ginn, S. L., Alexander, I. E., Edelstein, M. L., Abedi, M. R. & Wixon, J. Gene therapy clinical trials worldwide to 2012 - an update. *Journal of Gene Medicine* vol. 15 65–77 (2013).
164. Liu, J. *et al.* Triggerable tough hydrogels for gastric resident dosage forms. *Nat. Commun.* **8**, 1–10 (2017).
165. Lee, K. Y., Peters, M. C., Anderson, K. W. & Mooney, D. J. Controlled growth factor release from synthetic extracellular matrices. *Nature* **408**, 998–1000 (2000).
166. Huebsch, N. *et al.* Ultrasound-triggered disruption and self-healing of reversibly cross-linked hydrogels for drug delivery and enhanced chemotherapy. *Proc. Natl. Acad. Sci. U. S. A.* **111**, 9762–9767 (2014).

Chapter 1

Chapter 2

Chapter 2 : Materials, Methods and Instrument Theory

2.1 Materials

2.1.1 Bacterial Strains

Staphylococcus aureus (*S. aureus*) strain H560, Methicillin-resistant *Staphylococcus aureus* (MRSA) strain MRSA252, *Pseudomonas aeruginosa* (*P. aeruginosa*) stain PAO1 were obtained from the Jenkins Collection, University of Bath. *Escherichia coli* (*E. coli*) strain NCTC 10418 was obtained from the Yves-Mallard Group, University of Cardiff. *E. coli* strains BW25113, WP2 and *uvrA*⁻ were purchased from the Yale *E. coli* stock centre. *E. coli* strains PNW11-1, PNW11-2 and PNW11-4A were donated from the University of British Columbia.

2.1.2 Chemicals

Tryptic soy broth (TSB), tryptic soy agar (TSA), brain heart infusion agar (BHIA), fetal bovine serum, agarose, H₂O₂ solution (33% (v/v)), titanium oxysulphate solution, potassium iodide, crystal violet, gelred[®], glycerol, polyvinyl alcohol (PVA) (MW 146000-186000), Whatman[®] nuclepore[™] track-etched membranes (diameter 25 & 19 mm, pore size 0.2 μm, polycarbonate) were purchased from Sigma-Aldrich (Poole, Dorset, UK).

Invitrogen[™] molecular probes[™] LIVE/DEAD[™] BacLight[™] bacterial viability kit for microscopy L7007, Luria Bertani agar (LBA), Luria broth base (Miller's LB broth base)(LB), phosphate buffer saline (PBS) tables, D (+) glucose, TAE buffer and primers were purchased from Fischer Scientific (Leicestershire, UK).

X2 GoTaq mastermix was purchased from New England Biolabs (Ipswich, UK).

2.2 Bacterial Growth

2.2.1 Principles of Bacterial Growth

For consistent and reproducible microbiological data, bacteria are first grown within liquid culture medium, containing optimum nutrient concentrations and growth conditions for maximum bacterial proliferation and growth. Cultures can then be streaked onto solid agar plates to separate out species and obtain pure cultures from mixed broth or maintain pure stocks of individual species. From these pure plate cultures, bacterial isolates can be stored in 15% (v/v) of glycerol at $-80\text{ }^{\circ}\text{C}$ creating freeze stocks for long term storage. Alternatively, liquid cultures can be aliquoted onto solid agar to enumerate the total number of bacterial cells present within the culture.

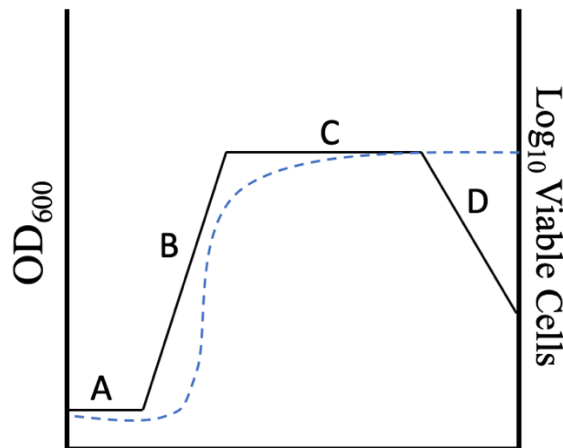


Figure 2.1: Standard bacterial growth curve showing change in OD (dotted line) changing with viable bacterial cells (solid line) over time. (A) lag phase, (B) exponential phase, (C) stationary phase and (D) death phase.

Bacterial growth consists of four distinct phases lag, exponential, stationary and death phase (**Figure 2.1**) Lag phase consists of the bacteria preparing for replication, through DNA synthesis and upregulation and production of enzymes. Cells then enter the exponential phase, where cell replication occurs at that the maximum rate, increasing bacterial population at an exponential rate. Then, once the bacterial population have exhausted the available space and nutrients, they enter stationary phase where the rate of bacterial growth is equal to the rate of death, resulting in no net change. Finally, when conditions exceed the bacteria's tolerance, they move into death phase, when the bacterial population begins to decline. Bacterial growth can be monitored photometrically by measuring the optical density (OD) of the bacterial culture periodically over time. The OD reading correlates the light

scattering of the culture with the quantification of bacterial turbidity. Bacterial growth phase and viable cell counts over time are shown in **Figure 2.1**.

2.2.2 Growth Conditions

All bacteria were maintained in 15% (v/v) glycerol stocks at $-80\text{ }^{\circ}\text{C}$ and streaked out on agar plates as required. Gram-positive bacteria were grown statically at $37\text{ }^{\circ}\text{C}$ on TSA and Gram-negative were grown on LBA. Overnight (ON) cultures were grown by inoculating bacterial broth with a single bacterial colony and then grown at $37\text{ }^{\circ}\text{C}$ for 18 h at 200 rpm to maintain turbidity. Gram-positive bacteria were cultured in TSB and Gram-negative bacteria in LB. Subcultures were obtained through dilution of ON culture into either fresh broth or PBS, by carrying out a 1 in 1000 dilution to OD of ~ 0.1 (1.5×10^5 CFU/mL).

2.2.3 Quantification of Bacteria

Colony forming units (CFU) are used to estimate the number of viable bacterial cells in a culture as one viable cell gives rise to one colony. CFU enumeration is carried out through plate counting. The Miles & Misra method was used to enumerate viable bacteria cells.¹ Bacterial cultures were serially diluted ($100\text{ }\mu\text{L}$ in $900\text{ }\mu\text{L}$ of PBS) from 10^{-1} to 10^{-8} . $10\text{ }\mu\text{L}$ of each dilution was then spotted in triplicate, shown in **Figure 2.2**, to obtain single colonies onto the appropriate bacteriological agar.

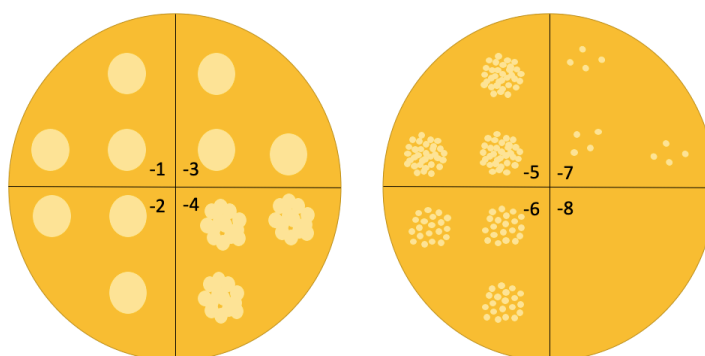


Figure 2.2: Schematic demonstrating the Miles & Misra method.

Plates were subsequently incubated, statically for 18 h at $37\text{ }^{\circ}\text{C}$. After incubation total number single colonies per spot were counted, ideally spots with between 20-50 colonies for increased accuracy. The average was taken then CFU/mL was calculated according to **Equation 2.1**.

$$\frac{\text{CFU}}{\text{mL}} = \frac{\text{Average number of colonies} \times \text{Dilution factor}}{\text{Amount aliquoted onto plate}} \quad (1)$$

Equation 2.1: Calculation for the enumeration of colony forming units per mL

2.3 Bacterial Biofilm Methods

2.3.1 96-well Plate Model

ON culture was subcultured by adding 10 μL of ON culture into 10 mL of D (+) glucose supplemented broth for the cultivation of biofilms. For Gram-negative species LB broth was supplemented with 50% (v/v) of D (+) glucose and for Gram-positive species TSB broth was supplemented with 1% (v/v). 200 μL of bacterial subculture was then added to wells of 96-well plate, with a column of wells with only supplemented 200 μL broth serving as a negative control. Plates were then grown statically at either 32 $^{\circ}\text{C}$ or 37 $^{\circ}\text{C}$ for desired time.

2.3.2 Crystal Violet Staining of 96-well Plate Model

96-well plate biofilms were prepared as per 2.3.1. After incubation the contents of the 96-well plate were removed, and all wells washed two times with sterile PBS (pH 7.4, 25 $^{\circ}\text{C}$) and left to dry at 25 $^{\circ}\text{C}$ for 2-3 h. 210 μL of 0.1% (w/v) crystal violet solution was added to all wells and left to incubate at 25 $^{\circ}\text{C}$ for 15 mins. Well content was removed, and all wells were washed with sterile PBS two times. The 96-well plate was left to dry for 2-3 h at 25 $^{\circ}\text{C}$. 210 μL of 30% (v/v) glacial acetic acid was added to all wells and left to elute dye for 15 mins. After incubation 125 μL was removed from each well and placed into a fresh 96-well plate. Absorbance was read at 510 nm using FLUROstart plate reader. All values were blank corrected to 125 μL of Glacial Acetic Acid.

P. aeruginosa biofilms, owing to their motility, form biofilms at the liquid-air interface, whereas *S. aureus* lacks motility and form biofilms by binding to the bottom of the well.

2.3.3 Polycarbonate Membrane – *In vitro* Wound Biofilm Model

Whatman polycarbonate membranes (white, 19/25 mm in diameter, pore size 200 nm) were placed shiny side up atop BHIA and were UV-C sterilised for 10 minutes (**Figure 2.3**). For 19 mm membrane: 20 μL of artificial wound fluid (AWF), 1:1 foetal calf serum and peptone, was added to the membrane and allowed to dry. 30 μL of bacterial subculture ($\sim 1 \times 10^5$ CFU/ml) was then added to the membrane. Plates were then incubated statically for desired time at either 32 °C or 37 °C. For 25 mm membrane: 30 μL of AWF was added and 50 μL of bacterial subculture. Biofilms were then exposed to antimicrobial treatment. After exposure to “antimicrobial” polycarbonate biofilms were removed from BHIA using sterile tweezers and placed into 5 mL of sterile PBS in 15 mL Falcon tube. The biofilm suspension was then vortexed for 1 minute and sonicated for 15 minutes. This was repeated twice to ensure removal of all bound cells. The biofilm suspension was then serially diluted and viable cells enumerated as in 2.2.3.

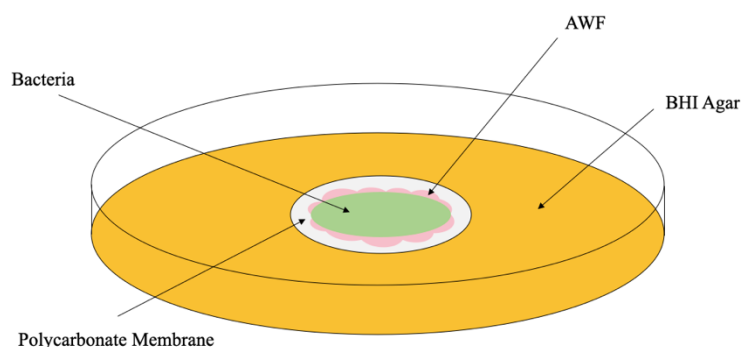


Figure 2.3: Schematic of polycarbonate membrane wound biofilm model.

2.4 Drug Susceptibility Assays

2.4.1 Minimum Inhibitory Concentration (MIC)

Antibiotic minimum inhibitory concentration (MIC)s were determined according to the Clinical and Laboratory Standards Institute guidelines.² Antimicrobial was made up to double the desired starting concentration in sterile H₂O, if appropriate, antimicrobials were filter sterilised prior to experimental use. 200 μL was added to the first column of a 96-well plate. 100 μL of antimicrobial was then serially diluted into bacterial broth across the plate to column 10. 100 μL of bacterial subculture ($\sim 1 \times 10^6$ CFU/mL) was added into all wells in column 1-10. 200 μL of broth only was added to column 11 serving as a negative control.

200 μL of bacterial subculture was added to column 12 serving as a positive control. MIC was defined as between the lowest concentration of antimicrobial that inhibited growth and the highest concentration that permitted bacterial growth. This was scored first through visualisation, and subsequently quantitatively using FLUROstar plate reader. Absorbance was read at 600 nm at 0 h and plates were then grown at 200 rpm for 18 h at 37 °C overnight.

2.4.2 Minimum Biofilm Inhibitory Concentration (MBIC)

ON culture of bacteria was subcultured as before (2.2.2). Serial dilution of antimicrobial was carried out as before (2.4.1). Plates were incubated statically for 18 h at 37°C. After incubation biofilm inhibition was evaluated using crystal violet staining (2.3.2)

2.4.3 Minimum Biofilm Eradication Concentration (MBEC)

Bacteria were grown as previously described (2.2.2). After 18 h growth contents were removed from all wells and 100 μL of fresh glucose supplemented broth was added to columns 2-10. Serial dilution of antimicrobial was carried out as in 1.2.4. After serial dilution 100 μL of fresh broth was added to all wells in columns 1-10. 200 μL was added to columns 11 and 12 which serve as positive and negative controls respectively. Plates were then incubated for 18 h at 37 °C and remaining biofilm was then evaluated using crystal violet staining (2.3.2)

2.5 Microscopy

2.5.1 Scanning Electron Microscopy

2.5.1.1 Theoretical Background

Scanning electron microscopy (SEM) creates images by scanning the sample surface with a focused beam of electrons, upon interaction with atoms of the sample the electrons produce signals which correspond to the topography and composition of the sample. Electrons are produced at the top of the microscope column and accelerated down through a series of apertures and lenses to produce a focused beam of electron. This electron beam will hit the sample that is mounted on the stage at the bottom of the microscope. The position the beam

hits on the sample can be controlled by the coils above the objective lens. When the electrons interact with the sample, they produce secondary electrons, backscattered electrons and characteristic X-rays. These signals are collected and form a visual display of the sample. Unlike conventional light microscopy, SEM can achieve a resolution of up to 1 nm.

SEM samples require advanced preparation to enable them to withstand the high vacuum operating system. Samples often require preparation to increase their electrical conductivity and their stability. Non-conducting materials are coated with a thin layer of electrically conducting material such as gold or platinum, deposited by low-vacuum sputter coating. In addition to metal coating, biological samples are often impregnated with an osmium-based stain, like osmium-tetroxide, to increase their bulk conductivity and thus the image quality. SEM samples are required to be completely dry owing to the high vacuum within the chamber. As such, biological samples require fixation using a chemical fixative and then dehydration, air drying causes collapse and shrinkage of cells, therefore water is replaced with ethanol to maintain structural integrity of sample to produce a representative image.^{3,4}

2.5.1.2 Sample Preparation

Biofilms were prepared and treated as before (2.3.3). After treatment they were suspended in 1 mL PBS to remove any unbound, planktonic bacteria. Biofilms were then fixed overnight in a solution of 3% (v/v) paraformaldehyde, 1.5% (v/v) glutaraldehyde in PBS (pH 7.4). Samples were rinsed in osmium tetroxide and dehydrated in ethanol of increasing concentrations (70, 80, 90 & 95 % (v/v)). Samples were left to dry and then fixed onto SEM platforms using carbon tape. Samples were then stored under vacuum until required. Before imaging sputter coated with gold. Imaging was performed using field emission scanning electron microscope and standard scanning electron microscope. (JEOL SEM6480LV, Bath, UK).

2.5.2 Confocal Laser Scanning Microscopy (CLSM)

2.5.2.1 Theoretical Background

Confocal light scanning microscopy (CLSM) utilises a pinhole conformation to focus light onto both living and fixed sample, therefore only what is in the geometric focus of the lens is detected. Owing to the pinhole configuration light can be focused onto separate planes while eliminating the out of focus light above and below the sample.⁵ As such high-powered lasers, either argon or krypton/argon, are used to illuminate sample to collect enough light to enable resolution as desired plane. CLSM use multiple mirrors enabling scanning linearly across x and y axis.⁶

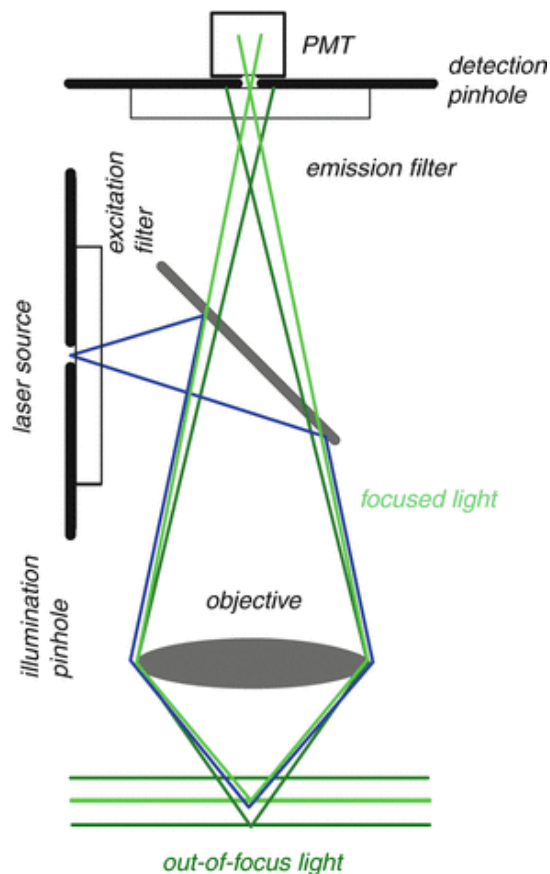


Figure 2.4: Schematic of CLSM optical pathway. (Reproduced with permission from Springer).

CLSM has frequently been used to study both planktonic bacteria and biofilms. Within bacterial biofilms CLSM has assisted in elucidating composition, metabolism and structure.^{7,8} The ability to study different depths of the biofilm without damage to the biological structures is a huge advantage.

LIVE/DEAD Assay Theory

LIVE/DEAD staining is used as an indicator of cell viability through determination of the cell walls integrity in bacteria including biofilm structures. LIVE/DEAD BacLight® uses a dual staining system: SYTO9 and propidium iodide (PI).⁹ The dyes have two distinct wavelengths 510-540 nm for SYTO9 and 620-650 nm for PI. While they both intercalate with nucleic acids, enhancing the fluorescence signal, they differ in their cell membrane permeability.¹⁰ SYTO9 can cross bacterial cell membranes emitting a green signal, enabling total cell count, PI can only cross into cells with disrupted membranes, emitting a red fluorescence signal.¹¹

2.5.2.2 LIVE/DEAD Staining

Biofilms were grown as per Section 2.3.3. Membranes were carefully removed from agar and washed with PBS three times to remove unbound, planktonic bacterial cells. BacLight™, consisting of two nucleic acid dyes: SYTO9 and PI, which were prepared according to manufacturer's instruction. Each biofilm was immersed in 1.5 mL of the combined stain mixture for 15 min in the dark at 25 °C. Post staining the biofilms were rinsed once with PBS and fixed onto microscope slides. These were then imaged using a confocal scanning laser microscope (Zeiss LSM510META). Manipulation of the images and 3D reconstruction was performed using LSM Image Browser and Imaris 7.4.2 software.

2.6 Cold Atmospheric Pressure Plasma

2.6.1 Helium Jet Set Up

CAP jet was used as outlined by Szili *et al.*¹² A single copper electrode was attached to either a tapered or non-tapered glass tube, helium gas fixed at 40 was run through the system controlled by a digital flow meter (either 0.6 or 2 standard litres per minute (SLPM)), **Figure 2.5**. Power and voltage were controlled using digital oscilloscope and conditions were fixed at 25 kHz and 10 kV. Distance between the bottom of the jet and the treatment substrate, known as the gap distance, was fixed at 5 mm unless otherwise specified. Jet was either fixed or manually moved by hand.

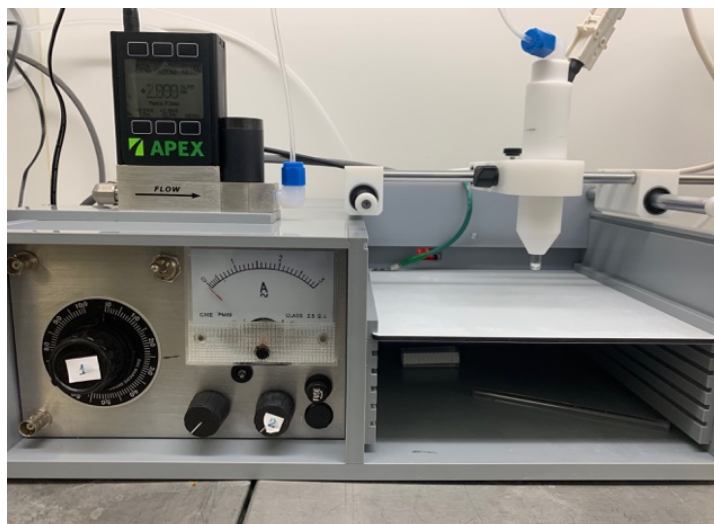


Figure 2.5: CAP jet set up.

2.6.2 CAP Treatment of Biological Substances

CAP jet was applied atop biological substance, either in wells of a 96-well plate or a polycarbonate membrane biofilm on agar surface. The gap distance between CAP jet and treatment surface was fixed at 5 mm and was checked before ignition. Jet was either fixed in a stationary position or carefully moved by hand on a lever system across treatment surface. After treatment biological material was left to incubate at 25 °C for 30 mins.

2.6.3 PVA Hydrogels

PVA (14,600-18,600 gmol⁻¹, 20% (w/v)) was made up to desired concentration by dissolving PVA into milliQ water, and then dissolved and sterilised by autoclaving. Solution was stored at room temperature until required. As needed, gels were then cast to desired thickness in a petri dish or on 24-well plate. Gels were then cryo-crosslinked at -20 °C and thawed. This process was carried out by removing gels from the freezer and defrosting for 4-6 h at 25 °C, this was considered one freeze/thaw cycle. The hydrogels were placed back into the -20 °C overnight and then taken out and defrosted for 4-6 h at 25 °C. This was considered two freeze/thaw cycles. This process can be repeated for a number of times, as the number of freeze/thaw cycles increases, the density of crosslinking will increase.

2.6.4 Absorbance and Fluorescence

Absorbance is the interaction of light with matter, when exposed to light it is either taken in, this is called absorbance or lost through scattering. Biomolecules absorb at separate distinct wavelengths, for example, haemoglobin absorbs yellow-green light enabling the detection and quantification of specific analytes blank corrected to solvent without analyte. While traditionally absorbance measurements are carried out in a cuvette, for high throughput measurements microplates can be used. The portion of light through the sample is called transmission (**Equation 2.2**) where transmittance (T) is defined as the ration of transmitted intensity (I) over the incidence intensity (I_0). Absorbance (A) is related to transmittance and incident and transmitted intensities (**Equation 2.3**).¹³ Absorbance has a logarithmic relationship with transmarine, absorbance of 0 would have a transmittance of 1.

$$T = \frac{I}{I_0} \quad (2)$$

Equation 2.2: Transmission of light

$$A = -\log_{10} T \quad (3)$$

Equation 2.3: Absorbance of analyte

When required the absorbance value can then be used to calculate the concentration of the analyte of interest, through either a standard curve of known analyte concentrations against absorbance or using the Beer-Lambert law where absorbance (a) is linear to analyte concentration (c) multiplied by path length (l) and extinction coefficient (ϵ) (**Equation 2.4**).

14

$$A = c\epsilon \quad (4)$$

Equation 2.4: Beer-Lambert law

2.6.5 Quantification of CAP Produced RONS

2.6.5.1 H₂O₂ Quantification - Potassium Iodide Method

1 M KI solution was made fresh by dissolving 0.83 g of KI into 5 mL of PBS (pH 7.4) as required to eliminate risk of degradation. KI standard curve was made by adding 100 μ L of

KI indicator to 100 μL of H_2O_2 of known concentrations (1000-100 μM) made from stock 33% (v/v) H_2O_2 in a 96-well plate. Plate was left to incubate at 25 $^\circ\text{C}$ for 30 minutes to allow yellow colour to develop and then absorbance was read at 410 nm using FLUROstar Omega plate reader. Readings were blanked against absorbance of KI only.

2.6.5.2 H_2O_2 Quantification - Titanium Oxysulphate Method

100 μL of Titanium Oxysulphate solution was added to 50 μL of 100 μL of H_2O_2 of known concentrations (1000-100 μM) made from stock 33% (v/v) H_2O_2 made up in PBS for increased stability of H_2O_2 . On addition of titanium oxysulphate a yellow colour formed immediately. Absorbance was read immediately at 405 nm using FLUROstar Omega plate reader. Readings were blanked against the absorbance of TiOSO_4 only.

2.6.5.3 Nitrite Quantification – Griess Test

100 μM nitrite was prepared through diluting stock 0.1 M sodium nitrite. 100 μL of 100 μM nitrite standard was serially diluted across a 96-well plate into PBS giving final concentrations of 100, 50, 25, 12.5, 6.25, 3.13, 1.6 μM and final volume of 50 μL in each well. 50 μL of sulphanilamide solution (1% (w/v) of sulphanilamide, 5% (v/v) phosphoric acid) was then added to each well and incubated in the dark for 10 minutes. 50 μL of NED solution was then added to all wells and left in the dark for 5-10 minutes, purple/magenta colour formed immediately. Absorbance was read at 540 nm immediately.^{15, 16}

2.7 DNA Methods

2.7.1 Principles of PCR

Developed in the 1980's by Karl Mullis, PCR enables the synthesis of specific DNA fragments using the enzyme DNA-polymerase. Polymerase synthesises a complementary sequence of DNA while a specific primer is bound to one of the DNA strands within the specific site to initiate synthesis.¹⁷ PCR is made up of three steps: denaturation, annealing and extension. Denaturation is when the target double stranded DNA is heated to cause the strands to separate, then annealing occurs when the primers bind to the regions flanking the

desired DNA sequence and finally extension occurs when DNA polymerase extends the 3' end of each primer along the target template strand. These steps are repeated between 25-40 times, these are referred to as cycles and produce exact replicates of the target sequence at an exponential rate.¹⁸

To analyse whether the desired PCR product has been produced, PCR products are run on an agarose gel using a method known as gel electrophoresis. Gel electrophoresis separates out DNA fragments by size using electrical current. DNA is negatively charged so samples are loaded in the agarose gel next to the negative electrode and DNA samples will move towards the positive electrode. Smaller samples will move through the gel quicker and thus move furthest away from the loading wells. Samples are run against a ladder, which contains DNA fragments of known lengths for internal comparison and estimation of unknown fragment size.

2.7.2 Colony PCR

Single colony was picked and suspended into 2 µl of PBS (pH 7.4) and then added to 15 µl of X2 GoTaq master mix with 1 µl of Forward primer and reverse primer. Primers were designed specifically for desired fragment and thermocycler conditions were optimised for desired product.

2.7.3 Agarose Gel Electrophoresis

Agarose gel electrophoresis was performed to analysis if PCR amplification had been successful. A 1% (w/v) agarose gel was prepared using 1x TAE buffer. 1 µl of GelRed dye (1:10,000) was added once agarose had cooled to 65°C prior to casting in the gel mould. Agarose was then cast into the gel tray and left to set for ~30 mins. 10 µl of 1 kB DNA marker was added. 20 µl of DNA sample was loaded into wells and the gel was run at 100 volts for 45-60 minutes. Bands were visualised under UV light and gel images were taken and stored.

2.8 Data Analysis

Comparisons between data sets was done either with a Students *t*-test or a One-way ANOVA depending. *P*-value of <0.05 was considered statistically significant for all cases. Graphs were plotted using GraphPad 8.0. Three biological replicates (n=3) were used throughout unless otherwise specified and error bars represent standard deviation, unless otherwise specified.

2.9 References

1. Miles AA, Misra SS, Irwin JO. The estimation of the bactericidal power of the blood. *J Hyg (Lond)*. 1938;38(6):732–49.
2. Jorgensen JH, Hindler JF. New consensus guidelines from the Clinical and Laboratory Standards Institute for antimicrobial susceptibility testing of infrequently isolated or fastidious bacteria [Internet]. Vol. 44, *Clinical Infectious Diseases*. Oxford Academic; 2007 [cited 2020 Sep 28]. p. 280–6. Available from: <https://academic.oup.com/cid/article-lookup/doi/10.1086/510431>
3. Suzuki E. High-resolution scanning electron microscopy of immunogold-labelled cells by the use of thin plasma coating of osmium. *J Microsc* [Internet]. 2002 Dec 1 [cited 2020 Sep 28];208(3):153–7. Available from: <http://doi.wiley.com/10.1046/j.1365-2818.2002.01082.x>
4. Smith KCA, Oatley CW. The scanning electron microscope and its fields of application. *Br J Appl Phys* [Internet]. 1955 Nov 1 [cited 2020 Sep 28];6(11):391–9. Available from: <https://iopscience.iop.org/article/10.1088/0508-3443/6/11/304>
5. Diaspro A, Bianchini P, Cella Zancacchi F, Usai C. Confocal Laser Scanning Fluorescence Microscopy. In: *Encyclopedia of Biophysics*. Springer Berlin Heidelberg; 2013. p. 362–6.
6. Paddock SW. *Confocal Laser Scanning Microscopy*. 1999.
7. González-Machado C, Capita R, Riesco-Peláez F, Alonso-Calleja C. Visualization and quantification of the cellular and extracellular components of *Salmonella Agona* biofilms at different stages of development. 2018 [cited 2020 Mar 23]; Available from: <https://doi.org/10.1371/journal.pone.0200011>
8. Maukonen J, Mattila-Sandholm T, Wirtanen G. Metabolic Indicators for Assessing Bacterial Viability in Hygiene Sampling Using Cells in Suspension and Swabbed Biofilm. *LWT - Food Sci Technol*. 2000 May 1;33(3):225–33.
9. Berney M, Hammes F, Bosshard F, Weilenmann HU, Egli T. Assessment and interpretation of bacterial viability by using the LIVE/DEAD BacLight kit in combination with flow cytometry. *Appl Environ Microbiol*. 2007 May 15;73(10):3283–90.
10. LIVE/DEAD® BacLight™ Bacterial Viability Kits MP 07007 LIVE/DEAD ® BacLight™ Bacterial Viability Kits L7007 LIVE/DEAD ® BacLight™ Bacterial

Chapter 2

Viability Kit *for microscopy* L7012 LIVE/DEAD ® BacLight™ Bacterial Viability Kit *for microscopy and quantitative assays* L13152 LIVE/DEAD ® BacLight™ Bacterial Viability Kit *10 applicator sets* [Internet]. [cited 2020 Mar 23]. Available from: www.omegafilters.com

11. Robertson J, McGoverin C, Vanholsbeeck F, Swift S. Optimisation of the Protocol for the LIVE/DEAD® BacLight™ Bacterial Viability Kit for Rapid Determination of Bacterial Load. *Front Microbiol* [Internet]. 2019 Apr 12 [cited 2020 Mar 23];10(APR):801. Available from: <https://www.frontiersin.org/article/10.3389/fmicb.2019.00801/full>
12. Szili EJ, Oh JS, Fukuhara H, Bhatia R, Gaur N, Nguyen CK, et al. Modelling the helium plasma jet delivery of reactive species into a 3D cancer tumour. *Plasma Sources Sci Technol* [Internet]. 2018 Jan 1 [cited 2020 Sep 28];27(1):014001. Available from: <https://doi.org/10.1088/1361-6595/aa9b3b>
13. Swinehart DF, The E, Law B-L. The Beer-Lambert Law [Internet]. [cited 2020 Mar 24]. Available from: <https://pubs.acs.org/sharingguidelines>
14. Stevenson K, McVey AF, Clark IBN, Swain PS, Pilizota T. General calibration of microbial growth in microplate readers. *Sci Rep*. 2016 Dec 13;6(1):1–7.
15. Dawson TM, Dawson VL. Review ■ Nitric Oxide: Actions and Pathological Roles. Vol. 1, *The Neuroscientist*. SAGE Publications Inc.; 1995. p. 7–18.
16. Bredt DS, Snyder SH. Nitric Oxide: A Physiologic Messenger Molecule. *Annu Rev Biochem* [Internet]. 1994 Jun [cited 2020 Mar 23];63(1):175–95. Available from: <http://www.ncbi.nlm.nih.gov/pubmed/7526779>
17. Valones MAA, Guimarães RL, Brandão LAC, De Souza PRE, De Albuquerque Tavares Carvalho A, Crovela S. Principles and applications of polymerase chain reaction in medical diagnostic fields: A review. *Brazilian J Microbiol*. 2009;40(1):1–11.
18. Mullis KB, Faloona FA. Specific Synthesis of DNA in Vitro via a Polymerase-Catalyzed Chain Reaction. *Methods Enzymol*. 1987 Jan 1;155(C):335–50.

Chapter 3

Chapter 3

Chapter 3 : Characterisation of Helium Driven Cold Atmospheric Plasma Jet

3.1 Aims

The aims of the work described in this chapter were to characterise and optimise the treatment parameters of a helium driven cold atmospheric plasma jet (He-CAP) to maximise bacterial killing/inhibition, while maintaining favourable interactions with a hydrogel screen. Owing to the large number of variables within the He-CAP set up, the jet nozzle conformation, helium flow rate and treatment time were the three variables altered. The operating parameters of power and voltage remained constant. Characterisation was performed via the quantification of the bactericidal components produced by the He-CAP jet, which included: reactive oxygen and nitrogen species (RONS), specifically hydrogen peroxide (H_2O_2) and nitrites and nitrates ($\text{NO}_2^-/\text{NO}_3^-$). Moreover, localised elevation in temperature and pH change were likely to have an effect on microbial growth. Subsequently, the variation in treatment parameters was then evaluated on bacteria both in the planktonic state and within biofilms. While He-CAP may be effective in the decontamination of bacterially infected wounds, the potentially harmful and mutagenic effects of He-CAP derived RONS on healthy mammalian cells is of paramount concern.

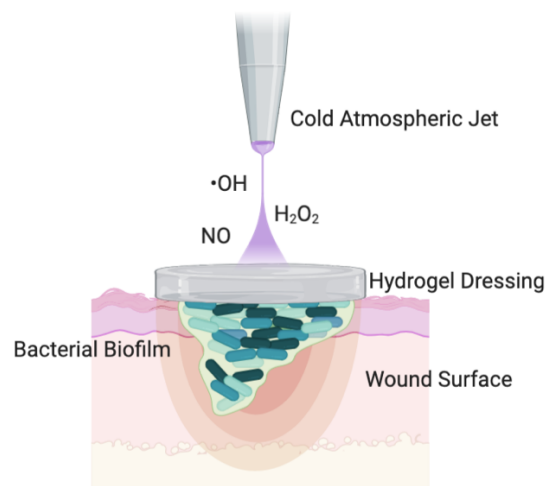


Figure 3.1 Schematic representation of a hydrogel “screen” wound dressing applied to a bacterially infected wound. He-CAP treatment will then be applied atop the hydrogel dressing, allowing bactericidal RONS to diffuse through into the wound bed, where they will decontaminate the wound bed and potentially promote healing, whilst also screening out RONS which could be harmful to healthy mammalian cells such as keratinocytes.

Chapter 3

Hydrogel dressings are frequently used in wound care owing to their beneficial healing effects such as the ability to maintain a moist healing environment. However, as with all conventional wound dressings, they must be changed regularly to observe wound healing and to ensure the wound is clean. This process can be painful and can cause trauma to the patient and can actually slow healing by removal of new epithelial tissue. Limiting the need for dressing changes would improve patient experience as well as potentially aid in healing. The utilisation of a hydrogel screen within He-CAP treatment could filter out harmful and potentially mutagenic RONS while enabling transport of bactericidal species through into the wound milieu for decontamination. This chapter also seeks to characterise the interactions of He-CAP and simple, potential hydrogel screens, assessing the delivery of RONS through the hydrogel as well as the reduction of bacterial load, both planktonic and biofilm, underneath the protective screen.

3.2 Chapter Background

3.2.1 Characterisation of CAP

Cold atmospheric plasmas (CAP) are formed in air via through the partial ionisation of an inert gas, and via the through interaction with the atmosphere to produce RONS. RONS are widely recognised for their reactivity with biological material. There are numerous variables that effect the RONS composition of the plasma: properties of the carrier gas (helium, argon, oxygen), flow rate of gas, gap distance (distance from treatment surface to plasma jet), voltage, power, treatment time, substrate (earthed or not earthed), direct/ indirect application, and physical properties of treatment “tissue” (liquid or solid).

Even small alterations in the CAP configuration can hugely impact the CAP interactions with bacterial and mammalian cells. The highly sensitive nature of CAP generation is advantageous in that it enables users to tailor the chemical composition for clinical use. For medical applications plasmas need to be able to operate under stable, reproducible, atmospheric conditions and remain $<40^{\circ}\text{C}$ at the tissue contact point.¹ Furthermore, within wound care, CAP should ideally produce a high concentration of bactericidal RONS to enable a significant reduction in the contaminating bacterial load while limiting damage to healthy, mammalian cells.

A key concern in plasma medicine is the control and speciation of secondary RONS generated within the activated medium. Owing to complex, plasma-induced liquid phase chemistry, (as outlined in Chapter 1), a variety of downstream RONS are generated after plasma activation of the substrate, varying from short-lived to long-lived species. Therefore, the cocktail of reactive species present within an activated substrate may differ to those generated at the point of plasma initiation. To ensure the safety and reproducibility of CAP treatment the RONS concentrations must be quantified. Previously, a range of methods have been used to gain a comprehensive characterisation of the generated components of CAP devices. These methods have included electrical, optical and spectroscopic techniques, flux analysis, UV and FTIR absorption spectroscopy and mass spectrometry to quantify ions and reactive species.^{2,3} H_2O_2 concentration can be quantified using colorimetric assays including titanium oxysulphate or potassium iodide as can the nitrite/nitrate ion concentrations through the use of the Griess assay (discussed 3.4.1.2).⁴⁻⁶

Table 3.1: All possible free-radical and non-radical RONS generated through cold atmospheric pressure plasma.⁷

Free Radical	Non-Radicals
Superoxide $O_2^{\bullet-}$	Hydrogen peroxide H_2O_2
Hydroxyl $\bullet OH$	Ozone O_3
Hydroperoxyl HO_2^{\bullet}	Singlet 1O_2
Alkoxy RO^{\bullet}	Organic peroxides $ROOH$
Peroxy RO_2^{\bullet}	Peroxynitrite $ONOO^-$
Carbon dioxide radical $CO_2^{\bullet-}$	Nitrosoperoxycarbonate $ONOOCO_2$
Nitric oxide $\bullet NO$	Nitrous acid HNO_2
Nitrogen dioxide $\bullet NO_2$	Peroxynitrite $ONOO^-$

It is important to note that the generation of RONS has been found to vary significantly between cell culture media and biocompatible liquids, such as phosphate buffered saline (PBS) or Ringer's solution, with higher concentrations of RONS being generated in cell culture media as a result of their higher organic component content.⁸ This phenomenon could have a serious impact on the cytotoxicity data of CAP treatment if not taken into account.

Szili *et al.* report the major bactericidal, long-lived RONS generated within PBS after exposure to He-CAP to be H_2O_2 and NO_2/NO_3 .^{3,9} The focus in this work for characterising the He-CAP jet are the bactericidal components H_2O_2 , NO_2/NO_3 and characteristics that could impact the morphology of the hydrogel i.e. temperature and pH. As previously discussed, the gas type, voltage, power, earthing and gap distance were maintained at constant values throughout, however, the flow rate of the gas, whether a non-tapered or tapered glass tube was used, and treatment times were varied to optimise and maximise RONS production for bacterial killing, while limiting damage to the hydrogel screen. While there is a large body of research on the optimal CAP conditions for high levels of RONS production and optimised conditions for killing various bacterial species, the addition of a hydrogel screen is novel, therefore there were no standard treatment conditions.

3.2.2 Biological Interactions of CAP

CAP derived RONS, UV and electromagnetic fields are known to have an impact on the biological function of both bacterial and mammalian cells. CAP produces both H₂O₂ and nitric oxide (NO). Topical H₂O₂ solution is used within wound clinics at high concentrations (1.5-3% (v/v)) for the decontamination of heavily colonised wounds. NO is synthesised by inflammatory cells, chiefly macrophages and has been shown to increase healing rates. NO promotes angiogenesis, modulates inflammation and effects cell proliferation.^{10,11} Like H₂O₂, NO is also known to have antimicrobial properties. At low concentrations NO promotes the activity and proliferation of immune cells and at high concentrations NO will covalently bind to DNA, proteins and lipids, inhibiting and killing the target pathogen.¹² CAP devices can be supplemented with O₂, which has been shown to increase oxygenation within the treated tissue.¹³ As chronic wounds are often in a state of chronic hypoxia, which impedes healing, oxygenation could prove advantageous within a wound environment.¹⁴

While UV's toxic and mutagenic impact on mammalian cells has been widely studied and is a causative agent in some of skin cancers, UV is also known to be toxic to bacteria and is a widely used for sterilisation of bacterially contaminated clinical equipment.¹⁵ Electromagnetic fields are also thought to impact bacteria with reports citing impact on DNA stability influencing interactions with oxidative radicals,¹⁶ increasing the effects of NO¹⁷ and limiting bacterial growth.¹⁸

3.2.3 PVA Hydrogels

Polyvinyl alcohol (PVA) is one of the oldest, most frequently used polymers in wound dressings, drug delivery systems, and contact lenses.¹⁹ Owing to its high biocompatibility and hydrophilic properties PVA hydrogels create a moist environment to promote wound healing and can be cross-linked for added structural integrity.²⁰ While aqueous solutions of PVA will partially gel at room temperature, increasing elasticity, PVA can be made into a more desirable gel by crosslinking. The crosslinking of polymers is broken into two categories: physical crosslinking and chemical crosslinking.

Chapter 3

To create a strong elastic hydrogel with PVA, the aqueous solution is heated to dissolve the PVA fully, then the hydrogel is subjected to a series of freeze-thaw cycles. The properties can be influenced through alteration of polymer concentration, molecular weight of PVA (Mw 146,000-186,000) and number of freeze-thaw cycles.²¹ Freeze-thawing crosslinks the PVA through the formation of crystalline regions. During freezing the densification of the PVA macromolecules through the formation of ice crystals (freezing) occurs, then the formation of an ordered structure during thaw (heating) period.²²

PVA can be mixed with additives such as nanoparticles or other polymers to make complex hydrogels. When blended with other substrates crystallisation by heat may be insufficient, instead chemical modification will be required. This process involves the modification acetalization of the PBA hydroxyl group using a mono-aldehyde like formaldehyde or di-aldehyde like glutaric aldehyde or glyoxal to form intermolecular crosslinking.²³

3.3 Methods

3.3.1 Thermal Imaging

A Xenics® GOBI-640-GigE thermal imaging camera was used to capture relative temperature change. Thermal imaging was calibrated against a carbon sheet of known temperature. The camera was then set up according to manufacturer's instructions. Temperature was recorded at second intervals using the software and calculated relative to surroundings.

3.3.2 pH and Temperature

1 mL of sterile PBS (pH 7.4, 25°C) was aliquoted into a 12-well plate. CAP treatment was applied for 1, 5, and 10 minutes, with a gap distance of 5 mm, under standard operating conditions with varying flow rate and jet tube conformation. The temperature and pH were measured before, immediately after He-CAP treatment and after 30 minutes incubation at 25°C using Jenway's temperature and pH probe as per the manufacturer's instructions.

3.3.3 Scanning Electron Microscopy of PVA Hydrogels

The external topography of the PVA hydrogel surface was analysed by scanning electron microscopy (SEM). Gels were freeze-dried (6 hours) and stored under vacuum overnight to ensure complete dehydration. SEM was then carried out as per section 2.5.1.2

3.3.4 Rheology

Experiments were run in triplicate. The sample was positioned on the rheometer (AR 2000 EX) and set with a relaxation time of 60 minutes. Oscillatory amplitude experiments maintained a frequency of 10 rad s⁻¹ and performed with the amplitude of oscillation from 0.01 % up to 100 % at 298 K. Oscillatory frequency sweep experiments maintained a constant shear strain (γ) of 0.0925 % with an increasing frequency from 0.1–100 rad s⁻¹ at 298 K.

3.4 Results and Discussion

3.4.1 Quantification of RONS from He-CAP Jet

He-CAP is known to produce a range of RONS through interactions with the atmosphere, however, the majority of these are short-lived and, as such, are difficult to measure directly. Owing to their short life, it is likely these species play little role in killing bacteria, instead reacting with other species forming longer-lived species.

The plasma plume formation varies visually with the change in helium flow rate and jet conformation, with the plume for the tapered jet appearing to be more intense than the non-tapered jet (**Figure 3.2**). This finding supports that of Laroussi *et al.*²⁴ The He-CAP jets plume is known to be of a low temperature and so can make contact with biological surfaces with reduced impact. Interestingly, previous work has shown that plasma plumes do exhibit a high, instantaneous and localised electric field at its tip.²⁵ Owing to the appeared intensity of the 0.6 standard litres per minute (SLPM) jet plume and the topography of treatment surfaces after exposure, this localised electric field could be the cause of the apparent scorching of hydrogels and biofilms surface.²⁶

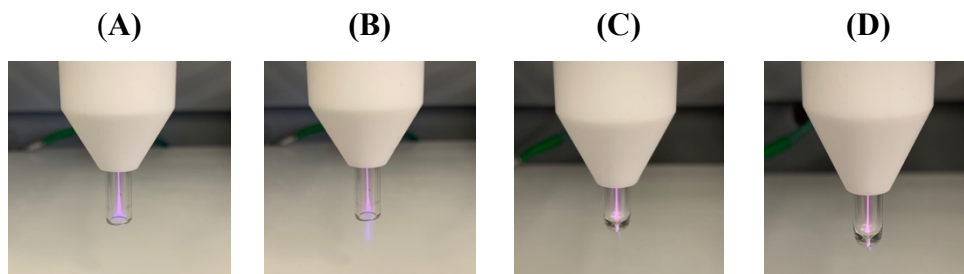


Figure 3.2 He- CAP jet plume when ignited at 25 kHz, 10 kV using non-tapered glass tube (**A-B**) and tapered glass tube (**C-D**). (**A**) and (**C**) used 0.6 standard litres per minute (SLPM) and (**B**) and (**D**) used 2 SLPM.

3.4.1.1 Quantification of Hydrogen Peroxide

H₂O₂ production was quantified under varying He-CAP jet operating conditions to determine optimum conditions for bacterial killing. H₂O₂ concentration was found to increase linearly with an increase in CAP application time and varied, dependent on helium flow rate and jet tube conformation. Helium flow rate of 0.6 SLPM was found to produce higher concentrations of H₂O₂ than 2 SLPM regardless of jet conformation (**Figure 3.3**).

There is a significant difference in the concentrations of H_2O_2 produced using the tapered jet upon altering the helium flow rate $p < 0.0001$ (****) for the difference between tapered and non-tapered using 0.6 SLPM of helium and $p = 0.0272$ (*) for 2 SLPM. This could be due to the alteration of air flow from laminar to turbulent mode, a phenomenon previously observed by Baek *et al.*²⁷ The group observed that, as flow rate was increased the density of OH increased, corresponding to the generation of RONS, yet when flow rate was increased to 4L/min the OH density was found to decrease. The group attributed this to change of flow from laminar to turbulent which resulted in the length of the helium gas stream with low air fractions decreasing significantly.²⁷ Further to this, Labay *et al.* also found that with an increase in flow rate there was a decrease in RONS production, however, the group attribute this decrease to the acidification of the treatment solution causing NO_2^- and H_2O_2 to react and produce peroxyntrites.²⁸

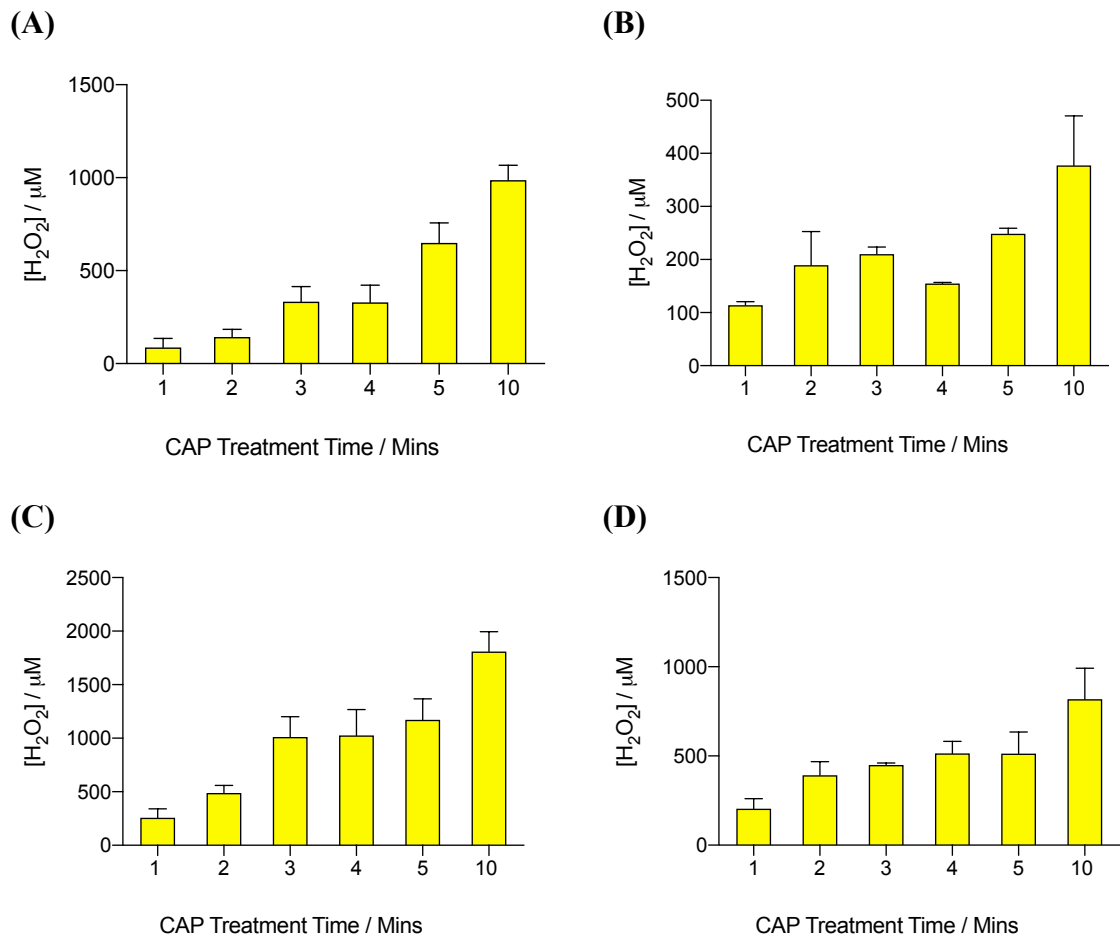


Figure 3.3 H_2O_2 quantification for various He- CAP jet conditions 0.6 SLPM of helium through non-tapered jet (A), 2 SLPM of helium through non-tapered jet (B), 0.6 SLPM of helium through tapered jet (C) and 2 SLPM of helium through tapered jet (D). Measured after 30 mins post treatment incubation at 25°C using KI reporter system. Error bars denote standard deviation (n=3).

3.4.1.1.1 Background and Sensitivity of H₂O₂ Detection Assays

Two colourmetric assays were found to detect H₂O₂ Titanium oxysulphate and Potassium iodide, the protocol and details of the assays are outlined in section 2.6.5. The concentrations of peroxide generated by CAP treatment is known to vary greatly depending on the operating parameters, as such the sensitivity of the two assays was assessed to attain when to use them. It is important to note that while these assays do quantify the amount of peroxide present it is possible that other CAP generated RONS are allowed being quantified.

Titanium Oxysulphate



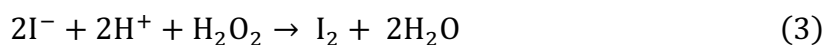
Equation 3.1 Titanium reaction with peroxide

Titanium oxysulphate reacts with H₂O₂ to produce perititanic acid, which produces an instantaneous yellow colour, which is stable for 6 h.²⁹ As He-CAP is known to produce nitrites, sodium azide was added to eliminate the decomposition of H₂O₂ by nitrites under acidic conditions as it reduces nitrites into molecular nitrogen, as such this method measures exclusively H₂O₂.³⁰ The limit of detection (LoD) was calculated to be 110 µM. (Standard Curve in Appendix 3.8.3).

$$\text{Limit of detection} = \frac{3 \times \text{standard deviation of lowest used concentration}}{\text{gradient of standard curve}} \quad (2)$$

Equation 3.2 Limit of detection

Potassium Iodide



Equation 3.3 Iodide ions and hydrogen peroxide



Equation 3.4 Iodine and iodide ion reaction

On addition of H₂O₂ the iodide ions (I⁻) within the potassium iodide (KI) are slowly oxidised to iodine (I₂), in the presence of iodide, iodine reacts to form triiodide (I₃⁻) which is yellow in colour.³¹ This can be quantified at absorbance 400 nm. LoD for KI is 11.77 µM. While the LoD for KI is lower than TiOSO₄, at higher concentrations KI tops out and ceases to be readable by absorbance owing to the production of O₂. This is commonly referred to as the

“Elephant’s toothpaste” reaction. O_2 is produced during the catalysed decomposition of H_2O_2 .³²

As such, when high concentrations of H_2O_2 were expected $TiOSO_4$ was used whereas KI was chosen when concentrations were expected in the millimolar range. It is important to note that while both methods will quantify H_2O_2 they are not selective and could be quantifying other CAP produced RONS (Standard Curve in Appendix 3.8.1).

3.4.1.2 Quantification of Nitrites

Nitric oxide (NO) is also known to be a product of He-CAP. One method to quantify NO production is by the through measurement of NO_2^- , one of two non-volatile, stable products of NO. The Griess assay uses sulphanilamide and *N*-1-naphthyethylenediamine dihydrochloride (NED) under acidic conditions (in phosphoric acid). The system is capable of detecting nitrites in various environments: serum, urine and plasma.^{33,34} Importantly it has proved highly useful in the quantification of nitrites from CAP sources.³⁵ (Standard Curve in Appendix 3.8.2)

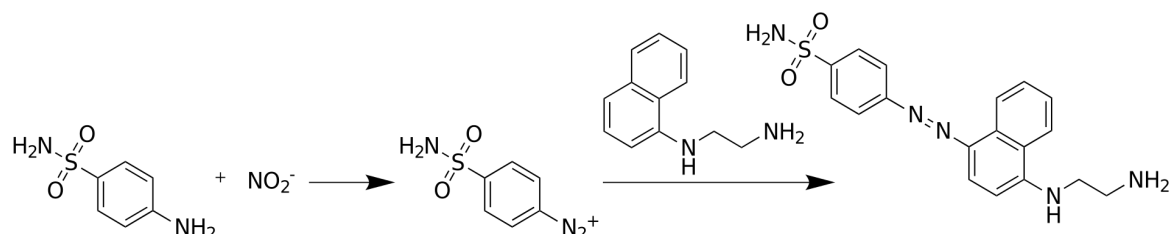


Figure 3.4 Chemical reaction for measuring NO_2^- using the Griess reagent system

The LoD of the Griess test was found to be $1.73 \mu M$, making the test reasonably sensitive, which is important given that the concentrations of nitrites produced by He-CAP treatment were expected to be low. Unlike peroxide, the generation of nitrites within He-CAP treated liquids was instantaneous, yet owing to their instability, nitrites were not observed after 30 minutes incubation post He-CAP treatment. Interestingly, nitrite concentration was found to be higher with shorter treatment times, decreasing as He-CAP application time increased. As treatment time increases there is more time for the nitrites to degrade into more stable RONS. This finding was concurrent with literature reporting that, nitrites are short lived and will break down into more stable species.⁸ A gas flow rate of 0.6 SLPM with tapered jet conformation was found to give the highest concentration of nitrite ions, similarly with

peroxide, this is thought to be owing to the turbulent airflow from the tapered jet conformation resulting in an increase in the formation of RONS

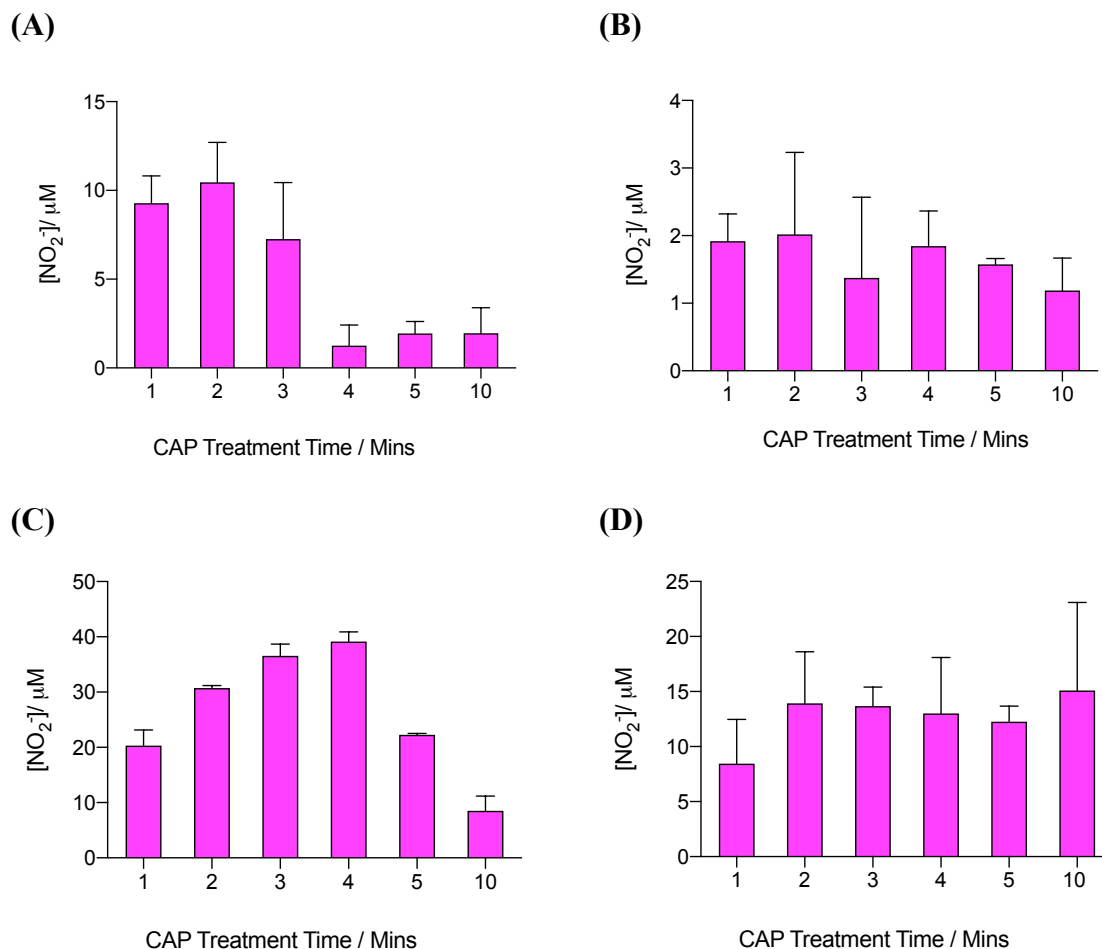


Figure 3.5 NO_2^- quantification for various He- CAP jet conditions: 0.6 SLPM of helium through non-tapered jet (A), 2 SLPM of helium through non-tapered jet (B), 0.6 SLPM of helium through tapered jet (C), and 2 SLPM of helium through tapered jet (D). Error bars denote standard deviation (n=3).

3.4.2 Temperature and pH

While He-CAP jets are reported to be “cold”, for direct application onto human skin to be tolerated the temperature needs to be below 40°C and, as previously discussed, the pH of the He-CAP treatment environment could have an impact the RONS generated. Moreover, pH plays an important role in maintaining homeostasis. Healthy skin has a pH between 4.0-6.3, however, chronic wounds have an alkaline pH of 7.15-8.93.³⁶ Wounds with an alkaline pH have been found to have a slower rate of healing. Yet acidic wound pH is associated with faster wound healing.³⁷

Temperature was measured for plasma-liquid treatments to mimic the interactions between plasma and the wound interface and plasma-surface biofilm treatments closely representing bacterial biofilm-associated wounds as biofilms consist of 90% water. Temperature change was measured using a temperature probe for liquids; the thermal imaging camera for the surface temperature of polycarbonate membrane biofilms; and pH was recorded using a pH probe.

Liquid-Plasma Temperature & pH

Temperature and pH change were measured in He-CAP treated PBS to assess whether there were any significant alterations that may have physiological impact. Owing to experimental constrictions temperature and pH had to be measured in 1 mL of PBS rather than the standard treatment volume of 350 μ L. This was deemed acceptable as previous papers used similar volumes.^{38,39} While the values in **Figure 3.6** will not be the same in the standard treatment volume, the trend is representative. No significant increase in pH or temperature is observed with any He-CAP conditions. This is surprising as literature reports a decrease in pH and increase in temperature with increased, He-CAP treatment time but is likely owing to the large volume used for the methodology.

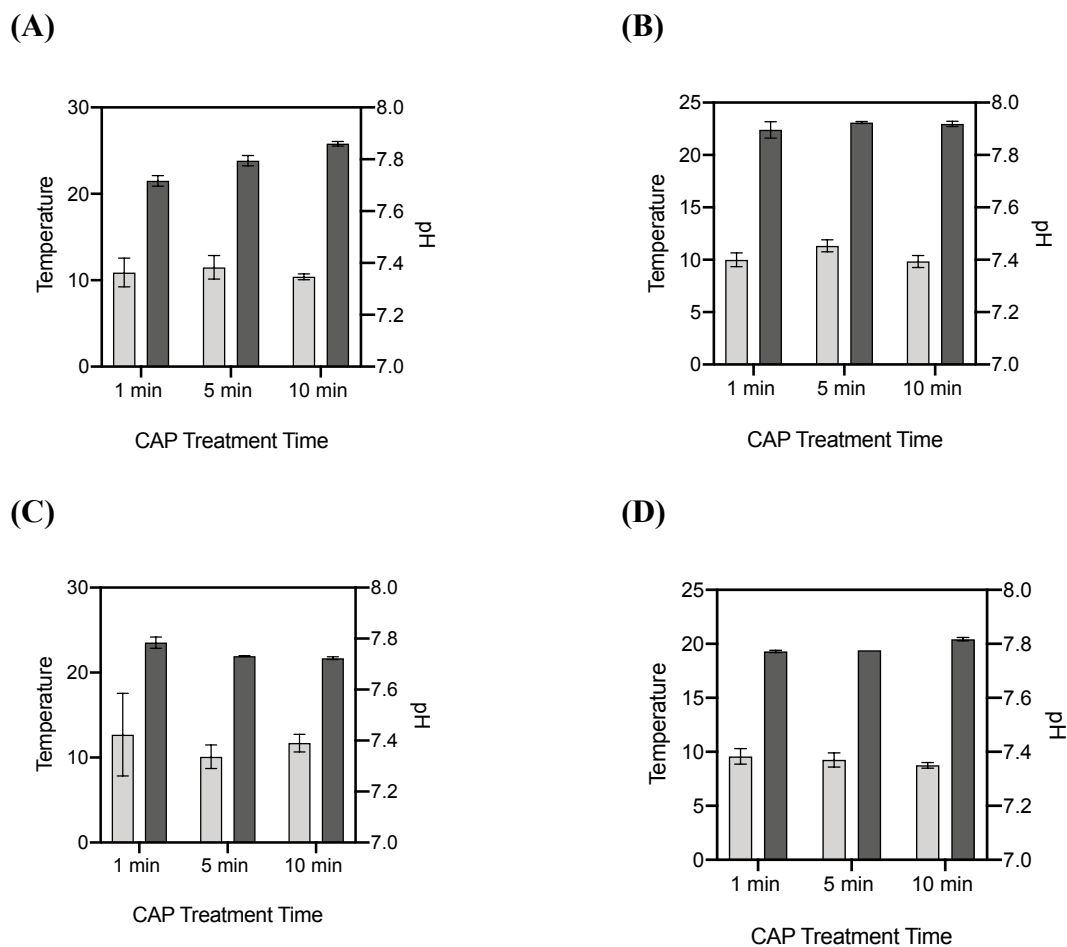


Figure 3.6 Temperature (shown in dark grey and recorded on the left axis) and pH change (shown in light grey and recorded on the right axis) in 2 mL of PBS (pH 7.4, 21°C) at varying times of exposure to He-CAP jet with different jet conformations: 0.6 SLPM He non-tapered jet (**A**), 2 SLPM He non-tapered jet (**B**), 0.6 SLPM tapered jet (**C**), & 2 SLPM tapered jet (**D**). Error bars denote standard deviation (n=3).

Surface Biofilm – Plasma Temperature

He-CAP jet was applied to *P. aeruginosa* polycarbonate biofilm to assess if there was any heating over time. While the temperature of the biofilm) was found to increase when He-CAP was applied to the surface, the temperature was found to be between 34 – 40 °C. Thus, it was concluded that direct application of the He-CAP jet to skin could be tolerated. Jet flow rate of 0.6 SPLM can be seen to emit more heat within its plume (**Figure 3.7A**) than 2 SLPM (**Figure 3.7B**). Moreover, the addition of a hydrogel screen would be likely to reduce any heating effect on the skin surface.

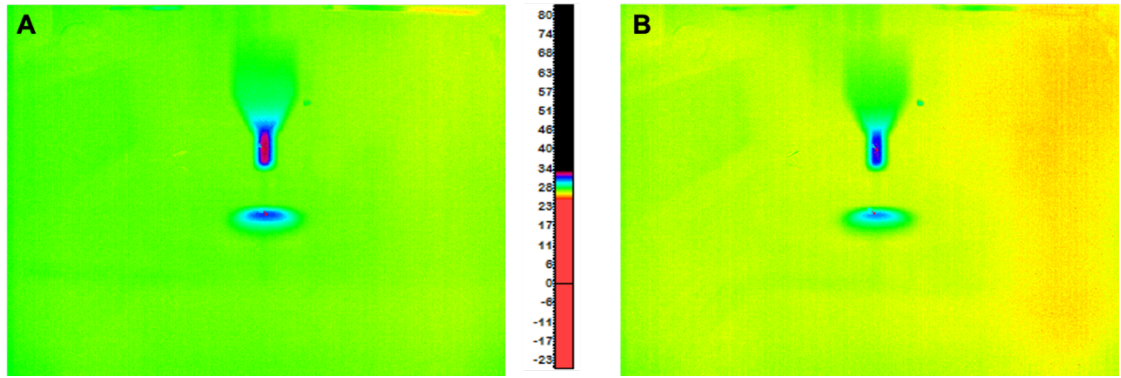


Figure 3.7 Thermal image of He-CAP jet demonstrating the variation in temperature between helium gas flow rates using Xenics GOBI-640-GigE thermal image camera 0.6 SLPM He flow rate **(A)** 2 SLPM He flow rate **(B)** when treating *P. aeruginosa* (PAO1) biofilm atop PBS buffer.

3.4.3 Interaction of He-CAP Jet with PVA Hydrogel

The overarching aim was to apply the He-CAP jet atop a hydrogel to reduce the penetration of damaging RONS, while maximising the bactericidal effects of the longer-lived He-CAP-generated RONS. The interactions between the hydrogel and He-CAP treatment were a key consideration. When operated with a flow rate of 0.6 SLPM, the He-CAP jet produces significantly more H_2O_2 than with a flow of 2 SLPM, thus, 0.6 SPLM would be the optimum flow rate to maximise antimicrobial effects. The model hydrogel used was PVA owing to its favourable biological interactions and biocompatibility, moisture content and durability.

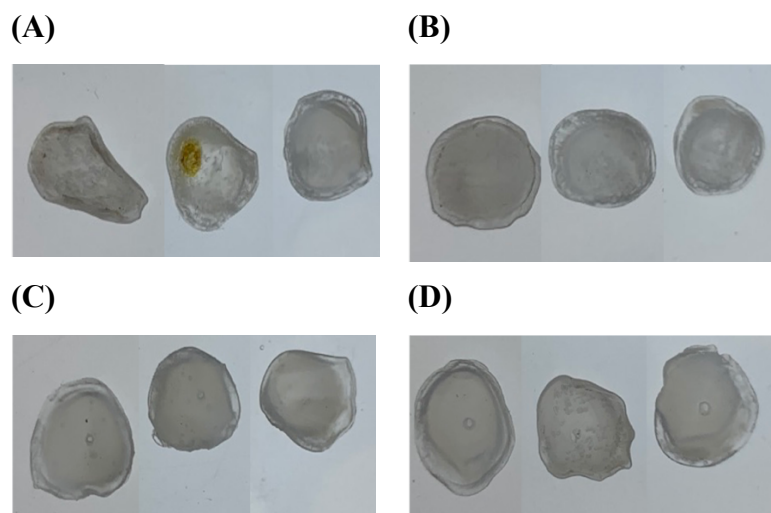


Figure 3.8 Photos of the visible, structural impact of He-CAP 0.6 SLPM of helium through tapered jet **(A)**, 2 SLPM of helium through tapered jet **(B)**, 0.6 SLPM of helium through non-tapered jet **(C)** and 2 SLPM of helium through non-tapered jet **(D)**.

Through simple visual and microscopic examination (**Figure 3.8** & **Figure 3.9**) the structural impact of He-CAP exposure, with variation in operating conditions, on PVA hydrogels was assessed. **Figure 3.8** shows the visual impact the He-CAP treatment has on the PVA gels. When exposed to 0.6 SLPM tapered He-CAP the PVA hydrogels appear to dry out and become scorched, as indicated by the yellowing of the gel seen in **Figure 3.8A**. However, none of the other conditions appear to have any significant impact, aside from some mild dehydration. Yet, through microscopic examination in **Figure 3.9** it can be seen that non-tapered 0.6 SLPM (**Figure 3.9B**) and 2 SLPM (**Figure 3.9 C&D**) are altering the surface morphology of the hydrogel. The increased impact on the hydrogel from the He-CAP at 0.6 SLPM could be owing to the increase in temperature of the plume as shown in Section 3.4.2.

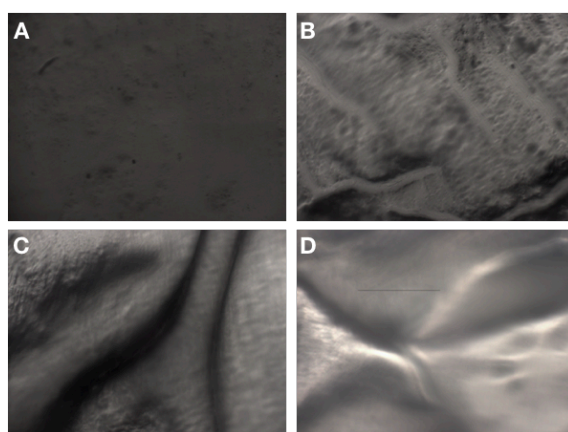


Figure 3.9 Microscopic analysis of the structural integrity of 5% (v/v) PVA gel treated with non-tapered He-CAP jet of varying conditions (x40 magnification) untreated control gel (**A**) 45 seconds with helium flow of 0.6 SLPM (**B**) 45 seconds with helium flow of 2 SLPM (**C-D**).

The topography of the PVA hydrogel surface after treatment with the varying He-CAP operating systems was further investigated using SEM. Owing to the increase in resolution it was hoped SEM would give a greater understanding of the impact of the He-CAP plume and the hydrogel surface. While the results were impacted by the freeze-drying step of the sample preparation, the hydrogels are compared to an untreated, control hydrogel for continuity. **Figure 3.10** shows the impact He-CAP treatment has on the hydrogel surface. **Figure 3.10A&B** show the smooth surface expected of a PVA hydrogel. However, after CAP treatment there is clear change in the surface morphology after both variations of flow rate.

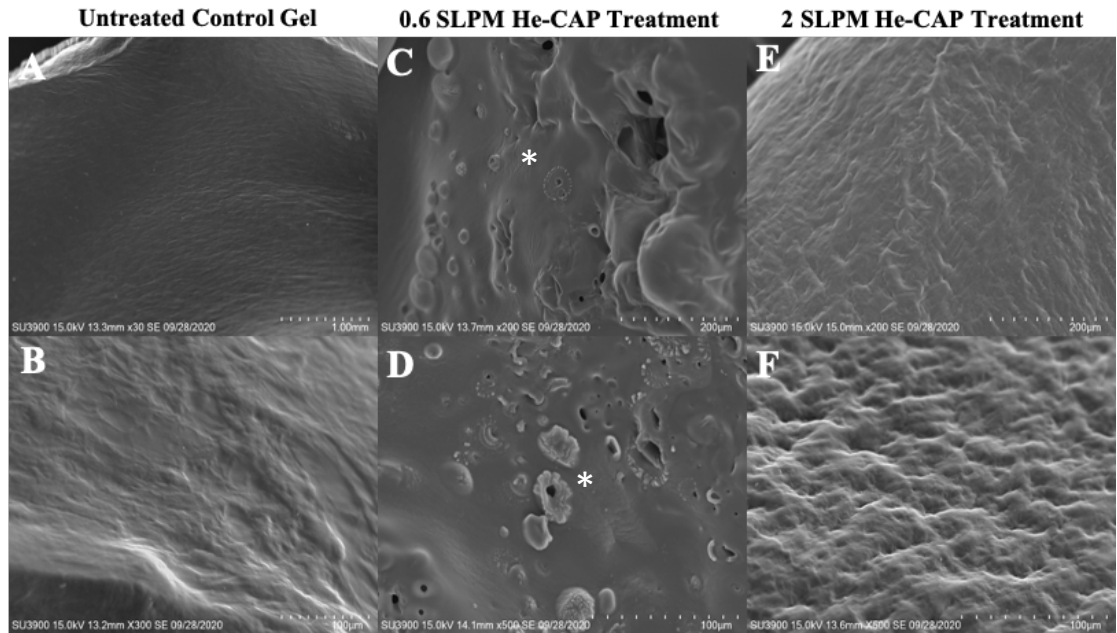


Figure 3.10 SEM images of 5% (w/v) PVA hydrogel. Untreated control gel (**A&B**), 5% PVA hydrogel after 5 min treatment with He-CAP jet operated at 0.6 SLPM (**C&D**) & 5% PVA hydrogel after 5 min treatment with He-CAP jet operated at 2 SLPM (**E&F**). He-CAP induced damage is indicated (*).

Rheology is sensitive to the internal structures of a polymer. The storage modulus (G') reflects the strength of a hydrogel, a larger G' means a greater strength. G' measures the materials elastic response. The loss modulus (G'') measures the materials viscous response. The G'' values were ten-fold lower than the G' value which indicates the gels were quite rigid, however this did not change post He-CAP treatment or vary between flow rates (**Figure 3.11**). Interestingly there is a 10-fold decrease in the G' value post He-CAP treatment this would seem to indicate some loss in strength. This could be owing to the changes in surface topography observed in **Figure 3.10**.^{40,41}

Chapter 3

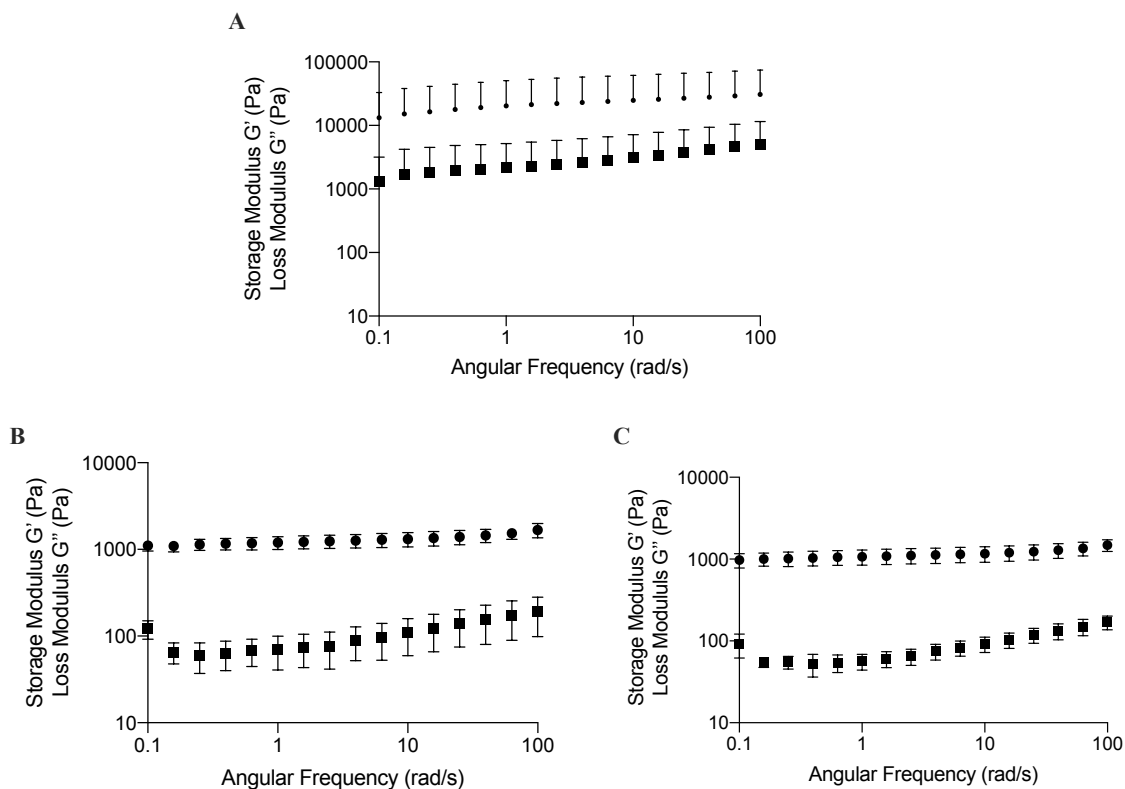


Figure 3.11 Rheology data for 5% (w/v) PVA hydrogels after He-CAP treatment. Untreated 5% PVA gel (A), 0.6 SLPM He-CAP treated 5% PVA gel (B) and 2 SLPM He-CAP treated 5% PVA gel (C) (●) storage modulus (G') (■) loss modulus (G''). Error bars denote standard deviation (n=3).

To further conclude the appropriate, He-CAP conditions for application atop a hydrogel, the RONS concentration recovered beneath the hydrogel screen was assessed. Both nitrite and H_2O_2 concentrations were assessed below a 5% (w/v) PVA hydrogel after 1 h incubation post exposure to five minutes of He-CAP treatment, with varying operating parameters. **Figure 3.12** shows that the highest concentration of both NO_2^- and H_2O_2 was recovered when treated with tapered jet with 0.6 SLPM. However, this operating condition had a detrimental effect on the structural integrity of the hydrogel. Thus, it was concluded that tapered jet with 0.6 SLPM helium flow was not appropriate for use with a hydrogel screen. Interestingly, the RONS recovered in all other conditions were comparable.

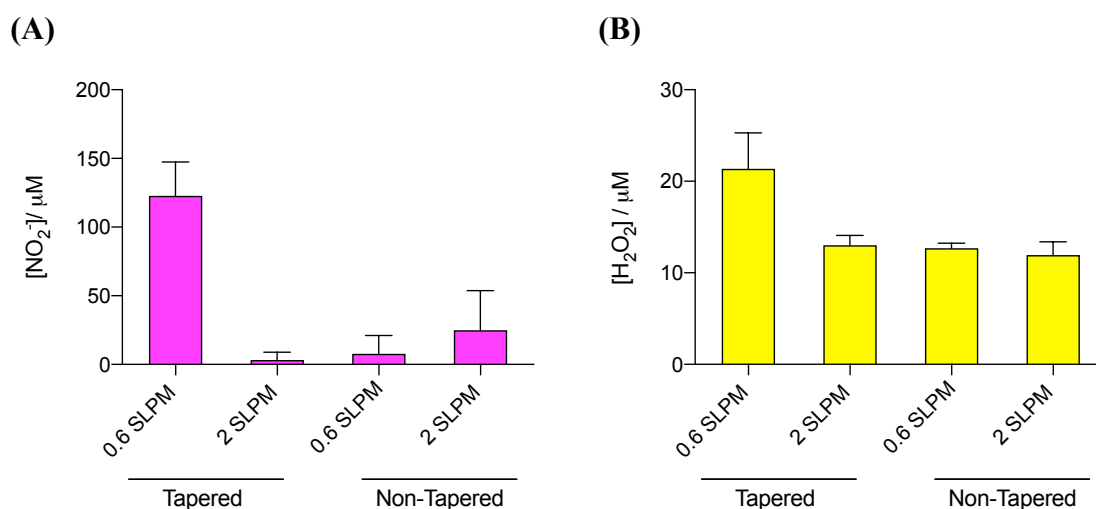


Figure 3.12 recovery of H_2O_2 and NO_2^- below 5% (w/v) PVA hydrogel after 1 h incubation at 25°C after 5 min of He-CAP treatment using: 0.6 SLPM of helium through non-tapered jet (A), 2 SLPM of helium through non-tapered jet (B), 0.6 SLPM of helium through tapered jet (C) and 2 SLPM of helium through tapered jet (D). Error bars denote standard deviation (n=3).

As a result of favourable gel interactions, the non-tapered He-CAP conformation was concluded to show best potential for application with a hydrogel screen. These conditions were therefore assessed for their bactericidal effects.

3.4.4 He-CAP Killing of Planktonic Bacteria

Planktonic bacteria were exposed to He-CAP treatment for varying times. The aim was to elucidate He-CAP's effect on bacterial viability and if, like many antibiotics, He-CAP was more effective on specific species of bacteria. Within the literature He-CAP is widely hailed as highly bactericidal against planktonic bacteria.⁴²⁻⁴⁴ Importantly, these studies use a multitude of different devices and do not consider the interactions between He-CAP device and a hydrogel screen.

Initially He-CAP was applied to subcultures of *Pseudomonas aeruginosa* (*P. aeruginosa*) (PAO1) *Staphylococcus aureus* (*S. aureus*) (H560) with CFU/mL of $\sim 1 \times 10^5$, as would be used within an MIC assay, the He-CAP was applied, and the bacterial cultures were left to grow for 18 h. Five minutes of He-CAP treatment was able to inhibit the proliferation of *P. aeruginosa* but not effective against *S. aureus*. However, as bacterial cultures of 1×10^5 CFU/mL would not be considered an infection within wound care, this was irrelevant. The MIC of H_2O_2 for *P. aeruginosa* (PAO1) is between 0.7-1.4 mM, *S. aureus* (H560) and

Methicillin-resistant *Staphylococcus aureus* (MRSA) (MRSA252) is between 3-6 mM (Appendix Figure 3.22). As the five minutes of He-CAP treatment produces $\sim 300 \mu\text{M}$ and $600 \mu\text{M}$ at 2 SLPM and 0.6 SLPM respectively, it is unsurprising no significant reduction is observed for stationary cultures of any of the strains.

He-CAP was then applied to stationary phase bacterial culture to assess its efficacy against high titre planktonic infection (at around 1.5×10^9 CFU/ml). To ensure that there was no bacterial proliferation, overnight cultures were suspended in PBS prior to He-CAP exposure. Cultures were then treated with either 2 SLPM or 0.6 SLPM of helium for 1, 5 and 10 minutes. After treatment bacteria were left to incubate to allow, He-CAP-produced RONS to have time to act, then the viability of remaining culture was enumerated Figure 3.13. No significant reduction on bacterial viability was observed with either flow rate or increased exposure time.

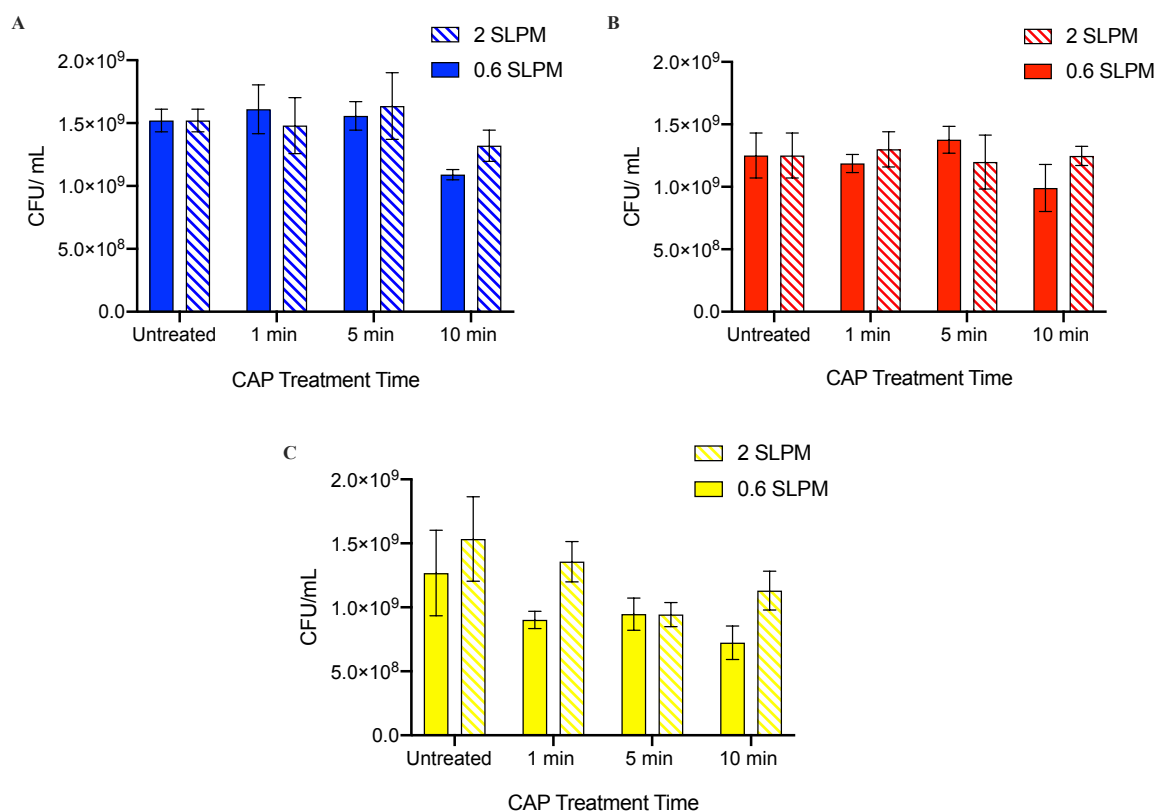


Figure 3.13 Effects of varying He-CAP helium flow rate and exposure time, using non-tapered jet, on viability of stationary phase, planktonic *P. aeruginosa* (PAO1) (A), *S. aureus* (H560) (B) and MRSA (MRSA252) (C) cultures in PBS. Error bars denote standard deviation (n=3).

3.4.5 He-CAP Eradication of Biofilms

He-CAP's efficacy in reducing bacterial biofilm bioburden has been widely reported within the literature, owing to the novel jet set up, the efficacy of the He-CAP jet was tested against the most prevalent bacterial species within wounds: *P. aeruginosa*, *S. aureus* and MRSA.⁴⁵ He-CAP was applied directly to established, 24 h biofilms of area 280 mm² for 5 minutes **Figure 3.14**). A treatment time of five minutes was used as it was thought to be a feasible treatment time for admission within a standard wound clinic.

He-CAP was found to significantly reduce the biofilm bioburden of all three bacterial species. This was unexpected, given that He-CAP had such a poor efficacy against planktonic cultures of the same bacterial strain, and that each mm² of biofilm would theoretically be exposed to the plasma for 0.945 seconds. This could potentially be as a result of changes in metabolic state for bacterial cells within a biofilm causing the bacteria to be more susceptible to RONS mediated killing. Alternatively, this unexpected reduction could be as a result of an increase in RONS generation on a solid surface. *P. aeruginosa* biofilms were most susceptible to He-CAP treatment, confirming literature reports that Gram-negative bacteria are more susceptible to He-CAP treatment.⁴⁶ Interestingly, a greater reduction was observed in MRSA than *S. aureus*. While it is uncertain what caused this difference, it is likely owing to variation in peroxide susceptibility or through variation in biofilm formation. No significant difference was observed between the two gas flow rates. However, qualitatively, the biofilms treated with 0.6 SLPM appear to have some surface scorching, which is thought to be as a result of the intensity of the 0.6 SLPM plume, as previously discussed. This phenomenon would not be favourable within a clinical environment.

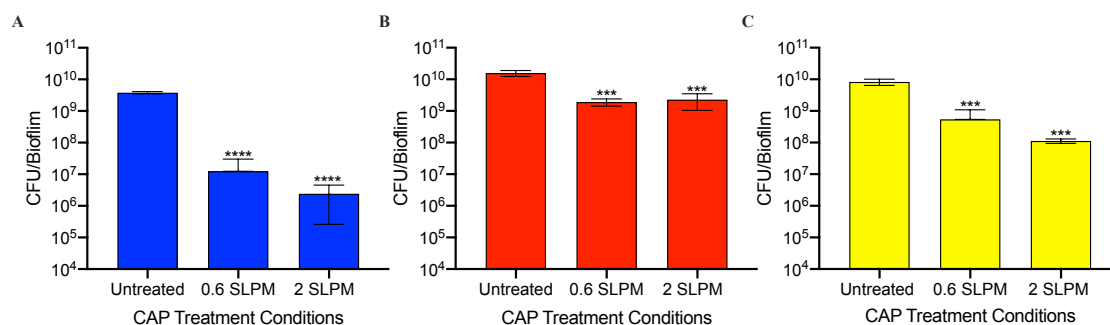


Figure 3.14 Reduction in viable cell count of *P. aeruginosa* (PAO1) (A), *S. aureus* (H560) (B) and MRSA (MRSA252) (C) 19 mm, 24 h biofilms after exposure to He-CAP for 5 mins at varying helium flow rate (0.6 & 2 SLPM). One-way ANOVA, (****) $p < 0.0001$ and (***) $p < 0.001$ compared to untreated. Error bars denote standard deviation (n=3).

The addition of a dressing on the wound is standard practice within wound care, providing a barrier to limit infection and providing a positive environment for healing to occur. The addition of a hydrogel dressing would enable the standard wound care to continue in tandem with He-CAP decontamination treatment. The He-CAP would be applied on to the hydrogel allowing the bactericidal RONS to diffuse into the wound bed and reduce bacterial load, while providing a screen from potentially harmful He-CAP-produced RONS and limiting the need for painful dressing changes owing partially to the transparency of the hydrogels, allowing basic wound assessment to continue without removal. Wound assessment is critical and if it can be done without the added infection risk of dressing removal this is highly beneficial. The 5% (w/v) PVA “model” hydrogel dressing was applied atop established 24 h biofilms of three common wound pathogens: *P. aeruginosa*, *S. aureus* and MRSA.

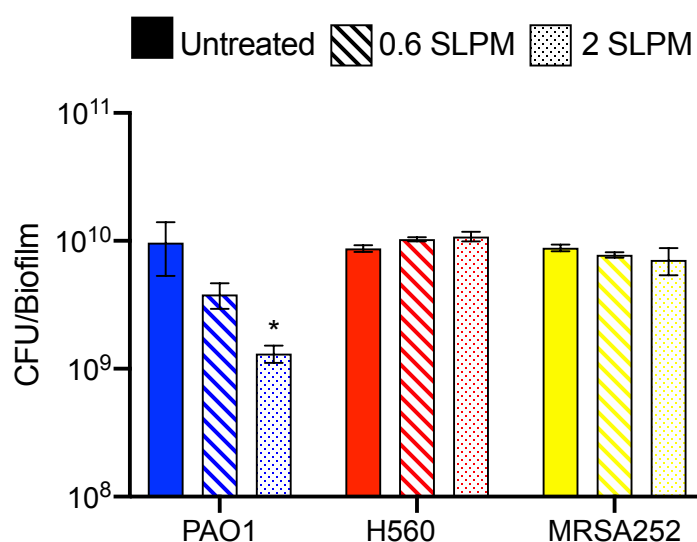


Figure 3.15 Reduction in viable cell count of *S. aureus* (H560), *P. aeruginosa* (PAO1) and MRSA (MRSA252) 24 h biofilms after 5 mins treatment with He-CAP at helium flow rate 0.6 SLPM or 2 SLPM atop a 5% (w/v) PVA hydrogel. Students *t*-test were carried out for statistical analysis. * $p = 0.0265$, all other comparisons were not significant. Error bars denote standard deviation (n=3).

Despite the unfavourable He-CAP-gel interactions both flow rates were used for comparison of efficacy. Treatment time of five minutes was found to effectively reduce the bioburden in direct treatment and was thought to be a reasonable treatment for use within wound clinics, thus five minutes of He-CAP was applied to the PVA gel biofilms. No reduction in viable cell counts was found for either H560 or MRSA252 strains. However, 2 SLPM He-CAP treatment on *P. aeruginosa* (PAO1) was found to significantly reduce bacterial counts, yet 0.6 SLPM was not found to have significant effect. While the reduction in viability was only 0.87 log (± 0.23) given that only 20 μM of H_2O_2 was recovered under the PVA gel after 5 mins He-CAP treatment, no reduction in bioburden had been expected. The delivery of H_2O_2 through a PVA hydrogel was quantified in section 3.4.3, however, previous quantification was carried out in a liquid medium (PBS), whereas here we observe the bactericidal effects of He-CAP generated RONS through a PVA hydrogel onto a surface biofilm, while biofilms are, as previously mentioned, 90% water, it is likely that there are different interactions occurring here than in previous experiments. Owing to the observed reduction in bacterial cell death in *P. aeruginosa* (PAO1) biofilms it is likely that greater concentrations of H_2O_2 or other RONS have been generated either within the gel or on the biofilm after He-CAP treatment. However, further work is required to understand this phenomenon.

3.4.6 He-CAP Inhibition of Biofilm Formation

While He-CAP jet treatment was found to be relatively ineffective for the eradication of an established biofilm-associated bacterial infection, it was considered that He-CAP may be able to inhibit the formation of a bacterial biofilm during the colonisation stage. As previously discussed, when a wound occurs the skin's integrity is compromised, enabling usually harmless bacteria to enter and colonise the wound. When the bacterial population outweighs the patient's immune response an infection occurs. Often when bacteria reach this density, known as the "critical threshold", they form biofilms, which is thought to occur at between 8-12 h into colonisation.⁴⁷ This anticipation of infection based on bacterial cell density is a relatively generalised and simplistic model of wound biofilm formation. As every patient/ wound is different (based on aetiology, comorbidities, treatment protocols, immune system responses/ complications etc.) it is challenging to predict wound progression based on microorganism colonisation alone. However, as biofilms are known to be hard to treat much research is now focused on the prevention and limitation of biofilm formation,

thus enabling easier treatment of bacterial infections and the reduction of antibiotic use. Bacterial biofilms were inoculated at 0 h and left to grow on a polycarbonate *in vitro* wound biofilm model for a total of 24 h at 37°C. At various stages during growth the developing biofilms were treated for 5 minutes with He-CAP jet. After a total 24 h of growth, biofilms were analysed.

3.4.6.1 Reduction in Viability

Biofilms were stripped and viable cells enumerated as previously described. A significant reduction in viable cells was observed at all treatment intervention times for *P. aeruginosa* (**Figure 3.16**). When treatment was administered at 0, 4 and 8 h the total biofilm was reduced below 10^5 CFU/ml, which would no longer be clinically considered as a wound infection.⁴⁸ After 8 h the bioburden is still significantly reduced, resulting in the likelihood that antimicrobials will be more effective, as well as improving the likelihood of the patient clearing the infection through a reduction in the burden on the host immune system and not overwhelming the innate immune response. He-CAP intervention was not found to be as effective on the developing MRSA252 biofilms. It is known that Gram-positive bacteria, such as MRSA, are not as susceptible to He-CAP. This is likely owing to their higher MIC (3-6 mM) for H_2O_2 when compared to Gram-negative bacteria like *P. aeruginosa* (700-350 μ M).

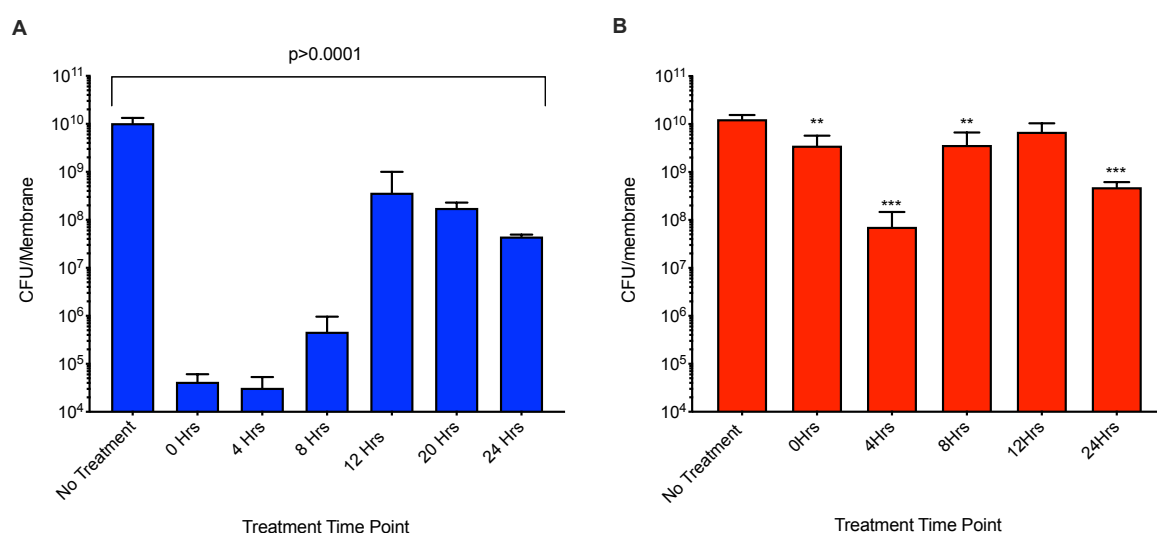


Figure 3.16 Comparison of viable bacterial cells at 24 h growth after varying He-CAP treatment intervention times during bacterial biofilm development. *P. aeruginosa* (PAO1) (A) MRSA (MRSA 252) (B). One-way ANOVA was performed (****) $p < 0.0001$ and (***) $p < 0.001$ (**) $p < 0.01$ (*) $p < 0.05$. Error bars denote standard deviation (n=3).

3.4.6.2 SEM Visualisation of Treated Biofilm

To further understand the potential mechanism of He-CAP on limiting biofilm formation, qualitative visualisation of the biofilms was carried out using SEM. Owing to the high-resolution, SEM enables visualisation of biofilm architecture, as well as morphology of bacterial cells at high resolution. The untreated *P. aeruginosa* biofilm displays typical biofilm morphology, the bacterial cells are densely packed, with an intricate web like structure, known as the extracellular matrix (ECM), holding them together (**Figure 3.17A**). After intervention at 8 h into bacterial growth where biofilm formation is likely to begin to occur, although this will vary between species, a visible reduction in bacterial density can be observed, with vast amounts of cellular debris and loss of the ECM (**Figure 3.17B**). Subsequently, after intervention 12 h into development (**Figure 3.17C**), there is some evidence of the web-like matrix, yet it appears altered when compared to the untreated biofilm. Moreover, despite the increase in bacterial cell density relative, in comparison to the **Figure 3.17B**, which is thought to be as a result of having 4 h extra to reach critical mass, the bacterial cells morphology appears altered. The cells appear puckered and no longer uniform in their appearance. This alteration in morphology was thought to indicate cellular death, Lekbach *et al.* report comparable *P. aeruginosa* morphology as cellular death, further confirming He-CAP induced death.⁴⁹ However, despite the evidence of considerable He-CAP induced cell death and structural alterations, the viable cell counts of biofilms with treatment intervention times of 12 h are still $\sim 1 \times 10^9$ CFU/mL (**Figure 3.16**).

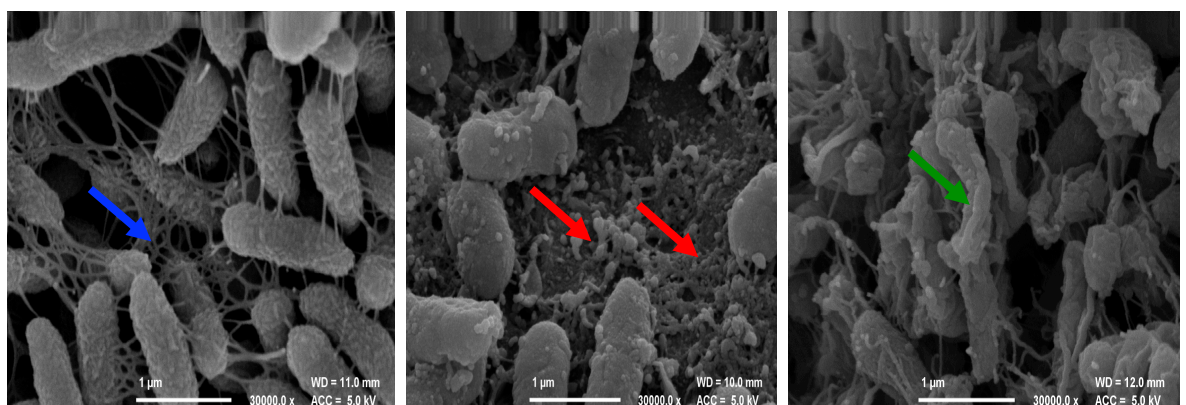


Figure 3.17 SEM images of *P. aeruginosa* (PAO1) biofilm after 24 h growth with varying treatment intervention times with 5 min exposure to He-CAP jet. Untreated control (A) blue arrow indicating the biofilm extracellular matrix. Treatment was applied 8 h into biofilm development, red arrow indicating cellular debris (B). Treatment was applied 12 h into biofilm development. Green arrow indicating dead *P. aeruginosa* cell (C).

3.4.6.3 Confocal Scanning Laser Microscopy of Biofilms using LIVE/DEAD Staining

Due to the disparity between SEM and viability data, LIVE/DEAD staining was carried out to further understand to impact of He-CAP treatment intervention. The LIVE/DEAD assay indicates cellular death through dye uptake. Cells which are dead, have ruptured membranes, those that are alive do not. All cells will take up the green dye, however, only dead cells with ruptured outer membrane will take up the red dye indicating their death.

The 24 h biofilm that was treated at 8 h, appears to lack cell density, shown by its thin Z axis, however, there is a thin green layer suggesting that although there is a loss of bacterial cell density, the cells are beginning to recover (**Figure 3.18A**). At 12 h a thick layer of red, dead, cells on the top layer of the markedly denser biofilm, which is indicative of the cellular death observed in the SEM results. Yet a thinner, green, live layer of cells remains. A 12 h biofilm will have reached a viable cell count of approximately 1×10^9 CFU/mL, which is a considerable cellular density, however, this biofilm would not have the same level of ECM as a 24 h biofilm. The significant amount of red, dead cells is likely owing to the lack of biofilm architecture providing protection. Yet, the thin green, viable layer underneath is thought to be what gives rise to the high number of viable cells found in **Figure 3.16A**.

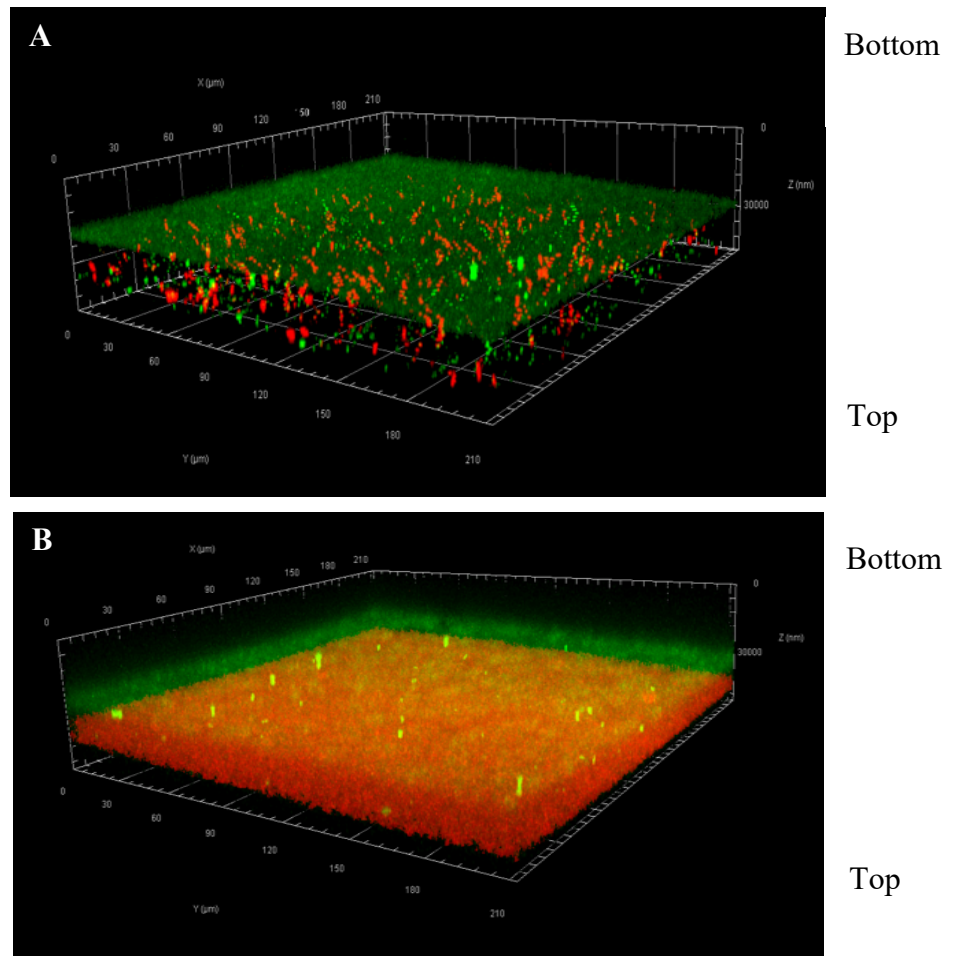


Figure 3.18 LIVE/DEAD results *P. aeruginosa* (PAO1) biofilm after 24 h growth with varying treatment intervention times with 5 min exposure to He-CAP jet **(A)** He-CAP intervention 8 h into growth **(B)** He-CAP intervention 12 h into growth. Images are inverted.

3.5 Conclusion

This chapter established that the He-CAP treatment applied atop a simple 5% (w/v) PVA hydrogel screen was not sufficient for the treatment of bacterial biofilm-associated infections within wounds. He-CAP conditions were optimised for maximum bacterial killing by quantifying the key bactericidal components: H_2O_2 and NO , while others may have an effect these are the predominant species, while retaining favourable interactions with a model hydrogel wound dressing made from PVA. Through cryo-crosslinking the PVA, hydrogel has the durability and flexibility to make it a good model wound dressing. A non-tapered jet configuration using 2 SLPM of helium was found to produce $\sim 600 \mu\text{M}$ of H_2O_2 and $5 \mu\text{M}$ of NO_2^- upon direct treatment, and while this was not found to have the greatest concentrations of RONS of all jet set ups, these conditions interacted the best with the hydrogel.

Gas flow rate did not appear to exhibit any effect on the viability of planktonic *P. aeruginosa*, *S. aureus* or MRSA strains post He-CAP exposure. Interestingly, when used to treat established 24 h biofilms, both 0.6 and 2 SLPM were found to significantly reduce the bacterial load, with Gram-negative *P. aeruginosa* being more susceptible to He-CAP treatment. This indicates that the He-CAP interactions at liquids and solid interfaces differ substantially. This could be owing to the difference in dilution factor between the liquid treatment and the polycarbonate membrane or that the generation of bactericidal RONS occurs more readily within the biofilm matrix or wound milieu.

The addition of the PVA hydrogel aimed to limit the delivery of potentially harmful RONS into the wound while providing a positive healing environment for the wound, with the intention of potentially propagating the generation of bactericidal RONS *in situ*. However, on addition of the hydrogel, He-CAP treatment no longer resulted in a reduction of bacterial load in drug-resistant or susceptible *S. aureus*. This was unsurprising, as the concentration of H_2O_2 recovered below the hydrogel was $< 50 \mu\text{M}$. Interestingly, when using 2 SLPM flow rate, a ~ 1 -log reduction in bioburden was observed in *P. aeruginosa*, however, a biofilm of 10^9 CFU/mL would still be hard to treat and be considered a serious infection.

Importantly, He-CAP application on a developing biofilm was found to significantly reduce the formation of *P. aeruginosa* biofilms in a time-dependent manner. Although He-CAP therapy has been found to induce significant bacterial death, the presence of both living and dead cells and impacted the structural integrity of the ECM within an established biofilm appears to offer some level of protection to the lower layers of biofilm, resulting in retention of viable cells. Treating within the early stages of development, before the biofilm has become established which would be before 12 h, significantly reduces the bacterial bioburden and limits the biofilms development, wherein traditional treatment strategies may become more effective. This finding was very encouraging as the reduction in bacterial load could increase the efficacy of antimicrobial treatments which would otherwise ineffective against the established biofilm.

A therapeutic release system could work well within the envisaged care pathway. In that, any large open wound could be treated with He-CAP to reduce bacterial load and limit biofilm formation. For example, at the 8 h stage for example a therapeutic hydrogel wound dressing could then be added and the He-CAP could be used to release an antibiofilm agent further preventing the biofilm formation and ideally eradicating any infection.

3.6 Future Work

The He-CAP jet used fails to generate high enough concentrations of H_2O_2 to have a significant impact on bacteria. Owing to the range of variables associated with He-CAP therapy, an improved He-CAP jet could be created which generates higher concentrations of H_2O_2 . If H_2O_2 were available in higher concentrations it is likely a greater reduction in biofilm bioburden would be observed both with and without a hydrogel wound dressing screen. While the simplistic PVA hydrogel failed to enable He-CAP-produced RONS to diffuse through it to produce a significant reduction in bacterial biofilm bioburden, the He-CAP treatment parameters were optimised for tolerable interactions between the hydrogel and He-CAP jet. Within the literature there are a range of H_2O_2 triggered release systems which could be added into the hydrogel to respond to He-CAP application, treating the wound infection, without the need for a dressing change.

Future work seeks to elucidate other potential biological interactions with He-CAP that may produce advantageous responses, such as those observed with the reduction of established biofilms and the time-dependent limitation of biofilm formation. Further to this, it would be interesting to see if He-CAP intervention during biofilm development makes the bacterial biofilm more susceptible to traditional wound infection treatments such as antibiotics. Direct treatment of He-CAP for decontamination of wounds is largely supported within literature without any consideration of the potentially harmful effects of exposing bacteria to He-CAP. Concerningly, direct He-CAP exposure could induce potentially harmful mutations within the bacteria and can bacteria mount resistance to He-CAP treatment, future work would seek to investigate the mutagenic effect of He-CAP treatment on bacteria. Further to this, while this work only quantifies and investigates the impact of H_2O_2 and nitrates/nitrites as these are reported to be the predominant reactive species, future work would seek to quantify and understand the role of other RONS and how they potentiate the bacterial reduction induced by He-CAP treatment.

3.7 References

1. Morfill, G. E. *et al.* Plasma medicine: an introductory review . *New J. Phys.* **11**, 115012 (2009).
2. Gorbanev, Y., Privat-Maldonado, A. & Bogaerts, A. Analysis of Short-Lived Reactive Species in Plasma-Air-Water Systems: The Dos and the Do Nots. *Anal. Chem.* **90**, 13151–13158 (2018).
3. Liu, Z. *et al.* Quantifying the concentration and penetration depth of long-lived RONS in plasma-activated water by UV absorption spectroscopy. *AIP Adv.* **9**, 015014 (2019).
4. Hathaway, H. J. *et al.* Delivery and quantification of hydrogen peroxide generated via cold atmospheric pressure plasma through biological material. *J. Phys. D. Appl. Phys.* (2019) doi:10.1088/1361-6463/ab4539.
5. Govaert, M., Smet, C., Verheyen, D., Walsh, J. L. & Van Impe, J. F. M. Combined Effect of Cold Atmospheric Plasma and Hydrogen Peroxide Treatment on Mature *Listeria monocytogenes* and *Salmonella Typhimurium* Biofilms. *Front. Microbiol.* **10**, 2674 (2019).
6. Pai, K. *et al.* Investigation of the Roles of Plasma Species Generated by Surface Dielectric Barrier Discharge. *Sci. Rep.* **8**, 16674 (2018).
7. Arjunan, K., Sharma, V. & Ptasinska, S. Effects of Atmospheric Pressure Plasmas on Isolated and Cellular DNA—A Review. *Int. J. Mol. Sci.* **16**, 2971–3016 (2015).
8. Khlyustova, A., Labay, C., Machala, Z., Ginebra, M.-P. & Canal, C. Important parameters in plasma jets for the production of RONS in liquids for plasma medicine: A brief review. *Front. Chem. Sci. Eng.* **13**, 238–252 (2019).
9. Szili, E. J., Hong, S. H., Oh, J. S., Gaur, N. & Short, R. D. Tracking the Penetration of Plasma Reactive Species in Tissue Models. *Trends in Biotechnology* vol. 36 594–602 (2018).
10. Witte, M. B. & Barbul, A. Role of nitric oxide in wound repair. *Am. J. Surg.* **183**, 406–412 (2002).
11. Luo, J., Chen, A. F. & Chen P, A. F. Nitric oxide: a newly discovered function on wound healing. (2005) doi:10.1111/j.1745-7254.2005.00058.x.
12. Schairer, D. O., Chouake, J. S., Nosanchuk, J. D. & Friedman, A. J. The potential of nitric oxide releasing therapies as antimicrobial agents. *Virulence* vol. 3 271–279 (2012).

13. Borchardt, T. *et al.* Effect of direct cold atmospheric plasma (diCAP) on microcirculation of intact skin in a controlled mechanical environment. *Microcirculation* **24**, (2017).
14. Kimmel, H., Grant, A. & Ditata, J. The Presence of Oxygen in Wound Healing | Wounds Research. *Wounds* **28**, 264–270 (2016).
15. Guffey, J. S. & Wilborn, J. In vitro bactericidal effects of 405-nm and 470-nm blue light. *Photomed. Laser Surg.* **24**, 684–688 (2006).
16. Li, S. H. & Chow, K. C. Magnetic field exposure induces DNA degradation. *Biochem. Biophys. Res. Commun.* **280**, 1385–1388 (2001).
17. Kohno, M., Yamazaki, M., Kimura, I. & Wada, M. Effect of static magnetic fields on bacteria: *Streptococcus mutans*, *Staphylococcus aureus*, and *Escherichia coli*. in *Pathophysiology* vol. 7 143–148 (Elsevier, 2000).
18. Tessaro, L. W. E., Murugan, N. J. & Persinger, M. A. Bacterial growth rates are influenced by cellular characteristics of individual species when immersed in electromagnetic fields. *Microbiol. Res.* **172**, 26–33 (2015).
19. Kamoun, E. A., Kenawy, E. R. S. & Chen, X. A review on polymeric hydrogel membranes for wound dressing applications: PVA-based hydrogel dressings. *Journal of Advanced Research* vol. 8 217–233 (2017).
20. Oliveira, R. N., McGuinness, G. B., Ramos, M. E. T., Kajiyama, C. E. & Thiré, R. M. S. M. Properties of PVA Hydrogel Wound-Care Dressings Containing UK Propolis. *Macromol. Symp.* **368**, 122–127 (2016).
21. Stauffer, S. R. & Peppast, N. A. Poly(vinyl alcohol) hydrogels prepared by freezing-thawing cyclic processing. *Polymer (Guildf)*. **33**, 3932–3936 (1992).
22. Tavakoli, J., Gascooke, J., Xie, N., Zhong Tang, B. & Tang, Y. Enlightening Freeze–Thaw Process of Physically Cross-Linked Poly(vinyl alcohol) Hydrogels by Aggregation-Induced Emission Fluorogens. *Cite This ACS Appl. Polym. Mater* (2019) doi:10.1021/acsapm.9b00173.
23. Kumeta, K., ãã, ãã. ;, Nagashima, I., Matsui, S. & Mizoguchi, K. Crosslinking of Poly(vinyl alcohol) via Bis(-hydroxyethyl) Sulfone. doi:10.1295/polymj.36.472.
24. Laroussi, M. & Lu, X. Room-temperature atmospheric pressure plasma plume for biomedical applications. *Appl. Phys. Lett.* **87**, 113902 (2005).
25. XinPei Lu *et al.* A long atmospheric pressure cold plasma plume for biomedical applications. in 1–1 (Institute of Electrical and Electronics Engineers (IEEE), 2008). doi:10.1109/plasma.2008.4590777.

26. Joh, H. M., Kang, H. R., Chung, T. H. & Kim, S. J. Electrical and optical characterization of atmospheric-pressure helium plasma jets generated with a pin electrode: Effects of the electrode material, ground ring electrode, and nozzle shape. *IEEE Trans. Plasma Sci.* **42**, 3656–3667 (2014).
27. Baek, E. J., Joh, H. M., Kim, S. J. & Chung, T. H. Effects of the electrical parameters and gas flow rate on the generation of reactive species in liquids exposed to atmospheric pressure plasma jets. *Phys. Plasmas* **23**, 073515 (2016).
28. Labay, C., Hamouda, I., Tampieri, F., Ginebra, M. P. & Canal, C. Production of reactive species in alginate hydrogels for cold atmospheric plasma-based therapies. *Sci. Rep.* **9**, 1–12 (2019).
29. Eisenberg, G. M. *Colorimetric Determination of Hydrogen Peroxide Optimum Quantity of Test Reagent for Maximum Color Development*. <https://pubs.acs.org/sharingguidelines>.
30. Machala, Z. *et al.* Formation of ROS and RNS in Water Electro-Sprayed through Transient Spark Discharge in Air and their Bactericidal Effects. *Plasma Process. Polym.* **10**, 649–659 (2013).
31. Junglee, S., Urban, L., Sallanon, H. & Lopez-Lauri, F. Optimized Assay for Hydrogen Peroxide Determination in Plant Tissue Using Potassium Iodide. *Am. J. Anal. Chem.* **05**, 730–736 (2014).
32. Hernando, F. *et al.* Another Twist of the Foam: An Effective Test Considering a Quantitative Approach to ‘elephant’s Toothpaste’. *J. Chem. Educ.* **94**, 907–910 (2017).
33. Chae, S. Y., Lee, M., Kim, S. W. & Bae, Y. H. Protection of insulin secreting cells from nitric oxide induced cellular damage by crosslinked hemoglobin. *Biomaterials* **25**, 843–50 (2004).
34. Campos-Neto, A. *et al.* CD40 ligand is not essential for the development of cell-mediated immunity and resistance to Mycobacterium tuberculosis. *J. Immunol.* **160**, 2037–41 (1998).
35. Kim, S. J. & Chung, T. H. Cold atmospheric plasma jet-generated RONS and their selective effects on normal and carcinoma cells. *Sci. Rep.* **6**, (2016).
36. Kumar, P. & Honnegowda, T. Effect of limited access dressing on surface pH of chronic wounds. *Plast. Aesthetic Res.* **2**, 257 (2015).
37. Percival, S. L., McCarty, S., Hunt, J. A. & Woods, E. J. The effects of pH on wound healing, biofilms, and antimicrobial efficacy. *Wound repair and regeneration* :

official publication of the Wound Healing Society [and] the European Tissue Repair Society vol. 22 174–186 (2014).

38. Yadav, D. K. *et al.* Cold atmospheric plasma generated reactive species aided inhibitory effects on human melanoma cells: an in vitro and in silico study. *Sci. Rep.* **10**, 1–15 (2020).
39. Schneider, C. *et al.* Acidification is an essential process of cold atmospheric plasma and promotes the anti-cancer effect on malignant melanoma cells. *Cancers (Basel)*. **11**, (2019).
40. Ou, K., Dong, X., Qin, C., Ji, X. & He, J. Properties and toughening mechanisms of PVA/PAM double-network hydrogels prepared by freeze-thawing and anneal-swelling. *Mater. Sci. Eng. C* **77**, 1017–1026 (2017).
41. Haines, L. A. *et al.* Light-Activated Hydrogel Formation via the Triggered Folding and Self-Assembly of a Designed Peptide. (2005) doi:10.1021/ja054719o.
42. Theinkom, F. *et al.* Antibacterial efficacy of cold atmospheric plasma against *Enterococcus faecalis* planktonic cultures and biofilms in vitro. *PLoS One* **14**, e0223925 (2019).
43. Mai-Prochnow, A., Bradbury, M., Ostrikov, K. & Murphy, A. B. *Pseudomonas aeruginosa* biofilm response and resistance to cold atmospheric pressure plasma is linked to the redox-active molecule phenazine. *PLoS One* **10**, (2015).
44. Ziuzina, D., Patil, S., Cullen, P. J., Keener, K. M. & Bourke, P. Atmospheric cold plasma inactivation of *Escherichia coli* in liquid media inside a sealed package. *J. Appl. Microbiol.* **114**, 778–787 (2013).
45. Bowler, P. G., Duerden, B. I. & Armstrong, D. G. Wound microbiology and associated approaches to wound management. *Clinical Microbiology Reviews* vol. 14 244–269 (2001).
46. Mai-Prochnow, A., Clauson, M., Hong, J. & Murphy, A. B. Gram positive and Gram negative bacteria differ in their sensitivity to cold plasma. *Sci. Rep.* **6**, (2016).
47. Rasamiravaka, T., Labtani, Q., Duez, P. & El Jaziri, M. The formation of biofilms by *pseudomonas aeruginosa*: A review of the natural and synthetic compounds interfering with control mechanisms. *BioMed Research International* vol. 2015 (2015).
48. Hurlow, J. *et al.* Clinical Biofilms: A Challenging Frontier in Wound Care. *Adv. Wound Care* **4**, 295–301 (2015).
49. Lekbach, Y. *et al.* Catechin hydrate as an eco-friendly biocorrosion inhibitor for 304L

Chapter 3

stainless steel with dual-action antibacterial properties against *Pseudomonas aeruginosa* biofilm. *Corros. Sci.* **157**, 98–108 (2019).

3.8 Appendix

3.8.1 KI Standard Curve

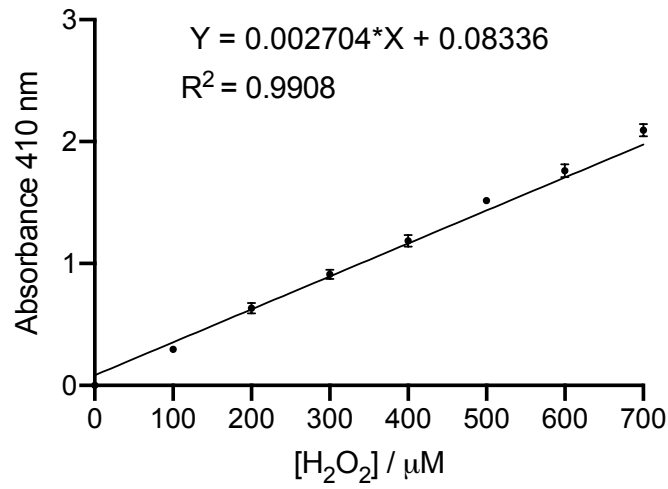


Figure 3.19 Standard curve using 1 M KI for the quantification of H₂O₂. Error bars denote standard deviation (n=3).

3.8.2 Griess Test Standard Curve

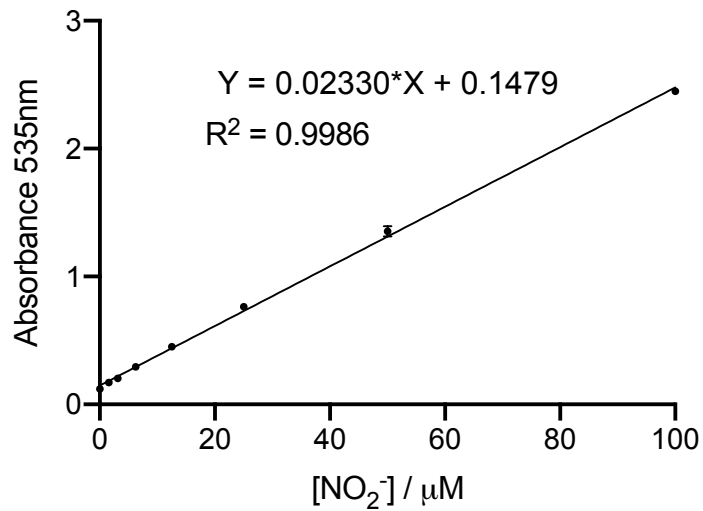


Figure 3.20 Standard curve using Griess reagents against known concentrations of sodium nitrate (NO₂⁻). Error bars denote standard deviation (n=3).

3.8.3 Titanium Oxysulphate Standard Curve

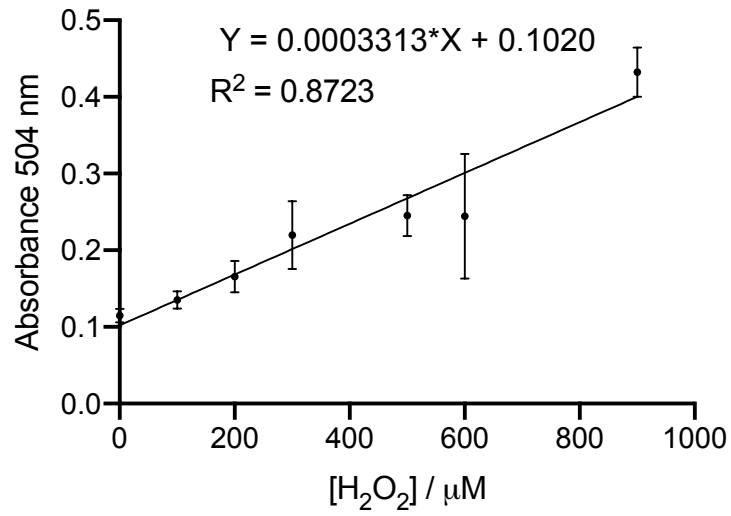


Figure 3.21 Standard curve of TiOSO_4 for the quantification of H_2O_2 . Error bars denote standard deviation ($n=3$).

3.8.4 MIC of H_2O_2

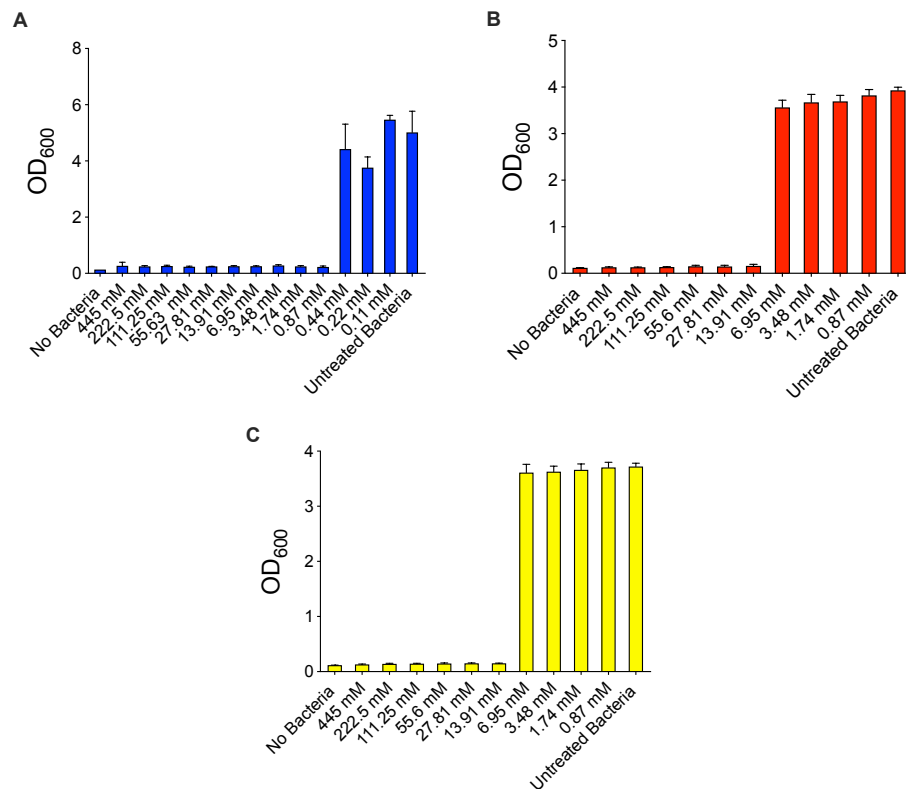


Figure 3.22 MIC of H_2O_2 for *P. aeruginosa* (PAO1) (A), *S. aureus* (H560) (B) and MRSA (MRSA252) (C). Error bars denote standard deviation

Chapter 4

Chapter 4 : Role of Biofilm Formation and Bacterially Produced Catalase in Mitigating CAP Damage

4.1 Overview

The interactions of cold atmospheric pressure plasma (CAP) and bacteria are still relatively unknown, as CAP is championed for application on biofilm-associated wound infection this chapter seeks to elucidate the interactions between CAP with bacteria and the effects this has on the efficacy of CAP decontamination of wounds. The complex architecture of biofilms is known to limit the diffusion of antibiotics through a biofilm, resulting in an increase in therapeutic dose. The structure and interactions within a biofilm denote a high level of resistance to mechanical and antibiotic treatments.

Szili *et al.* showed that plasma produced reactive oxygen and nitrogen species (RONS) were able to transverse a “tissue model” for enhanced delivery with ROS delivery being recorded 150 µm – 1.5 mm below the tissue surface.¹ While topical treatments struggle to transverse the bacterial biofilm matrix, these finding suggest that CAP may enable enhanced delivery of RONS through the biological interface delivering bactericidal RONS deep into the biofilm and thus enable a greater antibacterial/antibiofilm properties and help account for high efficacy against biofilms observed in Chapter 3.

This chapter seeks to elucidate the role of a developing bacterial biofilm in terms of bacterial density and species in limiting the transversion of helium-driven cold atmospheric pressure plasma (He-CAP) produced RONS into the wound bed compared topical H₂O₂. Bacteria produce a range of defence mechanism to mitigate cellular death, thus it is hypothesised that they will produce a response to limit the damage of He-CAP treatment. This chapters seeks to understand the role bacterially produced enzymes play in limiting cellular death from He-CAP exposure.

4.2 Chapter Background

4.2.1 Delivery of CAP RONS into Tissue Model

The use of plasmas for the modification of organic surfaces has been widely reported², yet in this application only 1-2 nm of the uppermost surface is modified. Photons and charged species are confined to this outer surface and RONS and radicles will react quickly thus having limited penetration. However, CAP produced RONS are known to penetrate into wounds covered with exudate and clotting blood. Further to this, our work has shown that CAP is effective in the treatment of thick biofilms. Szili *et al.* used a gelatin hydrogel to mimic skin with a vesicle-based sensor system suspended within the gel, which would rupture releasing a fluorescent dye in response to CAP induced damage. The group found that upon application of CAP treatment vesicles deep into the gelatin tissue (>150 μm) model were damaged. Further to this, despite the modest diameter of the CAP jet, the group found that a circular diameter of ~ 10 mm around the treatment area was subject to CAP induced damage, which is thought to be owing to the gas flow.¹

4.2.2 Oxidative Stress

Oxidative stress is caused by an imbalance between the systemic levels of reactive oxygen species (ROS) and the biological systems ability to mitigate their impact. While normally the system is able to detoxify the reactive species, when they cannot, oxidative damage will occur. Oxidative damage can occur in all living organisms and can be catastrophic in its effect altering the structure and activity of protein and can even lead to cellular death.³

Within human health, oxidative stress is involved in the development of a variety of medical conditions including cancer,⁴ Alzheimer's⁵ and Parkinson.⁶ However, ROS are produced endogenously by phagocytes within immune system to combat infection and also through leakage of activated oxygen from mitochondria during oxidative phosphorylation. But in order to maintain homeostasis cells have antioxidising systems, predominantly consisting of enzymes to mitigate or "mop up" excessive production of ROS and thus limit oxidative damage. Such enzymes include superoxide dismutase (SOD), catalase and glutathione peroxidase.⁷

4.2.3 *E. coli* Oxidative Stress Response

All aerobic bacteria, such as *Escherichia coli* (*E. coli*), require molecular oxygen (O_2) for respiration and the generation of energy. However, occasionally O_2 can be oxidised by redox enzymes in a process creating superoxide ($\bullet O_2^-$) a reactive oxygen species (ROS), that can cause damage to the bacteria.⁸ Further to this threat, the environment inhabited by bacteria is full of other harmful RONS such as H_2O_2 , NO and hydroxyl radicals ($\bullet OH$).⁹ The levels of RONS are kept in balance by bacteria using antioxidants, if the balance is disrupted, the bacteria's oxidative stress response (OSR) is engaged to prevent damage (**Figure 4.1**).

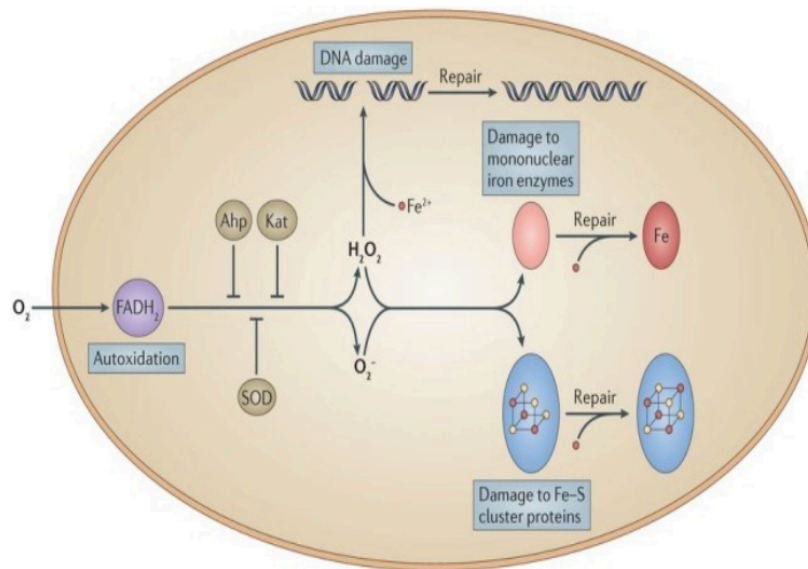


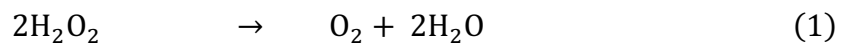
Figure 4.1: Schematic of reactive oxygen species induced damage in *E. coli* (Reproduce with permission from International Journal of Current Microbiology and Applied Sciences).¹⁰

E. coli's OSR is mediated by three key antioxidising pathways: SOD, catalase (*kat*) and alkyl hydroperoxide reductase (*Ahp*). SOD dismutates $\bullet O_2^-$ to H_2O_2 and *E. coli* has two distinct SOD Fe-SOD (encoded for by *sodA*) and Mn-SOD (encoded for by *sodB*).¹¹ Catalase catalyses the breakdown of H_2O_2 into H_2O and O_2 , *E. coli* has two catalases hydroperoxidase I (HPI) (*katG*) and hydroperoxidase II (HP II) (*katE*) (discussed further in section 4.2.5).¹² *Ahp* reduces various endogenous hydroperoxides (encoded for by *aphC* and *aphF*) (**Figure 4.1**).

4.2.4 Catalase

Catalase is an enzyme which catalyses the decomposition of H_2O_2 into oxygen and water, **Equation 4.1**, and is found in nearly all animals, plants and bacteria. Bacterial catalase is located intracellularly and is tested for within clinical microbiology, through application of a few drops of 30% (v/v) H_2O_2 . If effervescence is observed a positive result is recorded, to assist in classification of bacterial species.¹³

Catalase



Equation 4.1: Breakdown of H_2O_2 catalysed by catalase

4.2.5 *E. coli* Catalase

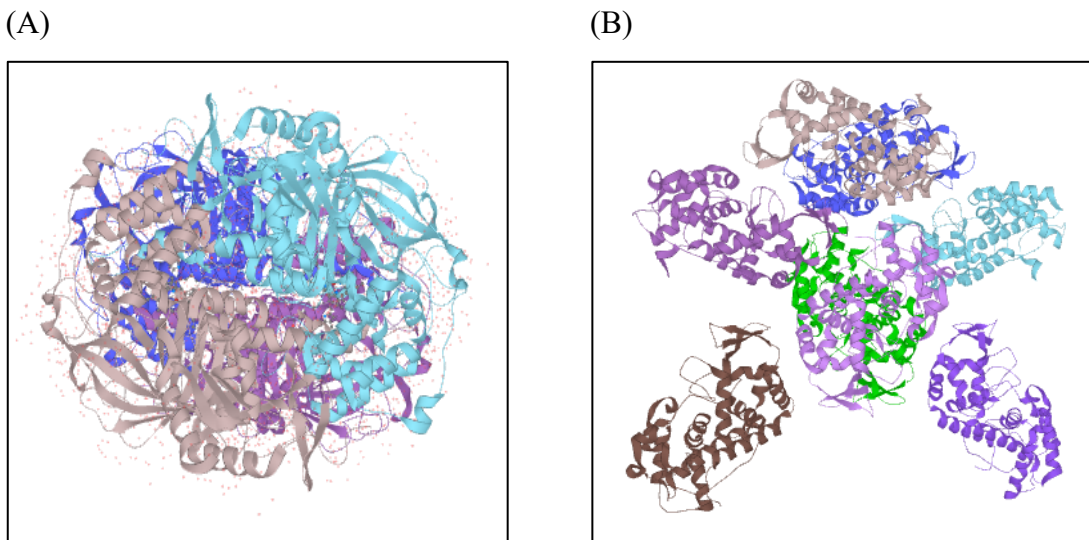


Figure 4.2: Structure of HPII (A) and HPI (B).

E. coli has been found to have two forms of catalase HPI and HPII. HPI is a bifunctional enzyme possessing both catalase activity and peroxidase activity, tetramer is structure with a molecular weight of 84,000 Daltons (Da), encoded for by *katG* (**Figure 4.2A**).¹⁴ HPII is monofunctional enzyme, with a molecular weight of 74000 Da, possessing only catalase activity and is encoded for by *katE* (**Figure 4.2B**).¹⁵

The expression of the two catalase enzymes is regulated independently of one another. HPI expression is induced in the presence of low concentrations of H₂O₂ through the detection of stress by *OxyR*, which is the main peroxide sensor that regulates the transcription of oxidative stress defence genes in response to low levels of H₂O₂. This results in a conformational change on the cysteine residues of *katG*. Whereas HPII is expressed during the transition between exponential growth phase and stationary phase through transcription of RNA polymerase containing σ^S subunit, a product of *rpoS* gene, which plays a key role in stress response.¹⁶

4.2.6 Gene Knockout

Gene function can be evaluated simply through removing the gene, this process is known as gene knock-out. After knock-out the gene's function can be elucidated through the evaluation of alterations to phenotype. Gene knockouts can be used to understand the complex network of regulation and the gene's function of a system wide level through the use of metabolomics, proteomics and transcriptomics.¹⁷ *E. coli* K-12 was first isolated from the stool of a diphtheria patient in 1922 and subsequently served as a standard culture in the laboratories of Stanford University owing to its high fertility within a laboratory setting.¹⁸ *E. coli* K-12 also has lambda phage (λ), which contains *lac* reporting system for isolation of mutants.

4.2.7 *E. coli* Catalase Mutants

Various strains of *E. coli* lacking the individual catalase have been used to analyse the role of the two catalase genes, Narita & Peng describe the construction of single knockouts and a catalase double knockout in *E. coli*. The group achieved this by knocking out the *katG* from the existing *katE* with kanamycin resistance cassette insertion using the Lambda Red recombination system, which is mediated by phage genes on a helper plasmid enabling scarless recombination and generation of the knockout. The kanamycin resistance cassette was then subsequently removed by the flippase recognition target (FRT) sites by the recombinase flippase (FLP) known as (FLP-FRT) recombination system, mediated by flippase on the helper plasmid.¹⁹

4.3 Methods

4.3.1 Materials

Ethylenediaminetetraacetic acid (EDTA), phenylmethanesulfonyl fluoride (PMSF), bovine serum albumin (BSA) and catalase from bovine liver were all purchased from Sigma-Aldrich (Poole, UK). Bradford reagent was purchased from Fischer Scientific (Ipswich, UK).

4.3.2 Recovery of RONS Through Bacterial Biofilm

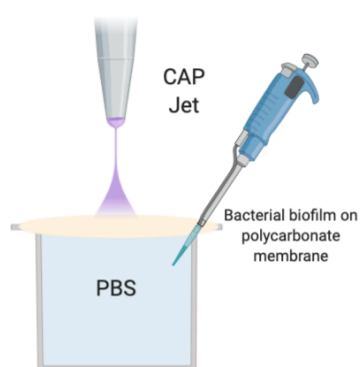


Figure 4.3: Experimental set up for the recovery of RONS beneath bacterial biofilm.

Biofilms were grown on polycarbonate membranes for 8, 12 and 24 h according to protocol in Section 2.3.3. Biofilms were removed using sterile forceps and placed atop 400 μL of sterile PBS in a 96-well plate as shown in **Figure 4.3**. Non-tapered CAP jet treatment was applied to the biofilm for 5 minutes (0.6 standard litres per minute (SLPM), 25 kHz, 10 kV, 5 mm distance) without movement. Post treatment biofilms were left to incubated at 25 $^{\circ}\text{C}$ for 30 minutes to allow the diffusion of H_2O_2 through the biofilm. After incubation 100 μL of PBS from below the biofilm was removed and the H_2O_2 concentration was subsequently quantified using KI reporter system as per section 2.6.5.1.

4.3.3 PVA/CMC Hydrogel

5% (w/v) solution of polyvinyl alcohol (PVA) was prepared as per 2.6.3. The solution was supplemented with carboxymethylcellulose (CMC) and case to a thickness of 10 mm and stored for 18 h at -20 $^{\circ}\text{C}$ to promote cryo-crosslinking. Gels were removed and defrosted at

room temperature after one freeze-thaw cycle, as per 2.6.3. As required gel discs were cut to a diameter 1 cm.

4.3.4 Bacterial Lysis

10 mL of bacterial overnight was centrifuged at 4,000 rpm for 10 minutes and resuspended in 1 mL of lysis buffer (Potassium phosphate buffer (5 mM), EDTA (5 mM), 10% (v/v) glycerol and PMSF (25 mM)). The suspension was then left to incubate at 37 °C for 1 h to completely lyse bacteria. After incubation, the lysis suspension was sonicated for 3 minutes with sonication probe (15 sec on ,15 secs off at 50% power). Suspensions were then centrifuged at 12,000 rpm for 10 minutes and supernatant, containing catalase, was removed and stored at -80 °C.

4.3.5 Protein Quantification – Bradford Assay

Bovine serum albumin (BSA)(Sigma) was diluted from stock (1 mg/mL) in DI water, to create a range of BSA concentrations: 100-1000 µg/mL. 10 µL of each concentration was added, in triplicate, to a 96-well plate with DI water used as a blank. Bradford reagent (Biorad)(Comassie Blue G) was equilibrated to room temperature and 300 µL was added to each well. The plate was mixed in a shaker incubator at 25 °C for 15 minutes. The absorbance was then read at 595 nm using microtiter plate reader (FluroSTAR, Omega). The absorbance from the blank sample was subtracted from all absorbance values, these corrected values were then used to create a standard curve – BSA concentration vs absorbance (**Appendix 4.8.1**). 10 µL of bacterial lysate containing unknown amounts of protein was added in triplicate to microtiter plate and 300 µL of Bradford reagent was then added, and the protocol was repeated as before. The absorbance readings for the unknown could then be used to calculate the protein concentration from the standard curve.

4.3.6 Catalase Activity Assay

Bacterial lysate was defrosted at room temperature and then incubated at 37 °C for 2 h to activate catalase enzyme. Agilent UV-Vis was blank corrected with 3 mL of PBS (pH 7.4, 25 °C) in 3 mL quartz cuvette. 100 µL of catalase lysate was added to 2.9 mL of 0.033% (v/v) of H₂O₂, diluted from 33% stock into PBS. The absorbance was recorded at 240 nm, at 10 second intervals for 60 seconds. Rate of decrease in absorbance of H₂O₂ corresponded to catalase activity. Activity was calculated using **Equation 4.2**, where absorbance was recorded at time (T) 60 s was subtracted from absorbance at 0 s multiplied by total volume (Vt) which was 3 mL. Where extinction coefficient at 240 nm (ϵ_{240}) was 43.6 mol⁻¹ cm⁻¹ multiplied by optical length of the cuvette (d), which was 10 mm, the volume of enzyme sample (Vs) which was 0.1 mL, the protein concentration (Cr) which was quantified using the Bradford assay as per section 4.3.5.²⁰

$$\text{Catalase} \left(\frac{\text{U}}{\text{mg}} \right) = \frac{(\text{AB}_{240 \text{ nm at } T = 0} - \text{AB}_{240 \text{ nm at } T = 60}) \times V_t}{\epsilon_{240} \times d \times V_s \times C_r \times 0.001} \quad (2)$$

Equation 4.2: Calculation for catalase activity using the change in H₂O₂ absorbance at 240 nm.

4.3.7 H₂O₂ Susceptibility

Bacteria were grown overnight as standard, washed and resuspended in 10 mL of PBS (pH 7.4, 25 °C). 400 µL of ON culture in a 12 well plate, was the treated with non-tapered He-CAP jet for 5 mins at (0.6 SLPM 25 kHz, 10 kV, 5 mm distance). After treatment bacteria was incubated for 30 mins at 25 °C. He-CAP treated bacteria and untreated bacteria were plated out onto LB agar for the enumeration of surviving CFU/mL. 200 µL of He-CAP treated bacteria and untreated bacteria were added to 200 µL of H₂O₂ (20 mM) and incubated for 1 h at 37°C. After incubation H₂O₂ treated bacteria were plated out to calculate survival. The susceptibility of bacteria to H₂O₂ was then calculated using **Equation 4.3**.

$$\text{Percentage Susceptibility (\%)} = \frac{\text{Number of bacteria after H}_2\text{O}_2}{\text{Number of bacteria without H}_2\text{O}_2} \quad (3)$$

Equation 4.3: Calculation of bacterial susceptibility to H₂O₂.

4.4 Results and Discussion

4.4.1 Transmission of RONS through Bacterial Biofilm

The findings of Szili *et al.* discussed in section 4.2.1 show that He-CAP can deliver ROS and theoretically induce cellular damage 150 μm deep into a biological tissue and effecting cells within a 10 mm circular radius. Within wound bacterial biofilm treatment this finding is encouraging and helps explain the efficacy of He-CAP against biofilms observed in Chapter 3. While the He-CAP jet was found to be relatively ineffective against planktonic culture of bacteria, its efficacy against bacterial biofilms was found to be significant, despite antimicrobials typically requiring 10-1000 times the MIC for biofilm eradication. The findings of Szili *et al.* potentially explain this phenomenon. Therefore, their methodology was adapted to assess the delivery of RONS through bacterial biofilms of progressive maturities to assess the effects of both bacterial cellular density and the maturation of biofilm formation. Methicillin-resistant *Staphylococcus aureus* (MRSA) and *Pseudomonas aeruginosa* (*P. aeruginosa*) are the most frequently isolated bacterial species from infected wounds, as such were thought to be the most relevant species to assess. Furthermore, they are Gram-positive and Gram-negative respectively, as He-CAP is known to have a greater effect on Gram-negative species it was important to include both.

During the development of bacterial biofilms there is an increase in cellular density owing to an increase in the number of viable cells, once biofilms reach the “critical colonisation threshold” they begin to form biofilms. Due to complex intercellular communication through quorum sensing, forming extra-cellular matrix and central cells becoming metabolically dormant biofilms are hard to treat. To understand the role of a developing biofilm on the effects of He-CAP, biofilms of varying maturity were used to assess the role of both cellular density and the formation of biofilm architecture.

The cellular density of the developing biofilms was elucidated first, both *P. aeruginosa* and MRSA biofilms were grown for 8, 12 and 24 h and found to have to comparable cell density at all three time points (**Figure 4.4**). After 12 h the biofilms reach the “critical colonisation threshold”, whereby the increase in number of viable cells stops and the community begin to form the architecture of a biofilm through release of toxins and development of extracellular matrix. Using these three stages in development we can assess the effects of

both an increase in bacterial cell density (between 8-12 hours) and the development of biofilm architecture (between 12-24 hours).

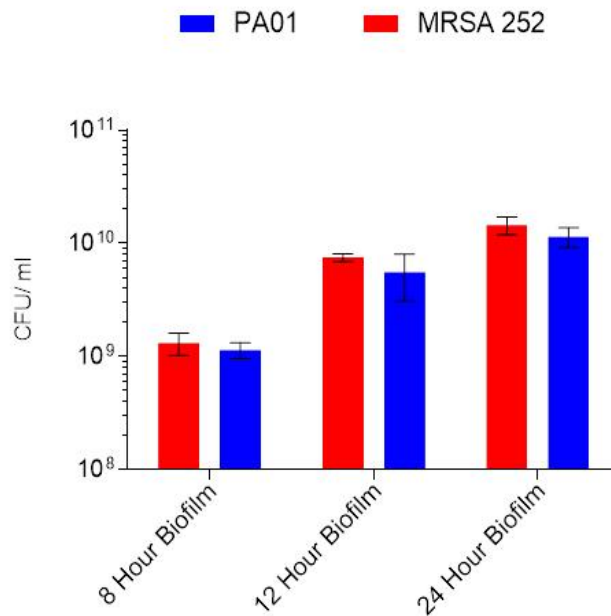


Figure 4.4: Quantification of viable cells of MRSA (MRSA252) and *P. aeruginosa* (PA01) biofilms at 8, 12 and 24 hours of growth. Error bars denote the standard deviation (n=3). (This graph was made in collaboration with Dr H. Hathaway and reproduced with her permission).

The *in vitro* wound biofilms are formed on a nano-porous polycarbonate membrane, to ensure any measured effect on RONS recovery was solely owing to the developing bacterial biofilm, the recovery beneath the membrane impregnated with artificial wound fluid (AWF) was assessed. After five minutes of CAP treatment, a 33% reduction in H₂O₂ recovered beneath the membrane was observed when compared to direct treatment of PBS. This was then taken into consideration as the transmission factor (TF) with a value of 0.67 to normalise values against the interference of the membrane. AWF impregnated membranes were incubated for 8, 12 and 24 h and the TF was measured to ensure there was no change. The results in **Figure 4.4** show that there is no significant difference in recovered H₂O₂ suggesting that AWF has little impact on H₂O₂ transmission.

Table 4.1: Concentration of H₂O₂ recovered beneath polycarbonate membrane impregnated with AWF after incubation for 8, 12 and 24 h at 37°C normalised to TF.

Incubation time	[H ₂ O ₂]/TF (μM)
8	374.9 ± 40.4
12	520.5 ± 13.1
24	400.2 ± 96.8

The concentration of H₂O₂ beneath bacterial biofilms was then analysed at 8, 12 and 24 h, relative to the membrane with AWF, **Figure 4.5**. 8 h biofilms with cell density of ~1x10⁹ CFU/mL were found to reduce the recovered H₂O₂ by half. 12 h and 24 h biofilms with density ~1x10¹⁰ CFU/mL almost completely prevent H₂O₂ from passing through them. The recovery of H₂O₂ beneath 24 h biofilms was found to be below the LoD of the KI reporter system. However, no significant difference was found between 12 and 24 h biofilms was observed between the two species, at the same time point (**Figure 4.5**).

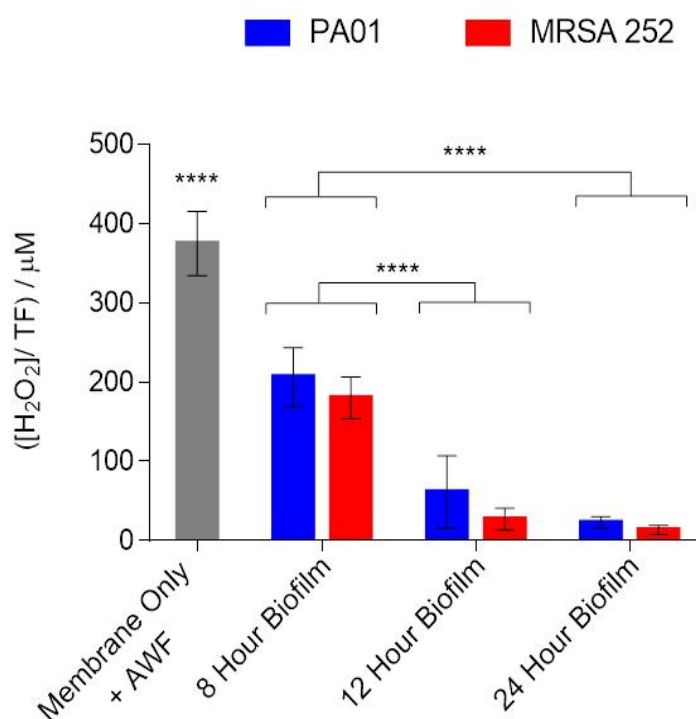


Figure 4.5: Recovery of H₂O₂ through MRSA (MRSA252) and *P. aeruginosa* (PAO1) biofilms (normalised to TF) of varying maturity from 8 – 24 h. Error bars denote the standard deviation (n=3). (This graph was made in collaboration with Dr H. Hathaway and reproduced with her permission).

Further to this, the time-dependent generation and/or diffusion of He-CAP generated H₂O₂ was assessed using a PVA/CMC hydrogel to mimic human skin on top PBS. He-CAP

treatment was applied to the hydrogel for five minutes, in the same way as in the bacterial biofilm experiment. The concentration of H_2O_2 beneath the hydrogel was analysed at various time points post treatment (**Figure 4.6A**). As post treatment incubation time was increased, the concentration of H_2O_2 recovered increased in a time dependent manner.

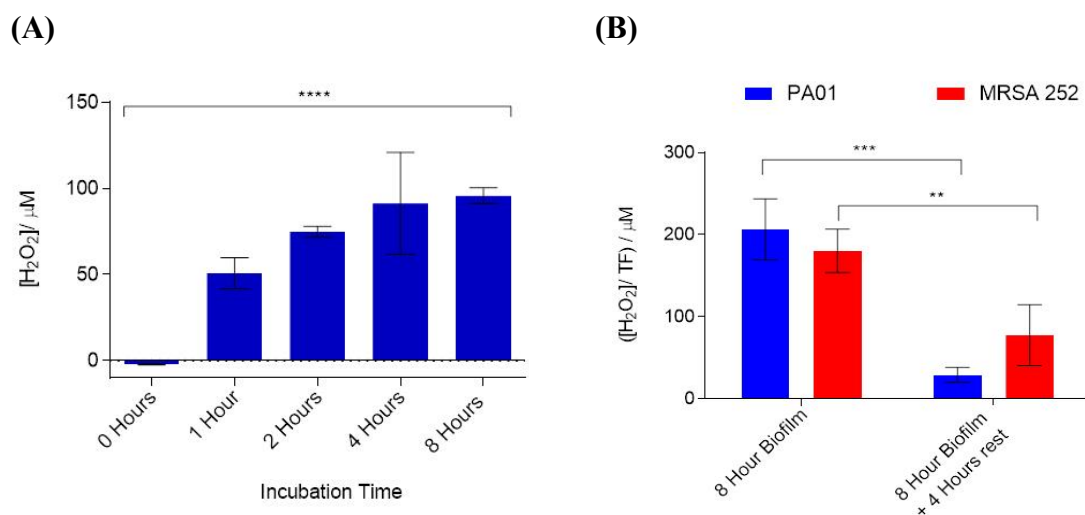


Figure 4.6: H_2O_2 recovery beneath PVA/CMC hydrogel after varying post CAP treatment incubation times (A) and recovery beneath *P. aeruginosa* (PAO1) and MRSA (MRSA252) biofilms after 4 hours rest (B). Error bars denote the standard deviation (n=3). (This graph was made in collaboration with Dr H. Hathaway and reproduced with her permission).

However, when the bacterial biofilms were left to incubate after He-CAP treatment the same trend was not observed **Figure 4.6B**. There was a significant reduction in the amount of H_2O_2 recovered beneath both *P. aeruginosa* and MRSA biofilms suggesting that there is a bacterial mechanism resulting in the reduction of the amount of H_2O_2 recovered. Previous studies have shown that bacterially produced enzyme catalase has a protective role mitigating H_2O_2 damage by catalysing its decomposition into water and oxygen. Both MRSA and *P. aeruginosa* are catalase-positive so this could explain the observed trend. Further work will seek to further elucidate this phenomenon.

4.4.2 Protective Role of Catalase Against CAP

Findings in section 4.4.1 suggest that bacterial biofilms are able to reduce the amount of He-CAP produced H_2O_2 , a potential mechanism of this reduction is thought to be owing to catalase, an enzyme which catalyses the decomposition of H_2O_2 to water and oxygen. To assess this, catalase knockout strains of *E. coli* were obtained and compared to wild type. If

catalase is playing a role in reducing CAP produced H₂O₂ the knockout strains will be more susceptible to CAP treatment and will permit greater concentrations of H₂O₂ through their biofilms.

4.4.3 Characterisation of Catalase Mutants

Catalase single and double knockout *E. coli* were made by Narita *et al.* and were acquired from the University of British Columbia and parental strain, which is a K-12 derivative, BW25113 was purchased from the Yale *E. coli* stock centre. The catalase test was used to confirm the absence of catalase within the *E. coli* strains. If catalase is present, then effervescence is observed owing to the breakdown of H₂O₂ into H₂O and O₂. **Table 4.2** shows that strain PNW11-2 and parent strain BW25113 are catalase positive. PNW11-2 is positive owing to the presence of *katE* gene, which is upregulated during stationary phase producing HPII. Whereas PNW11-1 has *katG* which is upregulated during the exponential phase of growth producing HPI, as such it would not be active in the stationary phase culture. As stationary phase bacteria are used for the catalase test a positive result was expected from PNW11-2 and the parental strains BW25113 as it is wild type for catalase activity. However, NW11-1 is devoid of catalase activity at stationary phase and PNW11-4A is null for catalase, so a negative result was expected. H₂O₂ susceptibility was further assessed using MIC testing, PNW11-1 was found to be least susceptible to H₂O₂, this is thought to be owing to the presence of *katG*, which will be upregulated in the presence of H₂O₂ to produce HPI. As the cultures are grown over 18 h in presence of H₂O₂, the H₂O₂ is thought to induce HPI production, resulting in degradation of H₂O₂ requiring a higher concentration of H₂O₂ to inhibit growth.¹⁶ Whereas PNW11-2 would only express *katE* during stationary phase at which stage the bacterial growth is likely to have been significantly inhibited by the presence of H₂O₂.

Table 4.2: Characteristics of *E. coli* knock-out strains, description of gene knockout, catalase test results and H₂O₂ MIC.

Strain Name	Catalase Present	Expression	Gene Knock-out	Catalase Test	H ₂ O ₂ MIC (mM)
PNW11-1	HPI	Exponential	$\Delta katE$	Negative	1.09-2.17
PNW11-2	HPII	Stationary	$\Delta katG$	Positive	0.27-0.54
PNW11-4A	None	None	$\Delta katE\Delta katG$	Negative	0.07-0.14
BW25113	HPI & HPII	Both	Parental Strain	Positive	0.27-0.54

As studies were focused on biofilms rather than planktonic bacteria, the strains were assessed for that biofilm formation abilities, as often genetic modification can alter bacterial growth. The four *E. coli* strains were used to grow simple 96-well plate biofilms and crystal violet staining was carried out on the 24 h biofilms. Their biomass was compared to the wild type, parental strain and no significant difference was found between the four strains used (**Figure 4.7**).

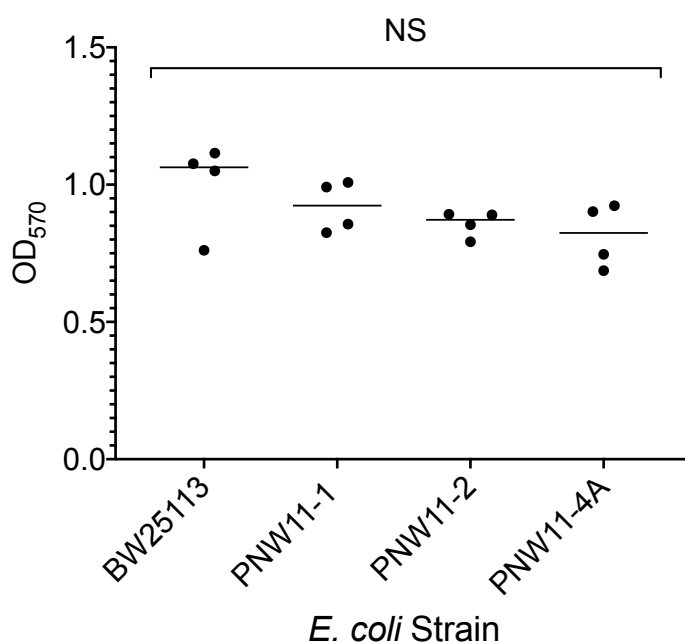


Figure 4.7: Analysis of *E. coli* strain biofilm biomass using 96-well plate assay after 24 h growth at 37°C. Absorbance at 570 nm corresponds to bacterial biofilm biomass (n=4).

4.4.4 CAP Susceptibility

As earlier hypothesised, if catalase was playing a key part in protecting bacterial biofilms from the damaging effects of CAP produced H₂O₂ then bacteria which are devoid of catalase would be more susceptible to CAP treatment. The *E. coli* catalase mutant strains were grown for 24 hours to produce mature biofilms. They were then treated with CAP for five minutes and reduction in viable cell count was compared to wild type parent strain *E. coli* BW25113 (**Figure 4.8**).

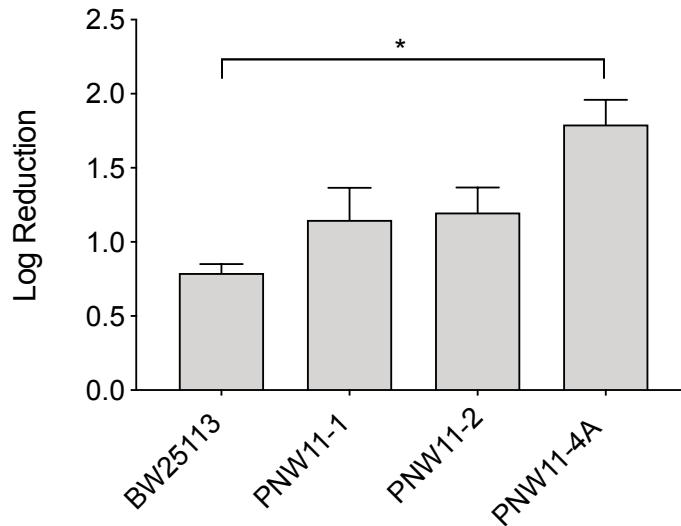


Figure 4.8: Log reduction of catalase mutant *E. coli* biofilms CFU/mL which were grown for 24 h and treated with CAP jet for 5 minutes using non-tapered jet at 5 mm distance. Error bars represent standard deviation, One-way ANOVA was carried out * $p = 0.0122$ ($n=3$).

E. coli catalase knockout biofilm He-CAP susceptibility reflects the trend of planktonic mutants in presence of H_2O_2 (**Table 4.2**). The parental strain, catalase wild type, BW25113 is least susceptible to He-CAP induced death, with double knockout PNW11-4A being most susceptible, with a significant reduction in bacterial viability when compared to the parental strain. Interestingly, there is no significant difference between the two single knockout strains. This is unexpected, as PNW11-1 lacks HP11, as HP11 is expressed during stationary phase, PNW11-1 was expected to be more susceptible to He-CAP induced killing. However, there is no significant difference between PNW11-1, PNW11-2 and BW25113.

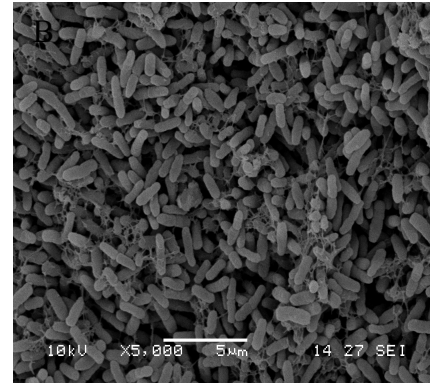
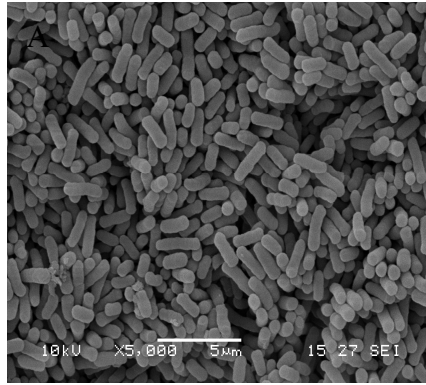
To further understand what effect the He-CAP was having on the *E. coli* mutant biofilms SEM was carried out to observe the morphology of biofilms post He-CAP treatment relative to untreated bacterial biofilms (**Figure 4.9**). While only a qualitative method, visually, the He-CAP induced damage to the *E. coli* biofilms does correspond to the quantitative viable cell data. Literature reports that the shortening of bacterial cells corresponds to bacterial death,^{21,22} which is what is observed in the He-CAP treated biofilms to increasing degrees between the parental wild-type stain, single knockouts and double knockout.

Chapter 4

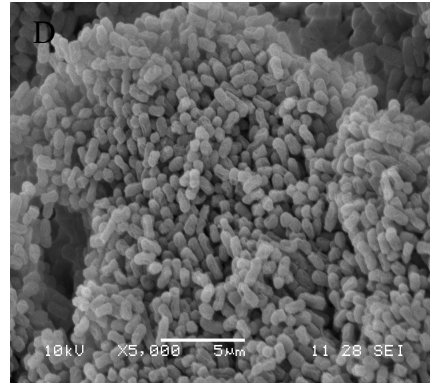
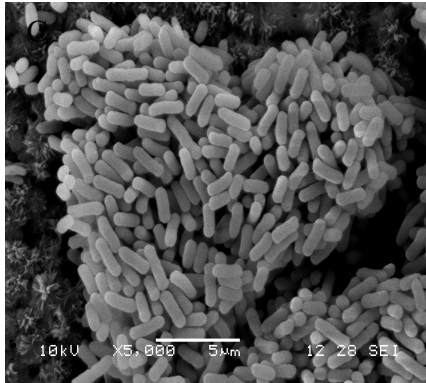
Untreated Biofilms

CAP Treated Biofilms

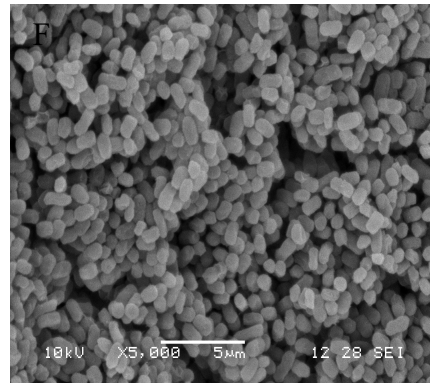
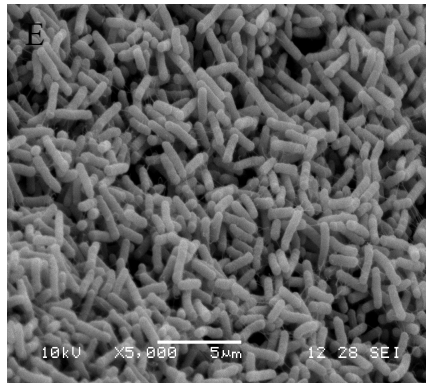
BW25113



PNW11-1
ΔkatE



PNW11-2
ΔkatG



PNW11-4A
ΔkatEΔkatG

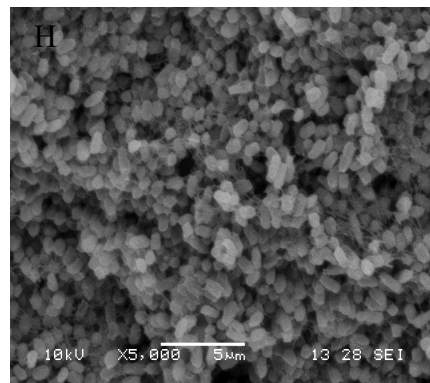
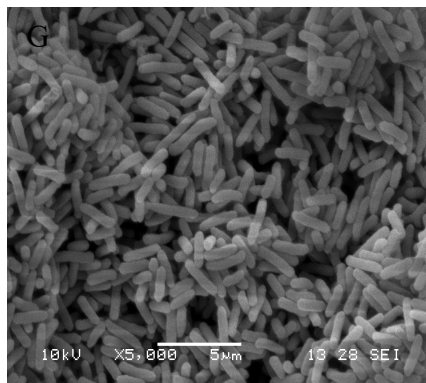


Figure 4.9: Scanning electron microscopy images of *E. coli* 24 h biofilms untreated control (A,C,E & G) and after 5 mins CAP treatment (B,D,F & H) at x5000 magnification. *E. coli* BW25113 (A-B), PNW11-1 (C-D), PNW11-2 (E-F), and PNW11-4A (G-H).

Untreated *E. coli* catalase mutant biofilms morphologically look like bacterial biofilms, with dense populations of bacteria although lacking the distinct extracellular matrix (ECM), this could be owing to sample preparation as control strain lacks ECM. Comparatively, post He-CAP *E. coli* biofilms look morphologically irregular, shorter in length, with distinct damage to cellular surface. This corresponds to the findings of previous research investigating the morphological effects of He-CAP treatment on bacteria and corresponds to the damage observed in Chapter 3. Further quantitative analysis, through measurement of cell length, confirms that *E. coli* $\Delta katE/\Delta katG$ biofilms are most susceptible to He-CAP induced death (Figure 4.10).

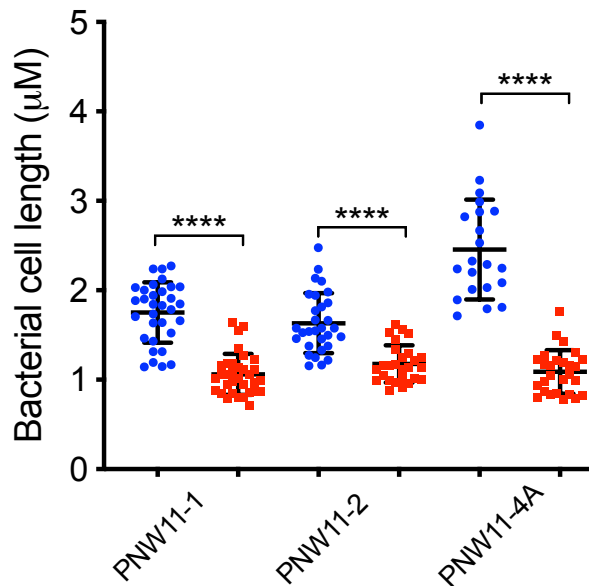


Figure 4.10: Comparison on *E. coli* bacterial cell length in untreated biofilms (●) compared to cellular length in biofilms after 5 mins treatment with CAP (■).

4.4.5 RONS Through Mutant Biofilm

To assess the role of catalase on hindering the delivery of CAP produced H_2O_2 through a biofilm, mutant biofilms were grown for 8, 12 and 24 h owing to the differing expression of HPI and HPII during biofilm growth and for comparison to initial study. As previous work confirmed that the bacterial density contributes to limiting H_2O_2 delivery viable bacteria were assessed for variance to ensure no significant difference. At 8 h growth (

Figure 4.11A) the greatest concentration of H_2O_2 was recovered through $\Delta katE/\Delta katG$ biofilm owing to complete absence of catalase. Interestingly, significantly more H_2O_2 was found beneath a $\Delta katG$ biofilm owing to presence of HPII. HPII is expressed during exponential growth phase resulting in degradation of He-CAP produced H_2O_2 . After 12 h growth (

Figure 4.11B) H_2O_2 delivery through wild-type and single knockout biofilms was reduced. While H_2O_2 recovery through $\Delta katE/\Delta katG$ is significantly higher, owing to lack of catalase activity. After 24 h H_2O_2 is only recovered through $\Delta katE/\Delta katG$ biofilms owing to a lack of catalase with all other biofilms have average H_2O_2 concentrations below the LoD for the KI assay ($\sim 11 \mu M$). These results conclude that catalase plays a key role in limiting the delivery of He-CAP produced H_2O_2 into the biofilm.

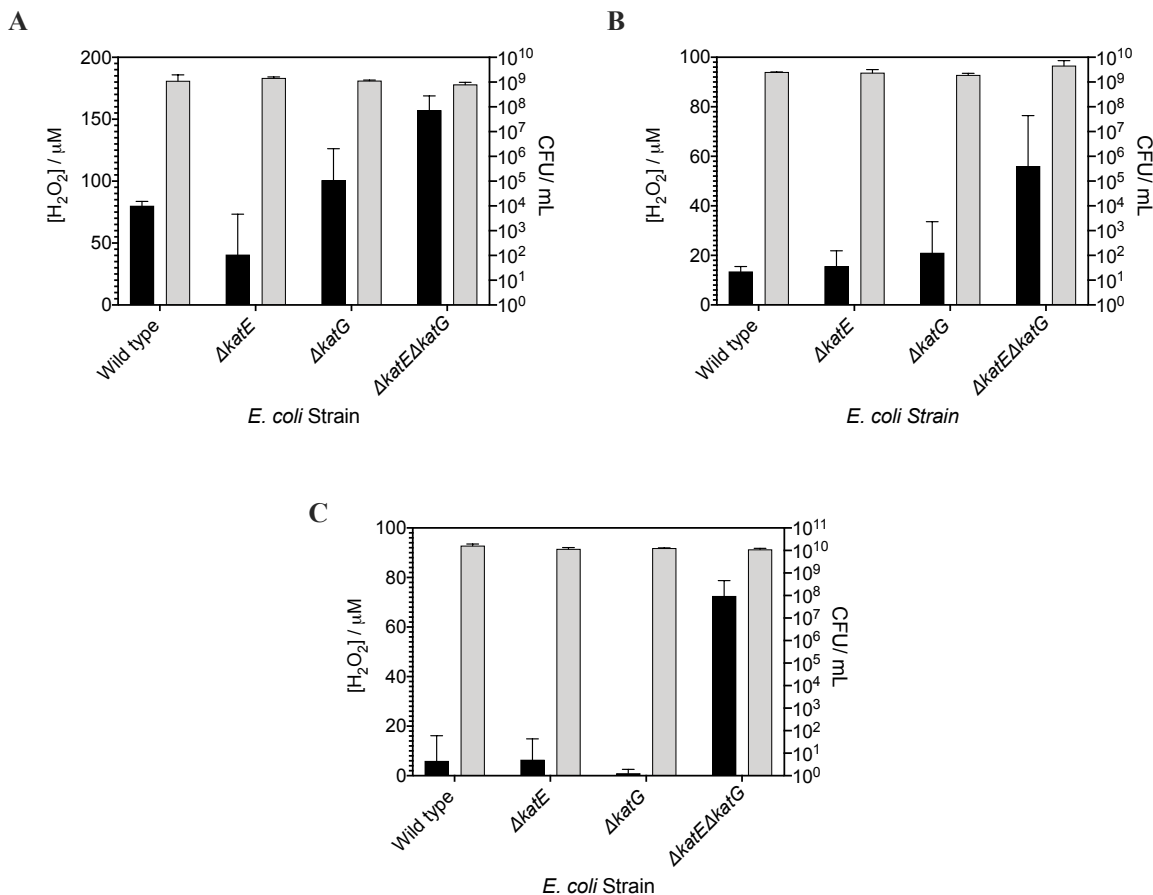


Figure 4.11: Recovery of H_2O_2 through knockout *E. coli* biofilms relative to CFU/ mL after 8 h (A) 12 h (B) and 24 h (C) of growth. H_2O_2 concentration is black and recorded on the left y-axis and CFU/mL is grey and recorded on the right y-axis. Error bars denote standard deviation (n=3).

4.4.6 Quantification of Catalase Activity

Catalase was extracted from *E. coli* samples after 5 mins He-CAP treatment and activity was assayed and compared to untreated control **Table 4.3**. There was found to be an upregulation of catalase after He-CAP treatment further indicating that He-CAP does cause an upregulation of catalase activity. This upregulation is thought to play a key role in limiting the delivery of H₂O₂ into the dense bacterial biofilms. *E. coli* BW25113 and NCTC 10418 were assessed as they are both wild type for catalase activity, BW25113 is the parental strain of the catalase knockouts, and NCTC 10418 is a clinically relevant strain.

Table 4.3: Quantification of *E. coli* catalase activity with and without He-CAP treatment.

Strain	Without He-CAP treatment (U/mg)	After 5 min He-CAP treatment (U/mg)
<i>E. coli</i> BW25113	0.24 ± 0.23	4.5 ± 0.45
<i>E. coli</i> NCTC 10418	0.32 ± 0.162	5.1 ± 0.071

4.4.7 Role of Catalase Concentration

To further prove the impact that catalase has on the delivery of H₂O₂ through a bacterial biofilm, exogenous bovine liver catalase was added to the double knockout strain PNW11-4A of various concentrations to understand the role of catalase concentration.

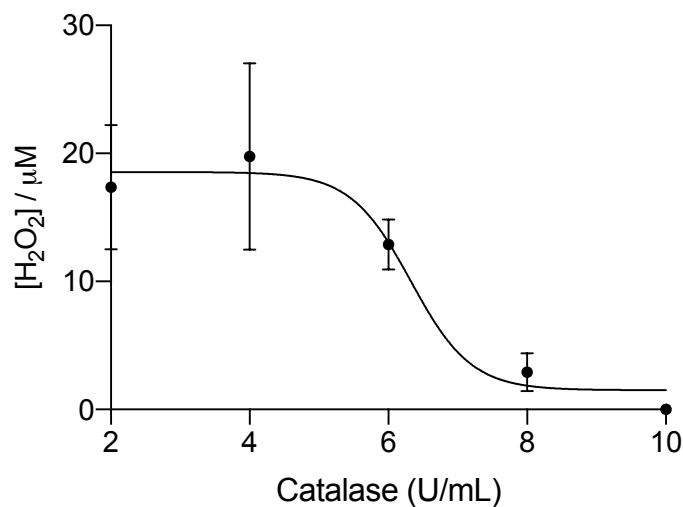


Figure 4.12: Inhibitor-response curve of H₂O₂ recovered through 24 h *E. coli* PNW11-4A biofilm impregnated with varying doses of bovine catalase. Error bars denote standard deviation (n=3).

24 h PNW11-4A biofilms were impregnated with bovine catalase and treated for 5 mins with He-CAP. After 30 minutes incubation the H_2O_2 below the biofilm was quantified and plotted (**Figure 4.12**). As the amount of catalase increases the H_2O_2 recovered decreases, owing to catalase degrading the H_2O_2 . The IC_{50} was found to be between 5.6 – 7.89 U/mL, meaning 5.6-7.89 U/mg of catalase will reduce the concentration of H_2O_2 recovered by 50%. This confirms the quantification of catalase (Section 4.4.6) as BW25113 produces approximately 4.5 U/mL of catalase and approximately 10 μM of H_2O_2 is recovered as would be expected from inhibition curve. While these mutant colonies have been well characterised by Narita *et al.* further work would seek to restore the functionality of the null mutant by knocking the gene back in to further confirm that the lack of catalase was impacting H_2O_2 recovery.

4.4.8 Susceptibility to H_2O_2

As He-CAP appears to upregulate catalase activity, to further test the potential implications of this H_2O_2 susceptibility was tested with and without He-CAP treatment (**Figure 4.13**). After 5 min He-CAP treatment *E. coli* BW25113 was found to be significantly less susceptible to H_2O_2 induced killing owing to the upregulation of catalase expression. Within a clinical environment this could have significant impact, if after only 5 minutes He-CAP treatment the bacteria are less susceptible to H_2O_2 killing is it likely that with repeated He-CAP application the therapeutic effects will lessen.

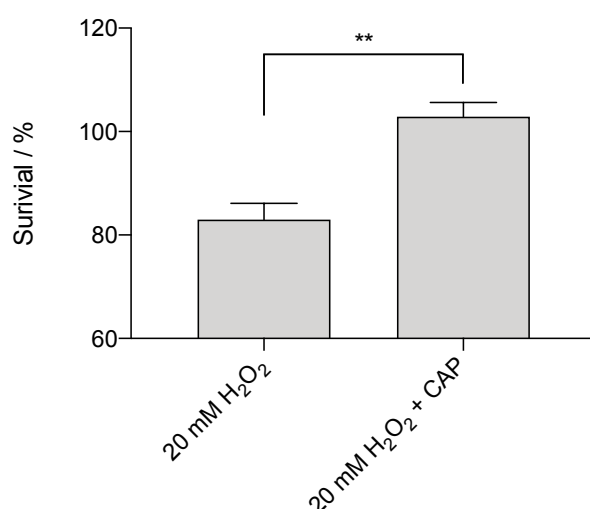


Figure 4.13: *E. coli* BW25113 was treated for 5 mins with CAP and then exposed to H_2O_2 (20 mM) for 1 h at 37°C, survival was calculated. Error bars denote standard deviation (n=3) Students *t*-test was carried out, $p < 0.01$.

4.5 Conclusion

He-CAP has been shown to deliver RONS deep into a tissue model and is effective in reducing the bioburden of bacterial biofilms despite producing low concentrations of RONS. Here, it has been shown that He-CAP can deliver RONS through a thick biofilm of $\sim 1 \times 10^9$ CFU/mL after 8 hours of growth, however, the recovery of H_2O_2 is reduced by half by the biofilm. After 12 and 24 hours of biofilm growth, the recovery of H_2O_2 is almost completely prevented by the bacterial biofilm. While the results at 8 h help explain the results observed in Chapter 3, where He-CAP intervention up to 8 h was found to significantly limit the formation of *P. aeruginosa* biofilms. After He-CAP was applied to a PVA/CMC hydrogel “model biofilm”, under the same conditions as the bacterial biofilm and left to incubate after treatment, the amount of H_2O_2 recovered was found to increase with increased incubation time, suggesting the H_2O_2 takes time to diffuse through a physical barrier. However, when the 8 h bacterial biofilms were left to incubate for 4 h post treatment no H_2O_2 was recovered beneath them, implying that the bacteria are removing the H_2O_2 .

Using *E. coli* mutant strains which had either HPI, HPII or both knocked out the role of catalase was elucidated, and it was shown that if catalase was completely removed the recovery of H_2O_2 beneath the biofilm was significantly higher than the strains that had catalase activity. Catalase activity was found to play a protective role against He-CAP induced damage within biofilms, the *E. coli* biofilm null of catalase activity was significantly reduced by He-CAP treatment whereas those with either HPI or HPII activity or wild type parent strain were not affected. Catalase has also been shown to be upregulated after He-CAP exposure, accounting for the reduction in H_2O_2 recovery and lack of effect on the catalase positive *E. coli* biofilms, further evidence of the protective effect of catalase against He-CAP treatment is an observed decrease in susceptibility of bacteria to H_2O_2 after He-CAP exposure.

4.6 Future Work

This work shows that there is a strong correlation between catalase activity and complete reduction of delivery of H₂O₂ deep into the biofilm after 24 h, yet within null catalase species of *E. coli* there is only a 50% reduction owing to the bacterial density or alternatively through the protective role of alternative oxidative stress enzymes such as SOD or glutathione oxidase. Future work would seek to elucidate the role of these enzymes in mitigating CAP induced death.

Further to this, owing to the apparent prevalent role of catalase in mitigating the effect of He-CAP it is possible that catalase negative strains of bacteria would be more susceptible to CAP treatment such as *Streptococci*. *Streptococcus* is known to cause cellulitis, as well as impetigo which are both common skin infections. While multiple studies have investigated the efficacy of cold plasma against a variety of different bacterial species no studies thus far have compared the efficacy of He-CAP on catalase positive strains comparing with catalase negative strains. Future work would seek to elucidate this and to create a library of catalase null-mutants for direct comparison.

4.7 References

1. Szili, E. J., Hong, S. H., Oh, J. S., Gaur, N. & Short, R. D. Tracking the Penetration of Plasma Reactive Species in Tissue Models. *Trends in Biotechnology* vol. 36 594–602 (2018).
2. Tatoulian, M. *et al.* Plasma Surface Modification of Organic Materials: Comparison between Polyethylene Films and Octadecyltrichlorosilane Self-Assembled Monolayers. *Langmuir* **20**, 10481–10489 (2004).
3. Pizzino, G. *et al.* Oxidative Stress: Harms and Benefits for Human Health. *Oxidative Medicine and Cellular Longevity* vol. 2017 (2017).
4. Saha, S. K. *et al.* Correlation between oxidative stress, nutrition, and cancer initiation. *International Journal of Molecular Sciences* vol. 18 (2017).
5. Huang, W. J., Zhang, X. & Chen, W. W. Role of oxidative stress in Alzheimer's disease (review). *Biomedical Reports* vol. 4 519–522 (2016).
6. Dias, V., Junn, E. & Mouradian, M. M. The role of oxidative stress in parkinson's disease. *Journal of Parkinson's Disease* vol. 3 461–491 (2013).
7. Maritim, A. C., Sanders, R. A. & Watkins, J. B. Diabetes, oxidative stress, and antioxidants: A review. *J. Biochem. Mol. Toxicol.* **17**, 24–38 (2003).
8. Zhao, G. *et al.* Biofilms and Inflammation in Chronic Wounds. *Adv. Wound Care* **2**, 389–399 (2013).
9. Halliwell, B. *Inflammation Biochemistry of oxidative stress*. <http://www.oup.com>.
10. Kashmiri, Z. N. & Mankar, S. A. Free radicals and oxidative stress in bacteria Free radicals and oxidative stress in bacteria. *Int.J.Curr.Microbiol.App.Sci* vol. 3 <http://www.ijemas.com> (2014).
11. Farr', S. B. & Kogoma², T. Oxidative Stress Responses in Escherichia coli and Salmonella typhimurium. *MICROBIOLOGICAL REVIEWS* vol. 55 (1991).
12. Ossowski, I. Von, Mulvey, M. R., Leco, P. A., Borys, A. & Loewen, P. C. Nucleotide Sequence of Escherichia coli katE, Which Encodes Catalase HPII. *JOURNAL OF BACTERIOLOGY* vol. 173 <http://jb.asm.org/> (1991).
13. Taylor, W. I. & Achanzar, D. Catalase Test as an Aid to the Identification of Enterobacteriaceae. *Appl. Microbiol.* **24**, 58 LP – 61 (1972).
14. Claiborne, A. & Fridovich, I. Purification of the o-dianisidine peroxidase from Escherichia coli B. Physicochemical characterization and analysis of its dual catalytic

- and peroxidatic activities. *J. Biol. Chem.* **254**, 4245–52 (1979).
15. Loewen, P. C. & Switala, J. Purification and characterization of catalase HPII from *Escherichia coli* K12. *Biochem. Cell Biol.* **64**, 638–646 (1986).
 16. Visick, J. E. & Clarke, S. RpoS- and OxyR-Independent Induction of HPI Catalase at Stationary Phase in *Escherichia coli* and Identification of rpoS Mutations in Common Laboratory Strains. *JOURNAL OF BACTERIOLOGY* vol. 179 (1997).
 17. McCloskey, D. *et al.* Evolution of gene knockout strains of *E. coli* reveal regulatory architectures governed by metabolism. *Nat. Commun.* **9**, 1–15 (2018).
 18. Bachmann, B. J. Pedigrees of Some Mutant Strains of *Escherichia coli* K-12. *Bacteriological reviews* (1972).
 19. Narita, L. & Peng, S. Construction of Catalase Double Knockout *Escherichia coli* Strain for Isogenic Strain Comparison Studies of the Role of Catalase. *Journal of Experimental Microbiology and Immunology (JEMI)* vol. 16 <http://www.bioinformatics.nl/cgi-> (2012).
 20. Weydert, C. J. & Cullen, J. J. Measurement of superoxide dismutase, catalase and glutathione peroxidase in cultured cells and tissue. *Nat. Protoc.* **5**, 51–66 (2010).
 21. Khan, I., Bahuguna, A., Kumar, P., Bajpai, V. K. & Kang, S. C. Antimicrobial Potential of Carvacrol against Uropathogenic *Escherichia coli* via Membrane Disruption, Depolarization, and Reactive Oxygen Species Generation. *Front. Microbiol.* **8**, 2421 (2017).
 22. Ramasamy, M., Lee, S. S., Yi, D. K. & Kim, K. Magnetic, optical gold nanorods for recyclable photothermal ablation of bacteria. *J. Mater. Chem. B* **2**, 981–988 (2014).

4.8 Appendix

4.8.1 Bradford Assay – Standard Curve

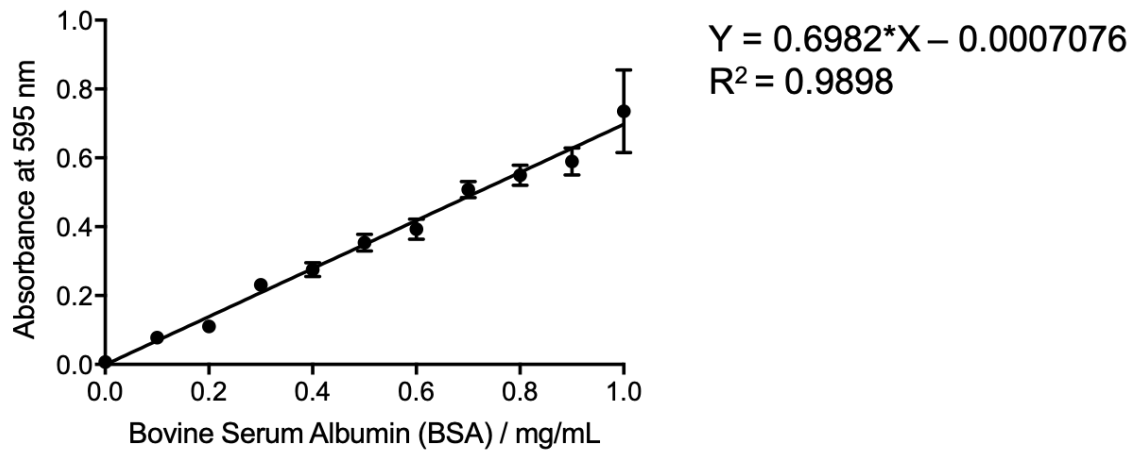


Figure 4.14: Standard curve for Bradford assay using bovine serum albumin (BSA) of varying concentrations. LoD 2.5 $\mu\text{g/mL}$. Error bars represent the standard deviation (n=3).

Chapter 5

Chapter 5 : Cold Atmospheric Plasma Induced Mutagenesis

5.1 Aims

The mutagenic effects of helium-drive cold atmospheric plasma (He-CAP) have previously been studied within mammalian cells, however their molecular interactions with bacterial cells have seldom been investigated. UV and X-ionising radiation are used within bacterial decontamination and are known to have mutagenic potential within bacteria and as such, they are assigned a mutagenic dose, whereby the mutagenic effects are estimated in accordance with the dose.

This chapter seeks to elucidate the mutagenic dose of He-CAP treatment through comparison with the known mutagens, UV and X-ionising irradiation. These mutagens were chosen as they are both well studied and have certain homology to components of, He-CAP. He-CAP is known to have a UV component and X-ionising radiation induces mutagenesis through the production of reactive oxygen and nitrogen species (RONS) that is comparable to He-CAP bactericidal mechanism which is through the production of RONS. Thus, they are logical comparisons for He-CAP mutagenesis. Furthermore, we seek to analyse the mutations induced both on a nucleotide and phenotypic level to investigate whether He-CAP induced mutations impact the bacteria virulence or have any impact upon patient care.

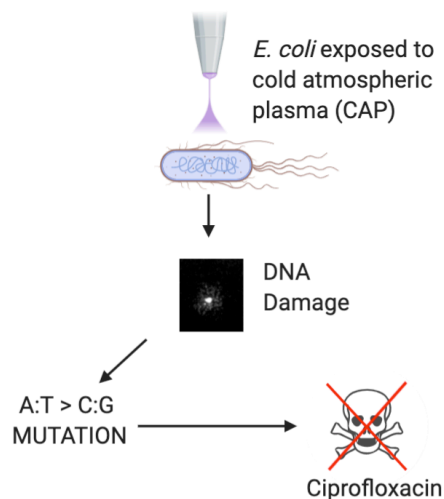


Figure 5.1: Graphical abstract for He-CAP induced mutagenesis workflow.

5.2 Chapter background

5.2.1 Mutagenesis

Mutagenesis is a process where genetic information of an organism is altered resulting in a mutation. This process can occur spontaneously or by exposure to a mutagen. Within mammals, spontaneous mutations often arise through misreading during transcription by DNA polymerase and can result in detrimental effects such as cancers or heritable diseases. A mutagen is defined as “any physical, chemical or biological agent that through exposure results in a mutation”. Hermann Muller, widely considered as the founding father of mutagenesis, discovered the mutagenic properties of X-rays for which he was awarded the Nobel Prize in 1946.^{1,2}

Within modern day biology, mutagenesis has become a seminal tool for elucidating the function and role of genes and proteins within complex systems through the creation of libraries of mutant genes, proteins and strains of bacteria. There are a number of methods used to induce mutations for biological study, including random mutagenesis, site-directed mutagenesis, insertional mutagenesis, homologous recombination and artificial gene synthesis. Mutations are classified by either the origin of mutation: whether is it spontaneous in origin or induced by the environment. Or alternatively by the type of mutation: mispairing, depurination, deamination or environmental. Mutations are then further characterised by the mechanism of mutation. The substitution of a nucleotide where a base with the DNA code is altered to another base is known as a point mutation. This mistake will then be copied into daughter cells and thus the mutation is permanent; if a purine base, Adenine (A) or Guanine (G) is changed to another purine base or a pyrimidine base, Cytosine (C) or Thiamine (T) is changed to another pyrimidine base this is known as transitional substitution; if a purine base is changed to a pyrimidine base this type of mutation is known as a transversion mutation. There are three types of single-base substitutions: silent substitutions are where one codon for an amino acid is altered to another codon for the same amino acid; missense mutations are where the codon for one amino acid is replaced with a codon for another amino acid and nonsense mutation is where the codon is replaced by a translation termination (stop) codon (discussed in section 5.2.4). The ramifications of point mutations are hard to predict. The consequences vary depending on the location or mutation, and whether it disrupts the

functional site. While some mutations may alter the amount of protein produced by a gene others may result in a complete loss of cellular function and as such are lethal.³

Random mutagenesis can be used to attain what the impact of such mutations are. This process was used by Muller to elucidate the mutagenic function of X-rays, through application of mutagen and assessment of change in phenotype.⁴ This method was also used to understand UV mutagenesis through its application upon *Escherichia coli* (*E. coli*).

5.2.2 Ionising Radiation

Energy emitted from a source is referred to as radiation, this encompasses everything from sunlight to UV to gamma rays. Radiation can be subcategorised into ionising and non-ionising radiation. Ionising radiation possess enough energy that upon interaction with an atom is capable of removing electrons from the atom, causing the atom to become charged – ionised. Whereas non-ionised radiation only exerts enough energy to cause atoms to vibrate, such as microwaves and infrared radiation.⁵ Owing to the omnipresence of radiation, exposure is unavoidable. However, exposure to radiation can have catastrophic effects to living things. The detrimental effects of radiation have been highlighted in famous disasters like Chernobyl and Fukushima, where nuclear meltdowns occurred releasing radioactive components. During the Chernobyl disaster 134 people were hospitalised, with acute radiation syndrome owing to patient absorbance of high doses of ionising radiation. 28 subsequently died and countless cases of cancer are attributed to the Chernobyl disaster.^{6,7}

The link between cancer and radiation has been studied for many years. Marie Curie won two Nobel prizes for her work on radiation, utilising radiation for the treatment of cancers and for X-ray imaging. However, owing to the lack of understanding of the damaging effects of ionising radiation, Curie worked unprotected and died of Leukaemia, attributed to exposure to radiation. As such, exposure to radiation is now tightly regulated. Radiation is typically valued in either Sievert (Sv), units of quantifying the effective dose or Gray (Gy) denoting the absorbed dose. 10-20 mSv or 0.01-0.02 Gy is the typical dose of radiation from a full body CT scan.^{8,9} Those working with radiation are limited on exposure to a maximum of 20 mSv per calendar year.¹⁰

Ionising radiation's mutagenic effects have been extensively studied, exposure to Ionising radiation results in a range of DNA damage including nucleotide modification and directly alters DNA structure by causing double-strand breaks (DSB). Secondary effects are as a result of the production of reactive oxygen species (ROS) which cause the oxidation of proteins and lipids and induce DNA Ionising radiation damage is particularly concerning as mutations can accumulate in the offspring of the irradiated parents.^{11,12}

5.2.3 Ultraviolet

UV is categorised into three types:

- 1.) UVA – 315 - 400 nm: Possesses the least energy and can cause skin damage through indirect damage.
- 2.) UVB – 280 – 315 nm: Has more energy than UVA and can cause direct damage to skin cells and are responsible for the majority of skin cancers.
- 3.) UVC – 100 – 280 nm: Has high energy reaction with ozone in the atmosphere and as such does not reach the ground. However, UVC can be made in man-made forms for sterilising surfaces.

UV light induces the formation of molecular lesions within DNA known as pyrimidine dimers. These are formed from thymine or cytosine bases via photochemical reactions. UV induces the formation of covalent linkages between consecutive bases along nucleotide chains. Cyclobutane pyrimidine dimers (CPD) (**Figure 5.2**) contains a four membered ring owing to the coupling of the two-carbon double-bonds of each pyrimidine base. 6-4 pyrimidine-pyrimidone (6-4 products) (**Figure 5.3**) is an alternative dimer consisting of single covalent bond between carbon-6 of one ring and carbon-4 of the neighbouring ring. 6-4 products occur at a third of the rate of CPD, however they are more mutagenic.

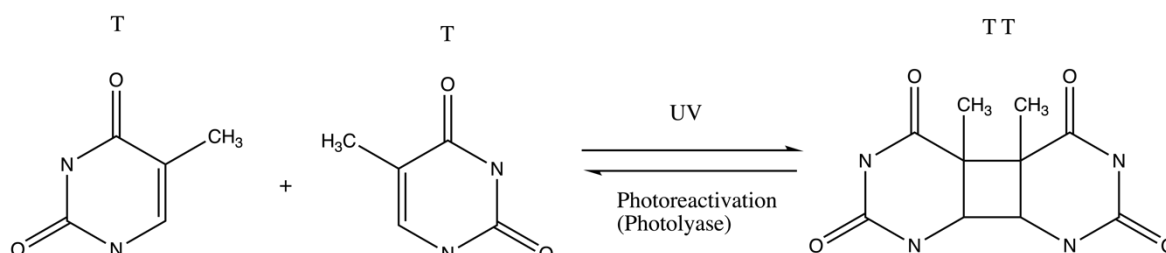


Figure 5.2: Formation of cyclobutane dimer in response to UV exposure.

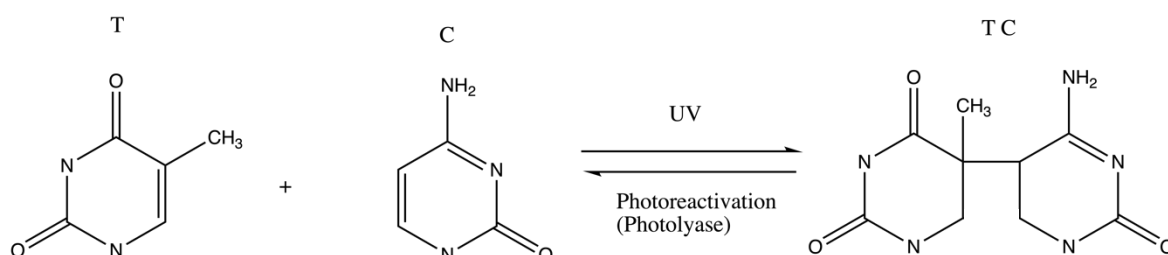


Figure 5.3: Formation of 6,4 pyrimidine-pyrimidine in response to UV exposure.

The most common source of UV is the Sun, to which we are all exposed to varying degrees, as such the mutagenic effects of UV have been studied extensively. UVB induced erythema, commonly known as sunburn is the most frequently observed photobiological response. A UVB dose sufficient enough to induce erythema will correspond to the formation of 10^5 CPD per epidermal cell, but these are usually corrected within seconds of formation by photolyase reactivation or through nucleotide excision repair. However, uncorrected lesions can inhibit the function of polymerases resulting in misreading during transcription and replication and thus cancer.

The most common types of cancer caused by UV are basal cell carcinoma, squamous cell carcinoma and cutaneous malignant melanoma. Patients who have *Xeroderma pigmentosa*, a rare genetic disorder, are very sun sensitive and at increased risk of skin cancer.

5.2.4 Ochre Stop Codon

A stop codon or termination codon is a nucleotide triplet within messenger RNA (mRNA) which signals for the termination of the translation of RNA into proteins. Stop codons signal the termination of translation by binding release factor which signals the dissociation of the ribosomal subunits and releasing the transcribed amino acid chain.¹³

Table 5.1: Nucleotide sequence for stop codons and their names.

Codon		Standard Codon	Name
DNA	RNA		
TAG	UAG	STOP	“Amber”
TAA	UAA		“Ochre”
TGA	UGA		“Opal”

Mutations which change a codon into a stop codon are known as nonsense mutations, there are three stop codons (**Table 5.1**) which are named according to their discovery. Nonsense mutations are frequently lethal (at a cellular level) owing to the degradation of protein through premature termination of translation.

5.2.5 Mutagenesis in Bacteria

The ability to alter DNA has enabled an enumerable number of scientific discoveries, often pertaining to protein and gene function. There are a variety of model organisms in existence where mutagenesis can be utilised. They vary in complexity from simple bacterial models included *E. coli*, *Caenorhabditis elegans* (*C. elegans*) worms, zebra fish and mice. *E. coli* is a simple model for genetic modification owing to its hardy nature and versatility within a variety of different growth nutrients where it grows easily. *E. coli* has proved its utility through a variety of landmark scientific discoveries, for example, the elucidation of the genetic code, discovery of restriction enzymes, and the discovery of the life cycle of lytic and lysogenic bacterial viruses.¹⁴

As previously discussed, mutagenesis can be induced through exogenous and endogenous environmental factors or self-induced in response to environmental conditions, for example in the presence of antibiotics. Mutagenesis can also be induced experimentally to attain a genes function. This can be achieved through a variety of methods. As discussed in section 5.2.1 mutations were induced through exposure to a mutagen, like Muller's work with X-rays where mutants with desired characteristic were then selected. Alternatively, modified oligonucleotides can be used in PCR to reduce fidelity and increase mutation rate. Mutant PCR products are then cloned in an expression vector for characterisation of proteins.¹⁵

Site directed mutagenesis gives control of the location of mutation. A common method for DNA manipulation, introduces mutations at a defined site in the target DNA fragment, including the genome and plasmid, via PCR or restriction endonuclease reaction. Depending on the number of mutational sites, site directed mutagenesis is divided into single site-directed mutagenesis and multiple site-directed mutagenesis. Site directed mutagenesis is simple, rapid and highly efficient and readily accessible.¹⁶ While site directed mutagenesis can be used for the deletion of bases, this is a small deletion, limited to ~170 bp. Whereas

gene knockout can be used to partially/completely delete a gene of up to 50 kb. Gene inactivation is carried out through plasma mediated homologous recombination, linear DNA-mediated homologous recombination or through insertional inactivation.¹⁷

5.3 Methods

5.3.1 Materials

Ammonium sulphate, sodium citrate, magnesium sulphate, thiamine, ciprofloxacin hydrochloride salt and lysozyme were purchased from Sigma-Aldrich (Poole, UK). Low-melting agarose, RNaseIF, SYBR Gold were purchased from Fischer scientific. *E. coli* WP2 and *uvrA*⁻ were purchased from the Yale *E. coli* stock centre.

5.3.2 Ames Test

5.3.2.1 Theory

The Ames test is used to determine the mutagenic potential of a chemical using bacteria as a reporter system. The test uses a library *Salmonella typhimurium* (*Salmonella*) strains with mutations in different genes in their His operon, which act as “hot spots” for mutations by mutagenic chemicals which cause DNA damage via various mechanisms. The *Salmonella* strains are auxotrophic, in that they require histidine for growth, but cannot produce it. If a chemical is mutagenic, it will cause either point mutations or frameshift mutations within the “hot spots” in the His operon, causing a reversion in phenotype (His⁻ → His⁺), enabling the *Salmonella* to produce histidine autologously. Owing to mammalian capability to metabolise chemicals into other molecules that may not be mutagenic, or vice-versa, rat liver extract is often added. This optional addition mimics metabolism breaking down chemicals to assess the mutagenic potential of the metabolites.¹⁹⁻²¹

While this simple mutagenic screening method has been used to identify 50-90% of all known carcinogens and is used as a multi test algorithm to assess novel drugs by the USA Toxic Substances Control Act. It is limited in that *Salmonella* is a prokaryotic, whereas humans are eukaryotic, moreover, human and rat metabolomics are not completely comparable.²²

5.3.2.2 *Salmonella* Ames Test

Figure 5.4 outlines the Ames test protocol. His⁻ *Salmonella* was grown up in broth supplemented with histidine to enable growth and, if required, rat liver extract was added. *Salmonella* suspension was then added to minimal agar, lacking histidine, and grown for 48 h to screen for natural revertant colonies, of which there should be few. Chemical or treatment condition of interest, henceforth referred to as “mutagen” was then added to *Salmonella* culture and plated on minimal agar lacking histidine, and incubated for 48 h. After incubation the total number of revertant colonies was counted. A significant increase in the number of revertant colonies compared to the untreated control suggests exposure to the potential mutagen is causing mutations and thus it is mutagenic.

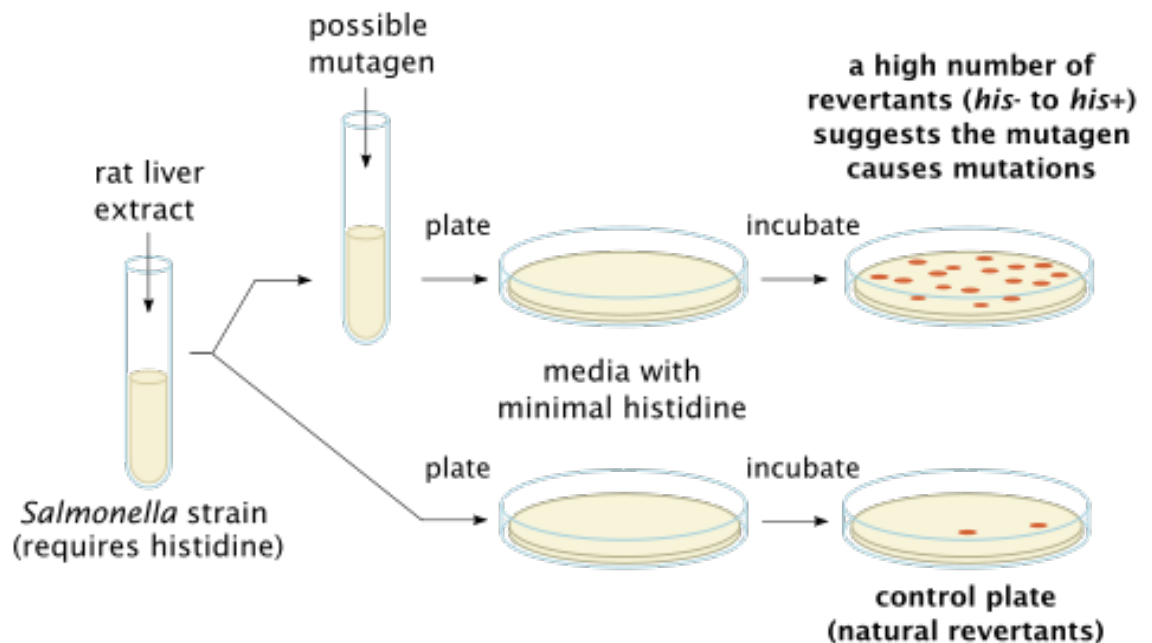


Figure 5.4: *Salmonella* Ames Test workflow.

5.3.2.3 *E. coli* Ames Test

5.3.2.4 Theory

Unlike the standard Ames test the modified Ames test uses *E. coli* with a mutation in the *TrpE* gene rendering it unable to synthesis tryptophan and as such the *E. coli* are unable to grow on agar unless it is supplemented with tryptophan. In the presence of a potential mutagen, in this case plasma, UV and ionising radiation, if point mutations are induced

during exposure the *E. coli* will revert to being able to produce tryptophan and will grow on the minimal agar identifying itself as a mutant colony. Further to this, the *E. coli* Ames test does not use rat liver extract as the system is applicable to bacterial mutagenesis not mammalian mutagenesis whereby the rat liver mimics the activity of mammalian liver enzymes which contribute to the breakdown of toxic compounds.

5.3.2.5 Bacterial strains

E. coli WP2 is a *E. coli* B/r strain derivative and wild type for DNA excision repair. WP2 *uvrA*⁻ is a mutated form of WP2, it has a mutation in the *trpE65* gene which removes accurate excision repair mechanism enabling for the detection of base-pair substitution mutations. This mutant strain was successfully used to study UV-induced mutagenesis.¹⁸

5.3.2.6 Minimal Agar

To prepare MA, components were prepared (as per **Table 5.2**) in separate bottles and combined after autoclaving. 1 mL of 10% (w/v) magnesium sulphate and 0.2 % (w/v) thiamine (B1) were added after combination.

Table 5.2: Minimal agar recipe for modified Ames test.

Bottle 1	
Potassium phosphate (Dibasic)	5.3g
Potassium phosphate (Monobasic)	2 g
Ammonium sulphate	1 g
Sodium citrate	0.5 g
dH ₂ O	333 mL
Bottle 2	
Agar	16 g
dH ₂ O	333 mL
Bottle 3	
D (+) Glucose	4 g
dH ₂ O	333 mL

5.3.2.7 Bacterial Growth Conditions

Bacterial stocks were maintained at -80 °C in 15% (v/v) glycerol and grown on LB agar as required. Overnight cultures were grown in LB broth (as previous 2.2.2). Subcultures were made through inoculation of 125 µL of ON culture into 5 mL of LB and grown for 2 h with shaking (200 rpm) at 37 °C.

5.3.2.7.1 Irradiation

The Cell-rad X-irradiator used in accordance with manufacturer's instructions. The treatment platform was placed on level one to allow treatment of six plates simultaneously, three LB agar survival plates and three minimal agar (MA) mutation plates, with a petri dish in the middle of treatment platform for constant measuring of delivered radiation dose, measured in Gy. The lids were kept on the plates.

5.3.2.7.2 UV

UVC supplied by a germicidal fluorescent tube (Philips) with peak output at 254 nm, was administered at an intensity of 1 W/m² for varying dosages. Bacteria was prepared as per **Error! Reference source not found.** 100 µL of bacteria was aliquoted on to MA agar in triplicate per treatment condition, which were treated in tandem with LB agar survival plates. Plates were exposed to varying dosages of UVC. Doses administered were 10, 20 and 30 J/m².

5.3.2.7.3 He-CAP

Bacterial cultures were prepared (Section 5.3.1) and 350 µL was treated for varying amounts of time with CAP jet (0-10 mins), and left for 30 mins to incubate at 25 °C. After CAP treatment, 100 µL of treated *E. coli* was aliquoted onto MA and spread evenly across the plate. Plates were incubated statically at 37°C for 48 h. 100 µL of untreated subculture was also added to MA to enumerate spontaneous mutants. CAP treated bacterial cultures were serially diluted in PBS and plated on LB agar to calculate number of surviving bacteria post

CAP treatment. Mutation rate was then normalised to the surviving CFU/mL of *E. coli* (Equation 5.1).

$$\text{Normalised Mutation Rate} = \frac{\text{No. of Mutant colonies post CAP treatment} - \text{No. of spontaneous mutants}}{\text{No. of surviving bacteria} \left(\frac{\text{CFU}}{\text{mL}}\right)} \quad (1)$$

Equation 5.1: Normalised mutation rate calculation

5.3.3 Antibiotic Susceptibility Assay

E. coli BW25113 was grown and treated with He-CAP (0-10 mins) as before (Section **Error! Reference source not found.**) and left to incubate for 30 mins to incubate at 25 °C. After treatment 100 µL of bacterial suspension was added to LB agar supplemented with 0.03 µg/mL of ciprofloxacin and spread across surface evenly. 100 µL of untreated subculture was also added to ciprofloxacin supplemented agar to enumerate spontaneous mutants. He-CAP treated bacteria were serially diluted in PBS and plated on LB agar to calculate number of surviving bacteria post He-CAP treatment.

5.3.4 Comet Assay

E. coli WP2 was grown and treated with He-CAP as before (Section **Error! Reference source not found.**). After 30 mins incubation at 25 °C 2.5 µL of CAP treated *E. coli* was added to readymade suspensions of: 90 µL low-melting agarose (equilibrated to 37 °C), 5 µL of lysozyme (20 mg/mL) and 2 µL of RNaseIF (50 U/mL), this was then incubated at 37 °C for 10 mins. 75 µL of suspension was then spread onto comet assay slides (EnzoLife Sciences) ensuring slides are kept flat and no air bubbles are produced. Slides were then left to dry at 25 °C for 10 mins. Slides were immersed in lysis solution and incubated at 4 °C for 30 mins. They were then immersed in alkaline solution (300 mM NaOH, 1 mM) and incubated at 25 °C in the dark. Slides were then washed twice with 1XTBE for 5 mins. Slides were then run in electrophoresis tank (12V, 10 mins). Slides were then washed for 5 mins in 70% ethanol before being stained with 1:10,000 SYBR Gold as per manufacturer's instructions. Slides were then imaged using confocal microscope and analysed using ImageJ/Fiji.

5.3.5 PCR

Colony PCR was carried as per Section 2.7.2 using the primers in **Table 5.3** using the thermocycling conditions in **Table 5.4**. Products were run against a 100 bp ladder as per section 2.7.3. Positive products are shown by band at 350 bp as seen in **Figure 5.5**.

Table 5.3: Primer sequence for amplification of *trpE* gene.

Primer Name	Sequence (5' – 3')
TrpE_for	CTTCCTGAAACGGGCAGTGT
TrpE_rev	AGGGCGTTATCCAGTAGTGC

Table 5.4: Thermocycler conditions for the amplification of *trpE* gene.

PCR Stage	Temperature	Time
Initial denaturation	94°C	30 seconds
30 Cycles	94°C	15-30 seconds
	45-68°C	15-60 seconds
	68°C	1 min/kb
Final extension	68°C	5 mins

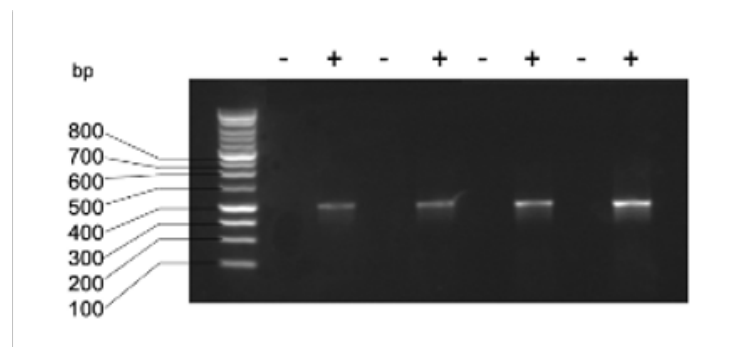


Figure 5.5: PCR result of *trpE* positive and negative colonies against 100 bp ladder.

5.3.6 Sequencing

Isolates were amplified and checked for successful amplification of *trpE* gene and cleaned up using GeneJET kit as per manufacturer's instructions. Samples were prepared to 5 ng/μL using sterile ddH₂O and sent off to Eurofins with forward primer (10 pmol/μL) for

Chapter 5

sequencing. Sequencing data was analysed to ensure clearly defined peaks, using 4Peaks and FASTA sequence was compared to *trpE* and analysed for any mutations using a simple, self-written Python script.

```
ACTTCCTGAAACGGGCAGTGTATTCACCATGCGTAAAGCAATCAGATACCCAGCCCGCCTAATGAGCGGGCTT
TTTTTGAACAAAATTAGAGAATAACAATGCAAACA_TAA_AAAACCGACTCTCGAACAGCTAACCTGCGAAGGCG
CTTATCGCGACAATCCCACCGCGCTTTTTTACCAGTTGTGTGGGGATCGTCCGGCAACGCTGCTGCTGGAATC
CGCAGATATCGACAGCAAAGATGATTTAAAAAGCCTGCTGCTGGTAGACAGTGCGCTGCGCATTACAGCTTTA
GGTGACACTGTCACAATCCAGGCACTTTCCGGCAACGGCGAAGCCCTGCTGGCACTACTGGATAACGC
```

Figure 5.6: Sequence of *trpE* gene showing forward and reverse primers in green, start codon in red and the mutation in blue

5.4 Results and Discussion

5.4.1 Comet Assay

Conventionally the Comet assay is used to detect DSB within human DNA, however, through modification, can be used to detect DSB within bacteria. According to Luis Fernández *et al.* ROS induced DNA damage can be detected using a modified Comet assay. The group found that fragmented DNA halos were observed around the dense, bright nucleoids of *E. coli* after exposure to H₂O₂. As H₂O₂ is the dominant, active species produced this method was deemed appropriate for the investigation of He-CAP induced DNA damage.

23

E. coli WP2 cells were treated with He-CAP for five minutes and the comet assay was carried out. After visual analysis, DNA fragmentation was observed in a halo conformation, comparable to those seen for H₂O₂ treated *E. coli* Luis Fernández *et al.* The dense nucleotides observed in the untreated control (**Figure 5.8A**) show undamaged DNA. After He-CAP exposure, halos of fragmented DNA were observed, which is indicative of DNA damage, which is thought to be owing to ROS induced damage as it closely resembles the findings of Luis Fernández *et al.* Quantitative analysis of the results found that post He-CAP treatment 25% of nucleoids were fragmented. This was found to be significantly higher than the percentage of fragmentation in the untreated control, which was only ~10% (**Figure 5.8D**).

Zeocin is a formulation of phleomycin, which is toxic against a range of bacteria, upon entry into a cell the copper cation Cu²⁺ to Cu¹⁺ activating the Zeocin, which then binds and cleaves DNA resulting in cell death.²⁴ Owing to Zeocin's ability to induce DNA damage, fragmented DNA halos were expected if the experimental procedure was correct (**Figure 5.7C**) confirming successful experimental procedure and indicates the expected conformation of fragmented DNA halos. Results from the He-CAP experiments were expressed as a percentage of fragmentation halos produced by zeocin. While there are fewer halos observed in DNA samples treated with He-CAP than Zeocin, this was expected as He-CAP was administered as sub-lethal doses, whereas Zeocin was used at a high concentration of 1 mg/mL, which is above the MIC. From these results it can be inferred that He-CAP induces DNA damage, through the production of ROS, to a greater extent than in untreated

control, producing similar DNA damage in the form of fragmented DNA halos, to positive Zeocin control and those found in literature.

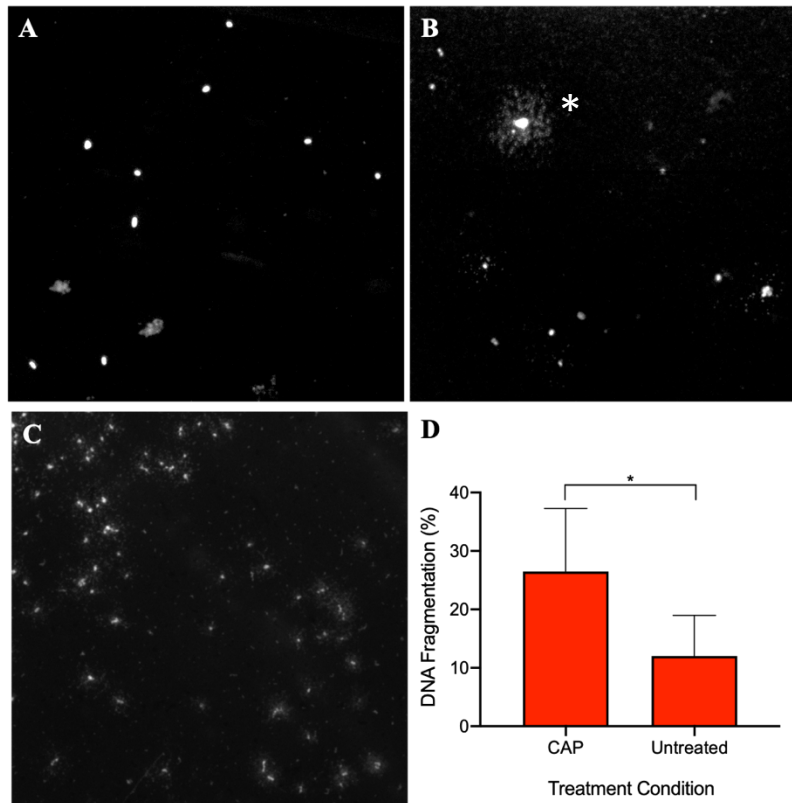


Figure 5.7: Diffusion-based DNA fragmentation assay was performed on *E. coli* WP2 cells to assess DNA damage. Untreated *E. coli* exhibit bright, dense nucleoids (A). After 5 min of He-CAP treatment evidence of DNA damage is observed, seen as speckling around the nucleoid (*) (B). *E. coli* treated with 1 mg/mL of Zeocin (C) DNA fragmentation (%) in Comet assay of *E. coli* WP2 after 5 minutes treatment with He-CAP jet compared to untreated control (D). The percentage of nucleoids with detectable fragmentation relative to intact nucleoids was calculated. A total of 138 nucleoids for He-CAP-treated and 157 nucleoids for untreated were analysed from 3 biological replicates. Error bars show standard deviation of the mean. Data was plotted using GraphPad 8.0, students t-test was performed (*) $p < 0.1$.

5.4.2 Survival

He-CAP devices are being introduced into clinical practice and are classed as medical devices, much like UV and X-irradiation. As previously outlined UV and X-irradiation have been extensively studied for their mutagenic properties and have set mutagenic dose thresholds. He-CAP devices such as the kINPen are approved for clinical use and as such He-CAPs mutagenic effect on mammalian cells has been studied to some extent. However, there has been little investigation of He-CAPs mutagenic effects upon bacteria.

For decontamination treatment, the application of a sublethal dose poses an increased risk of mutations and resistance.²⁵ *E. coli* WP2 was grown to log phase, to ensure the cells were metabolically active and then exposed to three mutagens: UV, X-irradiation and He-CAP. For the purpose of mutagenesis studies sublethal doses are required to observe alterations in phenotype. Therefore, sublethal doses of the three mutagens were elucidated (**Figure 5.8**). The maximum treatment time of the He-CAP and X-irradiation were found to have no significant impact on viability of *E. coli* WP2. Although UV was found to result in a 1-log reduction it recovered after 30 seconds (**Figure 5.8C**). These results confirm that sublethal doses of treatment were being administered enabling subsequent study of potential mutations. The reduction in viable cells observed after UV treatment is significantly higher than the reduction induced by, He-CAP exposure. Thus, there is an indication the He-CAP is lacking a strong UV component as it would be expected that there would be a reduction in viability. However, neither He-CAP nor X-irradiation have any effect on bacterial viability which is indicative of a similarity in bactericidal mechanism. This is further supported by the DNA fragmentation observed in the Comet assay results.

As can be seen from **Figure 5.8C**, He-CAP had no significant effect on WP2 strain viability even at the extended exposure time of 5 minutes treatment. This effect was comparable to ionising X-irradiation, which also had no effect on the viability of WP2 at the doses tested (**Figure 5.8B**), consistent with previous work, demonstrating that this B/r derivative is resistant to ionising radiation owing to combined deficiencies in Lon protease and the cell division inhibitor, Sula protein. It was also observed that the WP2 strain is more resistant to He-CAP than other common strains of *E. coli*. This supports the idea that whilst the He-CAP produced RONS play an important role in inducing bacterial cell death, He-CAP, like X-irradiation, is mutagenic even at the sublethal doses used.

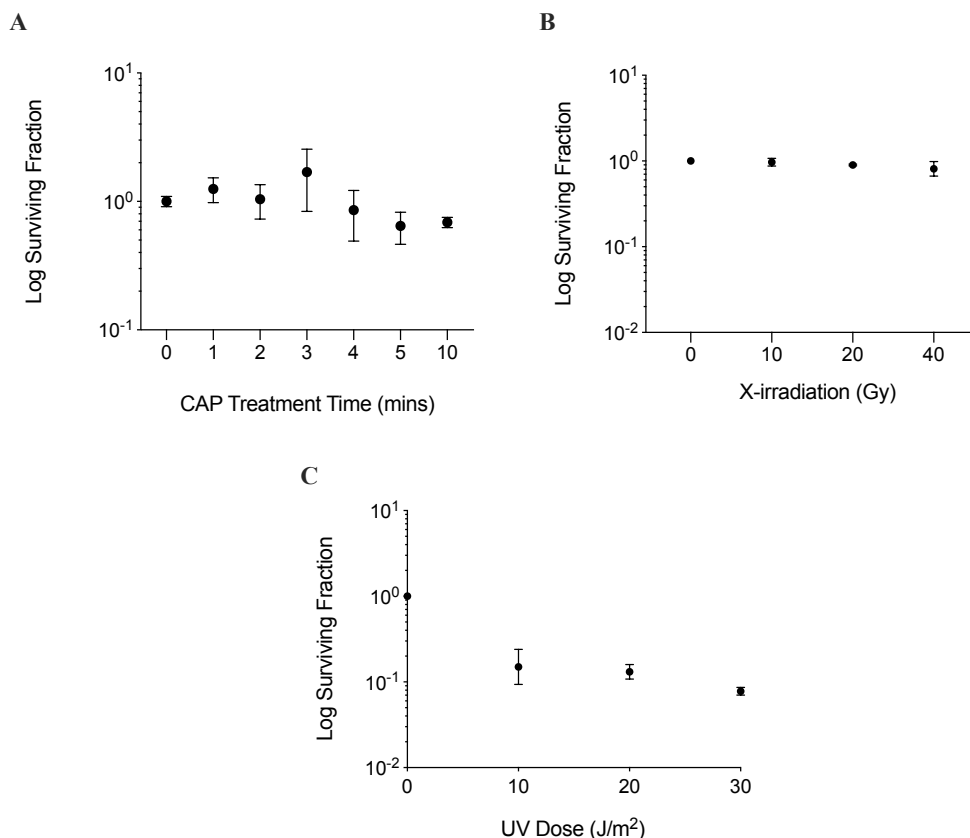


Figure 5.8: Effects of varying dosages of He-CAP, treatment time (mins) (A), UV dosage(J/m²) (B) and X-irradiation dosage (Gy) (C) on survival of *E. coli* WP2 strain. Plated to measure survival as per materials and methods and plotted as survival fraction relative to untreated control. Error bars represent the standard deviation of the mean (n=3).

5.4.3 Mutation Rate

E. coli WP2 has an ochre stop codon in the tryptophan marker gene *trpE*, removing the bacteria's ability to produce tryptophan. On introduction of a mutation, a reversion will occur, and the colony will grow on the media without tryptophan. According to Ames *et al.* if the number of revertant mutants from auxotrophy to prototrophy is higher than the rate of spontaneous mutations the “chemical” is mutagenic.²¹

This modified Ames test was used to assess the mutagenic effects of UV, He-CAP and X-irradiation. A dose-dependent increase in reversion mutation rate was observed for UV and X-irradiation, with highest overall rates seen with the highest dose of UV (30 J/m²) (Figure 5.9). A mutagenic dose threshold was observed in the treatments, meaning if exposure exceeds a certain dosage there is a significant increase in mutation rate. For X-irradiation

this was found to be above four minutes treatment for He-CAP (**Figure 5.9A**), 40 Gy for ionising radiation (**Figure 5.9B**) and for UV above 10 J/m² (**Figure 5.9C**).

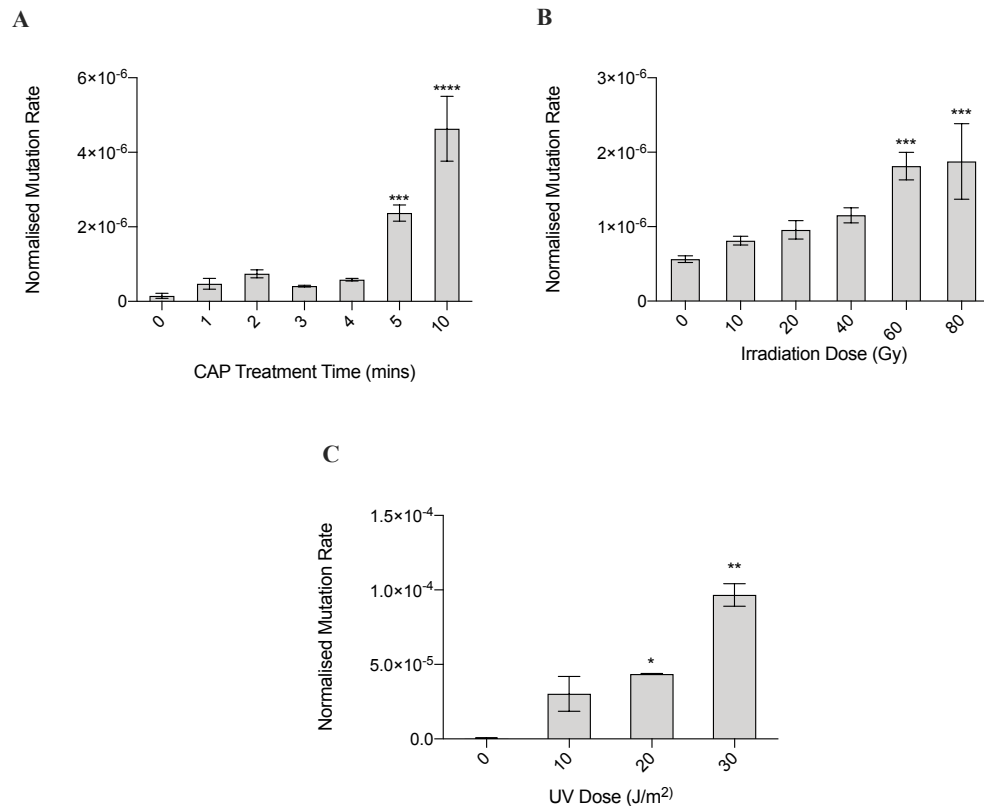


Figure 5.9: *TrpE* revertant mutants for *E. coli* WP2 after exposure to varying dosage of He-CAP (**A**) X-ionising radiation (**B**) and UV (**C**). Data was plotted using GraphPad 8.0. Error bars represent the standard deviation of the mean (n=3), significance was analysed using a one-way ANOVA comparing significance to the untreated control (****) p<0.0001, (***) p<0.001, (**) p<0.01 & (*) p<0.1.

To further assess if He-CAP treatment was inducing bulky lesions, more commonly associated with UV, as opposed to the oxidative lesions associated with X-irradiation, He-CAP treatment was applied to *E. coli* WP2*uvrA*⁻ strain. This *E. coli* strain is sensitive to ultraviolet radiation owing to loss of nucleotide excision repair function. If an increase in mutation rate was observed after He-CAP treatment, this would suggest that UV induced pyrimidine dimers, or another type of bulky, helix-destabilising damage was involved. As expected, an increase in mutants with WP2*uvrA*⁻ strain suggesting that nucleotide excision repair (NER)-dependent damage is produced. After treatment with He-CAP fewer mutants were found in the WP2 strain than the WP2*uvrA*⁻ strain (**Figure 5.10**). WP2*uvrA*⁻ were not treated with UV or X-irradiation as this is irrelevant to the study. It is known that the WP2*uvrA*⁻ strains are unable to repair UV induced damage, owing to absence of excision-

repair mechanism and as such the effects of X-irradiation will be the same as the WP2 strain as both strains remain competent for X-irradiation mutation repair.

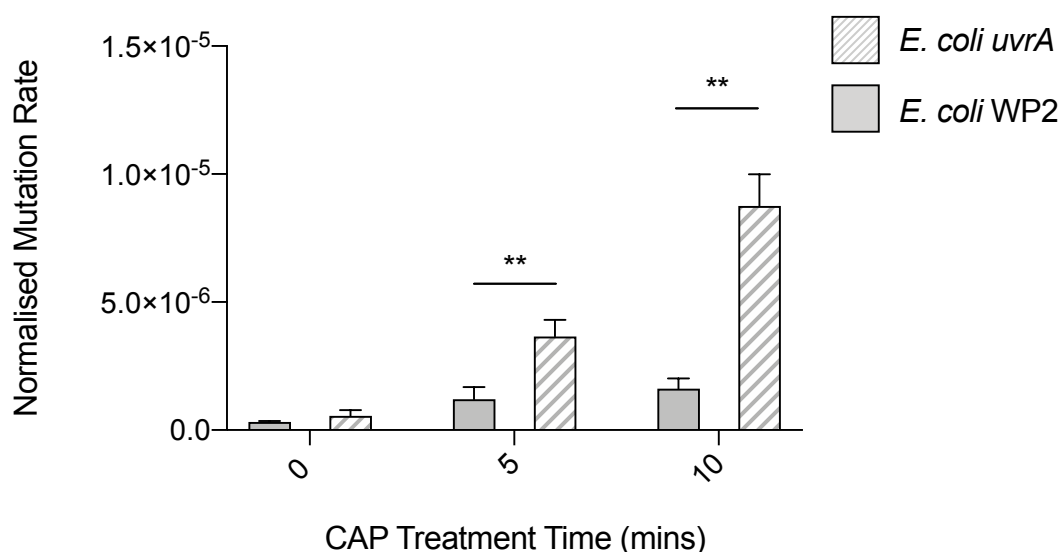


Figure 5.10: Comparison of the mutation rate with increased He-CAP treatment time between *E. coli* WP2 strain than in the *E. coli* WP2*uvrA*⁻ strain. Error bars denote standard deviation of the mean (n=3). Data was plotted using GraphPad 8.0. Unpaired *t*-test performed to assess statistical significance. (**) $p < 0.01$.

The *trpE* gene of *E. coli* has been well studied as a screening method for mutagen; there are seven known point mutations within the Ochre codon (**Table 5.5**). These point mutations result in reversion of nonsense phenotype of the *trpE* gene, enabling the production of tryptophan, changing the phenotype from Trp⁻ to Trp⁺.²⁶ Alternatively, suppressor mutations in genes encoding tRNAs can also arise, enabling the Ochre codon to be read through by the ribosome. There are four possible suppressor mutations that can suppress ochre mutations: anticodon changes UUG→UUA in *supB*, UUU→UUA in *supG*, and GUA→UUA in both *supC* and *supM*.

Table 5.5: Within the ochre codon of the *trpE* gene of *E. coli* there are known to be 7 possible point mutations which result in a change in stop codon, these are outlined below.

Mutation	Type of Mutation	Wild Type Codon	Point Mutation	Amino Acid Change
A•T → G•C	Translation	TAA	CAA	Glutamine (Gln)
A•T → T•A	Transversion		AAA	Lysine (Lys)
A•T → T•A	Transversion		TTA	Leucine (Leu)
A•T → T•A	Transversion		TAT	Tyrosine (Tyr)
A•T → C•G	Transversion		GAA	Glutamic Acid (Glu)
A•T → C•G	Transversion		TCA	Serine (Ser)
A•T → C•G	Transversion		TAC	Tyrosine (Tyr)

To assess which point mutations were more frequently induced by known mutagens (UV and X-irradiation) revertant colonies were analysed and compared to the unknown mutagen CAP (**Table 5.5**). As shown in **Table 5.5**, there is a distinct difference in the spectrum of point mutations induced by the two known mutagens. A sample of the amino acid sequences observed after exposure to the mutagens compared to the untreated reference sequence is shown in **Figure 5.11**.

X-irradiation predominantly causes CAA transition mutations and AAA/TCA transversions, yet these are not observed after UV treatment. Importantly, there are mutations induced by He-CAP treatment that are not documented as being induced by either X-irradiation or UV: TCC & TTT. This type of mutation could be what is causing the difference in mutation rate between the WP2 and WP2*uvrA*- strains. There is also a high number of suppressor mutations. Suppressor mutations denote a mutation that has altered the phenotype from *trpE*⁻ to *trpE*⁺; where the Ochre stop codon remained unchanged. Therefore, it can be concluded a mutation has occurred elsewhere in the genome. For example, mutations within tRNA can increase reading error rate, enabling stop codon to be misread.

Chapter 5

Treatment Conditions	<i>trpE</i> Amino Acid Sequence
Ref Sequence	-----FEQN--*RITMQT-----*KPTLEQLTCEGAYR-
40Gy	-----FEQN--*RITMQT-----*KPTLEQLTCEGAYR-
10UV	-----FEQN--*RITMQT-----*KPTLEQLTCEGAYR-
10Gy	-----FEQN--*RITMQT-----*KPTLEQLTCEGAY--
20Gy	-----FEQN--*RITMQT-----*KPTLEQLTCEGAY--
20Gy	-----FEQN--*RITMQT-----*KPTLEQLTCEGAY--
60Gy	-----FEQN--*RITMQT-----*KPTLEQLTCEGAY--
60Gy	-----FEQN--*RITMQT-----*KPTLEQLTCEGAY--
60Gy	-----FEQN--*RITMQT-----*KPTLEQLTCEGAY--
60Gy	-----FEQN--*RITMQT-----*KPTLEQLTCEGAY--
10UV	-----FEQN--*RITMQT-----*KPTLEQLTCEGAY--
240CAP	-----FEQN--*RITMQT-----*KPTLEQLTCEGAYR-
240CAP	-----FEQN--*RITMQT-----*KPTLEQLTCEGAYR-
300CAP	-----FEQN--*RITMQT-----*KPTLEQLT*RRRLS-
240CAP	-----FEQN--*RITMQ-----TPTLEQLTCEGAYR-
120CAP	-----FEQN--*RITMQT-----QKPTLEQLTCEGAYH-
30UV	-----FEQN--*RITMQT-----QKPTLEQLTCEGAY--
80Gy	-----FEQN--*RITMQT-----QKPTLEQLTCEGAY--
60CAP	-----FEQN--*RITMQT-----QKPTLEQLTCEGAYR-
180CAP	-----FEQN--*RITMQT-----QKPTLEQLTCEGAYR-
10Gy	-----FEQN--*RITMQT-----SKPTLEQLTCEGAY--
10Gy	-----FEQN--*RITMQT-----SKPTLEQLTCEGAY--
240CAP	-----FEQN--*RITMQT-----SKPTLEQLTCEGAYR-
120CAP	-----FEQN--*RITMQT-----SKPTLEQLTCEGAYR-
20Gy	-----FEQN--*RITMQT-----YKPTLEQLTCEGAYR-
10Gy	-----FEQN--*RITMQT-----YKPTLEQLTCEGAY--
180CAP	-----FEQN--*RITMQT-----YKPTLEQLTCEGAYR-
300CAP	-----FEQN--*RITMQT-----*KPTLEQLTCEGAYR-
300CAP	-----FEQN--*RITMQT-----*KPTLEQLTCEGAYR-
30CAP	-----FEQN--*RITMQT-----*KPTLEQLTCEGAYR-
30CAP	-----FEQN--*RITMQT-----*KPTLEQLTCEGAYR-
60CAP	-----FEQN--*RITMQT-----*KPTLEQLTCEGAYR-
120CAP	-----FEQN--*RITMQT-----*KPTLEQLTCEGAYR-
180CAP	-----FEQN--*RITMQT-----*KPTLEQLTCEGAYR-
240CAP	-----FEQN--*RITMQT-----*KPTLEQLTCEGAYR-
240CAP	-----FEQN--*RITMQT-----*KPTLEQLTCEGAYR-
240CAP	-----FEQN--*RITMQT-----*KPTLEQLTCEGAYR-
240CAP	-----FEQN--*RITMQT-----*KPTLEQLTCEGAYR-
180CAP	-----FEQN--*RITMQT-----*KPTLEQLTCEGAYR-
30CAP	-----FEQN--*RITMQT-----EKPTLEQLTCEGAYR-
180CAP	-----FEQN--*RITMQT-----EKPTLEQLTCEGAYR-
5Gy	-----FEQN--*RITMQT-----LKPTLEQLTCEGAYR-
180CAP	-----FEQN--*RITMQT-----LKPTLEQLTCEGAYR-
240CAP	-----FEQN--*RITMQT-----LKPTLEQLTCEGAYR-
10Gy	-----FEQN--*RITMQT-----KKPTLEQLTCEGAYR-
10Gy	-----FEQN--*RITMQT-----KKPTLEQLTCEGAY--
60Gy	-----FEQN--*RITMQT-----KKPTLEQLTCEGAY--
180CAP	-----FEQN--*RITMQT-----KKPTLEQLTCEGAYR-

Figure 5.11: Amino acid sequence alignment data for comparison of mutations between a range of mutagen treatments.

While there are clear distinctions in the frequency of individual point mutations between the three treatment groups, the mutagenic signature of He-CAP seems to resemble that of the X-irradiated group more closely than the UV exposed group. The spectra induced by both He-CAP and X-irradiation are also more similar to each other than either is to any induced by the range of mutagens tested by Ohta *et al.* Taken together these data indicate that He-CAP mutagenesis is similar to X-irradiation mutagenesis and therefore likely involves oxidative stress via the RONS component.²⁷

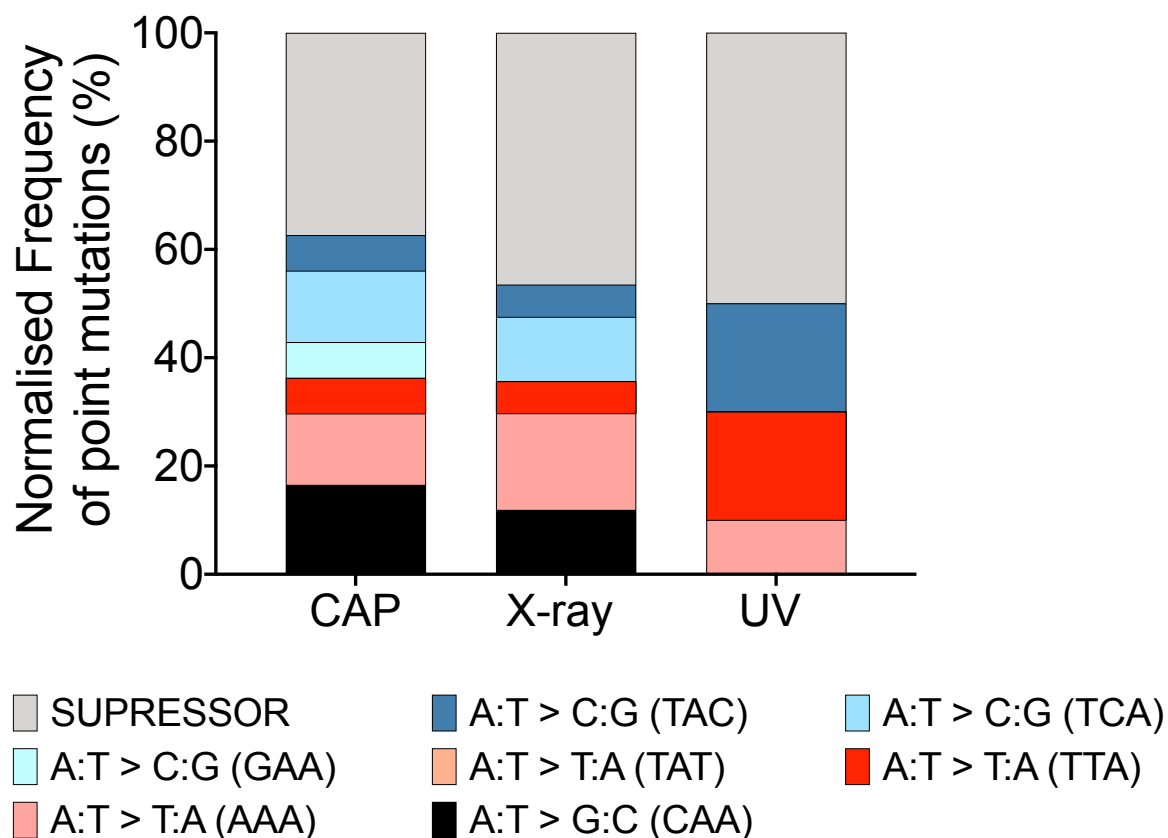


Figure 5.12: After analysis of the *trpE* gene of *E.coli* WP2 a broad spectrum of point mutations was observed in the Ochre region (TAA)(details outlined in **Table 5.5**). The frequency was calculated as percentage relative to total number of samples sequenced per condition.

5.4.4 He-CAP Induced Antibiotic Mutations

Resistance to ciprofloxacin, a widely used fluoroquinolone antibiotic, can occur as a result of single point mutations, similar to those the He-CAP jet appear to induce. Fluoroquinolone resistance is primarily caused by mutational alterations in the target genes of fluoroquinolones DNA gyrase and topoisomerase IV (at codons 80 or 84 of *parC*).²⁸ Hamed *et al.* reported a least one missense mutation in a variety of genes in fluoroquinolone resistant

bacteria.²⁹ As such, after He-CAP treatment *E. coli* suspensions were challenged with plates supplemented with ciprofloxacin at above MIC concentrations (0.03 $\mu\text{g}/\text{mL}$). As He-CAP treatment time increased, the number of mutant colonies capable of growing in the presence of ciprofloxacin also increased, further indicating that He-CAP induces point mutations, which can have important phenotypic effects. Interestingly, the mutation rate is non-linear suggesting that there is a threshold effect. He-CAP induced point mutations were found to increase *E. coli* resistance to ciprofloxacin treatment (**Figure 5.13**).

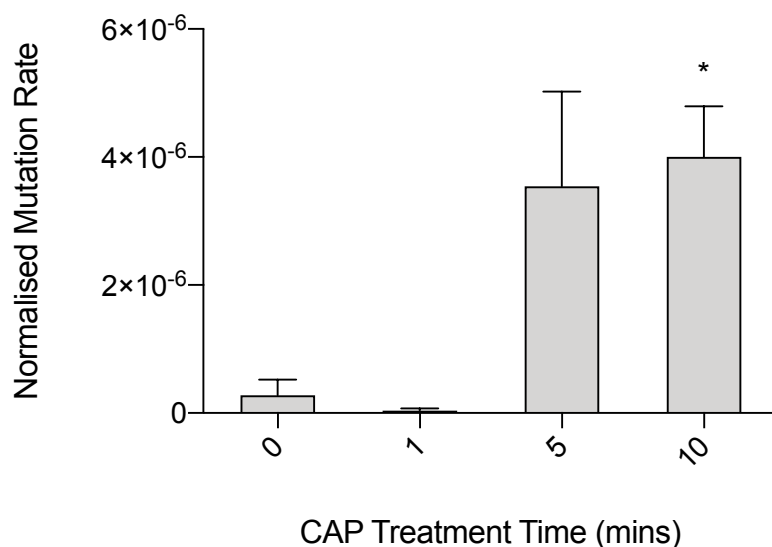


Figure 5.13: Normalised mutation rate of *E. coli* BW25113 in the presence of ciprofloxacin (0.03 $\mu\text{g}/\text{mL}$) after He-CAP treatment for varying amounts of time. Mutation rate is defined as number of ciprofloxacin-resistant *E. coli* cells per total surviving. Error bars represent standard deviation (n=3) Unpaired *t*-test performed to assess statistical significance. (*) p<0.1

There are a number of potential explanations for this. It is known that ROS scavengers such as superoxide dismutase (SOD) and catalase, which are enzymes from bacteria that can reduce the effect of ciprofloxacin and other antibiotics, owing to their bactericidal mechanisms including generation of ROS for bacterial killing. It was found in Chapter 4 that He-CAP treatment does upregulate the expression of catalase. Therefore, it is likely that the increased presence of catalase plays some role in mitigating the bactericidal effects of the ciprofloxacin increasing tolerance.

5.5 Conclusions

These findings indicate that the mutagenic effects of the He-CAP jet on bacteria are more comparable to X-irradiation than UV. Although it is known that He-CAP jets produce some UV radiation, our observations of the absence of a dramatically increased mutation rate or decreased survival rate in a WP2*uvrA* strain, together with differing mutagenic spectra for Trp reversion, strongly suggest that He-CAP-produced UV is not the dominant mutagen in our system.

The mutation spectrum induced by He-CAP appears to be more similar in pattern to those found in the X-irradiated samples than those with UV treatment (**Figure 5.12**). These findings suggest that He-CAP-produced RONS are the dominant mutagenic factor in our treatment conditions, as a consequence of inducing DNA damage (**Figure 5.7**), although the possibility of adaptive mutagenesis cannot be wholly discounted. This is consistent with previous studies that have separated out the particle and UV components of plasma to demonstrate that the UV component makes a comparatively minor contribution to decontamination when O₂ is present^{30,31} and a recent report that *E. coli* relies on genes associated with detoxification of RONS for resistance to He-CAP.³²

He-CAP induced mutations were found to impact *E. coli*'s susceptibility to a ciprofloxacin, which is commonly used to treat wound infection (**Figure 5.13**). While this was a simple study using only a single type of antibiotic this finding should be explored further with some urgency owing to the potential ramifications for the clinical use of He-CAP. As He-CAP treatment is intended for decontamination of bacterial infected wounds, including chronic wounds, where patients will often be on antibiotic treatments it is thus important to ensure there is no risk of increasing resistance through the use of He-CAP treatment.

5.6 Future Work

While *E. coli* is a good model bacterium to study mutagenesis, future work would seek to replicate the studies above using a Gram-positive strain of bacteria, to elucidate if similar results are displayed. Furthermore, wounds are frequently colonised and infected with multiple bacterial species, understanding the effects on Gram-positive bacteria is of paramount importance.

While sequencing has been carried out, further work would be required to understand the mutagenetic effects of He-CAP treatment on a whole genome basis, investigating the effects of both one-off treatment and repeated exposure to He-CAP. While preliminary data here suggests that exposure to He-CAP can denote an increased tolerance to ciprofloxacin, it would be interesting and of clinical importance to assess a range of other antibiotics for potential alterations in susceptibility, with particular focus on those used within wound care and to assess this library of antibiotics on a range of species and isolates. Further to this, assessing the susceptibility to topical antimicrobials such as povidone-iodine or hydrogen peroxide. Moreover, as there appears to be some level of genetic alteration that infers changes to antibiotic susceptibility it would be interesting to see if there is a further increase with repeated treatments.

Owing to the application of CAP being focused upon the decontamination of infected wounds, it would also be of interest to assess the antibiotic susceptibility of clinical wounds that have been CAP treated and isolate these after each treatment to understand the mutagenic effects *in vivo*. This could easily be done with high throughput screening of bacterial strains isolated from wounds before, during and after CAP treatment as assessing their phenotype and genotype for changes in correlation with treatment.

5.7 References

1. Muller, H. J. Artificial transmutation of the gene.
2. Muller, H. J. *The measurement of gene mutation rate in drosophila , its high variability and its dependence upon temperature.*
3. Griffiths, A. J., Gelbart, W. M., Miller, J. H. & Lewontin, R. C. *The Molecular Basis of Mutation.* (1999).
4. Muller, H. J. *The Production of Mutations by X-Rays.* *Amer. J. Physiol* vol. 13 (1928).
5. Kadhim, M. *et al.* Non-targeted effects of ionising radiation-Implications for low dose risk. doi:10.1016/j.mrrev.2012.12.001.
6. Mccall, C. Chernobyl disaster 30 years on: Lessons not learned. *Lancet* **387**, 1707–1708 (2016).
7. Nagataki, S. *Latest Knowledge on Radiological Effects: Radiation Health Effects of Atomic Bomb Explosions and Nuclear Power Plant Accidents.* *Jpn. J. Health Phys* vol. 45 (2010).
8. Smith-Bindman, R. *et al.* Radiation dose associated with common computed tomography examinations and the associated lifetime attributable risk of cancer. *Arch. Intern. Med.* **169**, 2078–2086 (2009).
9. Ionizing radiation, health effects and protective measures. <https://www.who.int/news-room/fact-sheets/detail/ionizing-radiation-health-effects-and-protective-measures>.
10. The Ionising Radiations Regulations 2017.
11. Adewoye, A. B., Lindsay, S. J., Dubrova, Y. E. & Hurler, M. E. The genome-wide effects of ionizing radiation on mutation induction in the mammalian germline. *Nat. Commun.* **6**, 1–8 (2015).
12. Borrego-Soto, G., Ortiz-López, R. & Rojas-Martínez, A. Ionizing radiation-induced DNA injury and damage detection in patients with breast cancer. *Genetics and Molecular Biology* vol. 38 420–432 (2015).
13. Clark, D. P., Pazdernik, N. J. & McGehee, M. R. Mutations and Repair. in *Molecular Biology* 832–879 (Elsevier, 2019). doi:10.1016/b978-0-12-813288-3.00026-4.
14. Blount, Z. D. The Natural History of Model Organisms: The unexhausted potential of E. coli. *eLife* vol. 4 (2015).
15. Smith, A. M. Oligonucleotide-directed mutagenesis using plasmid DNA: a screening step to confirm the first successful step to positive mutagenesis. *Tech. Tips Online* **6**,

- 10–11 (2001).
16. Shortie, D., Dimaio, D. & Nathans, D. *Directed Mutagenesis*. www.annualreviews.org (1981).
 17. Xu, J. zhong & Zhang, W. guo. Strategies used for genetically modifying bacterial genome: site-directed mutagenesis, gene inactivation, and gene over-expression. *Journal of Zhejiang University: Science B* vol. 17 83–99 (2016).
 18. Witkin, E. M. Ultraviolet mutagenesis and inducible DNA repair in *Escherichia coli*. *Bacteriol. Rev.* **40**, 869–907 (1976).
 19. Ames, B. N., Durston, W. E., Yamasaki, E. & Lee, F. D. Carcinogens are mutagens: a simple test combining liver homogenates for activation and bacteria for detection. *Proc. Natl. Acad. Sci. U. S. A.* **70**, 2281–2285 (1973).
 20. Antonoplis, A. *et al.* A Dual-Function Antibiotic-Transporter Conjugate Exhibits Superior Activity in Sterilizing MRSA Biofilms and Killing Persister Cells. *J. Am. Chem. Soc.* **140**, 16140–16151 (2018).
 21. Mortelmans, K. & Zeiger, E. The Ames Salmonella/microsome mutagenicity assay. *Mutat. Res. - Fundam. Mol. Mech. Mutagen.* **455**, 29–60 (2000).
 22. McCann, J., Choi, E., Yamasaki, E. & Ames, B. N. Detection of carcinogens as mutagens in the Salmonella/microsome test: assay of 300 chemicals. *Proc. Natl. Acad. Sci. U. S. A.* **72**, 5135–5139 (1975).
 23. Fernández, J. L. *et al.* DNA fragmentation in microorganisms assessed in situ. *Appl. Environ. Microbiol.* **74**, 5925–5933 (2008).
 24. Chankova, S. G., Dimova, E., Dimitrova, M. & Bryant, P. E. Induction of DNA double-strand breaks by zeocin in *Chlamydomonas reinhardtii* and the role of increased DNA double-strand breaks rejoining in the formation of an adaptive response. *Radiat. Environ. Biophys.* **46**, 409–416 (2007).
 25. Kohanski, M. A., DePristo, M. A. & Collins, J. J. Sublethal Antibiotic Treatment Leads to Multidrug Resistance via Radical-Induced Mutagenesis. *Mol. Cell* **37**, 311–320 (2010).
 26. Yanofsky, C. *et al.* The complete nucleotide sequence of the tryptophan operon of *Escherichia coli*. *Nucleic Acids Res.* **9**, 6647–68 (1981).
 27. Ohta, T. Characterization of Trp⁺reversions in *Escherichia coli* strain WP2uvrA. *Mutagenesis* **17**, 313–316 (2002).
 28. Hooper, D. C. & Jacoby, G. A. Topoisomerase inhibitors: Fluoroquinolone mechanisms of action and resistance. *Cold Spring Harb. Perspect. Med.* **6**, a025320

- (2016).
29. Hamed, S. M. *et al.* Multiple mechanisms contributing to ciprofloxacin resistance among Gram negative bacteria causing infections to cancer patients. *Sci. Rep.* **8**, 1–10 (2018).
 30. Schneider, S. *et al.* Summarizing results on the performance of a selective set of atmospheric plasma jets for separation of photons and reactive particles. *J. Phys. D: Appl. Phys.* **48**, 444001 (2015).
 31. Kogelheide, F. *et al.* To cite this article: Friederike Kogelheide et al. *J. Phys. D: Appl. Phys.* **53**, 13 (2020).
 32. Krewing, M. *et al.* Plasma-sensitive *Escherichia coli* mutants reveal plasma resistance mechanisms. *J. R. Soc. Interface* **16**, 20180846 (2019).

Chapter 6

Chapter 6 : Development of a Hydrogen Peroxide Responsive Hydrogel

6.1 Aim

The aim of this chapter was to develop a H_2O_2 responsive hydrogel which releases an antimicrobial moiety, for the inhibition of the formation of bacterial biofilms, in response to exposure to helium-driven cold atmospheric pressure plasma (He-CAP) produced reactive oxygen and nitrogen species (RONS) or alternatively through the application of topical H_2O_2 . Currently, topical H_2O_2 solution is used as an antimicrobial in woundcare, but the concentration of H_2O_2 needs to be carefully moderated, owing to the potentially detrimental effects that high concentrations of H_2O_2 can have on the healing process. However, the concentration needs to remain high enough to induce bacterial inhibition and death. The low levels of H_2O_2 produced by He-CAP treatment need to be sufficient to kill planktonic bacteria but not hinder wound healing.

Previous work described a displacement assay based on a boronic ester containing gel, in which the displacement of alizarin red S (ARS) by saccharides causes allows colorimetric determination of saccharide concentration. Sun *et al.* also reported a similar, reaction-based indicator, utilising the ability of RONS to oxidise boronic esters to produce a colorimetric response. This work aims to combine that these studies to develop a RONS responsive hydrogel that would be capable of releasing ARS into a wound, which we hypothesise will act as a biofilm inhibitor (**Figure 6.1**).

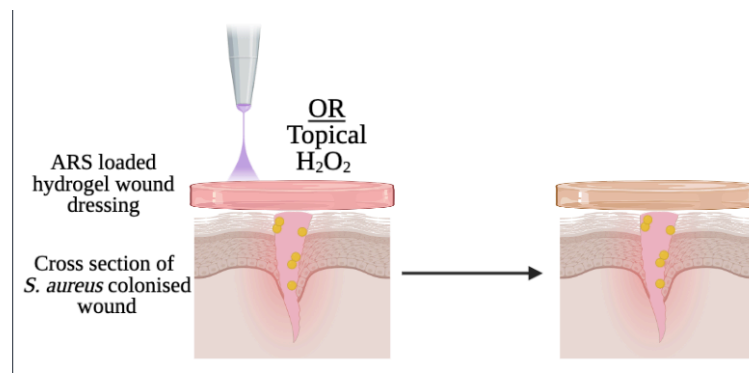


Figure 6.1: Schematic outlining the concept of the ARS-PBA hydrogel triggered release system for the inhibition of biofilm formation. The release of ARS in response to H_2O_2 diffuses through the hydrogel into the wound inhibits *S. aureus* biofilm formation.

6.2 Introduction

6.2.1 Boronic Acid and Ester Soft Materials

Boronic acid containing hydrogels have properties which may render potential utility in creating a matrix for drug delivery and wound care: they combine their unique reactivity of boronic acids with a hydrophilic, biocompatible matrix, capable of forming a range of macrostructures. Boronic acid macromolecules are effective in nanomaterials, sensors and in the delivery of therapeutics such as insulin. Effective polymeric systems for drug delivery are typically rigid and plastic, however, boronic esters dynamic nature offer better rheological characteristics for the development of wound dressings which need to conform to body shape and be comfortable to wear. These materials exhibit interesting physical properties, including the ability to self-heal, meaning the gel can be cut and reformed without external influence. Boronic acids are soft materials offering favourable biocompatibility and can act as a reservoir for drug release, which is utilised in the delivery of contraceptive drugs.¹

While there are a multitude of different boronic acids which can form esters, the most widely used is phenyl boronic acid (PBA) owing to its stability, availability and reactivity. PBA moieties can be incorporated into polymeric systems in a variety of ways. Existing polymers containing pendant groups that offer reactivity, including polyesters and amides, can have PBA groups coupled to them using a variety of coupling chemistries. The most commonly used coupling methods include: carbodiimide (CD) and EDC/NHS coupling. This was used by Chen *et al.* to functionalise hyaluronic acid with maltose or PBA, which produced a dynamic, covalently crosslinked hydrogel of hyaluronic acid. Hyaluronic acid is ubiquitous within human tissues and thus is highly biocompatible and the presence of the boronic acid offers glucose responsivity with the potential for application within drug release of biomedical sensing.²

6.2.2 Dye Displacement Saccharide Detector Assay

A monomer that has been synthesised containing PBA which can subsequently be polymerised forming polymeric chains featuring the previously mentioned boronic acid reactivity, which can then be crosslinked to form hydrogels. Lampard *et al.* developed a

hydrogel saccharide sensor which released chromophore ARS. ARS is deep red in colour, featuring a 1,2 diol in the form of a catechol and as such can form cyclic boronic esters in the presence of boronic acid functionalities. Upon esterification ARS exhibits a clear, visible colour change from red to orange. Quantification of this colour change within the hydrogel is difficult owing to the light-scattering nature of the material. This problem can be resolved by adding the gel into solutions of glucose, fructose, mannose and galactose of varying concentrations, and measuring the absorbance of the resulting solution. The sugars compete to bind to the boronic ester, displacing the ARS resulting in a colour change of orange back to red (**Figure 6.2**). The release of the ARS into the solution the hydrogel was suspended in could then be measured with UV-Vis at ARS's absorbance at 513 nm enabling the concentration of free ARS to be determined. This allowed for the subsequent back calculation of the saccharide concentration (**Table 6.1**).

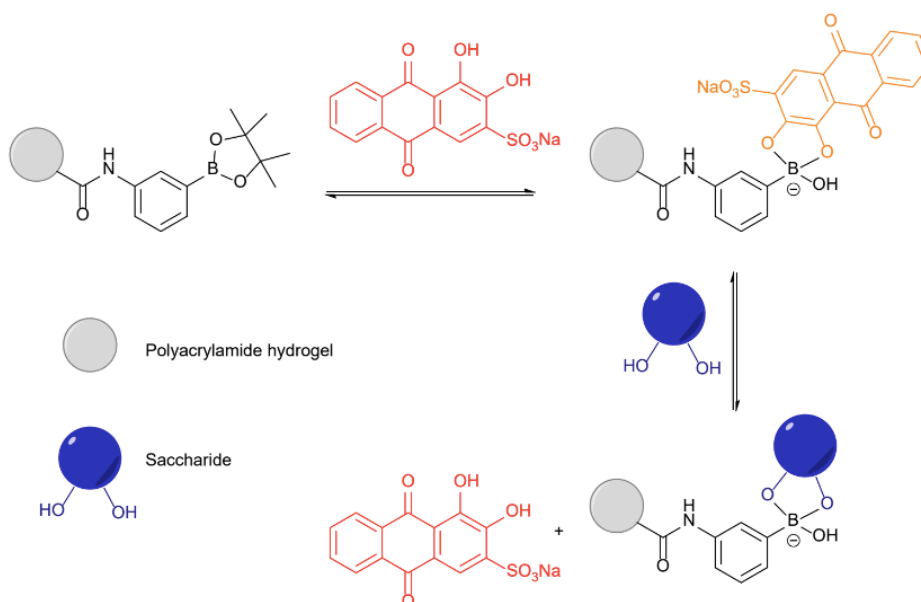


Figure 6.2: Displacement of ARS from PBA containing hydrogel matrices in the presence of saccharides owing to competitive binding.

Table 6.1: The amount of ARS release from PBA and Blank gels as abs g^{-1} at 513 nm

	Fructose	Galactose	Mannose	Glucose
PBA Gel	0.82	0.40	0.41	0.34
Blank Gel	0.23	0.21	0.22	0.19

6.2.3 Biofilm Inhibitors

The phenotypic transition of bacteria from their planktonic to biofilm state is associated with a significant increase in pathogenicity. Furthermore, biofilms are known to be significantly harder to treat than their planktonic counterparts as discussed in Chapter 1. As such, much research has gone into the development and discovery of molecules that can impact on biofilm formation. These include those which inhibit biofilm formation as well as those which disrupt preformed biofilms. This can be achieved in a number of ways, small organic compounds can inhibit bacterial surface adhesion, interference with the quorum-sensing pathways and altering biofilm formation.³

Nature has been a source of biofilm inhibiting compounds including ginseng and garlic. Emodin is a naturally occurring anthraquinone found in the roots of a number of moulds, plants and lichens. Ding *et al.* found that emodin inhibited biofilm formation at 20 μM in *Pseudomonas aeruginosa* (*P. aeruginosa*). This is thought to be owing to emodin's ability to penetrate into the biofilm and interfere with the QS system in *P. aeruginosa*.^{4,5} While the use of biofilm inhibitors are often employed to prevent the colonisation of surfaces through impregnation, for example within orthopaedic implants, they could also have application within wound care.⁶

6.2.4 Alizarin

Alizarin is an organic dye (**Figure 6.3A**), used throughout history, in 1869 it became the first natural dye to be synthetically produced. Alizarin is soluble in hexane and chloroform and exhibits pH dependent colour changes. Alizarin has been found to have antibiofilm properties against *Candida albicans* and MRSA.^{7,8} Alizarin red S (ARS) is the water soluble, sodium salt, of alizarin (**Figure 6.3B**). ARS is useful stain within histology; Dahl's method uses ARS for the highly specific staining of calcium within samples enabling the identification of calcification in the aorta and human kidney for effective medical diagnosis.^{9,10} While ARS is more soluble than alizarin, its maximum solubility is still relatively low at 2.5×10^{-4} M.

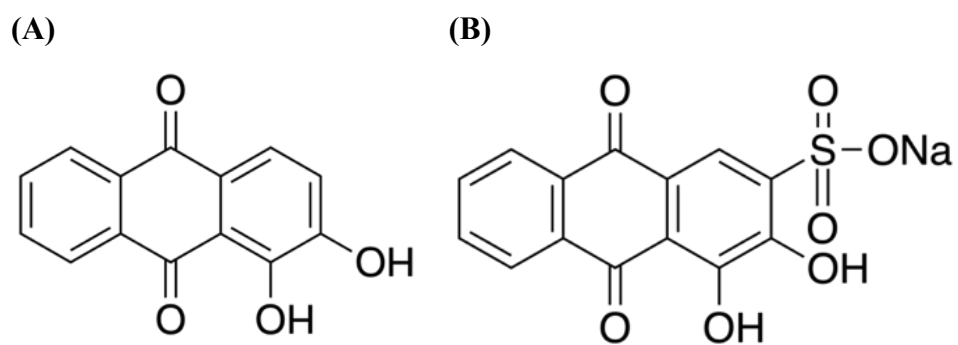


Figure 6.3: Chemical structure of Alizarin (A) and Alizarin red S (B).

6.3 Methods

6.3.1 General Information

All solvents and reagents were purchased from commercial suppliers and used without further purification unless otherwise specified. Proton and carbon NMR were recorded using a Bruker Advance 500. Chemical shifts were reported in ppm using TMS or solvent residual signals as internal reference standards. High-resolution mass spectrometry (HRMS) were performed on an Agilent 6545 LC/Q-TQF. UV-Vis were performed on a BMG Labtech CLARIOstar, BMG Labtech CLARIOstar data analysis software package MARS.

6.3.2 Blank Gel Synthesis

Hydrogels were formed through the dissolution of acrylamide (3.9 g) and methylene bisacrylamide (0.1 g) in distilled water (20 mL). Tetramethylethylenediamine (50 μ L) was added to freshly prepared ammonium persulphate solution (10% (w/v), 150 μ L), this was then added to the acrylamide solution with stirring at room temperature. This was then taken up into sterile 1 mL syringes, which were inverted and placed in racks to set. After 30-45 minutes incubation at room temperature the gels will have set, as determined by visual inspection. The end of the syringe was removed with scissors, and 0.1 mL pieces of gel were cut off using a sterile scalpel. Gels were stored in sterile phosphate buffer saline (PBS).

6.3.3 PBA Gel Synthesis

Hydrogels were made by dissolving acrylamide (3.8 g), methylene bisacrylamide (0.1 g) and PBA monomer (0.1 g) in distilled water (20 mL). Tetramethylethylenediamine (50 μ L) was added to freshly prepared ammonium persulphate solution (10% (w/v), 150 μ L), this solution was then added to acrylamide solution. This was then taken up into sterile 1 mL syringes, which were inverted and placed in racks to set. After 30-45 minutes incubation at room temperature the gels will have set, (as determined by visual inspection). The end of the syringe was removed, and 0.1 mL pieces of gel were cut off using a sterile scalpel. Gels were stored in sterile PBS.

6.3.4 PBA monomer synthesis

N-(3-(4,4,5,5-tetramethyl-1,3,2-dioxaborolan-2-yl)phenyl)methacrylamide (PBA) was synthesised (**Figure 6.4**). NEt_3 (0.49 g, 4.88 mmol) and methacryloyl chloride (0.51 g, 4.88 mmol) in DCM (4.0 mL) was added dropwise to a solution of 3-(4,4,5,5-tetramethyl-1,3,2-dioxaborolan-2-yl)aniline (1.00 g, 4.56 mmol) in DCM (60 mL) at 0 °C. The reaction mixture was stirred for 2 h and was allowed to warm to rt, which was then stirred for a further 30 min. It was ensured that the temperature did not rise above 30 °C in order to minimise the occurrence of side polymerisation products. The solution was then washed with H_2O (3 x 40 mL) and dried over MgSO_4 . The organic solvent was removed under reduced pressure and the title compound yielded as an off white solid (1.25 g, 95 %). ^1H NMR (δ ; 300 MHz; $\text{DMSO-}d_6$) 7.98 (1H, dq, CH), 7.68 (1H, d, CH), 7.56 (1H, d, CH), 7.36 (1H, t, AR CH), 5.79 (1H, s, CHH), 5.44 (1H, s, CHH), 2.05 (3H, s, CH_3), 1.35 (12H, s, 4 x CH_3). ^{13}C NMR (δ ; 75 MHz; $\text{DMSO-}d_6$) 166.54, 140.90, 137.32, 130.73, 128.74, 125.89, 123.23, 119.15, 84.14, 24.98, 18.85. FTIR (thin film) ν ; 1622 (C=C), 1662 (C=O), 2977 (C-H), 3355 (N-H). HRMS (FTMS): m/z calculated for $\text{C}_{16}\text{H}_{22}\text{BNO}_3$: requires 288.1768 for $[\text{M-H}]^+$, found 288.1795.

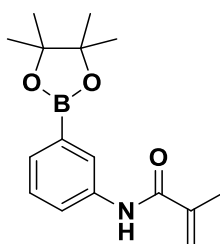


Figure 6.4 Structure of PBA

6.3.5 ARS loading

0.1 g of PBA hydrogel cylinder was immersed in 1 mL of 2.5×10^{-4} M ARS solution for 5 h at 25°C with rocking, to achieve maximum loading of ARS. ARS loading was monitored quantitatively through change in absorbance at 513 nm, read every 5 mins from 0 – 50 mins and then every 42 mins subsequently until there was no further decrease in absorbance. Gels were then placed into 1 mL of PBS for 3 h to wash out any non-bound ARS.

6.3.6 Removal of Excessive Dye

To measure the release of non-covalently bound dye from the gel, gel cylinder (0.1mL) loaded with ARS was weighed and placed into 24-well microtitre plate. 1 mL of PBS was then added. The initial absorbance at 513 nm using Spectrostar Omega plate reader from BMG Labtech. The aliquot was returned to the well to maintain volume at 1 mL.

6.3.7 ARS Release Studies with H₂O₂

To measure ARS release from PBA gel when exposed to H₂O₂ solution, a range of H₂O₂ solutions at differing concentrations were freshly made up in sterile PBS (0 to 4 mM) solution. ARS-PBA gels were placed into wells of a 24-well microtitre plate containing 1 mL of either sterile PBS or H₂O₂ solutions. 100 µL was taken from the well and absorbance was measured at 513 nm at regular time intervals. After readings 100 µL was replaced into the well to maintain volume. Values were blank corrected to PBS only.

6.3.8 Release Studies using Plasma Activated Buffer

1 mL of sterile PBS was treated with cold atmospheric plasma jet, using conditions: 10 kV, 25 kHz, helium flow rate of 0.6 SLPM and gap distance of 15 mm, non-tapered jet for varying amounts of time (0-30 mins). Once the plasma activated solution was generated the ARS-PBA gels were added and released ARS was added to bacteria to assess ability to inhibit biofilm formation as discussed in section 6.3.9.

6.3.9 Biofilm Inhibition Studies

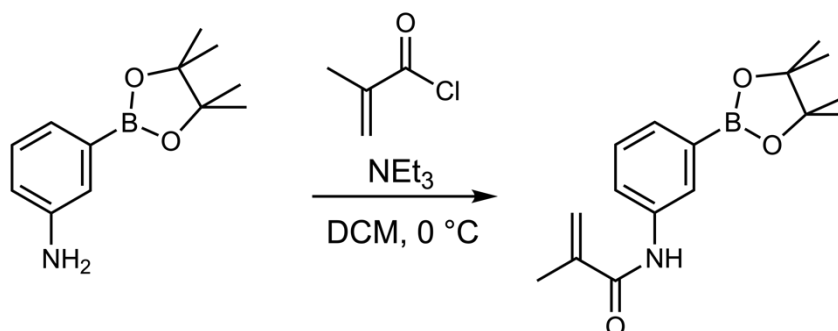
PBA-ARS gel was placed into a PBS solution (1 mL, pH 7.3) containing 2 mM H₂O₂ and incubated for 3 hours. Then 100 µL of the resulting PBS/H₂O₂/ARS solution (as discussed in 6.3.8) was then added to 100 µL of bacterial subculture (~2.5x10⁵ CFU/mL) in glucose supplemented broth (as per section 2.4.2) in 96-well plates. Biofilms were then statically incubated at 37°C for 18 h. After incubation biofilms were rinsed with PBS and stained with CV (as per section 2.3.2)

6.4 Results and Discussion

Initial release characterisation of the PBA hydrogel was carried out including quantification of ARS loading, washing and triggered release in the presence of varying concentrations of H_2O_2 in order to quantify optimal ARS release conditions. The antimicrobial efficacy of ARS and H_2O_2 both alone and in combination was then assessed on four strains of bacteria: two Gram-positive strains; methicillin-resistant *Staphylococcus aureus* (MRSA) and *Staphylococcus aureus* (*S. aureus*) and two Gram-negative; *P. aeruginosa* and *Escherichia coli* (*E. coli*), which are representative of the bacterial strains predominantly isolated from both acute and chronic wounds. The ARS-PBA gel was then tested for its ability to inhibit the formation of bacterial biofilms.

6.4.1 Synthesis of Boronic Acid Containing Hydrogel

The PBA monomer was prepared as shown in **Equation 6.1** according to the synthesis reported by Lampard *et al.*¹¹ The PBA hydrogel was made by dissolving acrylamide, methylene bisacrylamide and boronic ester monomer into distilled water. TMEDA and ammonium persulphate solution was added to initiate the polymerisations. After 40 minutes gelation was completed, and the cylinders were produced to a measurable volume. The gels created were clear in colour, as such, it was thought they could take on the colour of a dye.



Equation 6.1: The binding of PBA to acrylamide monomer

6.4.2 Determination of Loading of Hydrogel

The loading of the PBA hydrogel was conducted in multiple stages, initially the binding of ARS to the PBA gel was analysed, then the washing of unbound ARS from the PBA

hydrogel was monitored to ensure its total removal. Finally, the release of ARS from the PBA hydrogel in response to H_2O_2 was quantified.

To bind the ARS to the boronic ester moieties within the hydrogel, the PBA gel cylinders were placed into 2.5×10^{-4} M solution of ARS in PBS and left to incubate for 5 hours, to maximise ARS dye loading. The ARS binding to the hydrogel can be observed visually through the colour change from clear (unloaded PBA gel) to red (after loading with ARS for 5 hours). After the excess, unbound, ARS was washed away by placing gels in PBS for 3 hours, the final ARS-PBA gels were orange in colour as shown in **Figure 6.6**.

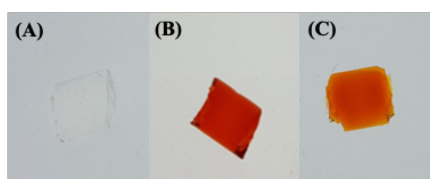


Figure 6.5: PBA hydrogel gel blank (A), loaded with ARS prewash step (B) and after washing in PBS (C).

6.4.2.1 Scheme for Triggered Release

Work by Lampard *et al.* outlined the release of ARS in response to the presence of sugars in equilibrium, the addition of the H_2O_2 prevents the backward reaction pathway. This is owing to the oxidation of the boron-carbon bond to the boron-oxygen bond, removing the binding site for the ARS catechol. The ARS binding and release should occur in a similar manner to that of the carbohydrate, with oxidation of the boronic ester causing the release of the bound dye, rather than the displacement in the presence of the saccharide. This would then result in the release of the ARS into the surrounding solution. Boronic esters are known to undergo H_2O_2 mediated oxidation to form the corresponding phenol. In the presence of H_2O_2 the ARS is cleaved and released into the aqueous solution (**Figure 6.6**). This can be visually monitored owing to the change in the colour of the gel as shown in **Figure 6.5**.

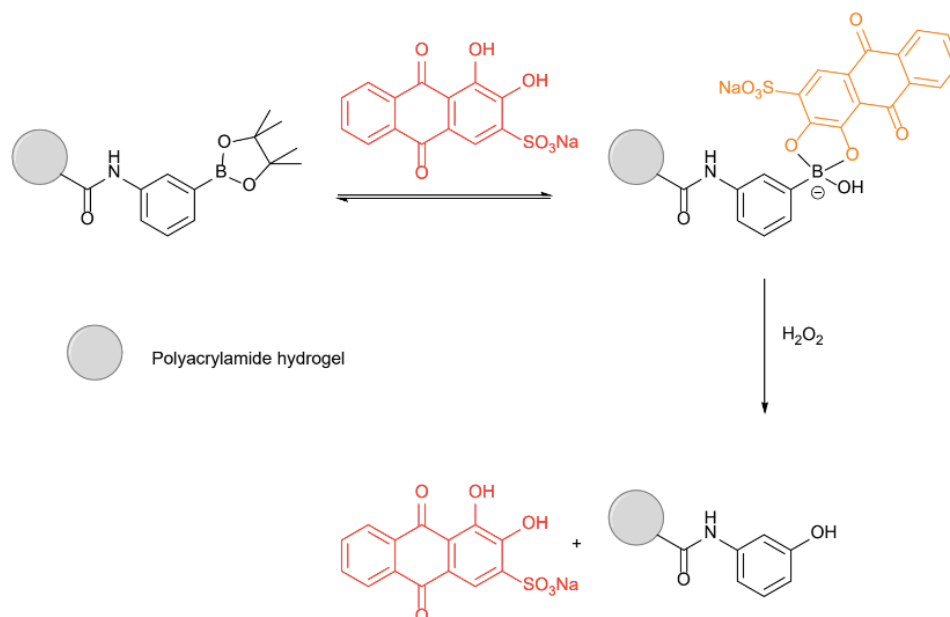


Figure 6.6: Schematic for the binding and triggered release of ARS to PBA hydrogel in the presence of H₂O₂ with the oxidative release of the ARS indicated by the reverse colour change on addition of H₂O₂

6.4.2.2 Loading of ARS to PBA Gel

The loading of ARS to the PBA gel can be quantified using absorbance. As the concentration of free ARS within the solution decreases, so does the absorbance, in accordance with the Beer Lambert law (**Equation 6.2**).

$$A = \epsilon Cl \quad (1)$$

Equation 6.2: Beer Lambert law

This absorbance change can be monitored over time. Aliquots were taken from the loading solution and measured at different time intervals. To allow for the discrepancies in gel swelling and size, absorbance was plotted as a function of the individual gel masses **Figure 6.7**. From these results, the minimum time required for the maximum loading of the dye where the gel is said to be saturated with ARS, can be elucidated. After 200 minutes the graph reaches a plateau, indicating no further decrease in absorbance, thus it can be concluded that PBA gel is saturated with ARS. While the PBA gels used are relatively small cylinders, if the gel size were to be increased, for example to make a larger sheet for wound dressing, the loading time would increase owing to an increase in the number of boronic acid binding sites and to account for the increased diffusion length.

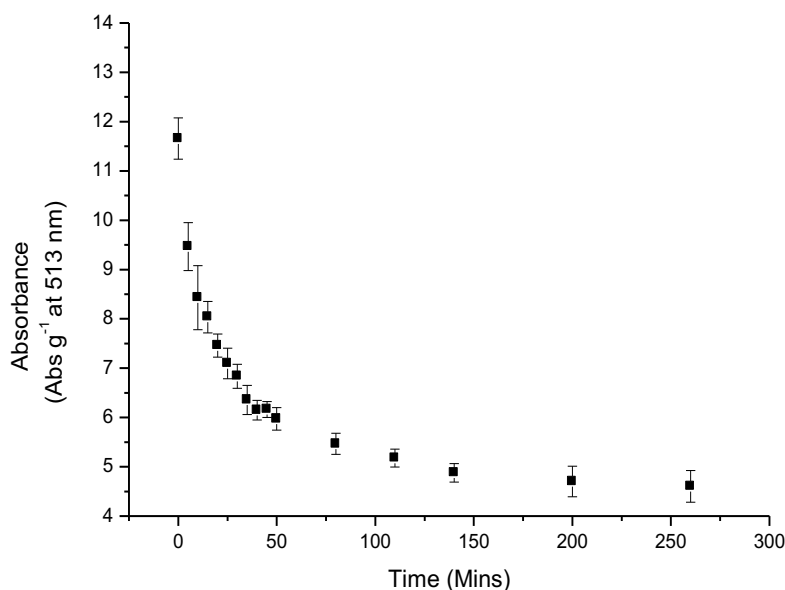


Figure 6.7: UV-Vis absorption per gram of PBA-based hydrogel at 513 nm over time in PBS (pH 7.3) at 25°C. Error bars indicate the standard deviation (n=3).

After ARS loading, to ensure that all non-specifically bound ARS was removed from within the hydrogel matrix structure the gels had to be washed. This was done by adding the gels to PBS solution and monitoring the increase of absorbance in the surrounding solution indicating release of ARS from the gels. Aliquots of the gel wash solution were periodically removed, and the ARS concentration measured through recording absorbance at 513 nm (**Figure 6.8**). Subsequently the aliquots were replaced to maintain the wash solution volume. The absorbance of the wash solution corresponded to the amount of un-bound ARS removed from the hydrogel. Once the wash solution absorbance ceased to increase, it was deemed sufficient washing had occurred and the remaining ARS was covalently bound to the gel. This was found to be at 180 mins.

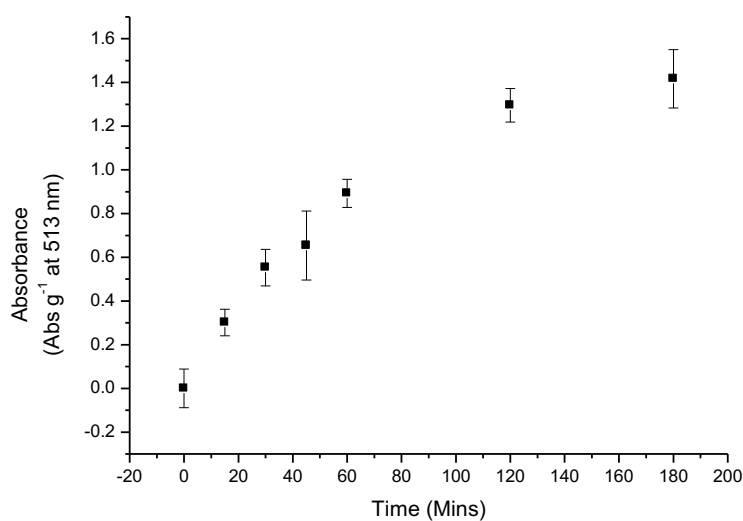


Figure 6.8: UV-Vis absorption per gram of PBA-based hydrogel at 513 nm over time in PBS (pH 7.3) at 25 °C. Error bars indicate standard deviation (n = 3).

6.4.2.3 Triggered Release of ARS from PBA Hydrogel

Following the loading and subsequent wash steps, the ARS-PBA hydrogels were ready for release studies. The gels were exposed to increasing concentrations of H₂O₂ made up in PBS (for increased stability of H₂O₂ and to maintain the pH of ARS) and the absorbance of the resulting solution was recorded. As the excess ARS has been removed as shown in **Section 6.4.2.2**, any release of ARS in the presence of H₂O₂ will be owing to the oxidation of the PBA and the subsequent triggered release of ARS. The rate of release of ARS was found to increase in the presence of higher concentrations of H₂O₂ (**Figure 6.9**). The release of ARS in the presence of H₂O₂ was found to increase as the concentration of H₂O₂ increased from 100 μM – 4 mM.

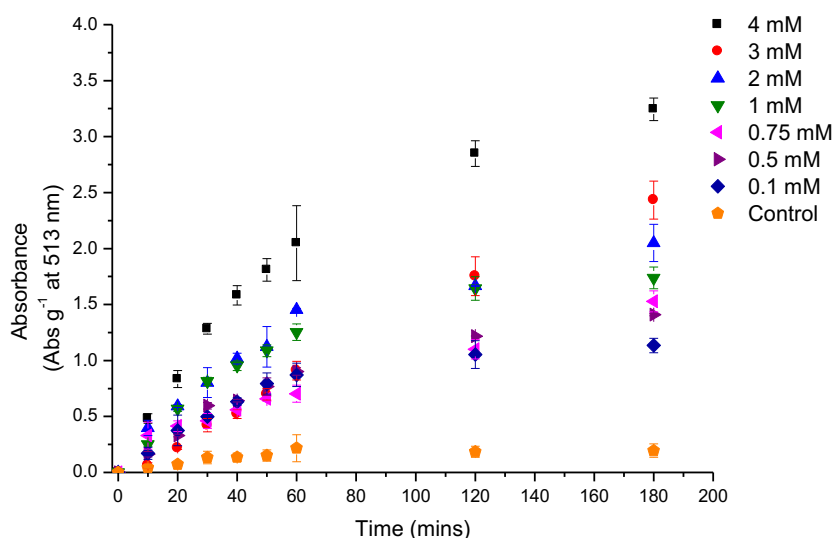


Figure 6.9: Absorbance at 513 nm of ARS released over time from PBA in the presence of varying concentrations of H_2O_2 (0-4 mM) in PBS.

As shown in **Figure 6.9**, the release of ARS begins to plateau at 180 minutes post exposure to H_2O_2 , the absorbance at 180 minutes was subsequently plotted in **Figure 6.10** for direct comparison of release after exposure to varying H_2O_2 concentrations. Interestingly, there was a significant release of ARS in the presence of 0.5 mM of H_2O_2 , which is the concentration of peroxide produced by He-CAP jet after five minutes, thus theoretically He-CAP treatment could release ARS from the PBA containing gel.

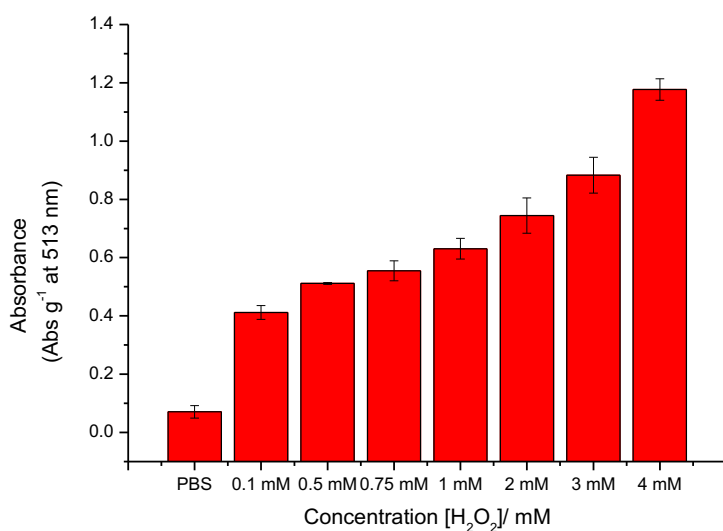


Figure 6.10: UV-Vis absorption per gram of PBA-based hydrogel in the presence of various concentrations of hydrogen peroxide (0.1 – 4 mM) in PBS (pH 7.3) after 3 hours. Absorbance was measured at 513 nm at 25 °C; error bars indicate standard deviation (n = 3).

6.5 Bacterial Studies

H₂O₂ is a known topical antimicrobial used within the decontamination of wounds. As it serves as a trigger within the hydrogel some H₂O₂ is likely to diffuse through the hydrogel into the wound bed in addition to the release of the ARS. As such the combination of ARS with H₂O₂ was assessed for antimicrobial effects.

6.5.1 Minimum Inhibitory Concentrations

As previously outlined, the MIC of an antimicrobial is indicative of the minimum concentration required to inhibit growth of bacteria. When tested on planktonic bacteria Gram-positive bacteria MRSA and *S. aureus* were found to be less susceptible to H₂O₂ than Gram-negative *P. aeruginosa* and *E. coli* (Table 6.2). MRSA252 and *S. aureus* have an MIC of 6.95-13.91 mM and *P. aeruginosa* and *E. coli* have an MIC of 0.43-0.87 mM (For absorbance data see Appendix 6.9.1). The MIC for all four strains was > 125 μM ARS, however, it is worth noting that the maximum solubility of ARS is 2.5x10⁻⁴ M and owing to the protocol, the maximum concentration of ARS that can be used in the MIC is 1.25x10⁻⁴ M.

Table 6.2: The MIC of MRSA (MRSA252), *S. aureus* (H560), *P. aeruginosa* (PAO1) and *E. coli* (NCTC10418) when treated with H₂O₂ and ARS using standard microplate dilution method. For absorbance data see Appendix 6.9.1 & 6.9.2.

Bacterial Species	MIC H ₂ O ₂ (mM)	MIC ARS (mM)
MRSA252	6.95-13.91	>125
<i>S. aureus</i> H560	6.95-13.91	>125
<i>P. aeruginosa</i> PAO1	0.43-0.87	>125
<i>E. coli</i> NCTC 10418	0.43-0.87	>125

6.5.2 Minimum Biofilm Inhibitory Concentrations

Alizarin is a known biofilm inhibitor; it was thus thought that ARS would also have biofilm inhibitory properties. The minimum biofilm inhibitory concentration (MBIC) is the minimum concentration of antimicrobial required to inhibit biofilm formation. Owing to the fact that alizarin is a calcium chelator as proven by Lee *et al.* and as calcium contributes to

adhesion of bacteria to surface, it was thought that ARS would reduce the amount of calcium available for the bacteria and thus would impact binding and reduce biofilm formation.⁷ To assess this, varying concentrations of ARS was added to lag phase bacteria ($\sim 1 \times 10^5$ CFU/mL) in a 96-well plate, the bacteria was then left to grow statically, to enable the formation of biofilms, for 24 h. After incubation the bacterial biofilm biomass was stained using crystal violet (CV) dye and its biomass was measured as a function of absorbance. An increased absorbance at 570 nm corresponded to an increase in bacterial biomass. It is important to note that while the methodology enables high throughput screening, as was required here, it is a crude method estimating only biomass not the viability or number of cells within the remaining biofilm. Further to this CV will stain all materials present, including extracellular (ECM) and biofilm slime not just the bacterial cells themselves.

As expected, the biofilms of the four species respond differently to the ARS; **Figure 6.11** shows the variation in the biomass of the biofilms varies between the species. Both MRSA and *S. aureus* biofilms are inhibited by ARS, however *P. aeruginosa* and *E. coli* are not. Their MBIC values are outlined in **Table 6.3**. This is potentially owing to *S. aureus* biofilms require greater concentrations of calcium for biofilm formation than the Gram-negative strains and as such, are more susceptible to the ARS owing to its ability to chelate calcium.

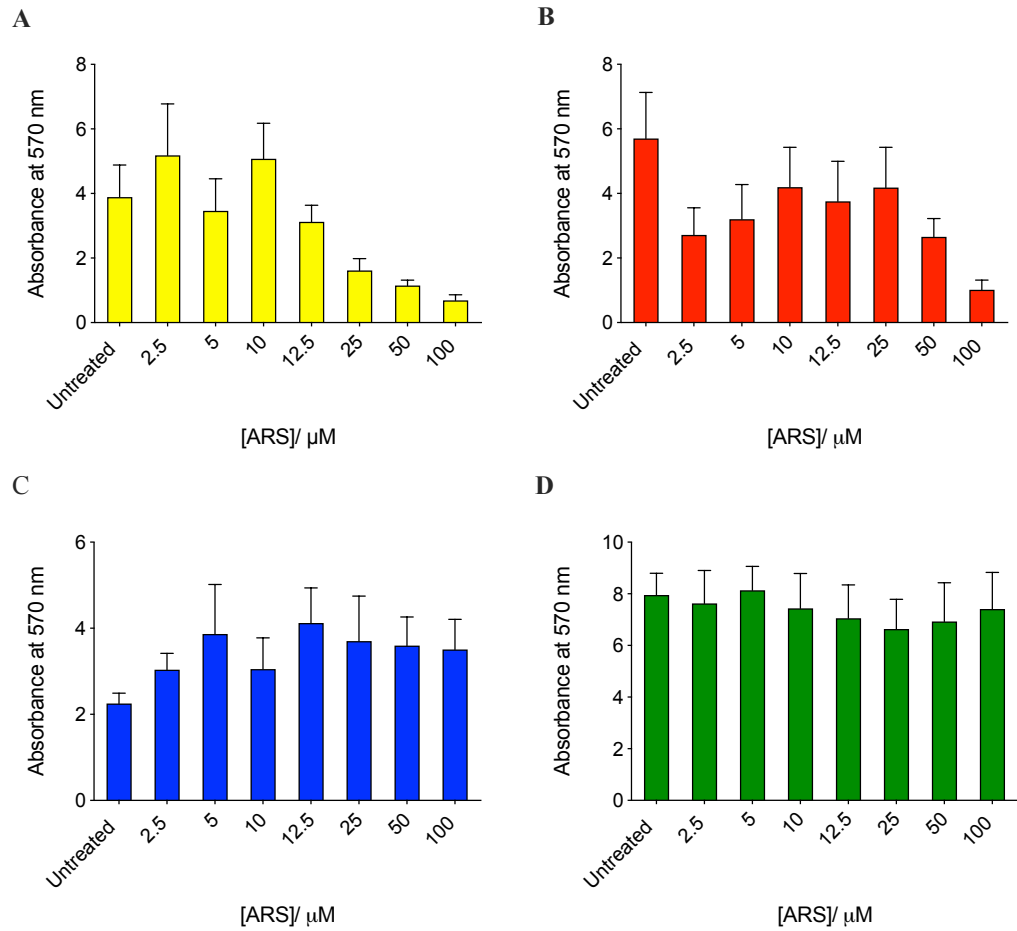


Figure 6.11: Varying concentrations of ARS (2.5-100 μM) were added at lag phase to MRSA (MRSA252) (A), *S. aureus* (H560) (B), *P. aeruginosa* (PA01) (C) and *E. coli* NCTC 10418 (D). After 24 hours growth at 37 $^{\circ}\text{C}$, absorbance was measured at 570 nm. Error bars indicate standard deviation (n = 4).

The same experimental procedure was repeated with H_2O_2 to elucidate the MBIC of H_2O_2 **Figure 6.12**. Gram-negative bacteria appear to be less susceptible to H_2O_2 . The MBIC of *P. aeruginosa* 25-100 mM which would seem to be an experimental anomaly.

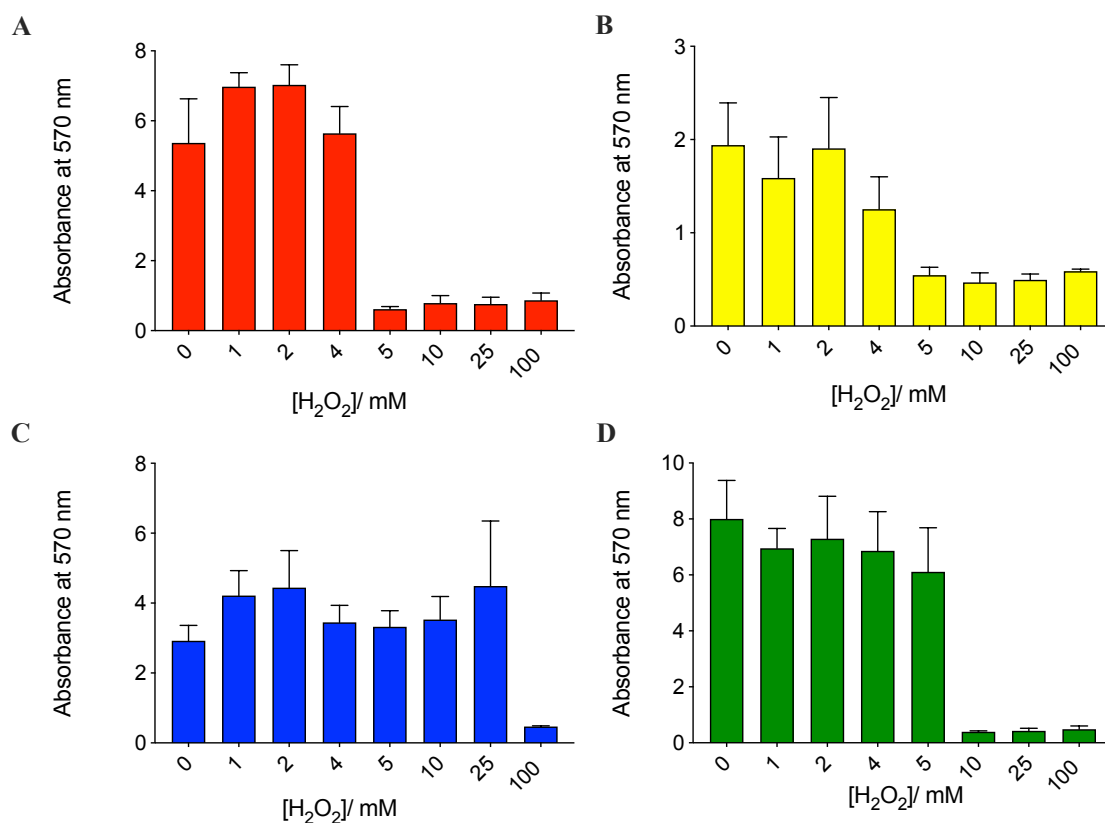


Figure 6.12: Varying concentrations of H₂O₂ (1-100 μM) were added at lag phase to MRSA (MRSA252) (A), *S. aureus* (H560) (B), *P. aeruginosa* (PAO1) (C) and *E. coli* (NCTC 10418) (D). After 24 hours growth at 37 °C, absorbance was measured at 570 nm. Error bars indicate standard deviation (n = 4).

The MBIC of MRSA252 and *S. aureus* for ARS is between 50-100 μM, however, the MBIC for *P. aeruginosa* or *E. coli* is above 100 μM (**Table 6.3**).

Table 6.3: The MBIC of MRSA (MRSA252), *S. aureus* (H560), *P. aeruginosa* (PAO1) and *E. coli* (NCTC10418) when treated with H₂O₂ and ARS using standard microplate dilution method. For absorbance data see Appendix.

Bacterial Species	MBIC H ₂ O ₂ (mM)	MBIC ARS (mM)
MRSA252	4-5	50-100
<i>S. aureus</i> H560	4-5	50-100
<i>P. aeruginosa</i> PAO1	25-100	>100
<i>E. coli</i> NCTC 10418	5-10	>100

To further assess the effect of ARS on bacteria, a viability assay using XTT was performed, to see whether the ARS was affecting the bacteria's viability while preventing it from forming a biofilm or if it is only preventing the biofilm formation leaving viable bacterial

cells. The metabolic activity of all four strains was found to be >50% showing that while the biofilm had not formed the bacteria are still metabolically active (**Figure 6.13**).

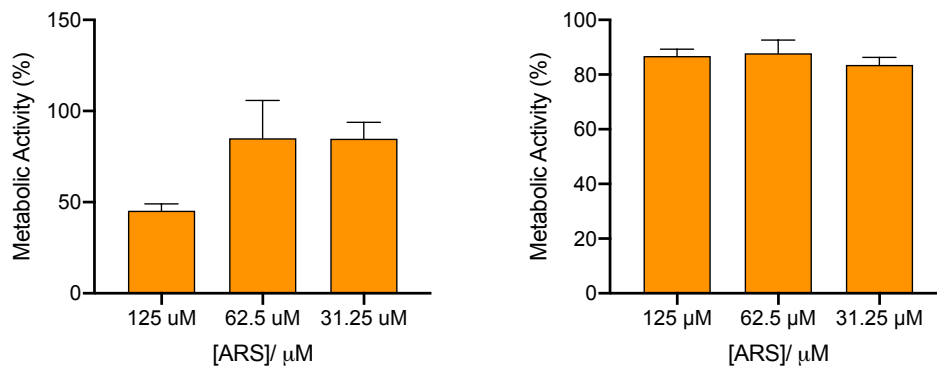


Figure 6.13: XTT Viability of ARS against bacterial strains *P. aeruginosa* (PAO1) and *S. aureus* (H560). Error bars indicate the standard deviation (n=3).

6.5.3 Minimum Biofilm Eradication Concentrations (MBEC)

As outlined in **Chapter 1**, the concentrations of drug required to eradicate a biofilm can be between 10-1000 times higher than the MIC of said drug. To further assess the utility of H₂O₂ and ARS were tested against 96-well plate, 24 h biofilms to elucidate their MBECs. The MBECs were found to be higher than the maximum solubility of ARS (**Table 6.4**).

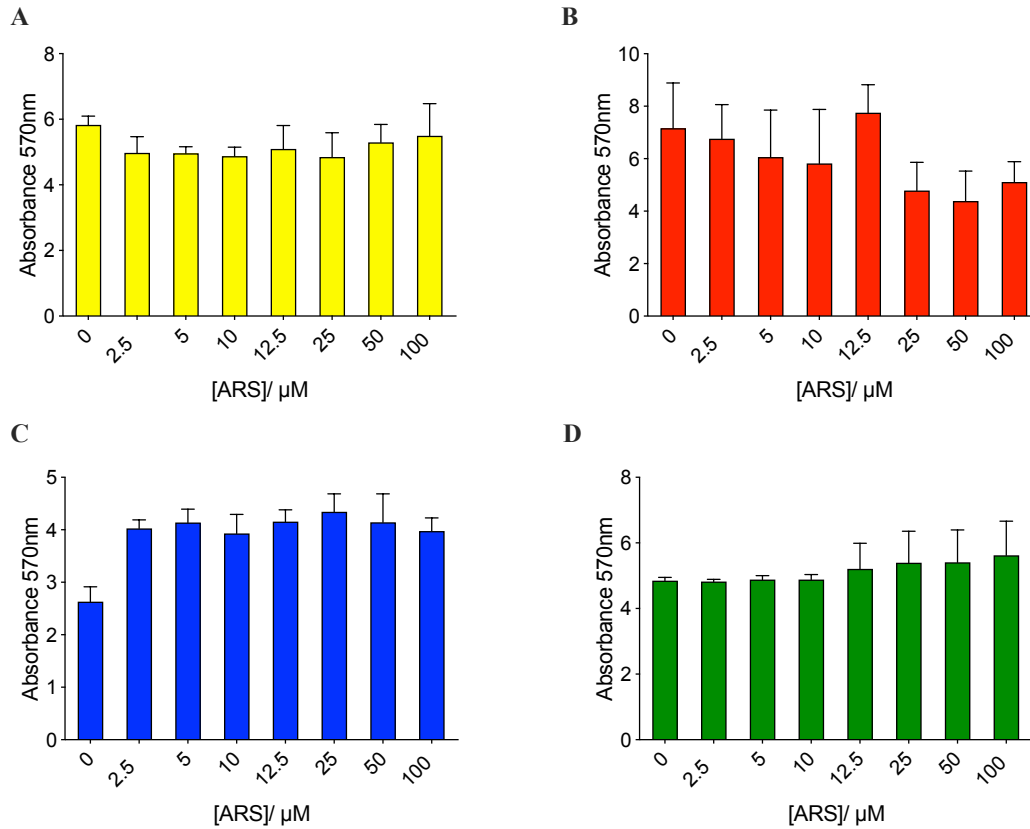


Figure 6.14: Varying concentrations of ARS (2.5-100 μM) were added at stationary phase to MRSA (MRSA252) (A), *S. aureus* (H560) (B), *P. aeruginosa* (PA01) (C) and *E. coli* (NCTC 10418) (D). After 24 hours growth at 37 $^{\circ}\text{C}$, absorbance was measured at 570 nm. Error bars indicate standard deviation ($n = 4$).

Unsurprisingly the MBEC of ARS was above 2.5×10^{-4} M, as ARS has no effect on the viability of the bacteria it was not expected that the ARS would have any effect on the established biofilms (**Figure 6.14**).

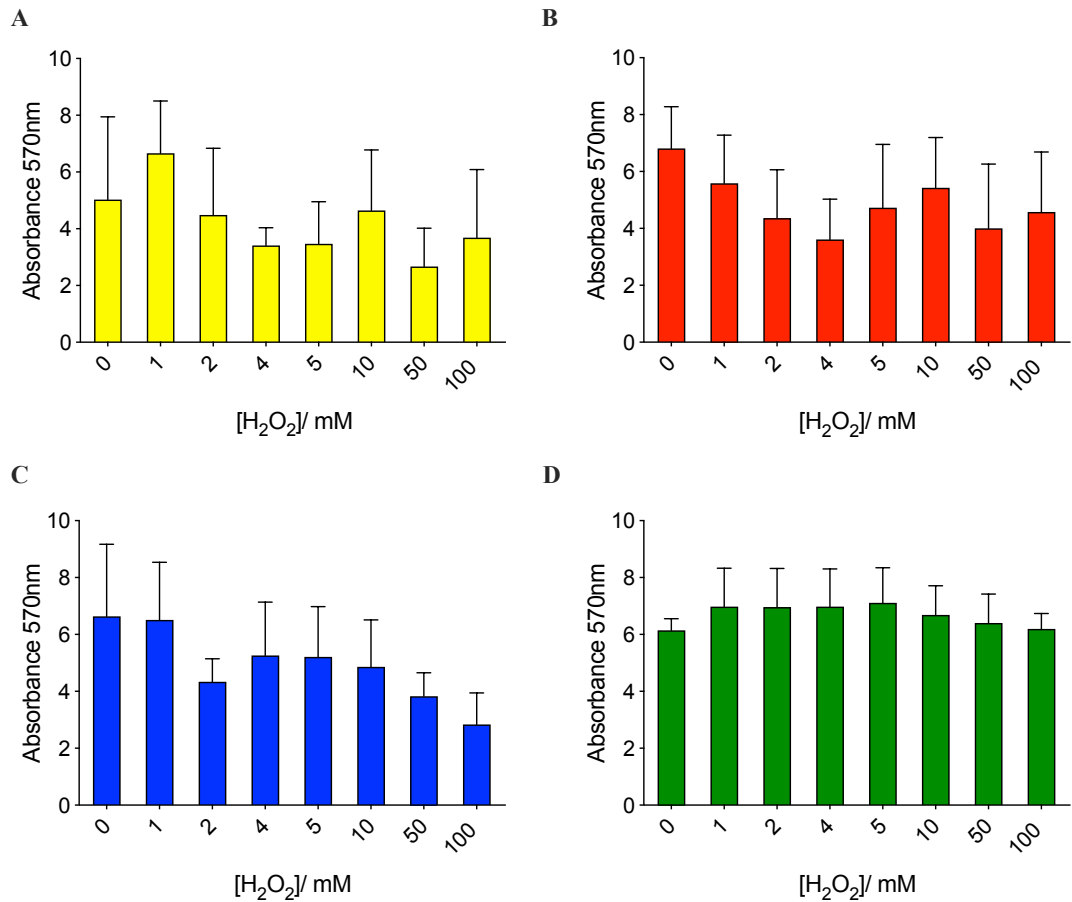


Figure 6.15: Varying concentrations of H₂O₂ (1-100 mM) were added at stationary phase to MRSA (MRSA252) (A), *S. aureus* (H560) (B), *P. aeruginosa* (PAO1) (C) and *E. coli* (NCTC 10418) (D). After 24 hours growth at 37 °C, absorbance was measured at 570 nm. Error bars indicate standard deviation (n = 4).

The MBEC of H₂O₂ was found to be above 100 mM for all four strains as shown in **Figure 6.15**, confirming that the MBEC is significantly higher than the MIC.

Table 6.4: The MBEC of MRSA (MRSA252), *S. aureus* (H560), *P. aeruginosa* (PAO1) and *E. coli* (NCTC10418) when treated with H₂O₂ and ARS using standard microplate dilution method. For absorbance data see Appendix.

Bacterial Species	MIC H ₂ O ₂ (mM)	MIC ARS (μM)
MRSA252	>100	>125
<i>S. aureus</i> H560	>100	>125
<i>P. aeruginosa</i> PAO1	>100	>125
<i>E. coli</i> NCTC 10418	>100	>125

6.5.4 Combination of ARS and H₂O₂

As both ARS and H₂O₂ would be released into the wound milieu, the combination of 2 mM H₂O₂ and either 50 µM or 100 µM ARS were added to developing biofilms at 0 h to assess whether the combination had an additive effect on the inhibition of biofilm formation. If the combination is additive or synergistic the absorbance for the combination will be significantly lower than the individual compounds.

For MRSA252 the combination of 2 mM H₂O₂ and 50 µM and 100 µM ARS was found to completely inhibit the formation of MRSA252 biofilms as denoted by a crystal violet absorbance of <0.5 at 570 nm, which corresponds to complete lack of biofilm biomass **Figure 6.16A**. As the combinations produced a significantly greater effect than the compounds alone it can be concluded that the combination is synergistic. While the combination of H₂O₂ and ARS significantly reduced the biomass of *P. aeruginosa*, the absorbance was still ~1.5 indicating the presence of bacterial biofilm. However, owing to the decrease in biomass it is hypothesised that the addition of further antimicrobials would be effective at lower concentrations as they would be able to penetrate the sparse biofilm easier than a dense biofilm. The combination of ARS and H₂O₂ was found to be ineffective on *S. aureus* (H560) and *E. coli* (NCTC10418). When the combinations were added to growing biofilms at 6 hours into growth or to established 24-hour biofilms the combination was found to be ineffective in both instances, as was expected owing to the lack of efficacy shown by the individual compounds.

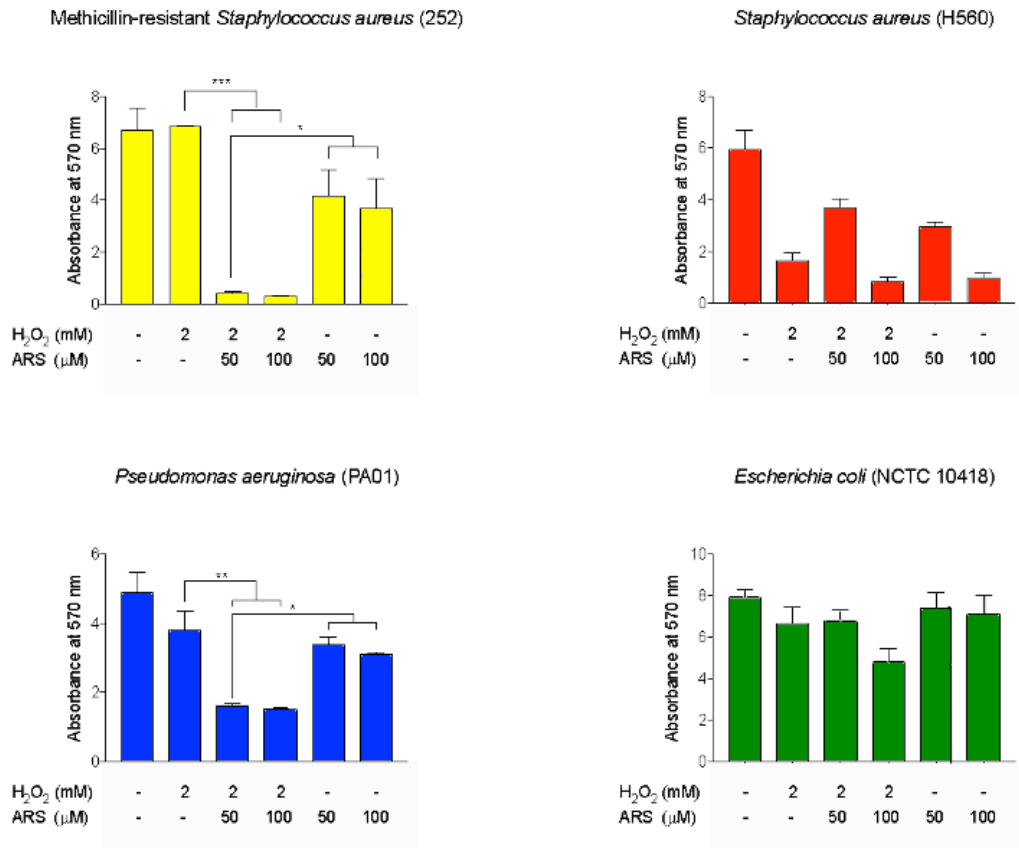


Figure 6.16: H₂O₂ (2 mM) was added to ARS (50 and 100 μM) during lag phase to MRSA252 (A), *S. aureus* H560 (B), *P. aeruginosa* (PAO1) (C) and *E. coli* (NCTC 10418) (D). After 24 h growth at 37 °C whereby absorbance was measured at 570 nm. Error bars indicate standard deviation (n=4).

6.5.5 ARS PBA Hydrogel Inhibition of Biofilm Formation

The ARS PBA gel was treated with H₂O₂ and the resulting solution was added to planktonic cultures of MRSA, *S. aureus*, *P. aeruginosa* and *E. coli* under the same conditions as the individual antimicrobials had been added previously. As the most promising results were observed when 2 mM H₂O₂, solutions were added in combination with ARS, 2mM of H₂O₂ was added to the PBA gel to trigger the release of the ARS. The resulting solution was found to significantly inhibit the formation of MRSA252 biofilms (**Figure 6.17**). However, it was ineffective against *S. aureus* H560, while this was to be expected owing to the observed results of the combination therapy, it was not expected that the treatment would be effective on MRSA and not *S. aureus*. This could potentially be as a result of MRSA252 using greater concentrations of calcium for the formation of its biofilm when compared to *S. aureus* (H560) thus accounting for the discrepancy. The combination was not found to be effective

against *P. aeruginosa* or *E. coli*. 2 mM of H₂O₂ was found to inhibit the formation of both species' biofilms, as such it could not be concluded that the ARS released from the PBA hydrogel was having any effect upon the biofilm formation. 1 mM of H₂O₂ was instead used to trigger the release of ARS (data not shown), however, this was not found to inhibit biofilm formation. It was thus concluded that the ARS-PBA hydrogel was ineffective against *P. aeruginosa* and *E. coli*.

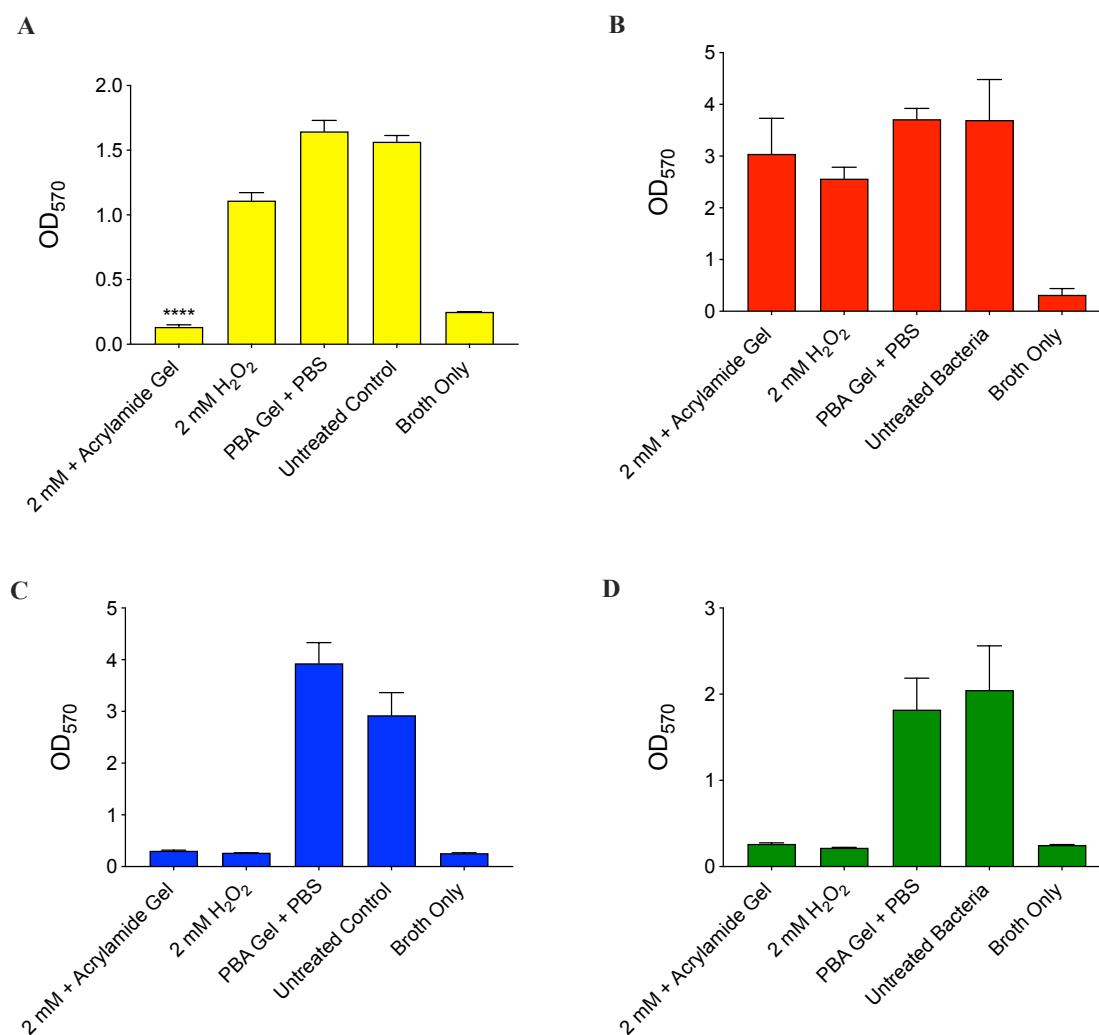


Figure 6.17: Biofilm biomass after 18 h growth at 37 °C in the presence of resultant solution after ARS loaded acrylamide gel was exposed to 2 mM H₂O₂, 2 mM H₂O₂ only, the resultant solution of PBA hydrogel in the presence of PBS compared to untreated bacterial control and broth only control for MRSA (MRSA252) (A), *S. aureus* (H560) (B), *P. aeruginosa* (PAO1) (C), and *E. coli* (NCTC10418) (D). Error bars represent standard deviation (n=3) One-way ANOVA was performed p<0.0001.

To ensure the antibacterial/antibiofilm properties of the ARS-PBA hydrogel were due to the combination of the H₂O₂ and ARS, and not the PBA containing hydrogel, the toxicity of the PBA gel was assessed without ARS bound to it and no H₂O₂. To mimic the triggered release conditions, 1 mL of PBS was added to the PBA gel, this was then added to the bacteria and

biomass was assessed after 24 h. The biomass was compared to untreated control. There was no significant difference between the untreated bacterial biomass and the bacterial biofilm treated with PBA gel solution. Upon oxidation of the boronic acid, boronic acid is produced, the potential toxicity of this was concerning, however, these results show that the boronic acid has no antimicrobial effect.

6.5.6 He-CAP Activation of PBA Gel

An overarching aim of the project was to develop a system where a molecule or molecules could be released from a hydrogel in response to exposure to He-CAP. As the ARS is released in the presence of H_2O_2 , which is the predominant RONS produced by He-CAP, it was thought that He-CAP would release the ARS and result in an antimicrobial effect within a contaminated wound.

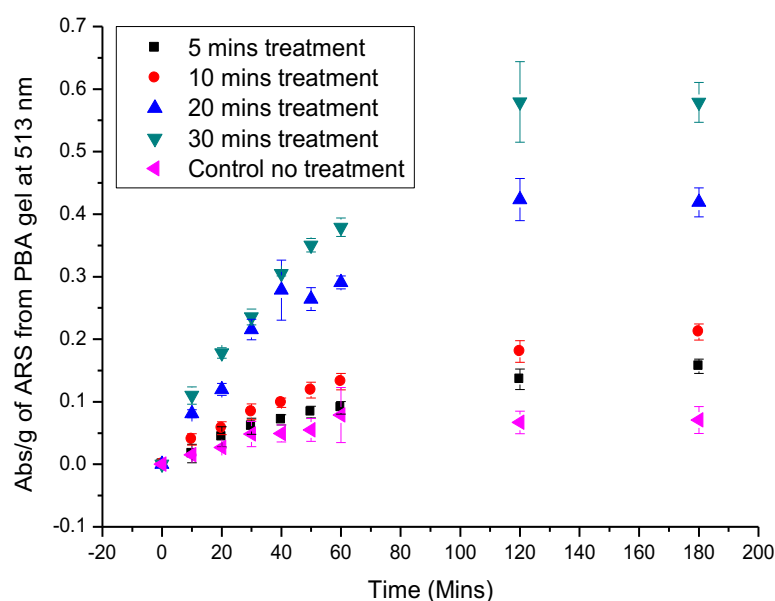


Figure 6.18: Absorbance at 513 nm of release of ARS from PBA gel after incubation with PBS treated with He-CAP for varying amounts of time (0-30 minutes). Error bars represent standard deviation (n=3).

As shown in Chapter 3, as He-CAP treatment time increases so does the concentration of RONS generated in treatment solution, with 5 minutes generation $\sim 650 \mu M$ of H_2O_2 . When ARS gels were added into plasma-activated PBS the absorbance at 513 nm increases owing to the He-CAP generated RONS mediating the release of ARS from the PBA gel, this is as a result of the He-CAP generated RONS within the PBS (**Figure 6.18**). The longer the PBS

has been exposed to the He-CAP, the greater the concentration of RONS generated and thus the increase in ARS released. This encouraging result indicates that the PBA is a potential candidate for a He-CAP responsive therapeutic hydrogel wound dressing.

As such, He-CAP was then applied directly to the PBA gel cylinders to trigger the ARS release. However, He-CAP treatment dehydrated the gels causing them to become brittle and there was a significant amount scorching observed (data not shown). Larger sheets of PBA gel were made to test with He-CAP treatment, in theory the larger volume should act as a reservoir allowing for the movement of water and decreasing the risk of burning and localised dehydration. However, this was not the case, the PBA gel dehydrated, and a hole was burned in the centre as shown in **Figure 6.19**.



Figure 6.19 He-CAP treated ARS-PBA hydrogel. Edges of the gel were taped down to prevent movement.

To attempt to limit this dehydration a PVA layer was added to the PBA. As shown in Chapter 3 PVA did not have any adverse response when treated with He-CAP, so a bi-layer gel was created. The PVA provides a more robust layer for the direct application of He-CAP and acts as a reservoir, for the He-CAP generated RONS, which would then diffuse down and trigger the release of the ARS from the PBA gel. However, the RONS reacted at the PBA/PVA interface and created an ARS concentration gradient resulting in the diffusion of ARS away from the wound surface as shown in **Figure 6.20**.

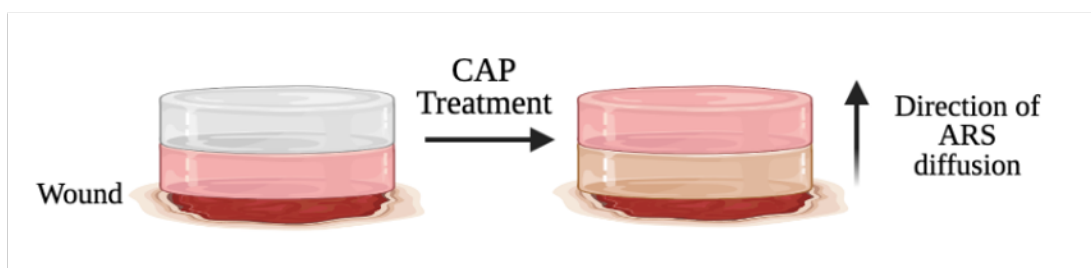


Figure 6.20: Bilayer ARS-PBA and PVA hydrogel before He-CAP treatment and after He-CAP treatment showing diffusion gradient of ARS post He-CAP treatment moving away from the wound.

Owing to the ARS gradient moving away from the contact surface, the tests were performed using the single layer PBA gel with H₂O₂ solutions and He-CAP activated solutions rather than direct He-CAP treatment.

6.6 Conclusions

A boronic ester containing acrylamide monomer was synthesised and successfully polymerised into a boronic ester functionalised polyacrylamide hydrogel known as PBA. PBA was found to be able to bind the diol containing dye, ARS. The ARS can be cleaved from the PBA in the presence of H_2O_2 , thus acting as a triggered release system. The release of ARS occurs in dose dependent manner in response to H_2O_2 .

Further to this, it was found that CAP treated PBS also triggered the release of ARS from the PBA hydrogel in a dose dependent manner, whereby the increased exposure time of the PBS to the CAP jet inferred an increased dose. This is thought to be due to the increased production of RONS, chiefly H_2O_2 , with increased CAP exposure time. This was thought to offer a promising alternative to the PVA hydrogel described in Chapter 3, as not only would it provide a screen from potentially damaging RONS produced by the CAP jet, it would also release an antibiofilm agent to prevent the formation of bacterial biofilms within the wound. However, when CAP treatment was applied directly to the gel, it was found to dehydrate and burn. The addition of a PVA layer, to form a dual layer hydrogel failed to mitigate this adverse response. Therefore, in order for this system to be compatible with CAP therapy further engineering of the hydrogel is required.

The ARS-PBA hydrogel system was found to be effective at inhibiting the formation of MRSA biofilms *in vitro*, but disappointingly, it was not found to be effective against *S. aureus* or Gram-negative *P. aeruginosa* or *E. coli* bacteria. However, as bacteria are not known to have any resistance to ARS, this could be administered as a prophylactic treatment although. Furthermore, as hydrogels and hydrogen peroxide are routinely used within wound care, this therapeutic option would require no alteration to existing clinical care pathways.

In addition to its utility as a therapeutic wound dressing, the ARS-PBA hydrogel system could be used as a solid state, reaction-based indicator of H_2O_2 concentration. This could have multiple applications within biology and for environmental detection.

6.7 Future Work

While 96-well plate biofilm models enable the high-throughput analysis of antibiofilm agents, they are simplistic and lack a multitude of physiological components that could influence the efficacy of the ARS-PBA hydrogel. Future work would seek to test the efficacy of the ARS-PBA hydrogel on both an *ex vivo* porcine skin model and potentially on animal models.

Further to this the ARS-PBA hydrogel could theoretically be used in tandem with an infection detection system, for example the commercially available *Wound Check* or *Moleculight* technologies or indeed the *SPaCE* sensor system developed within the Jenkins Group. On the detection of bacterial colonisation was detected then the H₂O₂ trigger could be applied either topically or via CAP therapy if the hydrogel were modified for optimal compatibility, to release ARS into the contaminated wound and prevent a biofilm-associated infection from forming.

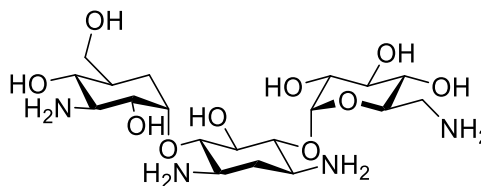


Figure 6.21: Structure of Kanamycin, an aminoglycoside antibiotic

Kanamycin is an aminoglycoside antibiotic, commonly prescribed within the clinic and historically was used to treat *Mycobacterium tuberculosis*, however there is growing kanamycin resistance within this species. The sugars that constitute the aminoglycosides offer a number of 1cis-,2 and 1,3 diols which act as binding sites for boronic acids. As such, kanamycin could be bound to the PBA gel for the RONS mediated triggered release of kanamycin to treat an infected wound.

6.8 References

1. Guan, Y. & Zhang, Y. Boronic acid-containing hydrogels: Synthesis and their applications. *Chem. Soc. Rev.* **42**, 8106–8121 (2013).
2. Dufort, B. M. & Tibbitt, M. W. Design of moldable hydrogels for biomedical applications using dynamic covalent boronic esters. *Materials Today Chemistry* vol. 12 16–33 (2019).
3. Ghosh, A., Jayaraman, N. & Chatterji, D. Small-Molecule Inhibition of Bacterial Biofilm. *ACS Omega* **5**, 3108–3115 (2020).
4. Rabin, N. *et al.* Medicinal Chemistry Review part of Agents that inhibit bacterial biofilm formation. *Futur. Med. Chem* **7**, 647–671 (2015).
5. Ding, X. *et al.* Screening for novel quorum-sensing inhibitors to interfere with the formation of *Pseudomonas aeruginosa* biofilm. *J. Med. Microbiol.* **60**, 1827–1834 (2011).
6. Verderosa, A. D., Totsika, M. & Fairfull-Smith, K. E. Bacterial Biofilm Eradication Agents: A Current Review. *Frontiers in Chemistry* vol. 7 824 (2019).
7. Lee, J. H., Kim, Y. G., Yong Ryu, S. & Lee, J. Calcium-chelating alizarin and other anthraquinones inhibit biofilm formation and the hemolytic activity of *Staphylococcus aureus*. *Sci. Rep.* **6**, 1–11 (2016).
8. Manoharan, R. K., Lee, J. H., Kim, Y. G. & Lee, J. Alizarin and chrysazin inhibit biofilm and hyphal formation by *Candida albicans*. *Front. Cell. Infect. Microbiol.* **7**, (2017).
9. Puchtler, H., Meloan, S. N. & Terry, M. S. ON THE HISTORY AND MECHANISM OF ALIZARIN AND ALIZARIN RED S ... ON THE HISTORY AND MECHANISM OF ALIZARIN AND ALIZARIN RED S ... Page 2 of 2. *J. Histochem. Cytochem.* **17**, 110–124 (1969).
10. Dahl, L. K. A Simple and Sensitive Histochemical Method for Calcium. *Proc. Soc. Exp. Biol. Med.* **80**, 474–479 (1952).
11. Lampard, E. V. *et al.* Dye Displacement Assay for Saccharides using Benzoxaborole Hydrogels. *ChemistryOpen* **7**, 266–268 (2018).

6.9 Appendix

6.9.1 MIC H₂O₂

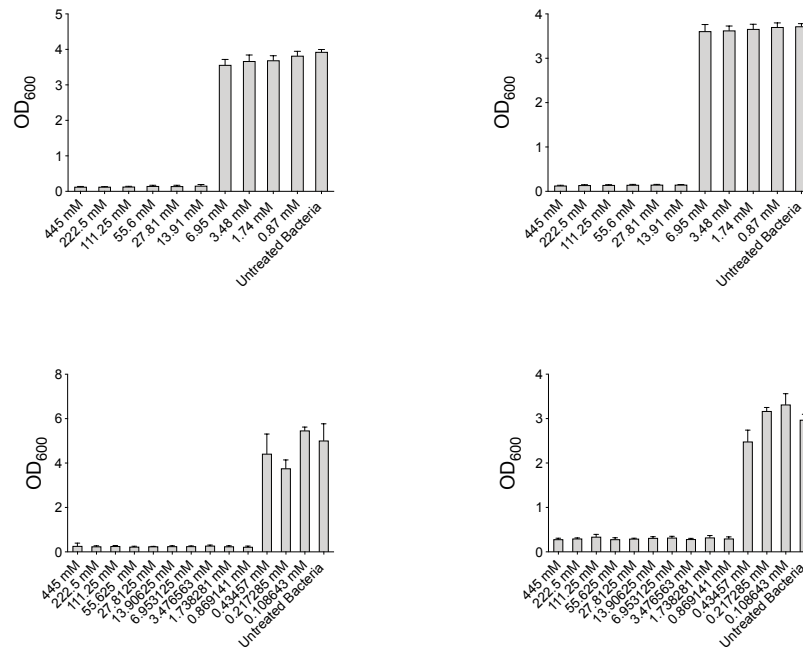


Figure 6.22: Minimum inhibitory concentration (MIC) of H₂O₂ against MRSA252, *S. aureus* (H560), *P. aeruginosa* (PAO1) and *E. coli* (NCTC10418). Absorbance at 600 nm corresponds to planktonic bacterial growth relative to untreated bacterial control (n=3).

6.9.2 MIC ARS

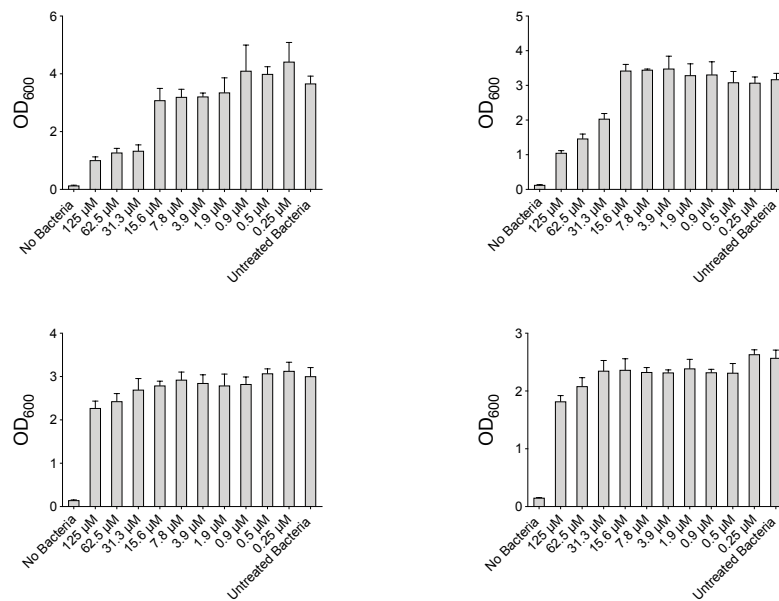
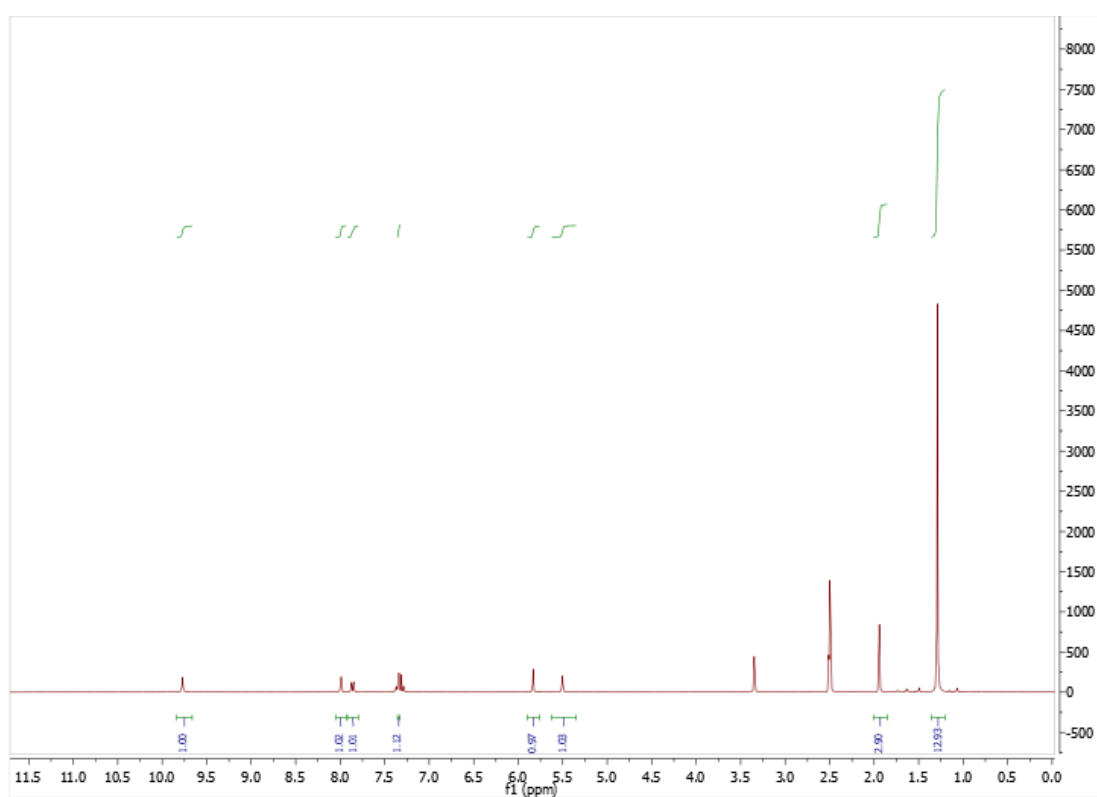
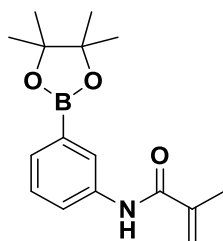


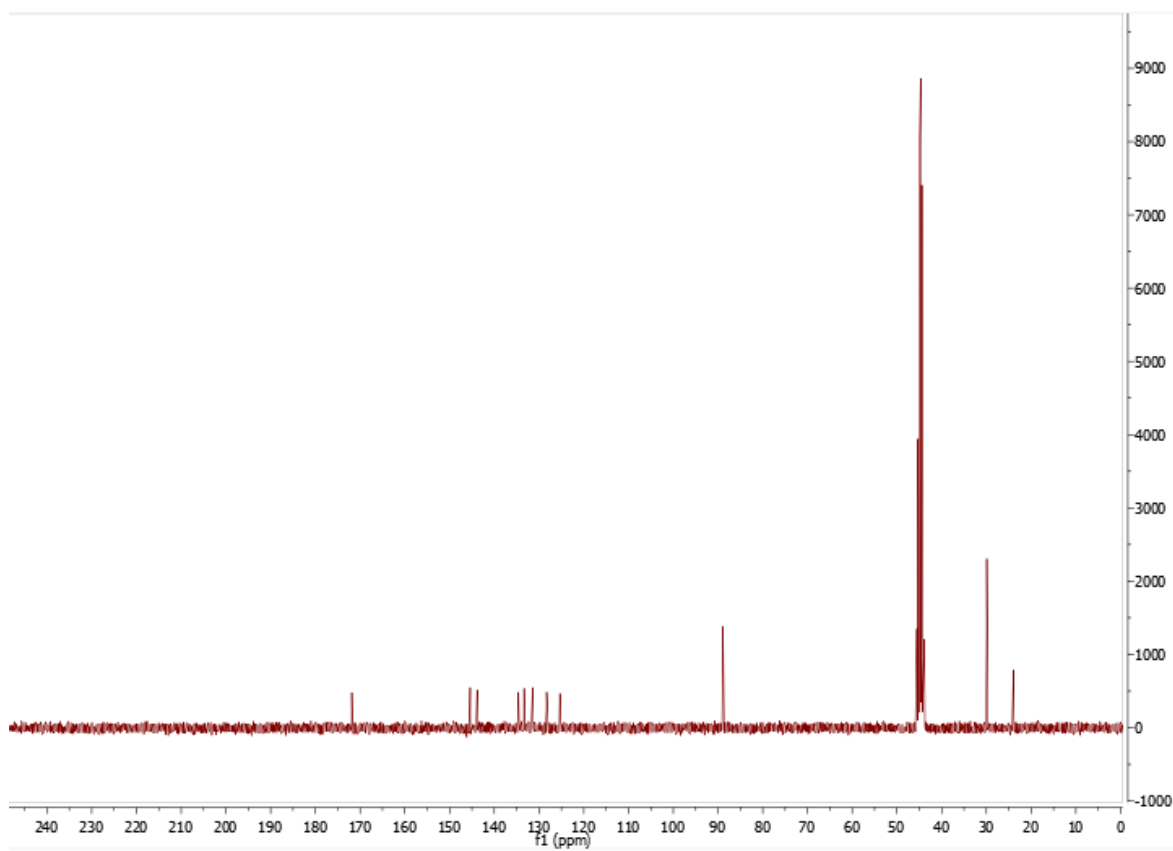
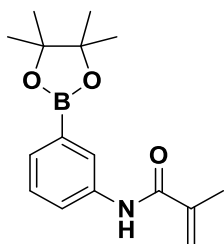
Figure 6.23: Minimum inhibitory concentration (MIC) of ARS against MRSA (MRSA252), *S. aureus* (H560), *P. aeruginosa* (PAO1) and *E. coli* (NCTC10418). Absorbance at 600 nm corresponds to planktonic bacterial growth relative to untreated bacterial control (n=3).

6.9.3 NMR Spectra

N-(3-(4,4,5,5-tetramethyl-1,3,2-dioxaborolan-2-yl)phenyl)methacrylamide (PBA) (^1H NMR, 300 MHz, DMSO- d_6)



N-(3-(4,4,5,5-tetramethyl-1,3,2-dioxaborolan-2-yl)phenyl)methacrylamide (PBA) (^{13}C NMR, 75.5 MHz, DMSO- d_6)



Chapter 7

Chapter 7 : Povidone Based Hydrogel Wound Dressing

7.1 Aims

Due to the low production of H_2O_2 by the helium-driven cold atmospheric pressure plasma (He-CAP) jet through a hydrogel wound dressing an alternative route for cold atmospheric pressure plasma (CAP) therapy with a hydrogel was to use He-CAP jet treatment in tandem with an antimicrobial to produce a synergistic response for the eradication of a bacterial infection. Theoretically, this could be done either through the topical application of the antimicrobial or by incorporating the antimicrobial into a hydrogel.

Within burn wound care, povidone-iodine (PVP-I), a polymeric iodophor, is commonly used like H_2O_2 , for the decontamination of burn wounds. Previous literature suggests that PVP-I can act synergistically with H_2O_2 in the treatment of bacterial infections. It was thus hypothesised that PVP-I could act synergistically with He-CAP treatment for the eradication of bacterial infection. Furthermore, as the He-CAP was sub-optimal in its efficacy, an alternative CAP jet using argon was investigated for its therapeutic potential. Ghimire *et al.* developed a novel argon driven cold atmospheric pressure plasma (Ar-CAP) jet tailored for the decontamination of infected wounds owing to its ability to generate high concentrations of H_2O_2 . The Ar-CAP was assessed to see if it would interact more favourably with a hydrogel and generate greater concentrations of H_2O_2 both with and without a hydrogel. Finally, the aim was to combine the PVP-I hydrogel with the modified Ar-CAP jet for the decontamination of *Pseudomonas aeruginosa* (*P. aeruginosa*) biofilm-associated wound infections.

7.2 Chapter Background

7.2.1 Povidone-Iodine

Povidone iodine (PVP-I) consists of the polymer polyvinylpyrrolidone (PVP) and triiodide (I_3^-) (**Figure 7.1**). The triiodide forms a complex with the carrier polymer povidone, which when in an aqueous environment will release iodine (I_2) and iodide (I^-) into the solution and establishes an equilibrium with free iodine being released following **Equation 7.1**: Triiodide equilibrium to iodine and iodide with an equilibrium constant of 0.000145 M at 298 K showing the majority “reservoir” species is I_2 .

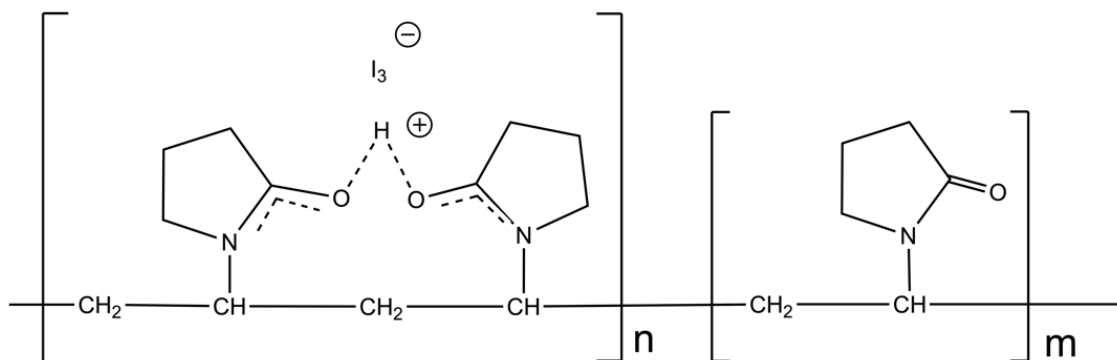


Figure 7.1: Chemical structure of PVP-I.



Equation 7.1: Triiodide equilibrium to iodine and iodide.

PVP-I has been found to be effective against a range of microorganisms. It is a broad spectra antimicrobial with efficacy against both Gram-positive and Gram-negative bacteria, in addition to this it is also effective against mycobacteria, yeasts, enveloped and non-enveloped viruses, including rabies, as well as protozoa.¹ As iodine crosses into bacteria it can induce cell death through the oxidation of amino acids and nucleic acids (**Figure 7.2**).² This gradual dissociation of iodine from PVP-I results in low associated cytotoxicity and sensitisation.

In addition to its antimicrobial activity, PVP-I also exhibits a range of anti-inflammatory properties on the host cells. Within the patient PVP-I modulates redox potential, exerts an inhibitory effect on inflammatory cells like $TNF-\alpha$ and enhances healing signals from

proinflammatory cytokines through the activation of monocytes, T-lymphocytes and macrophages. In the bacteria PVP-I can inhibit the production and release of bacterial exotoxins such as α -hemolysin and phospholipase C and can suppresses the activity of enzymes like elastase.³

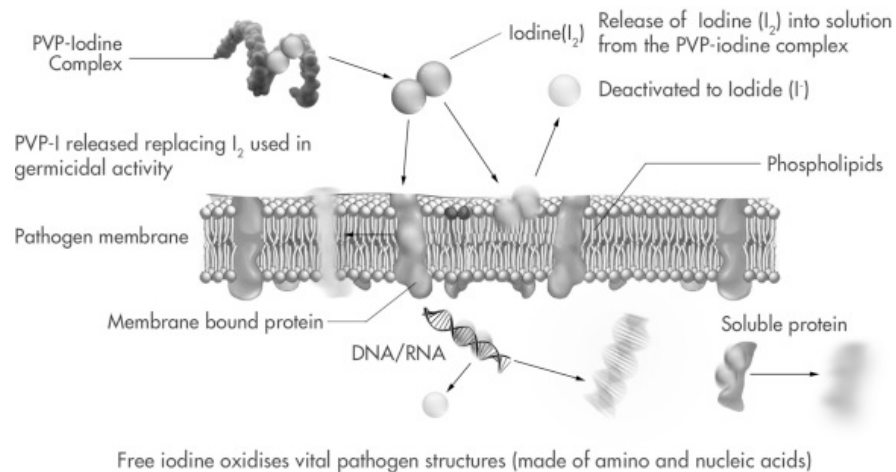


Figure 7.2: PVP-I antibacterial mechanism through the establishment of an equilibrium. (Reproduced with permission from Journal of Surgery).

As with all approved antimicrobials, the cytotoxicity of PVP-I has been extensively investigated, while there is a low level of cytotoxicity owing to nonspecific effects, it is at a significantly lower level than in other commonly used topical antimicrobials like chlorohexidine. PVP-I treatment is not recommended for patients with thyroid disorders, infants with low birth weight or patients receiving radio-iodine therapy. The absorption of PVP-I is determined by the condition of the skin barrier, absorption will increase if the skin barrier is broken and will also depend on the skins age and the surface area of the application area.⁴

PVP-I is used successfully within care regime for acute wounds, chronic wounds and burn wounds. The formulation used is dependent on its presentation, specifically its level of exudation and the extent of bacterial contamination (

Figure 7.3). Inadine, is a commercially available PVP-I based dressing, the non-adherent dressing using polyethylene glycol impregnated with PVP-I and has been used for the treatment of wound for over 30 years.⁵

Level of Exudation	High	Polyurethane foam with 3%		Dry powder spray/solution		
	Medium					
	Low	Liposomal 3%	Ointment 10%			
	Dry	Hydrogel				
		Contamination	Colonisation	Critical Colonisation	Sepsis	
	Increasing level of infection →					

Figure 7.3: Chart showing the selection of PVP-I formulation depending on requirements of the clinical wound.⁶

7.2.2 Argon Plasma

As already discussed, the engineering of plasma devices can be tailored for their use. The He-CAP jet previously described, was not found produce high enough concentrations of ROS, mainly H_2O_2 , for the decontamination of wounds. H_2O_2 in CAP jets is a secondary product of the reaction between hydroxyl ($\cdot OH$) radicals ($\cdot OH + \cdot OH \rightarrow H_2O_2$) and its production could be enhanced by a suitable choice of the working gas. Based on the literature^{7,8} the rate coefficient (k) for the formation of $\cdot OH$ radicals is an order of magnitude higher with argon metastables ($Ar_m + H_2O \rightarrow \cdot OH + H + Ar$, $k = 4.5 \times 10^{-10} \text{ cm}^3\text{s}^{-1}$) than that with helium metastables ($He_m + H_2O \rightarrow \cdot OH + H + He$, $k = 2.6 \times 10^{-11} \text{ cm}^3\text{s}^{-1}$). Also, results by Xian *et al.* suggest that the concentration of $\cdot OH$ radicals in Ar-CAP is higher than He-CAP. This higher concentration in Ar-CAP is mainly attributed to the morphology of the discharge. Ar-CAP discharge operates in filamentary mode with a lot of micro-discharges whereas discharge in helium is more diffuse. Higher energy and electron density in plasma filaments / streamers that are more likely to be formed in Ar-CAP are known to contribute to the higher concentration of $\cdot OH$ radicals.

Based on the above principle, the effect of inter-electrode separation distance along with the length of the plasma jets were investigated by Ghimire *et al.* (collaborators at Lancaster University). It was found that by increasing the inter-electrode separation distance from 5 mm to 160 mm increased the concentration of H_2O_2 from 0.4 mM to 1.2 mM in two minutes of plasma treatment in deionised water. This is significantly higher than the concentration produced by He-CAP in five minutes of plasma treatment. The higher inter-electrode

separation distance mainly facilitated the formation of energetic streamers, which increased the concentration of H_2O_2 . Further to this, the Ar-CAP jet was found to decrease the pH of the treatment solution owing to the generation of NO_2^- , which within a wound environment would be advantageous for healing. The Ar-CAP (described in the next section) was optimized to operate at room temperature by addition of an additional ground electrode, still producing higher concentration of H_2O_2 .

7.3 Methods

7.3.1 Bacterial Strains

Within this chapter a selection of *P. aeruginosa* strains were used outlined their origin is outlined in **Table 7.1**. They were maintained and cultured as per 2.2.2.

Table 7.1: *P. aeruginosa* strains name and origin

Strain Name	Origin
PAO1	ATCC Typed Strain
PAE45311	
PAE45321	Acute wound isolates from Bristol Southmead
PAE45325	Hospital
PAE45379	

7.3.2 Argon Plasma Jet

Developed at the University of Lancaster by Ghimire *et al.* the Ar-CAP jet shown in **Figure 7.4** consisted of an internal steel needle electrode (outer diameter = 0.9 mm, inner diameter = 0.6 mm, length 51 mm) sealed inside a quartz tube (inner diameter = 1.5 mm, outer diameter = 3 mm). Two external copper electrodes of length 4 mm 5.6 cm from electrode, spaced 5.4 cm apart and 6.6 cm from the bottom of the tube. Ar gas was kept at 1.0 standard litres per minute (SLPM) and generated at 10 kV at 23.5 kHz. Voltage and current waveforms were monitored using oscilloscope. The gap distance was 1.5 cm and the Ar-CAP jet was stationary unless otherwise stated.

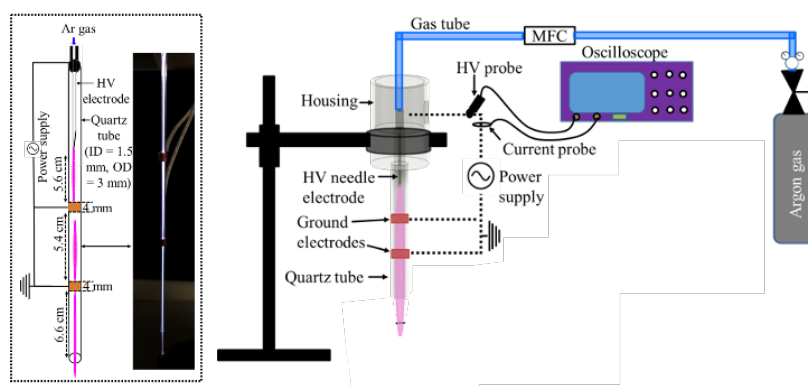


Figure 7.4: Schematic of Ar-CAP jet set up.

7.3.3 PVP-I Hydrogel

5% (w/v) PVA solution was made up as per section 2.6.3. This was then mixed 1:1 with 10% (v/v) Povidone Iodine (PVP-I) and vortexed to ensure homogenisation. The gels were then cast by aliquoting 500 μ L into wells of a 24-well plate and crosslinked through freeze thawing, from here referred to as cryogenic crosslinking (cryo-crosslinking). Cryo-crosslinking was achieved through two repeated freeze-thaw cycles at -20°C . As required gels were rinsed for 2 h in 1 mL of sterile PBS to remove excess PVP-I.

7.3.4 Checkerboard Assay

100 μ L of LB broth was added to all wells in a 96-well plate apart from 1A-G which were left empty. 200 μ L of antimicrobial A was added to wells 1A-G, then 100 μ L was removed from these wells and serially diluted across the plate, stopping before row 11. 100 μ L of antimicrobial A was added to well H1 and serially diluted across row H, providing the minimum inhibitory concentration (MIC) for antimicrobial A. 100 μ L of antimicrobial B was added to wells 1-10 in Row A, and serially diluted down the plate stopping before row G. 100 μ L of antimicrobial B was added to well A11 and serially diluted down the plate, providing the MIC for antimicrobial B. 100 μ L of bacterial subculture was then added to all wells aside from E-G12, providing a positive control. Finally, 100 μ L of broth was added to wells A-D12, providing a negative control. Plates were then incubated statically for 18 h at 37°C , and the absorbance of each well was then read at 600 nm corresponding to bacterial growth. Lack of turbidity indicated no cell growth. This was repeated three times per bacterial species.

7.3.5 Plasma Activation of Drug

7.3.5.1 Planktonic Treatment

150 μ L of PVP-I of $\frac{1}{2}$ MIC concentration was added to wells of a 96 well plate and then CAP treatment was applied for $\frac{1}{2}$ time required to generate MIC levels of antimicrobial activity from the jet (3 or 5 min depending on strain), 150 μ L of bacterial subculture was

then added atop CAP activated PVP (diluting PVP 1:2). In a separate well 150 μL of PVP-I was added and 150 μL bacterial subculture. In a final well $\frac{1}{2}$ MIC CAP dose was applied to 150 μL of PBS and 150 μL of bacterial subculture was then added. 150 μL of subculture was then added to PBS only to serve as a positive control. The plate was then incubated statically for 18 h at 37 °C.

7.3.5.2 Biofilm Treatment

100 μL of PVP was added atop 24 h biofilm, CAP jet treatment was then applied atop the biofilm for 5 minutes, under the conditions outlined above. After treatment biofilms were left to incubate for 1 h at 37 °C. Biofilms were then stripped and CFU/biofilm enumerated as previous. CFU was compared to untreated control. Biofilms were grown and enumerated as previously described in section 2.3.3.

7.3.6 FT-IR

PVP-I hydrogels were made as per section 7.3.3 and PVA hydrogels were made as per section 2.6.3. The gels were lyophilised and converted into powdered form. Samples were then analysed using the fourier transform infrared spectroscopy (FT-IR) at force 75%, over the range 600-4000 cm^{-1} using Spectrum100 (PerkinElmer).

7.3.7 MALDI-TOF

DCTB matrix (trans-2-[3-(4-terta-butylphenyl)-2-methyl-2-propenylidone] malononitrile and was dissolved in DI H_2O . to give a final concentration of 40 mg/mL. This was then mixed 1:1 with PVP-I hydrogel suspension solution. 10 μL was spotted onto a polished steel target plate and dried in air. Samples were measured on the Bruker Autoflex Matrix-assisted Laser Desorption Ionisation (MALDI) mass spectrometer. Spectra were normalised to plasma activated water.

7.3.8 Pyocyanin Expression Assay

Overnight cultures of *P. aeruginosa* were grown as per standard protocol and either synergy checkboard assay or MIC assay was carried out. 200 μL of bacterial culture was removed from the 96-well plate, post incubation and added to a sterile Eppendorf. This was then centrifuged at 10,000 rpm for 10 minutes to separate out whole cells and supernatant. 150 μL of the green/blue coloured supernatant was then removed and added into a 96-well plate. The absorbance was read at 691 nm which corresponds to the concentration of pyocyanin. Values were blank corrected against broth only control.

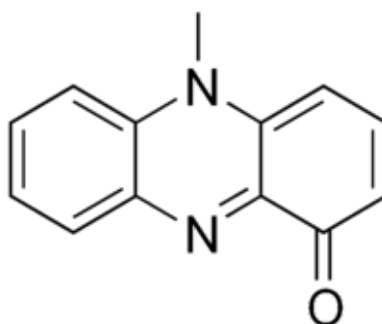


Figure 7.5: Structure of Pyocyanin (PCN).

7.4 Results and Discussion

7.4.1 Bacterial Activity of PVP-I

To assess its utility against *P. aeruginosa* infections, the MIC and minimum biofilm eradication concentration (MBEC) for four clinical isolates and one laboratory strain were assessed (**Table 7.2**). There was no measurable difference in MIC for the five isolates used, but there was variation in their MBECs. This is likely owing to the variation in biofilm formation between the isolates, those which form more dense biofilms are likely to have a higher MBEC owing to their complex architecture. The MIC and MBEC of H₂O₂ for these five strains were also attained, as the end goal was to combine the two treatments and assess synergistic interactions. More variation in susceptibility to H₂O₂ was observed between strains than was observed for PVP-I. There was no concordance observed between the results, the three strains which were most resistant to PVP-I treatment varied in the susceptibility to H₂O₂.

Table 7.2: MIC and MBEC of H₂O₂ and PVP-I for *P. aeruginosa* isolates.

Bacterial Strain	H ₂ O ₂ MIC (mM)	H ₂ O ₂ MBEC (mM)	PVP-I MIC (% (v/v))	PVP-I MBEC (% (v/v))
PAO1	0.435-0.87	1110-2230	0.63-0.31	1.25-2.50
PAE321	0.435-0.87	560-1110	0.63-0.31	>5
PAE379	1.73-3.48	1110-2230	0.63-0.31	>5
PAE325	1.73-3.48	560-1110	0.63-0.31	0.63-1.25
PAE311	0.435-0.87	1110-2230	0.63-0.31	>5

It is known that H₂O₂ and PVP-I are synergistic in their antimicrobial effects.¹⁰ To ensure that this was applicable to the strains used in this work, a checkerboard assay for drug synergy was conducted.¹¹ A simple assay used to determine the fractional inhibitory concentration index (FICI) of drug combinations, the checkerboard assay assesses a variety of combinations of the two drugs and compares them to the drugs individually as shown in **Figure 7.6**.

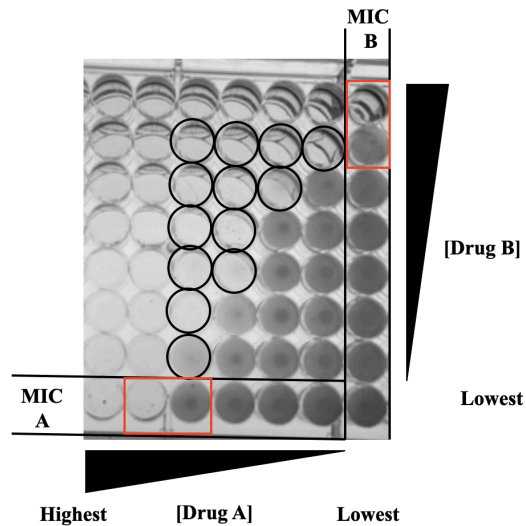


Figure 7.6: Layout of synergy plate. Black circles show wells where combination of drug has successfully inhibited growth below the MIC of the drugs individually. Red square shows where the MIC of Drug A and Drug B falls.

FICI is calculated as per **Equation 7.2**, using combination drug MIC and individual drug MIC values. The FICI value can then convey whether the drug combination is synergistic, FICI of less than 0.5 is a synergistic combination, an FICI of between 0.5-4 is additive and an FICI of >4 is antagonistic.¹¹

$$\text{FICI} = \frac{\text{MIC Drug A in combination}}{\text{MIC Drug A only}} + \frac{\text{MIC Drug B in combination}}{\text{MIC Drug B only}} = \text{FICA} + \text{FICB} \quad (2)$$

Equation 7.2: FICI calculation

The FICI was found to be 0.375 for four out of five strains used (**Table 7.3**), confirming the combination of PVP-I and H₂O₂ is synergistic in killing bacteria. For strain PAE45379 the combination was not found to be synergistic.

Table 7.3: FICI values for five *P. aeruginosa* strains used and FIC range (N=3).

Bacterial Strain	FICI	FIC Range
PAO1	0.375	0.313-1
PAE45321	0.375	0.313-1
PAE45379	Not Synergistic	Not Synergistic
PAE45235	0.375	0.282-1
PAE45311	0.375	0.31-1

As previously mentioned, CAP's main bactericidal component is H₂O₂ and as shown in Chapter 3, He-CAP treatment is ineffective in reducing viable cell counts of planktonic *P. aeruginosa* cultures. Owing to the synergistic interactions between H₂O₂ and PVP-I, it is hypothesised that He-CAP will also active synergistically with PVP-I, enabling a reduction of the bioburden of planktonic cultures of *P. aeruginosa*.

7.4.1.1 Plasma Activation of PVP-I

To assess the potential synergistic combination of He-CAP and PVP-I the checkboard assay was found not to be experimentally viable: it was conjectured that after multiple CAP treatments to “activate” PBS for the assay, the short lived RONS would have degraded and the assay would not be consistent. Instead, the protocol was modified (as per section 7.3.5.1). Sub MIC concentrations of both He-CAP and PVP-I had to be used to attain whether the combination was synergistic, if MIC values were used any bacterial death could not be attribute to the combination, instead it would be owing to the presence of the single drug at MIC concentrations. The He-CAP treatment was applied to the ½ MIC PVP-I to “activate” it, then planktonic cultures of bacteria were added and incubated for 18 h. If the combination is synergistic then the reduction in optical density would be significantly greater in the combination treatment wells than the reduction observed by the two single antimicrobials. All five *P. aeruginosa* strains were found to be susceptible to the He-CAP/PVP-I combination (**Figure 7.7**).

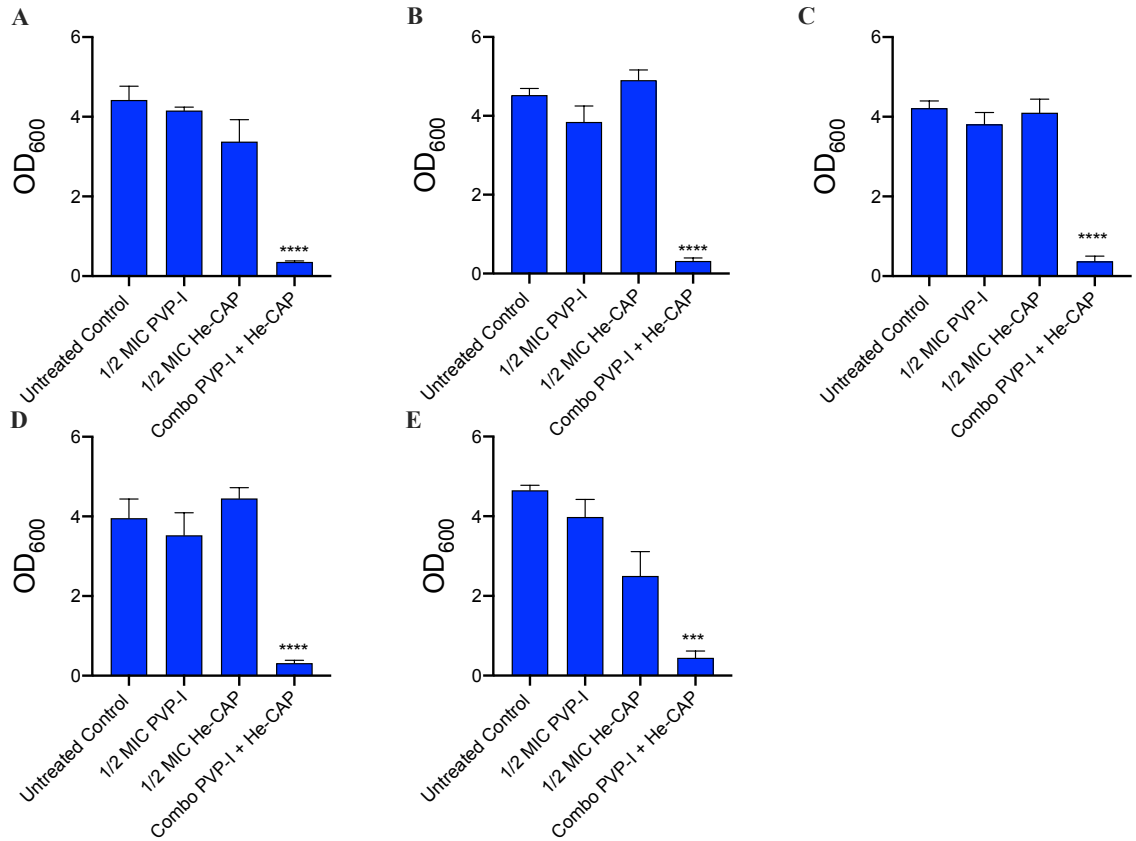


Figure 7.7: Optical density 600 nm of *P. aeruginosa* stains PAO1 (A), PAE45311 (B), PAE45321 (C), PAE45325 (D) & PAE45379 (E) after exposure to 1/2 MIC dose of PVP-I (0.33% (v/v)), 1/2 MIC He-CAP (3 & 5 mins) treatment and combination treatment relative to untreated control. (n=3) Error bars represent standard deviation. One-way ANOVA was performed in GraphPad 8.0 **** $p < 0.0001$ *** $p = 0.0009$ respectively.

During CAP activation of PVP-I a visible colour change of the PVP-I was observed with increased treatment times (**Figure 7.8**). Owing to the synergism observed in bacterial treatment it was hypothesised that this colour change could be indicative of chemical alterations that were responsible for the increased efficacy of PVP-I post CAP treatment.

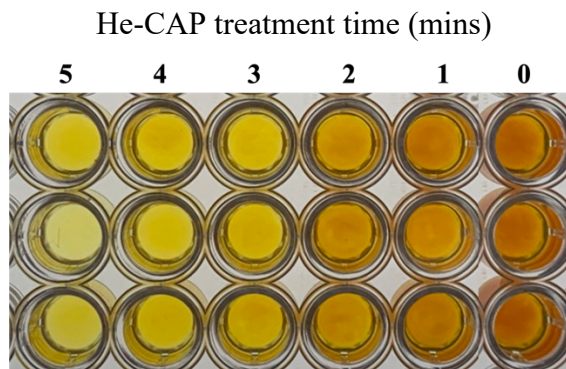


Figure 7.8 Visual analysis of PVP-I after He-CAP treatment of varying times (mins).

UV-Vis spectroscopy was carried out to analyse change in absorbance of PVP-I as He-CAP exposure time increased. As treatment time increased the absorbance peaks at 290 nm and 350 nm owing to I^- and I_2 were seen to decrease (**Figure 7.9**).¹²

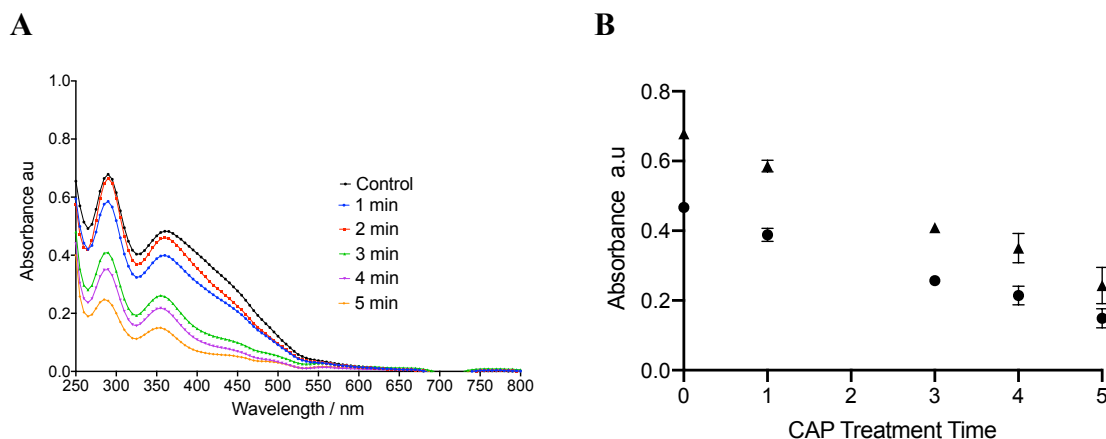
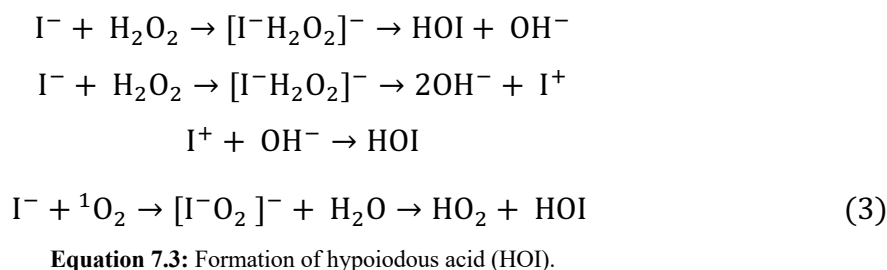
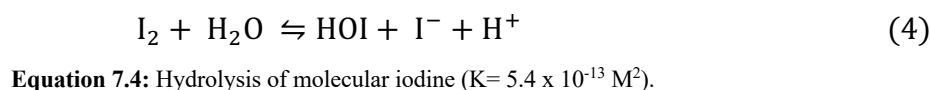


Figure 7.9: (A) UV-Vis Spectra of 0.33% (v/v) PVP-I with increasing He-CAP treatment (B) Absorbance change at 288 nm (▲) and 350 nm (●) after varying treatment time of He-CAP jet.

More liberation of I_2 is known to occur with an increase in temperature further to this, at a pH >8, the pH of CAP treated solutions is >8, the equilibrium state favours bactericidal species hypiodous acid (HOI) and I_2 . It was hypothesised that there is a further increase in the formation of bactericidal HOI owing to the interaction of iodide ions with He-CAP produced H_2O_2 to form HOI as per **Equation 7.3**.¹³



HIO is known to be antibacterial and antifungal.¹⁴ Elemental iodine is used for the disinfections of water and will hydrolyse in a pH-dependent manner forming HOI and I^- as per **Equation 7.4**.¹⁵



Both HOI and I₂ are active disinfectants, HOI has twice the oxidising power of I₂, yet I₂ has a greater capacity for penetrating into the cells than HOI. The hydrolysis of I₂ is pH dependent, at higher pH's the equilibrium will shift to the right so HOI will be the predominant active antimicrobial, whereas at low pH equilibrium will shift to the left, so I₂ is the main active antimicrobial. The optimal pH is 7 resulting in a 1:1 ratio of HOI: I₂. Importantly at pH<8 HOI is unstable and will decompose into iodate and iodide ions.¹⁶ Further to this, the observed decrease in absorbance is indicative of the triiodide ions being consumed, supporting the theory that the iodide and iodine are being utilised to produce other active iodide containing compounds.

7.4.1.2 Activity of CAP Activated PVP-I Against Model Wound Biofilms

As discussed earlier, targeting bacterial biofilms with novel treatments is of paramount importance as they exhibit resilience to conventional antimicrobial treatments due to their complex architecture. PVP-I is often applied to heavily contaminated wounds and CAP treatment is currently used within some clinics to decontaminate wounds. Hence the combination of the two therapies was assessed for efficacy against bacterial biofilms.

The synergistic combination of PVP-I and He-CAP treatment was applied to established 24 h *P. aeruginosa* biofilms. PVP-I was added topically to the biofilm, as is routine within the wound clinic, and He-CAP was applied to the PVP-I for five minutes with movement. The biofilms were then left to incubate for one hour to allow for the generation of RONS and subsequent PVP-I/RONS interactions to occur. In order to be synergistic, there must be a significant reduction in biofilm density observed with the combination of therapies when compared to both of the individual antimicrobials.

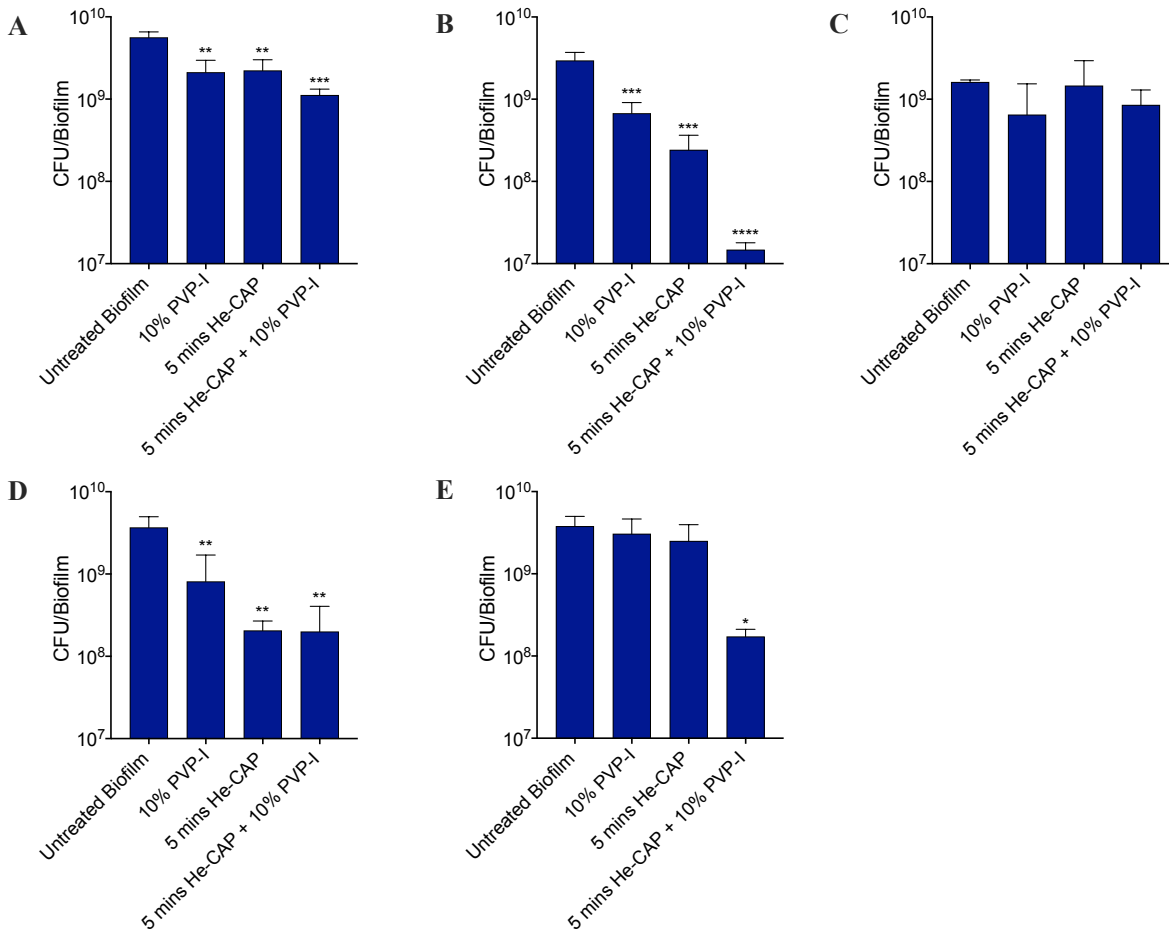


Figure 7.10: Quantification of viable cells in 24 h *P. aeruginosa* biofilms stains PAO1 $p = 0.0021, 0.0026$ & 0.0004 (A), PAE45311 $p = 0.0006, 0.002$ & <0.0001 (B), PAE45321 (C), PAE45325 $p = 0.0098, 0.0031$ & 0.0031 (D) & PAE45379 $p = 0.0295$ (E) after treatment with PVP-I, He-CAP and a combination of PVP-I and He-CAP. Error bars represent standard deviation (n=3), One-way ANOVA was performed (****) $p < 0.0001$, (***) $p < 0.001$, (**) $p < 0.01$ and (*) $p < 0.1$.

The combination of treatments was found to significantly reduce the bacterial bioburden in four out of five of the strains (**Figure 7.10**). However, the combination of He-CAP and PVP-I was not found to be synergistic, instead an additive effect was observed. This was concluded as while there was no significant difference found between the combination therapy and the individual treatments, there was a greater reduction in bacterial bioburden observed with the combination therapy in three of five strains **Figure 7.10A, B & E**. *P. aeruginosa* PAE45321 24 h biofilms were not reduced by PVP-I, He-CAP or combination treatment (**Figure 7.10C**) and *P. aeruginosa* (PAE45325) was not found to be additive as the combination therapy did not produce a greater reduction in bioburden than the individual treatments (**Figure 7.10**).

The lack of efficacy of He-CAP PVP-I on the PAE45321 strain could be owing to its pathogenicity, as previously mentioned, it was isolated from an acute wound infection. This environment often promotes an upregulation of virulence factors expression. Pyocyanin is a fluorescent molecule expressed by *P. aeruginosa* which is both cytotoxic to cells in the lung and other bacterial species. When the strains were assayed for pyocyanin activity, PAE45321 was found to have significantly higher pyocyanin expression than the other strains tested (**Figure 7.11**). Pyocyanin is controlled by QS and controls gene expression and community behaviour in bacteria, it also controls colony size and biofilm thickness. As such, it is likely that this increased pyocyanin expression is making the PA45321 biofilm more robust and resilient to treatments.¹⁷

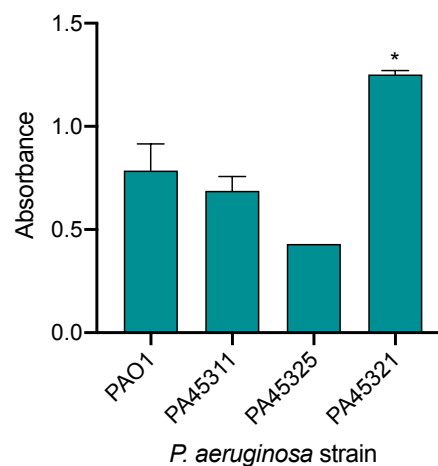


Figure 7.11: Pyocyanin for *P. aeruginosa* strains PAO1, PA45311, PA45325 & PA45321. Error bars represent standard deviation. One-way ANOVA performed (*) $p < 0.1$.

To assess whether the combination of the He-CAP and PVP-I was impacting the structural integrity of the biofilm scanning electron microscopy (SEM) imaging was carried out. Untreated *P. aeruginosa* (PAO1) 24 h biofilms (**Figure 7.12A**) showed densely packed bacterial cells with web-like structure visible, which is characteristic of the ECM in a healthy biofilm. These biofilms treated with He-CAP showed that whilst the bacteria are still dense, their morphology is shortened which is characteristic of cellular death (**Figure 7.12B**). Biofilms treated with 10% (v/v) of PVP-I (**Figure 7.12C**) are still visibly dense like the untreated control, however, the bacterial cells have a puckered morphology characteristic of cellular death and there is a lack of extracellular matrix (ECM) present suggesting the He-CAP treatment does have an impact on the biofilm integrity. The combination therapy appears induce a reduction in bacterial density, (the circular pores of the polycarbonate

membrane are visible), there is cellular death as observed with the PVP-I only treatment and no ECM was visible (**Figure 7.12D**).

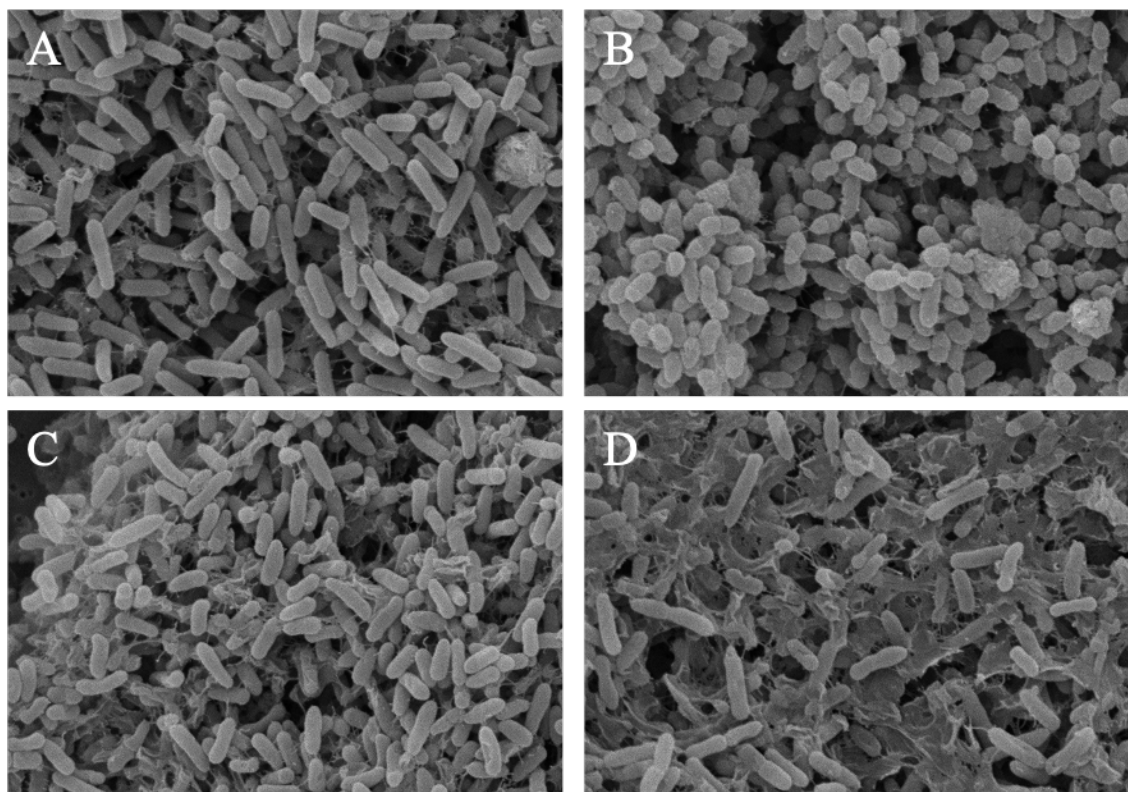


Figure 7.12: SEM at x5000 magnification, of 24h *P. aeruginosa* (PAO1) biofilm untreated control (**A**), He-CAP treatment for 5 mins (**B**), 10% (v/v) PVP-I (**C**) and 5 min CAP treatment of 10% (v/v) PVP-I (**D**).

7.4.1.3 Characterisation of Argon Plasma Jet

He-CAP, as previously discussed, was found to produce insufficient concentrations of RONS for the effective reduction of bacterial loads both planktonically and in biofilms. As the recovery of RONS beneath a hydrogel wound dressing was $\sim 20 \mu\text{M}$, which is significantly below the MIC for any bacterial species studied. Therefore, an alternative CAP jet was constructed to increase the concentration of H_2O_2 . Ar-CAP was found to produce a higher concentration of H_2O_2 in a shorter treatment period (**Figure 7.13**). $\sim 2 \text{ mM}$ of H_2O_2 was produced in two minutes which is significantly higher than the $\sim 650 \mu\text{M}$ produced by He-CAP. Importantly, 2 mM is above the MIC for *P. aeruginosa* and close to the MIC for *S. aureus* and MRSA. Therefore, it was hoped that Ar-CAP would be more effective at treating biofilm-associated wound infections.

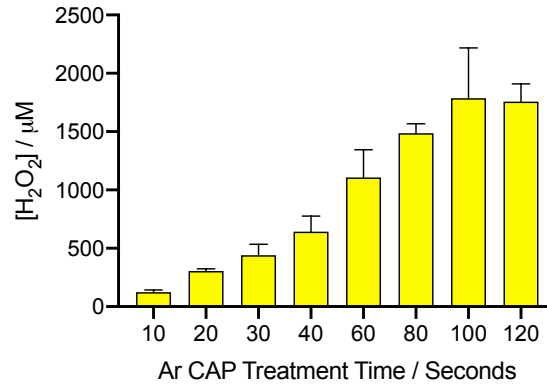


Figure 7.13 Quantification of H₂O₂ produced by Ar-CAP jet treatment. Error bars represent standard deviation (n=3).

Ar-CAP was tested for its efficacy against planktonic bacteria to attain its MIC using a modified MIC method known as the minimum inhibitory treatment time (MITT). Ar-CAP was applied to PBS for varying treatment times, this CAP-activated PBS buffer was then added to planktonic subcultures of *P. aeruginosa* and *S. aureus* and left to grow for 18h. The MITT was defined as the minimum CAP treatment time capable of completely inhibiting bacterial growth. Ar-CAP MITT was between 30-40 seconds for *P. aeruginosa* (**Figure 7.14A**) and 120-180 seconds for *S. aureus* (**Figure 7.14B**).

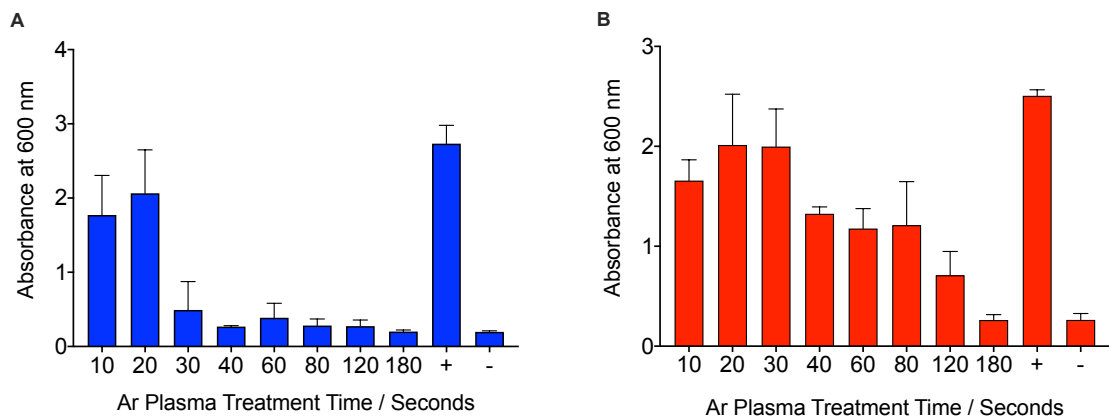


Figure 7.14: Minimum inhibitory Ar-CAP treatment time (MITT) for *P. aeruginosa* (PAO1) (**A**) and *S. aureus* (H560) (**B**) relative to untreated bacterial control. Error bars represent standard deviation (n=3).

These finds also support He-CAP results that found *P. aeruginosa* to be more susceptible to CAP treatment than *S. aureus*. Moreover, while this is a basic assay, results suggest that Ar-CAP treatment will be significantly more effective against bacterial infections than He-CAP was found to be. However, like He-CAP, the Ar-CAP jet was found to be ineffective at reducing the bioburden of established planktonic cultures of $\sim 10^9$ CFU/mL after five minutes of treatment (**Figure 7.15**).

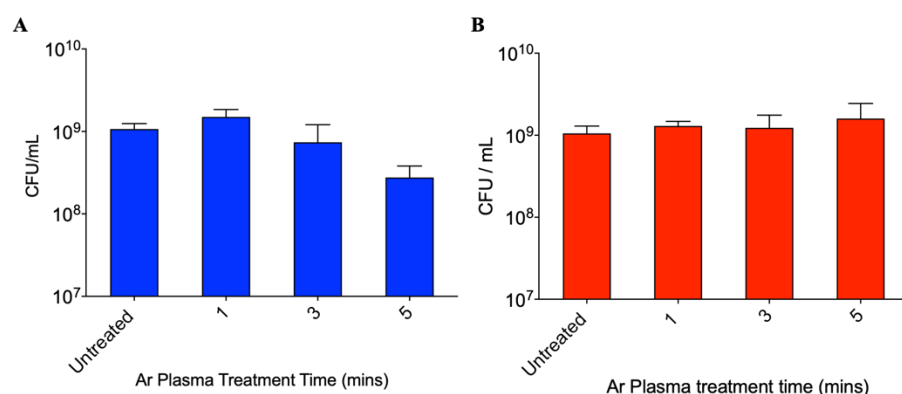


Figure 7.15: Reduction in viable planktonic bacterial cells of *P. aeruginosa* (PAO1) (A) and *S. aureus* (H560) (B) after varying treatment times with Ar-CAP. Error bars represent standard deviation (n=3).

Ar-CAP was also found to significantly reduce biofilm bioburden in *P. aeruginosa* (PAO1) and *S. aureus* (H560), however, it is important to note that while there was a significant reduction, visually the surface of the biofilm was very scorched, suggesting high local temperatures. This would be very undesirable on a wound surface, owing to its impact on healing. While this is concerning, the addition of a hydrogel would screen the skins surface and limit the topographical damage induced through Ar-CAP treatment. As such, the concentration of the RONS capable of penetrating a PVA hydrogel were investigated, **Figure 7.16**.

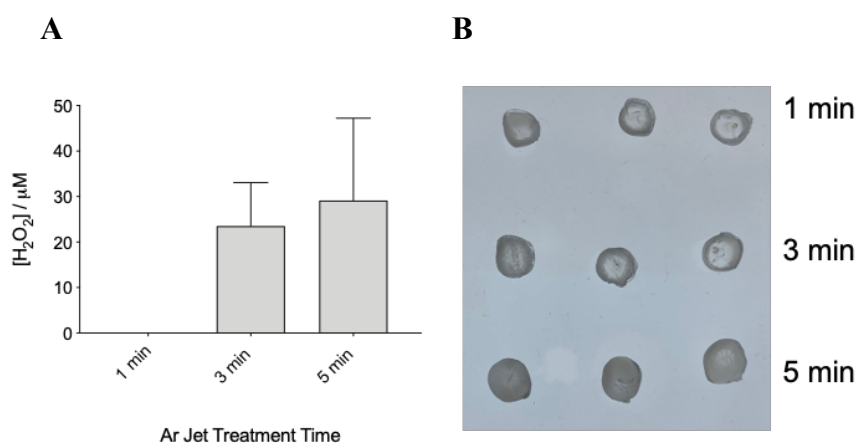


Figure 7.16: Analysis of 5% PVA hydrogel with varying Ar-CAP treatment. Recovery of H₂O₂ beneath the 5% PVA hydrogel after varying Ar-CAP treatment times (A). Visual analysis of the 5% PVA hydrogels after varying treatment times (B). Error bars represent standard deviation (n=3).

After five minutes of Ar-CAP treatment and a subsequent 30-minute incubation, ~28 µM of H₂O₂ was recovered beneath the hydrogel **Figure 7.16A**. While this is significantly lower than the MIC for either strain of bacteria, the recovered concentration is over double that recovered at He-CAP treatment. Furthermore, as shown in **Figure 7.16B**, the gels withstand

treatment well, with only slight dehydration. As such Ar-CAP treatment could potentially be more effective with a hydrogel than the He-CAP.

The addition of a PVA hydrogel significantly reduces the efficacy of Ar-CAP treatment, resulting in no significant reduction in *S. aureus* (H560) biofilms and only a 1-log reduction of *P. aeruginosa* (PAO1), which is no more effective than the He-CAP jet. However, the Ar-CAP interacts more favourably with the hydrogels, resulting in no observed scorching (Figure 7.17).

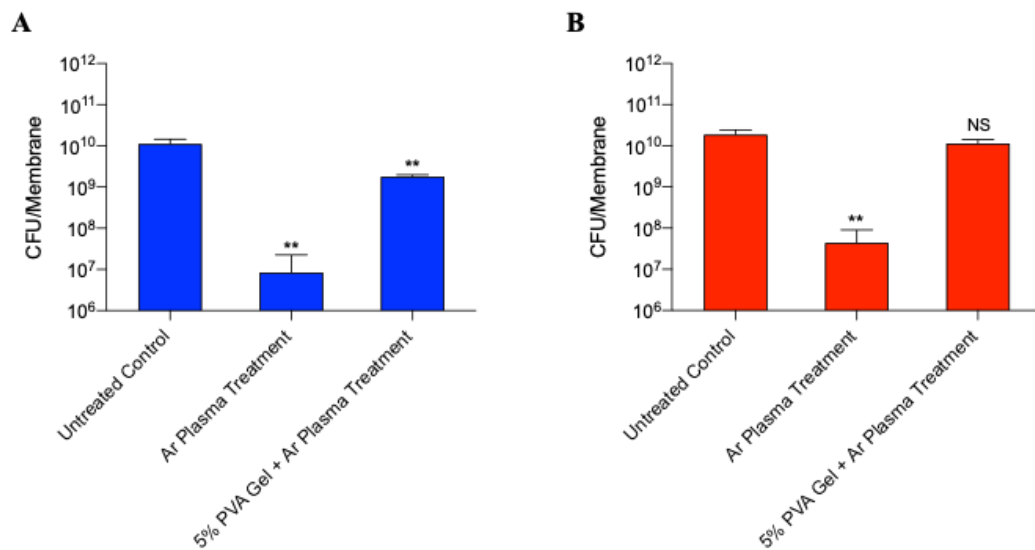


Figure 7.17: Reduction in viable cells of 24 h biofilm after treatment Ar-CAP for 5 min atop a 5% PVA hydrogel screen *P. aeruginosa* (PAO1) (A) & *S. aureus* (H560) (B). Error bars represent standard deviation (n=3). One-way ANOVA (***) $p < 0.001$.

7.4.1.4 Characterisation of PVP-I Gel

PVP-I was shown to act synergistically with He-CAP treatment against planktonic bacteria and bacterial biofilms and PVA hydrogels were found to withstand both He-CAP and Ar-CAP application. PVP-I was thus blended with PVA, which was shown previously to be resilient against CAP treatment, to form a potentially therapeutic hydrogel wound dressing for combination treatment with CAP therapy.

7.4.1.5 Scanning Electron Microscopy

SEM studies were carried out to assess the surface topography of the PVP-I/PVA hydrogel after treatment with Ar-CAP (Figure 7.18). The untreated hydrogel has a smooth surface

Figure 7.18A-C, whereas after Ar-CAP treatment there is a clear change in the morphology of the hydrogel, with surface dehydration, thought to be owing to the gas flow, resulting in a change from the smooth untreated surface, to ridged surface **Figure 7.18D&E**. In addition to this, after Ar-CAP treatment pores/holes appear in the surface of the gel **Figure 7.18E, G&H**.

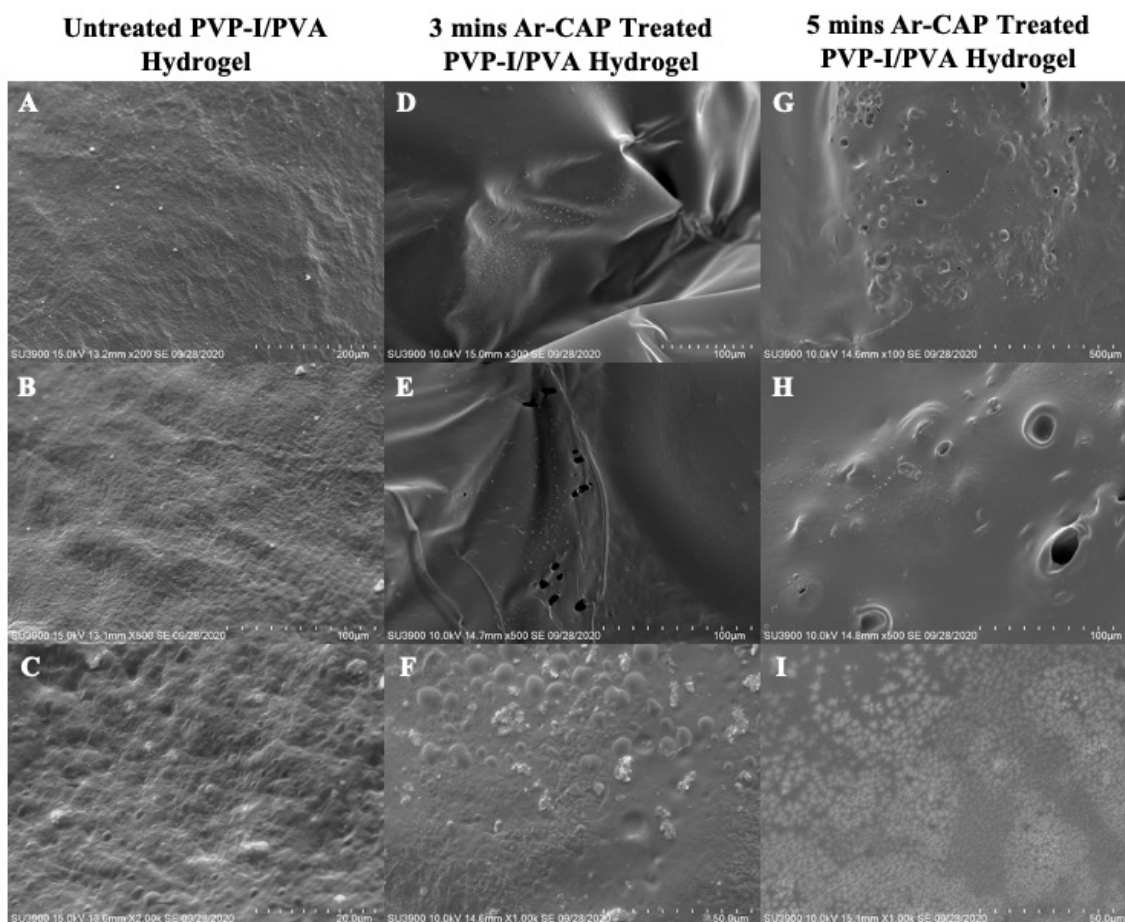


Figure 7.18: SEM images of PVP-I/PVA Hydrogel. Untreated PVP-I/PVA hydrogel gel control (**A-C**), PVP-I/PVA hydrogel after 3 mins Ar-CAP treatment (**D-F**) & PVP-I/PVA hydrogel after 5 min Ar-CAP treatment (**G-I**).

There is no significant change in rheology data before and after CAP treatment. Unlike the PVA only hydrogel discussed in Chapter 3, there is less of a disparity between the G' and G'' , indicating that the PVP-I hydrogel is less rigid in structure than the PVA hydrogel.

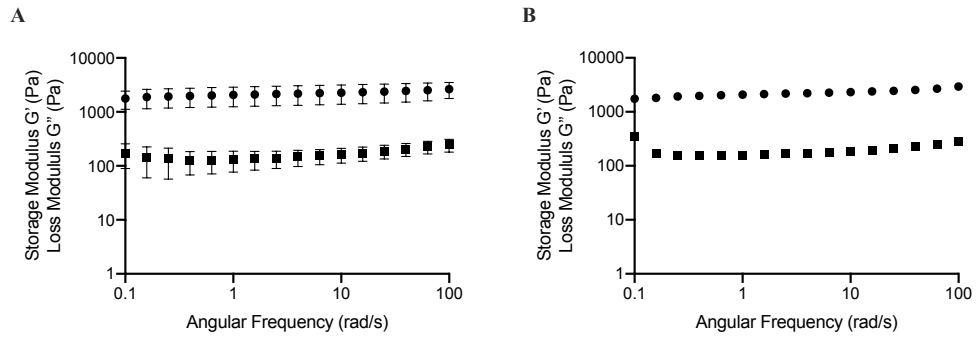


Figure 7.19: Rheology data for PVP-I hydrogel. Untreated control (A) and after 5 minutes of Ar-CAP treatment (B). Error bars represent standard deviation (n=3).

7.4.1.6 FT-IR

The FT-IR spectra of PVA and PVP-I was recorded: the stretching vibrations of (O-H) was found between 3500 and 3329 cm^{-1} and asymmetric and symmetric stretching vibration of (C-H) of CH_2 groups is visible between 2940 - 2907 cm^{-1} ; For PVP a strong peak was observed at 1650 - 1660 cm^{-1} which is characteristic of the carbonyl group of the PVP. In PVP-I both the PVA peaks and PVP carbonyl peak was present confirming that PVP is present within the hydrogel.

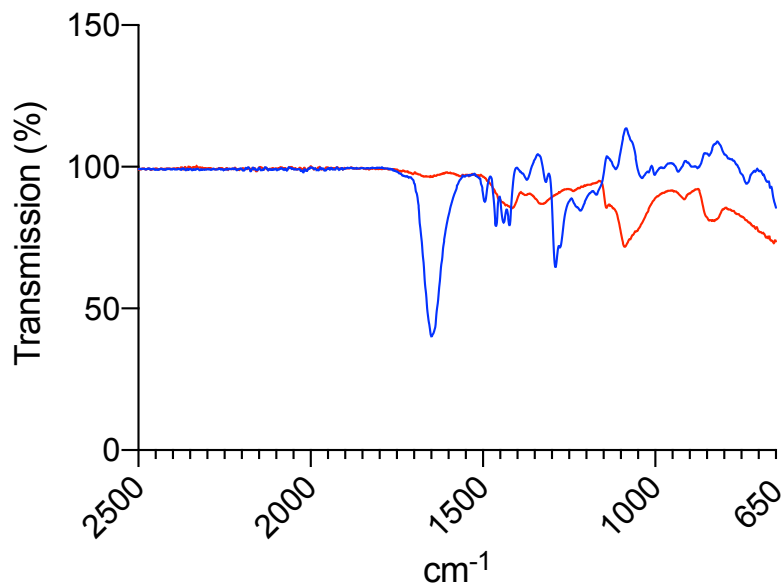


Figure 7.20 FT-IR analysis of PVP-I Gel (-) and 5 % PVA Hydrogel (-).

Whilst these results prove that the PVP-I is present within the PVA based hydrogel, it is impossible to ascertain the nature of the bonding between the two polymers for this data. It is possible that the carbonyl is involved in the hydrogen bonding processes caused during

the freeze-thaw process, or it may simply be physically contained within the pores of the PVA matrix.

7.4.1.7 MALDI-TOF

While UV-Vis showed that there was a change in absorbance of PVP-I after CAP treatment the chemical quantification was mostly conjecture. Matrix-assisted laser desorption/ionisation time of flight mass spectroscopy (MALDI-TOF) was used for high resolution characterisation of the species present in CAP treated PVP-I. There is a clear distinction between untreated PVP-I (blue) and Ar-CAP treated PVP-I (red) shown in **Figure 7.21**. Ar-CAP PVP-I shows clear sharp peaks corresponding to I^- ($m/z = 129$) and I_2 ($m/z=251$) which are within the accepted mass error, confirming the theory that CAP is causing a shift in equilibria causing triiodide to dissociate into iodine and iodide.

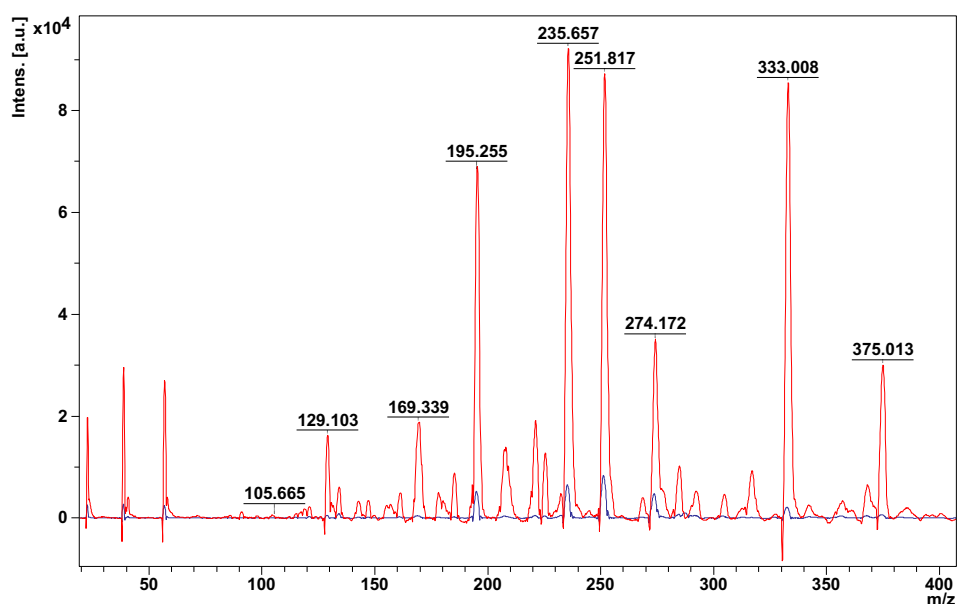


Figure 7.21: MALDI-TOF analysis of PVP-I gel 1h after 3 mins treatment with Ar CAP jet (-) compared with untreated control (-).

7.4.1.8 Efficacy of PVP-I Hydrogel Against Established Model Wound Biofilms

While the efficacy of CAP activated PVP-I on planktonic *P. aeruginosa* was a promising finding, as previously highlighted bacterial biofilms are significantly harder to treat and

associated with an increase in pathogenicity. Within burn wounds especially *P. aeruginosa* biofilms frequently form, hindering healing. As hydrogels and PVP-I are already used within burn care the combination of the two therapies would not deviate from the existing care pathway and could provide a therapeutic of increased efficacy, which could easily be integrated into the clinic.

5% (w/v) PVA hydrogels have proven mechanically stable after CAP exposure to both He-CAP and Ar-CAP, thus PVP-I was blended with PVA gels to create a hydrogel. The PVP-I/PVA hydrogel was washed in PBS for two hours to remove and excess PVP-I to reduce the risk of PVP-I leeching out of the hydrogel into the wound milieu. The hydrogels were placed onto established 24-hour *P. aeruginosa* biofilms, which mimic a heavily infected wound. Five minutes of Ar-CAP treatment was applied atop the hydrogel, with movement, to “activate” the PVP-I. Ar-CAP was used rather than He-CAP as it produces a greater concentration of H₂O₂ which is the known to be synergistic with the PVP-I. The reduction in viable bacterial cells was then compared with untreated control, PVP-I gel without plasma treatment and Ar-CAP treatment when applied directly to the biofilm (**Figure 7.22**). The biofilms were subsequently incubated statically at 37 °C for one hour to enable the PVP-I to have an effect.

Importantly, there was no significant reduction in bacterial cell count in the presence of PVA/ PVP-I gel only compared to the untreated control and therefore it can be concluded that if there is any PVP-I leeching from the hydrogel it is not enough to have any impact on the viability of the biofilms. A significant reduction in biofilm bioburden was observed in three out of the five *P. aeruginosa* strains tested. In the case of *P. aeruginosa* (PAO1) a 4-log reduction in bacterial cells was observed, this is very significant given than the biofilm was only exposed to the hydrogel for 1 hour. Two of the clinical isolates were also significantly reduced PA45321 and PA45379, while they were reduced by 3-log and 2-log respectively. Whilst this is less than PAO1, this is to be expected as they are clinical isolates, thus they are more likely to be virulent and have increased resilience to antimicrobial therapies. PA45311 and PA45325 were not reduced by CAP activated PVA/PVP-I hydrogels, despite encouraging planktonic results. It could be that these strains needed an increased exposure time.

Chapter 7

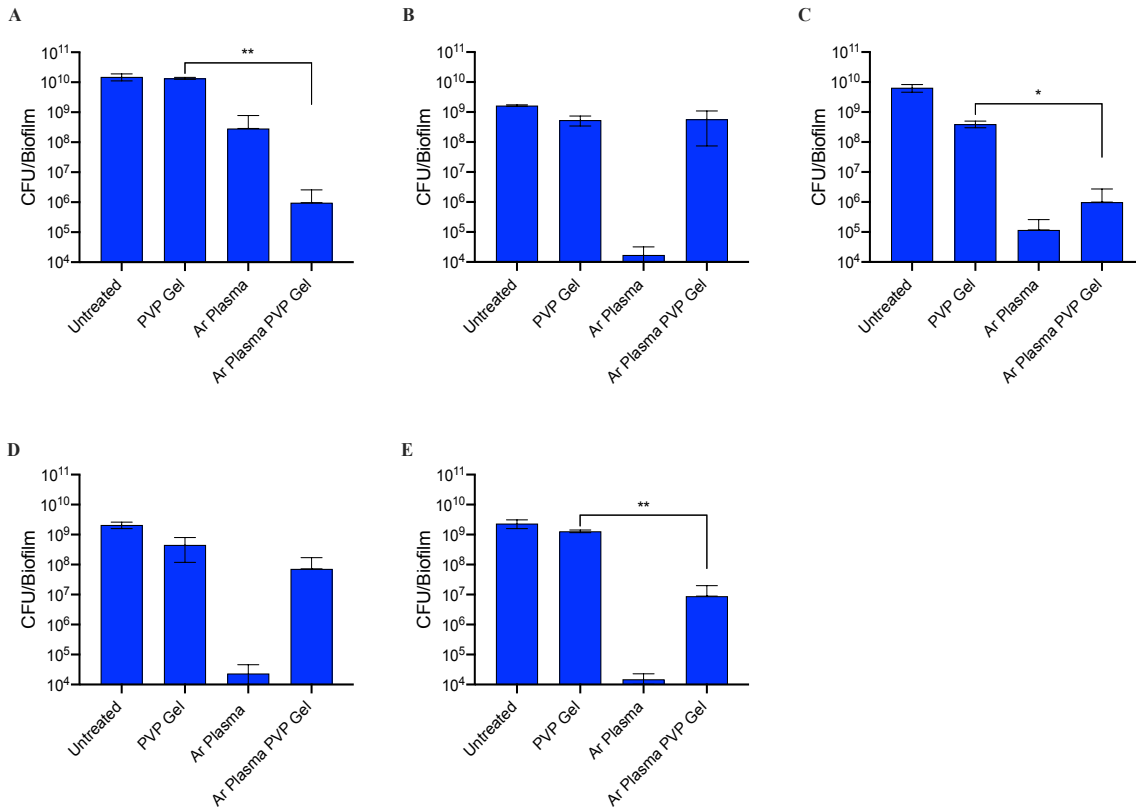


Figure 7.22: Reduction in viable bacterial after treatment for 1 h with PVP-I hydrogel and PVP-I hydrogel with 3 mins of Ar CAP jet treatment applied atop relative to untreated control and Ar plasma treatment without hydrogel. *P. aeruginosa* PAO1 (A), PAE45311 (B), PAE45321 (C), PAE45325 (D) and PAE45379 (E). *t*-test was carried out with Welch's correction $p = 0.0019$, $p = 0.0203$ and $p = 0.0033$ respectively. Error bars represent standard deviation (n=3). (**) $p < 0.01$ & (*) $p < 0.1$.

As already outlined, upon interaction with CAP, PVP-I undergoes a colour change from dark brown to yellow/clear. It is hypothesised that this is as a result of the liberation of triiodide from the PVP-I and an equilibrium shift from triiodide to iodine and iodide ions. This colour change is also observable within the PVA/PVP-I hydrogel where there was a noticeable change before and after treatment (**Figure 7.23**). There is a visible difference in the colour of the untreated control gels from brown to lighter brown, which was expected, as there would be the release of triiodide from the gel during the incubation, however, this release was found to be insignificant against the bacterial biofilms as shown in **Figure 7.22**. There is a significant colour change in the treated gels, from brown to yellow, indicating the increased liberation of the triiodide and subsequent iodine reactions discussed previously.

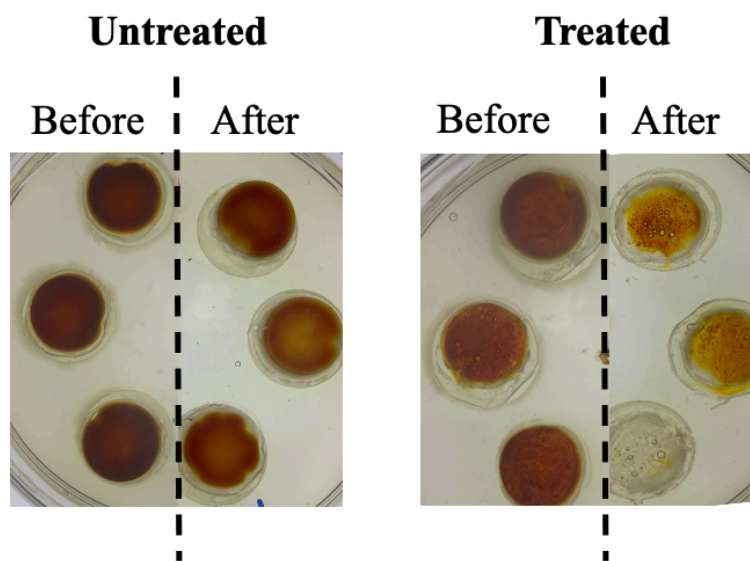


Figure 7.23: Qualitative analysis of untreated and Ar-CAP treated PVP-I hydrogels before and after 1 h incubation at 37 °C.

7.5 Conclusions

This chapter describes the synergistic interactions of both Helium and Argon CAP jets with PVP-I for the successful prevention and eradication of bacterial infections both planktonically and within a biofilm. Furthermore, the PVP-I can be blended with PVA to create a therapeutic hydrogel, which might have utility in a wound dressing that reduces the bacterial biofilm bioburden upon the addition of CAP therapy.

PVP-I has been shown to act synergistically with H₂O₂ against bacteria. As such, when PVP-I is applied in tandem He-CAP treatment complete inhibition of bacterial growth was observed in doses that individually were not effective in inhibiting bacterial growth. This combination therapy was found to be effective against the five *P. aeruginosa* strains, one laboratory strain and four clinical isolates tested. When the combination of PVP-I and He-CAP was applied to established, 24-hour *P. aeruginosa* biofilms, a significant reduction in bioburden was observed in three of the five test strains. However, the interaction of the two treatments was found to be additive rather than synergistic. The biofilms were only treated for one hour to assess the efficacy of the therapy, it is possible that with longer treatment exposure a greater reduction in bioburden would be observed.

As outlined in chapter 3, the He-CAP jet was not producing sufficient concentrations of RONS to significantly kill bacteria either planktonically or in a biofilm. As such, an alternative CAP jet was developed by Ghimire *et al.* with increased H₂O₂ and other RONS production to increase bactericidal efficacy. Ar-CAP was found to produce double the concentration of H₂O₂ beneath a PVA hydrogel, as well as reduce viable bacteria cell count.

Due to the success of the combination of topical He-CAP and PVP-I, it was thought that the PVP-I could be added into a PVA hydrogel to create a robust potentially therapeutic hydrogel which screens out damaging CAP RONS that are damaging to healthy tissues within the patient, while releasing an antibacterial moiety. While this system is not a triggered release system, the synergistic interactions of PVP-I with CAP does appear to affect a measurable reduction in bacterial biofilm compared to PVP-I hydrogel alone. The PVP-I hydrogel was characterised to confirm that the PVP-I was suspended in the cryo-crosslinked PVA hydrogel using FT-IR. The interaction of CAP with the PVP-I was

confirmed with MALDI-TOF which indicated the liberation of iodide ions and iodine which can then subsequently react with the CAP produced RONS. Due to the increased efficacy measured, it is hypothesised that the iodide ions react with CAP produced H_2O_2 to produce HOI, a potent antimicrobial. When the PVP-I hydrogel was applied to established 24-hour *P. aeruginosa* biofilms for one-hour significant reduction in bacterial bioburden was observed in three of the five strains. This was encouraging and with further incubation or longer treatment times the biomass reduction could potentially be further increased.

7.6 Future Work

Further work would seek to improve the PVP-I hydrogel for maximum bactericidal effect, varying post gel application incubation time, as well as testing the hydrogels resilience to increased CAP exposure. This could potentially be achieved through blending the PVP-I with a range of different polymer such as CMC or agarose, which have been shown to tolerate CAP exposure. This further optimisation of the hydrogel could tolerate repeated CAP exposure thus resulting in greater reduction of the biofilm bioburden. Moreover, owing to the desired application of the PVP-I hydrogel being for wound decontamination further microbiological tests would seek to test PVP-I hydrogels efficacy on other bacterial species, potentially on those isolated from chronic wound patients and on mixed species biofilms which is more representative of a clinical wound infection including *Klebsiella pneumonia*, *Streptococcus* sp, and *Candida albicans*.

The development of the Ar-CAP jet has potential for the use of CAP treatment with a hydrogel owing to the increased concentrations of RONS produced and seemingly favourable physical interactions with the hydrogel. Dr Bhagirath Ghimire, a collaborator at the University of Lancaster is seeking to develop a multi-tube plasma jet, which would greatly increase the treatment surface area as well increasing the concentration of RONS produced. At present the Ar-CAP jet has a treatment surface area of 5 mm² whereas the multi-tube jet would be able to treat ten-times the area in the same time (**Figure 7.24**).

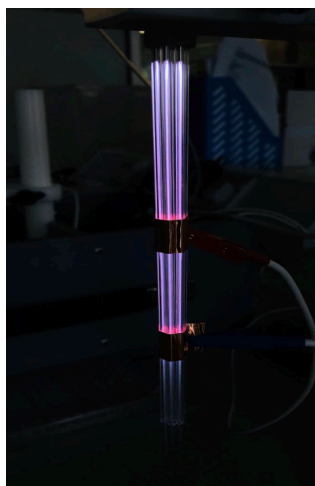


Figure 7.24: Prototype multi-jet

Overall, it was concluded that a simple hydrogel screen, while effective in preventing the delivery of damaging RONS to the wound bed, however, also prevented therapeutic

concentrations of RONS from being delivered into the wound. Therefore, the addition of antimicrobial moieties into the hydrogel for enhanced generation of RONS or alternatively the triggered release of antimicrobial moieties was required.

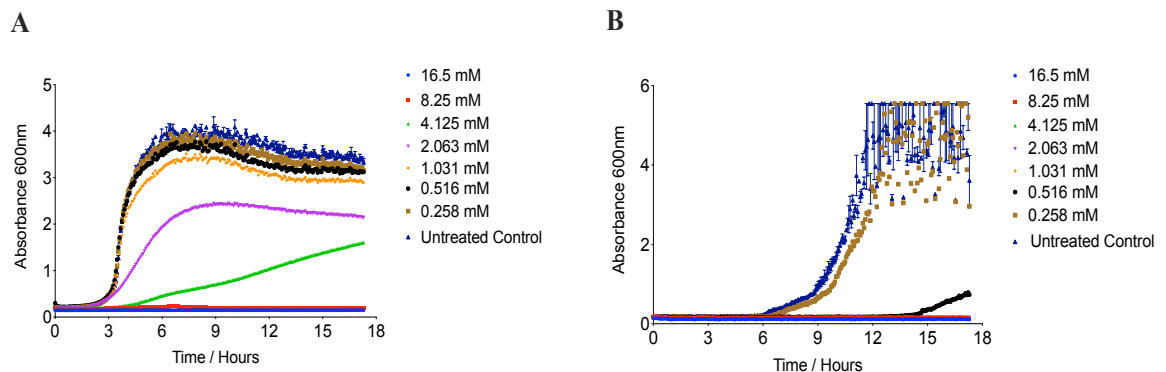


Figure 7.25: MIC of PAA for *S. aureus* (H560) (A) and *P. aeruginosa* (PAO1) (B).

One such possible compound is TAED – PAG particles which, in the presence of H_2O_2 , releases peracetic acid (PAA). PAA is known to be an effective antimicrobial against both *S. aureus* and *P. aeruginosa*. The MIC of PAA was found to be 4.13-8.23 mM for *S. aureus* and 0.26-0.52 mM for *P. aeruginosa* (Figure 7.25).

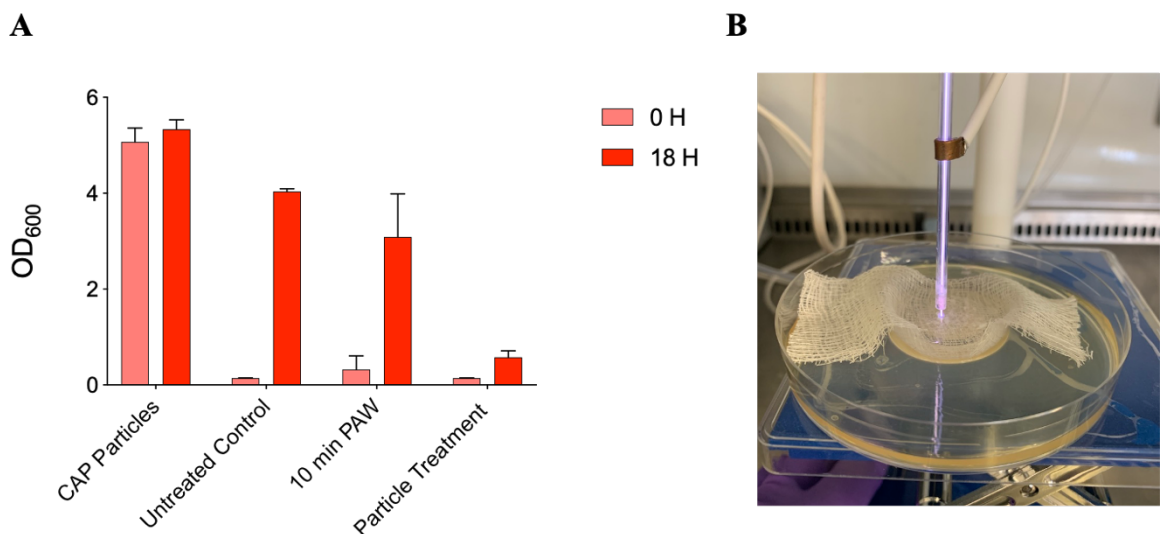


Figure 7.26: Reduction in optical density of *S. aureus* (H56) after 18 h growth at 37°C in the presence of TAED-PLGA particles, Ar-CAP activated water, Ar-CAP activated TAED-PLGA particles compared to untreated bacterial control (A), prototype TAED-PLGA wound dressing system (B).

Preliminary work has found that Ar-CAP activated TAED-PAG particles were effective at inhibiting *S. aureus* growth (Figure 7.26A). The TAED-PAG particles would be suspended in an agarose wound gel with a gauze layer to prevent adhesion to the wound bed and then Ar-CAP would be applied on to the gel to “activate” the particles, as shown in Figure 7.26B. If this concept was found to be effective in reducing *S. aureus* biofilms, then theoretically,

Chapter 7

the TAED-PAG gels could be combined with the PVP-I gel to create a CAP responsive, therapeutic hydrogel wound dressing, which is effective against both *P. aeruginosa* and *S. aureus*.

7.7 References

1. Eggers, M. Infectious Disease Management and Control with Povidone Iodine. *Infectious Diseases and Therapy* vol. 8 581–593 (2019).
2. Kanagalingam, J. *et al.* Practical use of povidone-iodine antiseptic in the maintenance of oral health and in the prevention and treatment of common oropharyngeal infections. *Int. J. Clin. Pract.* **69**, 1247–1256 (2015).
3. Bigliardi, P. L. *et al.* Povidone iodine in wound healing: A review of current concepts and practices. *International Journal of Surgery* vol. 44 260–268 (2017).
4. Globel, B., Globel, H. & Andres, C. Iodine absorption from iodine-containing PVP preparations in humans. *Dtsch. Medizinische Wochenschrift* **109**, 1401–1404 (1984).
5. Sibbald, R. G. & Elliott, J. A. The role of Iodine in wound care: a consensus document. *Int. Wound J.* **14**, 316–321 (2017).
6. Paulson, D. S. *Handbook of Topical Antimicrobials: Industrial Applications in Consumer Products and Pharmaceuticals.* (2005).
7. Verreycken, T., Sadeghi, N. & Bruggeman, P. J. Time-resolved absolute OH density of a nanosecond pulsed discharge in atmospheric pressure He-H₂O: Absolute calibration, collisional quenching and the importance of charged species in OH production. *Plasma Sources Sci. Technol.* **23**, 045005 (2014).
8. Li, L. *et al.* OH radicals distribution in an Ar-H₂O atmospheric plasma jet. *Phys. Plasmas* **20**, 093502 (2013).
9. Xian, Y. *et al.* Optical and electrical diagnostics of an atmospheric pressure room-temperature plasma plume. in *Journal of Applied Physics* vol. 107 063308 (American Institute of PhysicsAIP, 2010).
10. Zubko, E. I. & Zubko, M. K. Co-operative inhibitory effects of hydrogen peroxide and iodine against bacterial and yeast species. *BMC Res. Notes* **6**, 272 (2013).
11. Meletiadis, J., Pournaras, S., Roilides, E. & Walsh, T. J. Defining fractional inhibitory concentration index cutoffs for additive interactions based on self-drug additive combinations, Monte Carlo simulation analysis, and in vitro-in vivo correlation data for antifungal drug combinations against *Aspergillus fumigatus*. *Antimicrob. Agents Chemother.* **54**, 602–609 (2010).
12. Li, N., Shi, L., Wang, X., Guo, F. & Yan, C. Experimental Study of Closed System

- in the Chlorine Dioxide-Iodide-Sulfuric Acid Reaction by UV-Vis Spectrophotometric Method. *Int. J. Anal. Chem.* **2011**, 1–7 (2011).
13. Luther, G. W., Wu, J. & Cullen, J. B. Redox Chemistry of Iodine in Seawater. in 135–155 (1995). doi:10.1021/ba-1995-0244.ch006.
 14. Al-Baarri, A. N. *et al.* IOP Conference Series: Earth and Environmental Science Effect of Hypoiodous Acid (HIO) Treatment on Color and pH Changes in Snake Fruit (*Salacca edulis* Reinw.) during Room Temperature Storage Effect of Hypoiodous Acid (HIO) Treatment on Color and pH Changes in Snake Fruit (*Salacca edulis* Reinw.) during Room Temperature Storage. doi:10.1088/1755-1315/292/1/012042.
 15. Lengyel, I., Epstein, I. R. & Kustin, K. Kinetics of Iodine Hydrolysis. *Inorg. Chem.* **32**, 5880–5882 (1993).
 16. *Iodine as a drinking-water disinfectant Alternative drinking-water disinfectants: iodine.* (2018).
 17. Das, T., Kutty, S. K., Kumar, N. & Manefield, M. Pyocyanin Facilitates Extracellular DNA Binding to *Pseudomonas aeruginosa* Influencing Cell Surface Properties and Aggregation. *PLoS One* **8**, (2013).

Chapter 8

Chapter 8 : Conclusions & Future Perspectives

While cold atmospheric pressure plasma (CAP) treatment is approved for clinical use the field of plasma medicine is still in its infancy with many complex biological interactions not fully understood. This multidisciplinary approach sought to elucidate clinically relevant bacteria/CAP interactions to increase the clinical impact of what could be a great tool against the ever-mounting threat of antimicrobial resistant bacterial infections. The overarching objectives of this research were to further understand the biological interactions of CAP with bacteria, both their ability to mitigate and respond to CAP induced damage and the mutagenic potential of sub-lethal CAP treatment, and to develop a therapeutic hydrogel wound dressing for the delivery of an antibiofilm moiety for the inhibition or eradication of a bacterial biofilm within an infected wound.

After optimisation of operating conditions, the He-CAP jet was found to have little impact on the viability of planktonic bacteria, while administering He-CAP at various times during biofilm development was found to reduce the final viable cell counts of the biofilms after 24 h growth, overall, the He-CAP was not found to produce sufficient reductions in bacterial cells for the application of wound decontamination. Unsurprisingly the limited impact of He-CAP treatment was further diminished with the addition of a hydrogel wound dressing.

The developing bacterial biofilm impacted the delivery of He-CAP generated hydrogen peroxide, whereas the biofilm matured there was an increased reduction of hydrogen peroxide recovered beneath it, in both Gram-positive and negative strains of bacteria. This was subsequently found to be partially the result of He-CAP treatment upregulating the oxidative stress response in the treated bacteria. Their upregulation of catalase, an enzyme which breaks down hydrogen peroxide was found to significantly reduce the lethality of He-CAP treatment. This understanding somewhat explains the insufficiency of the He-CAP jet, its low concentration of hydrogen peroxide cannot overcome the bacterial response to induce a significant reduction in bacterial bioburden. Further to this, the mutagenic potential of He-CAP treatment was investigated. CAP generates a cocktail of RONS, some of which are known to be mutagenic to mammalian cells. While the mutagenic effects on human cells is relatively well understood, CAPs mutagenic potential upon bacteria is unknown. As already explained, He-CAP treatment is sub-lethal, which increases the likelihood that exposed cells

Chapter 8

could mutate post treatment. The He-CAP was found to induce a spectrum of mutations in *E. coli* which resulted in increased tolerance to the antibiotic ciprofloxacin. Within wound care the impacts of the could be huge. As such, the application of CAP within wound care should be administered with caution until further research into the phenomenon is conducted.

It was thought that the mutagenic risk of CAP application on mammalian cells and, theoretically, bacterial cells could be elevated through the addition of a hydrogel wound dressing. It was hypothesised that the hydrogel “screen” could filter out harmful RONS while providing a moist, protected healing environment for the wound. Two potential hydrogels were developed, one which releases an antibiofilm agent, ARS, which prevented the formation of MRSA biofilms the other combined povidone-iodine (PVP-I) which polyvinyl alcohol (PVA) into a hydrogel which acted synergistically with CAP to significantly reduce the bioburden of *Pseudomonas aeruginosa* biofilms. Theoretically either of the hydrogel systems could be combined with the diagnostic hydrogel developed by the Jenkins group to form a theragnostic hydrogel.

Although the presented findings are novel there are certain limitations which are important to address for the continuation of the research. The work on the biological interactions between CAP and bacteria predominantly use *Escherichia coli*, which is a Gram-negative bacterium. Further, the only oxidative stress related enzyme investigated is catalase whereas it is likely that superoxide dismutase and glutathione peroxidase play a role also. The ARS hydrogel system, while it releases ARS in response to hydrogen peroxide and plasma activated water, the application of He-CAP jet causes serious structural impact on the hydrogel, therefore optimisation of He-CAP conditions for this specific application would be required. Alternatively, the argon-driven CAP (Ar-CAP) jet could be assessed for interactions with the ARS hydrogel, owing to its more favourable interactions with PVA it is possible it would work well with the ARS gel. The PVP-I and PVP-I hydrogel shows great promise for clinical application; however, further quantification is required to fully understand the interactions between PVP-I and CAP generated RONS to confirm if the bactericidal moiety formed is HOI.

While future work has been outlined in individual chapters, the overall future of cold plasma medicine appears very promising, there are multiple CAP devices available for clinical use, with new clinical trial data being published monthly. While CAP provides a promising alternative therapy to traditional antibiotics, the excitement should be tempered with caution. While CAP has been shown to effectively reduce bacterial loads, further robust testing in the clinic and *in vitro* in the laboratory is required to assess the potential for resistance to for to CAP as well as further understanding the mutagenic effects of CAP treatment upon bacteria. A concerted multidisciplinary approach is required to further understand the risks of CAP, particularly within wound care.